

**Selective modulation of the Protein Kinase CK2:
discovery, syntheses and characterization
of non-ATP site inhibitors of CK2**

Dissertation

zur Erlangung des Grades
des Doktors der Naturwissenschaften
der Naturwissenschaftlich-Technischen Fakultät III
Chemie, Pharmazie, Bio- und Werkstoffwissenschaften
der Universität des Saarlandes

von

Benoît Bestgen

Saarbücken

2015

Tag des Kolloquiums: Freitag, 27. November 2015

Dekan: Prof. Dr.-Ing. Dirk Bähre

Vorsitzender: Prof. Ahcène Boumendjel

1. Berichterstatter: Prof. Dr. Rolf Hartmann

2. Berichterstatter: Prof. Dr. Joachim Jose

Akademischer Mitarbeiter: Dr. Matthias Engel

The present study was conducted from October 2011 to November 2015 under the supervision of Prof. Dr. Rolf W. Hartmann in the faculty of Pharmaceutical and Medicinal Chemistry of Natural Sciences and Technology of Saarland University, and under the supervision of Prof. Marc Le Borgne and Dr. Thierry Lomberget in the department of Medicinal Chemistry in the faculty of pharmacy of Lyon University.

Die vorliegende Arbeit wurde von Oktober 2011 bis November 2015 unter Anleitung von Herrn Prof. Dr. Rolf W. Hartmann in der Fachrichtung 8.2 Pharmazeutische und Medizinische Chemie der Naturwissenschaftlich-Technischen Fakultät III der Universität des Saarlandes angefertigt, und unter Anleitung von Herrn Prof. Marc Le Borgne und Herrn Dr. Thierry Lomberget in der Fachrichtung Medizinische Chemie der Pharmazeutische Fakultät der Universität des Lyon angefertigt.

Le travail présenté a été réalisé entre octobre 2011 et novembre 2015 sous la supervision du Prof. Dr. Rolf W. Hartmann au sein du département de pharmacie et de chimie médicinale de la faculté des sciences naturelles de l'Université de la Sarre, et sous la supervision du Prof. Marc Le Borgne et du Dr. Thierry Lomberget au sein du département de chimie thérapeutique de la faculté de pharmacie de l'Université de Lyon.

Saarland University, Pharmaceutical and Medicinal Chemistry & Helmholtz Institute for Pharmaceutical Research Saarland (HIPS), Department of Drug Design and Optimization, Campus C2.3, 66123 Saarbrücken, Germany

EA 4446 Biomolécules Cancer et Chimiorésistances, SFR Santé Lyon-Est CNRS UMS3453-INSERM US7, 8 avenue Rockefeller, F-69373 Lyon cedex 08, France

EA 4446 Biomolécules Cancer et Chimiorésistances, SFR Santé Lyon-Est CNRS UMS3453-INSERM US7, 8 avenue Rockefeller, F-69373 Lyon cedex 08, France.

"It was the best of times, it was the worst of times, it was the age of wisdom, it was the age of foolishness, it was the epoch of belief, it was the epoch of incredulity, it was the season of Light, it was the season of Darkness, it was the spring of hope, it was the winter of despair, we had everything before us, we had nothing before us, we were all going direct to Heaven, we were all going direct the other way [...]"

A Tale of Two Cities (Charles Dickens)

English summary

Selective modulation the Protein Kinase CK2: discovery, syntheses and characterization of non-ATP site inhibitors.

The protein kinase CK2 is a tetrameric enzyme composed of a dimer of regulatory subunits (β) and two catalytic subunits, CK2 α and/or CK2 α' . The catalytic subunit of CK2 is constitutively active, while the regulatory subunit modulates the selectivity toward a subset of substrate proteins. CK2 is a ubiquitous Ser/Thr protein kinase involved in the control of various signaling pathways, and dysregulation of CK2 promotes cancer development. CK2 has been proved to be a valuable target in cancer treatment.

Our objective was to target CK2 outside the ATP-pocket. Two independent classes of compounds were studied:

- Based on a first hit with a low potency ($IC_{50} = 30 \mu M$) but a non-ATP competitive mechanism of action, several 2-aminothiazole derivatives were synthesized to lead to a potent ($IC_{50} = 0.6 \mu M$) and cell efficient allosteric inhibitor of CK2. Using single mutation scanning, CD spectrometry, STD-NMR and docking experiments, the binding site of our compounds was precisely defined outside the ATP-pocket, at the interface of the glycine-rich loop and the αC -helix.
- Inhibitors of the α/β interaction were studied from a small cyclic peptide to the development of small molecules through Virtual Ligand Screening. Structures Activity Studies were conducted on the synthesized derivatives and cellular based assays to evaluate the α/β inhibitors were set up.

The two classes of compounds developed herein are valuable tools to understand the physiological regulation of the protein kinase CK2, and potential new opportunities in cancer treatment.

Key words: Oncology, Medicinal chemistry, Biology, Protein Kinase

German summary

Selektive Modulation der Proteinkinase CK2: Entdeckung, Synthese und Charakterisierung von nicht ATP-kompetitiven Hemmstoffen.

Das Protein Kinase CK2 ist ein tetrameres Enzym, das aus einem Dimer von regulatorischen Untereinheiten (β) und zwei katalytischen Untereinheiten (CK2 α und/oder CK2 α') besteht. Die katalytische Untereinheit der CK2 ist konstitutiv aktiv, während die regulatorische Untereinheit die Auswahl einiger der durch CK2 phosphorylierten Substrate steuert. CK2 ist eine ubiquitäre Proteinkinase, die an der Kontrolle zahlreicher Signalwege beteiligt ist. Eine Fehlregulation der CK2 fördert die Tumorenstehung. Es konnte gezeigt werden, dass CK2 eine vielversprechende Zielstruktur für die Entwicklung neuer Therapeutika ist. Unser Ziel war es, neue Hemmstoffe der Proteinkinase CK2 zu entwickeln, die an anderen Stellen als dem aktiven Zentrum angreifen.

Zwei Serien von Verbindungen sind untersucht worden:

- Basierend auf einem ersten schwach aktiven "Hit" ($IC_{50} = 30 \mu M$), der einen nicht-ATP-kompetitiven Wirkmechanismus aufwies, wurden einige neue 2-Aminothiazol-Derivate synthetisiert. Dadurch wurden allosterische Inhibitoren mit einer deutlich gesteigerten Potenz ($IC_{50} = 0,6 \mu M$) und einer beachtlichen Zellaktivität erhalten. Mittels eines CK2-Punktmutanten-Screenings, Zirkulardichroismus-Spektrometrie, STD-NMR und molekularer Docking-Simulationen konnte die Bindestelle unserer Hemmstoffe außerhalb der ATP-Bindetasche, zwischen der Glycin-reichen Schleife und der αC -Helix, lokalisiert werden.
- Desweiteren wurden niedermolekulare Inhibitoren der α/β -Interaktion entwickelt, ausgehend von einem zyklischen Peptid sowie von Hitverbindungen aus einem virtuellen Screening. Neue Verbindungen wurden synthetisiert und die Struktur-Wirkungsbeziehungen analysiert; zusätzlich wurde ein Zellaassay zur Überprüfung des postulierten Wirkmechanismus etabliert.

Die beiden entwickelten Verbindungsklassen sind interessante Werkzeuge, um die physiologische Regulation der Proteinkinase CK2 näher zu analysieren; überdies stellen sie Ausgangspunkte für die Entwicklung neuartiger Krebstherapeutika dar.

Stichworte: Onkologie, Medizinische Chemie, Biologie, Protein Kinase

French summary

Modulation sélective de la Protéine Kinase CK2 : Identification, synthèse et caractérisation d'inhibiteurs ne ciblant pas le site ATP.

La Protéine Kinase CK2 est une enzyme tétramérique composé d'un dimère de sous-unité régulatrice (β) et de deux sous-unités catalytiques, CK2 α et/ou CK2 α' . La sous-unité catalytique de CK2 est constitutivement active alors que la sous-unité régulatrice régule seulement la sélection des substrats phosphorylés par CK2. CK2 est une Ser/Thr protéine kinase ubiquitaire impliquée dans le contrôle de nombreuses voies de signalisations. La dérégulation de CK2 promeut le développement des cancers et il a été démontré que CK2 est une cible pertinente dans le traitement des cancers.

Notre objectif était de cibler la protéine kinase CK2 de manière indépendante du site actif. Deux séries de composés ont été étudiés :

- Basé sur un premier hit faiblement actif ($CI_{50} = 30 \mu M$) mais inhibant CK2 de manière non-ATP compétitive, des dérivés comportant le noyau 2-aminothiazole ont été synthétisés et un composé actif ($CI_{50} = 0,6 \mu M$) et efficace *in cellulo* a été obtenu. Grâce à des expériences sur des mutants ponctuels de CK2, des expériences de dichroïsme circulaire, de la STD-RMN et de la modélisation moléculaire, le site de fixation de nos inhibiteurs a été précisément défini à l'interface de la boucle riche en glycine et de l'hélice- αC .
- Des inhibiteurs de l'interaction α/β ont été étudiés à partir d'un peptide cyclique jusqu'au développement de petites molécules via un screening virtuel. Des études de relations structure-activité ont été réalisées sur la série de composés synthétisés et des tests cellulaires ont été mis en place afin d'évaluer ces composés.

Les deux classes de molécules décrites sont des outils intéressants pour comprendre la régulation physiologique de la protéine kinase CK2 et des opportunités prometteuses dans le traitement de certains cancers.

Mots-clés: Oncologie, Chimie Médicinale, Biologie, Protéine Kinases

Acknowledgments

I accomplished this work in the laboratory of “Biomolécules Cancer et Chimiorésistances” (University Lyon 1, EA 4446), under the supervision of Pr. Marc Le Borgne and Dr. Thierry Lomberget and in the laboratory of “Pharmaceutical and Medicinal Chemistry” (Saarland University), under the supervision of Pr. Rolf W. Hartmann and Dr. Matthias Engel. I would also like to thank Dr. Jean-Jacques Feige and Dr. Claude Cochet who accept me in their laboratory (Biology of Cancer and Infection, KIN, U1036).

First, I would like to thanks Pr. Marc Le Borgne and Pr. Rolf W. Hartmann for proposing me this fascinating topic of research and to allow me to work in this project. A special word for Dr. Claude Cochet, the father of this project, who let me enter in his “CK2 world” and show me why science will always be exciting, thank you. I am deeply grateful to Dr. Matthias Engel from who I have learned a lot and I am still learning. I would also like to thank Dr. Thierry Lomberget who helps me during my work in Lyon. I had the chance to be supervised by all of you, thank you for your precious help, I will never forget all the advices and what I have learned from you.

I would like to thank Pr. Ahcène Boumendjel (Université Joseph Fourier), Pr. Fabrice Anizon (Université Blaise Pascal) and Pr. Joachim Jose (Universität Münster) who accepted to read this work, as well as all the members of the jury.

I would like to thank Ruben Abagyan and Irina Kufareva (Skaggs School of Pharmacy and Pharmaceutical Sciences, University of California, San Diego, La Jolla) for your precious help in molecular modeling. Even if we could work only by email exchanges, I have learned a lot from our long emails, Irina.

It was a pleasure to work with you, Isabelle Krimm (Institut des Sciences Analytiques, UMR 5280), thank you for your help along this project, and thank you for your always quick reactivity.

I would like also to acknowledge Jean-Baptise Reiser (IBS) for your co-crystallization attempts even if unfortunately, the joy of the success was not with us.

I would like to thank Didier Bouyssi and Pierre Falson for your nice and helpful participation to all my PhD committees. Thank you for your help in the long road of a PhD.

The doctoral school, EDISS, always helps me during my PhD, thank you, and it was a pleasure to be a member of your board. I would like to thank Pr. Stéphanie Briançon (LAGEP, University of Lyon) to accept me as a part-time teacher during my 4th year of PhD. I discovered the galenic science thanks to the help of all the nice people from your team.

My thoughts are also going to all the wonderful people that I met in Lyon, Grenoble and Saarbrücken. I can't name all of you but you made this journey perfect. And I would like to thank you who help me in my work: Ahmed, mister CD; Caro, my professor in Western Blot; Marica, for your help in cell culture; Enrico, for sharing your chemistry; Lilli & Kristina, the SPR specialists; Dalila, for your kind help with the administration; Odile, for your advices; Nathalie, the LC-MS expert; Marlène, for your always perfect cell dishes... and all the others, in the labs and outside with who I really had fun!

I would like also to thank my family, my parents and my sisters for your support.

And finally, Dienabou, life is great by your side!

I could not be there without all of you.

Abbreviations

μ M: Micromolar

3D: Three-Dimensional

ADMET: Absorption, Distribution, Metabolism, and Excretion - toxicity

AGC: protein kinase A, G and C (PKA, PKC, PKG)

Akt: Protein kinase B (PKB)

AMPPNP: Adenosine 5'-(β,γ -imido)triphosphate

ANS: 8-Anilinonaphthalene-1-sulfonic acid

ATP: Adenosine TriPhosphate

Bcr-Abl: breakpoint cluster region - Abelson murine leukemia oncogene homolog 1

Bn: Benzyl

Boc: tert-ButOxyCarbonyl

br s: broad singlet

CaM: Calmodulin

CAMK: Calmodulin/Calcium regulated Kinases

ccRCC: clear cell Renal Cell Carcinoma

CDK: Cyclin-dependent kinases

CFTR: Cystic fibrosis transmembrane conductance regulator

CK1: Cell Kinase 1 group

CK2: Casein Kinase 2

Clk: Cdc2-like kinase

CMGC: CDK, MAPK, GSK3 and CLK families

Cpd: compound

d: doublet

DBC1: Deleted in Breast Cancer 1

dd: doublet of doublet

DIPEA: DiIsoPropylEthylAmine

DLS: Dynamic Light Scattering

DMAP: 4-(Dimethylamino)pyridine

DMAT: 4,5,6,7-tetrabromo-N,N-dimethyl-1H-benzimidazol-2-amine

DMF: N,N'-dimethylformamide

DMSO: DiMethylSulfOxide

DRB: 5,6-dichlorobenzimidazole 1- β -D-ribofuranoside
DSC: Differential Scanning Calorimetry
dt: doublet of triplet
DYRK: Dual specificity tyrosine-phosphorylation-regulated kinase
eg: *exemplia gratia*
ELISA: Enzyme-Linked ImmunoSorbent Assay
EMA: European Medicines Agency
EMT: Epithelial–Mesenchymal Transition
ERK: Extracellular signal-regulated kinases
ESI: Electro Spray Ionization
Et: Ethyl
Fig: Figure
GBD: Global Burden of Diseases
GPCR: G protein–coupled receptor
GST: glutathion S-transférase
GTP: Guanosine TriPhosphate
HATU: 1-[Bis(dimethylamino)methylene]-1H-1,2,3-triazolo[4,5-b]pyridinium 3-oxid hexafluorophosphate
HEPES: 4-(2-hydroxyethyl)-1-piperazineethanesulfonic acid
HPLC: High Performance Liquid Chromatography
HRMS: High Resolution Mass Spectrometry
HTRF: Homogeneous Time Resolved Fluorescence
HTS: High-throughput screening
IC₅₀: Concentration required for 50 % inhibition
ICM: International Computer Management
ie: *id est*
IQA: [5-oxo-5,6-dihydro-indolo(1,2-a)quinazolin-7-yl]acetic acid
ITC: isothermal titration calorimetry
K_A: Association constant
K_D: Dissociation constant
LC: Liquid Chromatography
LE: Ligand Efficiency
LogP: Octanol-water partition coefficient
m: multiplet
MDR: Multi-Drug Resistance

Me: Methyl
MEK: Mitogen/Extracellular signal-regulated Kinase
mM: Millimolar
MS: Mass Spectrometry
Ms: Mesylate (MeSO₂)
MTT: 3-(4,5-dimethylthiazol-2-yl)-2,5-diphenyl tetrazolium bromide
MW: Micro-Wave
NBS: N- bromosuccinimide
n-Bu: n-Butyl
NCS: N-ChloroSuccinimide
nM: Nanomolar
NMR: Nuclear Magnetic Resonance
Pc: cyclic peptide
PCNA: proliferating cell nuclear antigen
PDB: Protein Data Bank
PEI: Percentage Efficiency Index;
Ph: Phenyl
PK: Protein Kinase
POM: PolyOxoMetalate
PP2I: Protein-Protein Interaction Inhibitors
q: quadruplet
RCC: Renal Cell Carcinoma
RGC: Receptor Guanylate Cyclases
RMSD: Root-Mean-Square Deviation
RT: Room Temperature
s: singlet
SAR: Structure Activity Relationship
SAXS: Small-Angle X-ray Scattering
SD: Standard deviation
SPR: Surface Plasmon Resonance
SR: serine/arginine
STD: Saturation-Transfer Difference
t: triplet
Tab: Table
TAT: Trans-Activator of Transcription

TBB: 4,5,6,7-Tetrabromo-2-azabenzimidazole
TBBi: 4,5,6,7-tetrabromobenzimidazole
TBCA: (E)-3-(2,3,4,5-Tetrabromophenyl)acrylic acid
TBS: Tris-Buffer Saline
TBST: Tris-Buffer Saline Tween
TCA: Trichloroacetic-acid
td: triplet of doublet
TdCD: Temperature-dependent circular dichroism
TFAA: TriFluoroAcetic Anhydride
THF: TetraHydroFuran
TIBi: 4,5,6,7-tetraiodobenzimidazole
TIBI: 4,5,6,7-tetraiodobenzimidazole
TK: Tyrosine Kinase
TKL: Tyrosine Kinase-Like
TLC: Thin Layer Chromatography
TMSA: TriMethylSilylAcetylene
TPSA: Topological Polar Surface Area
Ts: Tosyl
TSA: Thermal Shift Assay
UV: Ultra-Violet
VLS: Virtual Ligand Screening

Contents

English summary	5
German summary.....	6
French summary.....	7
Acknowledgments.....	8
Abbreviations	10
Contents	14
1. Introduction.....	19
1.1 Cancer and cell signaling	20
1.1.1 Epidemiology.....	20
1.1.2 Cancer definition	20
1.2 Protein kinases in cell signaling.....	22
1.2.1 Cell signaling.....	22
1.2.2 Deregulation in cancer development.....	22
1.2.3 Protein Kinases	22
1.2.4 Human kinome	23
1.2.5 Protein Kinase structures	25
1.2.6 Protein Kinases as therapeutic targets.....	27
1.3 Protein kinase CK2.....	30
1.3.1 Overview.....	30
1.3.2 Structural specificities	31
1.3.3 CK2 implication in pathophysiology	40
1.3.4 Known CK2 inhibitors	48
1.4 Allosteric and non-ATP competitive inhibitors	56
1.4.1 Allosteric definition	56
1.4.2 Kinase inhibitor classes and allosteric.....	57
1.4.3 Examples of non-ATP competitive inhibitors of protein kinases	59
1.4.4 Allosteric inhibitors and CK2	67

1.5	Protein-Protein Interaction Inhibitors.....	71
1.5.1	Definitions and importance.....	71
1.5.2	Specific difficulties in PP2I discovery.....	71
1.5.3	Successful stories.....	73
1.5.4	PP2I and CK2.....	82
2.	Aim of the thesis.....	87
3.	Results	91
3.1	Modulation of protein kinase CK2 activity in cells through novel non-ATP competitive inhibitors	92
3.1.1	Scientific rationale.....	92
3.1.2	Hit compound 1 is a non-ATP competitive inhibitor of CK2.....	94
3.1.3	Structural requirements of the new inhibitors for CK2 α affinity	96
3.1.4	Identification of a putative allosteric pocket	96
3.1.5	Compounds 5 and 7 induce a thermal destabilization of CK2 α	99
3.1.6	The binding sites of compound 5 and the ATP-competitive inhibitor CX-4945 do not overlap	101
3.1.7	<i>In silico</i> prediction of the binding mode.....	103
3.1.8	Compound 7 retains its cell-free potency in cell-based CK2 inhibition assays	104
3.1.9	The inhibition of CK2 activity by compound 7 is substrate-dependent	105
3.1.10	Conclusion	107
3.2	2-Aminothiazole derivatives as potent and selective allosteric modulators of the protein kinase CK2	116
3.2.1	Scientific rationale.....	116
3.2.2	Chemistry.....	118
3.2.3	Structure-Activity Relationships	120
3.2.4	Enzymatic characterization of compound 8e effects on CK2.....	129
3.2.5	Compound 8e binds to an allosteric pocket of CK2 α	130
3.2.6	Compound 8e is a selective inhibitor of CK2.....	130
3.2.7	Inhibition of CK2 cellular activity and apoptosis induction by 8e	131
3.2.8	Conclusion	134
3.3	Identification of the first cellular efficient modulator of the protein kinase CK2 subunit interaction	135
3.3.1	Scientific rationale.....	135

3.3.2	Design of a cell permeable chimeric TAT-Pc	136
3.3.3	TAT-Pc suppresses the CK2 α /CK2 β interaction in living cells	137
3.3.4	CK2 subunits subcellular localization is altered by TAT-Pc.....	138
3.3.5	Epidermal growth factor receptor (EGFR) down-regulation upon TAT-Pc treatment	139
3.3.6	p21 phosphorylation is increased by TAT-Pc.....	140
3.3.7	Differential effects of CK2 α /CK2 β interaction inhibition and CK2 β knockdown	143
3.3.8	TAT-Pc decreases cancer cell viability	143
3.3.9	Conclusion	144
3.4	Structure-Based discovery of a small chemical scaffold targeting the CK2 Subunits interface	145
3.4.1	Virtual Screening and hit validation	145
3.4.2	Chemical synthesis	148
3.4.3	Cell-free biological evaluation.....	155
3.4.4	Structure-Activity Relationship Studies.....	157
3.4.5	Biological evaluation in living cells	157
3.4.6	Conclusion	159
4.	Final discussion.....	161
4.1	Allosteric modulator of CK2 α	162
4.1.1	CK2 specificities and allosteric inhibitors	162
4.1.2	X-ray structures	164
4.1.3	Similarities and differences with others allosteric inhibitors.....	168
4.1.4	Indirect effect in the single-alanine mutagenesis experiments	170
4.2	CK2 α /CK2 β interaction inhibitors.....	171
4.2.1	Structurale similarities with other related compound.....	171
4.2.2	Effects in cell signaling.....	172
4.3	Perspectives of further drug development	174
4.3.1	Allosteric modulator of CK2 α	174
4.3.2	CK2 α /CK2 β interaction inhibitors.....	175
4.4	Outlook.....	175
5.	Experimental section.....	178
6.1	Chemistry	179
6.1.1	Synthesis of compounds of chapter 3.1	179
6.1.2	Synthesis of compounds of chapter 3.2	183

6.1.3	Synthesis of compounds of chapter 3.4	199
6.2	Biology	209
6.2.1	Biology of the chapter 3.1	209
6.2.2	Biology of the chapter 3.2	214
6.2.3	Biology of the chapter 3.3	216
6.2.4	Biology of the chapter 3.4	218
References	221

1. Introduction

1.1 Cancer and cell signaling

1.1.2 Epidemiology

Cancers were responsible for 5660 thousands deaths in the world in 1990 and 8236 thousands in 2013, representing 15% of human mortality in 2013 (Fig 1). Deaths caused by cancer are generally increasing, mainly because of ageing of the world's population. Notably, death rates for cancers are not homogeneous, from cancer types but also from geographical area.^{1,2}

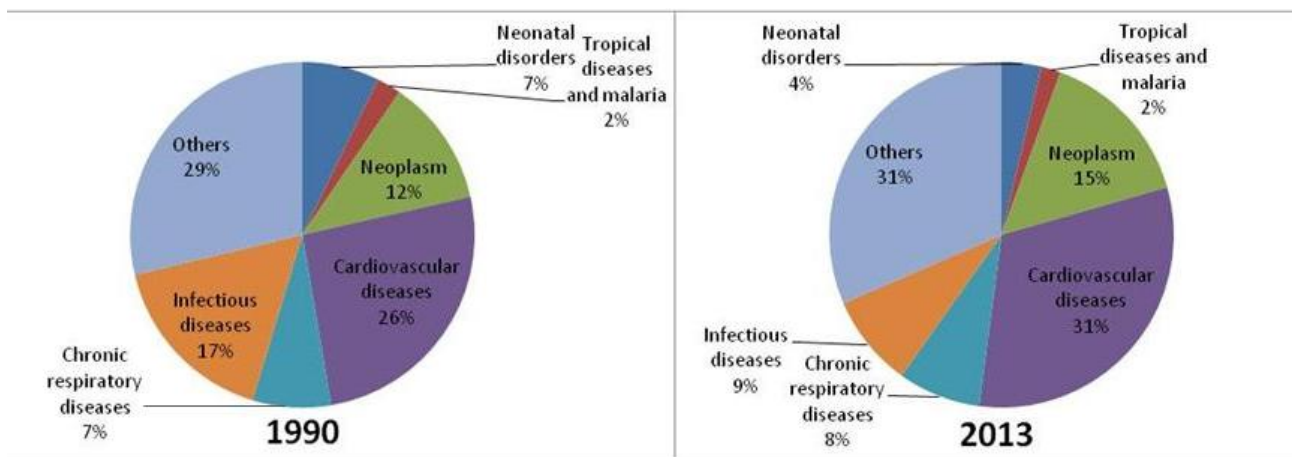


Fig 1: Percentages of death causes in the world in 1990 and 2013 (Reprinted from the Lancet GBD 2013², Copyright (2016), with permission from Elsevier).

In 2008, 12.7 million cancer cases and 7.6 million cancer deaths were estimated to have occurred. For females, the most frequent cancer is breast cancer with 23% of total cancer cases and 14% of cancer deaths. For males, lung cancer is the most frequent with 17% of the cases and 23% of deaths. Notably, mortality rates are similar in developing countries and in developed countries.³

1.1.3 Cancer definition

Sometimes, cancers are classified by the organ at the source of neoplasm but there are actually more than 100 distinct types of cancer and different types of cancer can exist in one organ. Nevertheless, all subtypes of tumors share six common hallmarks (Fig 2): (i) sustaining

proliferative signaling, (ii) inducing angiogenesis, (iii) insensitivity to anti-growth signals, (iv) evading apoptosis, (v) activating invasion and metastasis, (vi) enabling replicative immortality. These six characteristics are the common denominator of cancer cells.⁴

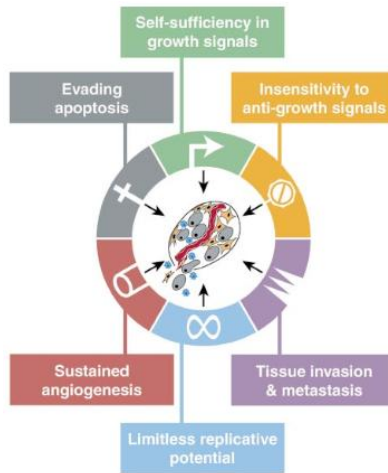


Fig 2: Hallmarks of cancer (Reprinted from Hanahan, D. *et al.*⁴, Copyright (2016), with permission from Elsevier)

More than one deregulation is required to transform a normal human cell into cancer cells. Globally, a succession of genetic changes, each one providing a step promoting a growth advantage, is required for the acquisition of the six characteristics of cancer cells. Each genetic change is responsible of a small deregulation in cell signaling, leading to tumor development.⁵

1.2 Protein kinases in cell signaling

1.2.1 Cell signaling

Cell signaling is the global system that enables cells to react properly to environmental factors. Indeed, cells are controlled by various internal or external factors. In order to respond to these stimuli, cells have to be able to detect them and to react specifically to them. A network of proteins is responsible of the signal carrying from the environment into the cells. Each protein inside the cell signaling network controls a specific part of the signal transduction. Together, they control specific responses to one stimulus.

1.2.2 Deregulation in cancer development

Cell signaling is responsible of the control of the cellular functions. Cell signaling regulates cell proliferation, cell differentiation, apoptosis, cell survival, cell mobility, cell cycle, metabolism, transcription, translation... In consequence, any small deregulation of this machinery could be the starting point of a complete change in cell behavior. In some cases, pro-survival and anti-apoptotic features can be acquired in normal cells that could be then transformed into cancer cells. Thus, deregulation of cell signaling is a common feature of cancer cells.

1.2.3 Protein Kinases

Protein Kinases are one of the major classes of protein involved in cell signaling. Protein kinases are a group of enzymes able to transfer a phosphate group from a phosphate donor such as ATP or GTP to a protein substrate (Fig 3). In living cells, phosphorylation is a reversible mechanism as dephosphorylation is operated by another class of proteins named protein phosphatases. Phosphorylation is a very well controlled mechanism enabling cells to react in a time frame of milliseconds to seconds. Indeed, each protein kinase is able to phosphorylated specific substrates at specific amino acids. According to recent estimations, at least 30% of proteins in eukaryotic cells are phosphorylated.⁶ Addition of phosphate groups can alter protein activity, stability, cellular localization and interactions. Consequently, protein phosphorylation is a key regulator of cellular physiology, and abnormal phosphorylation contributes to diseases such as cancer, diabetes and neurodegeneration.

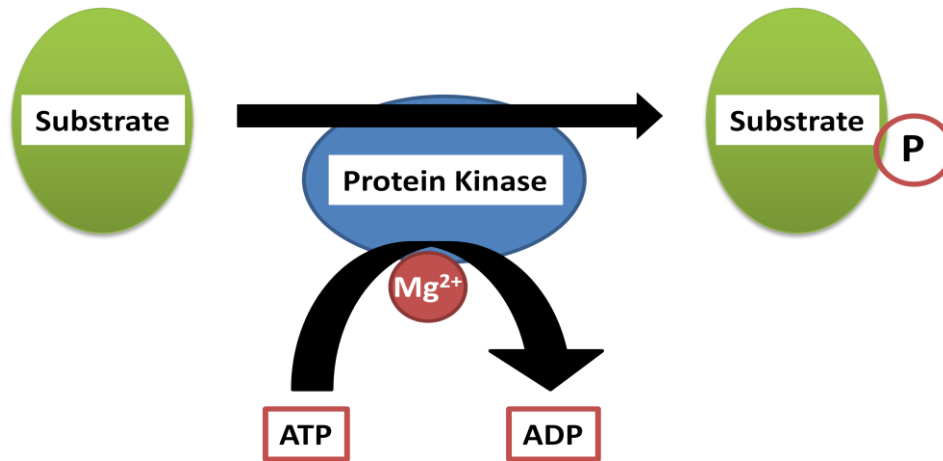


Fig 3: Schematic representation of protein phosphorylation.

1.2.4 Human kinome

The completion of the human genome sequence allows the classification of all the 518 kinases that represent about 1.7% of the human genome.⁷ The entire set of human protein kinases are called human kinome and could be divided into eight major subfamilies (Fig 4):

- TK for Tyrosine Kinase which phosphorylates almost exclusively tyrosine residues,
- TKL for Tyrosine Kinase-Like which are similar to TK but phosphorylates serine/threonine substrates,
- STE that are homologs of the yeast STE genes,
- CK1 for Cell Kinase 1,
- AGC for protein kinase A, G and C (PKA, PKC, PKG),
- CAMK for Calmodulin/Calcium regulated Kinases,
- CMGC named after CDK, MAPK, GSK3 and CLK families,
- RGC for Receptor Guanylate Cyclases.

Notably, some protein kinases do not belong to any of the major branches of the human kinome. As an example, CK2a is phylogenetically close to the CMGC family with similarities with DYRK, CLK and CDK but CK2a is located on a different branch in the kinome (Fig 4).

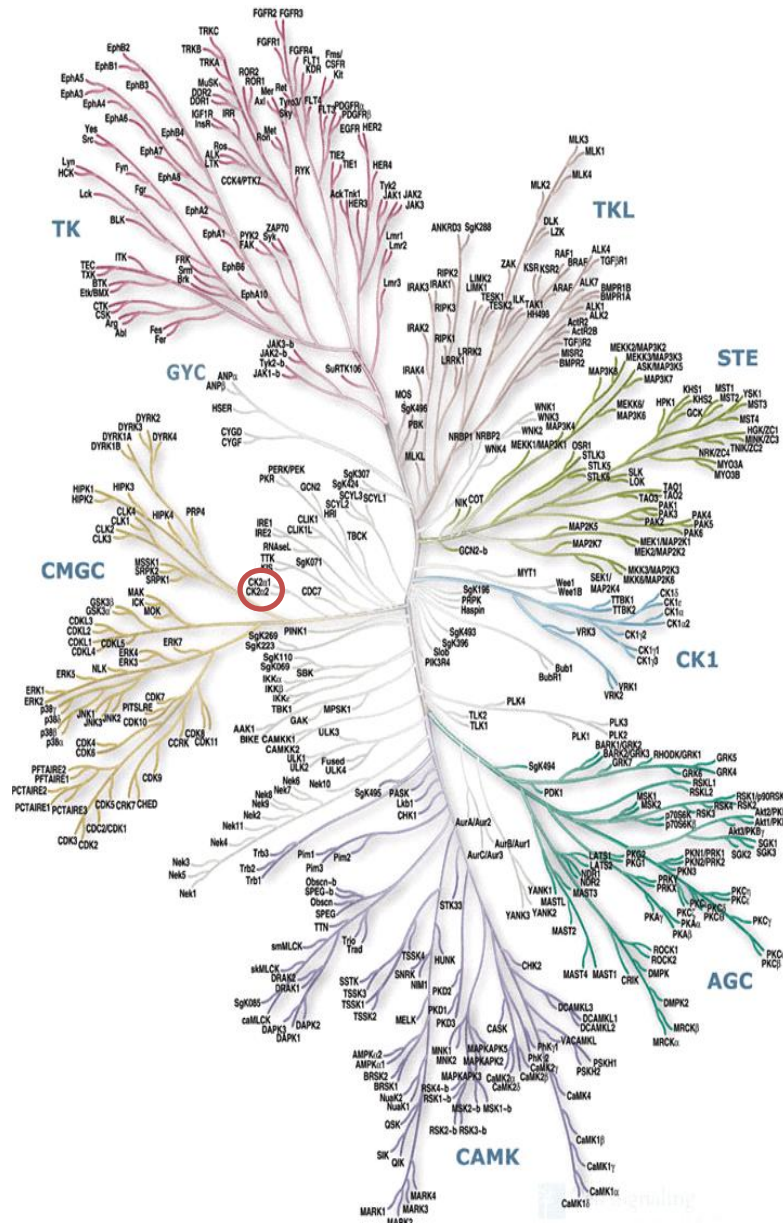


Fig 4: The Human Kinome (From Manning, G. et al.⁷). Each kinase is at the tip of a branch and the similarity between various kinases is inversely related to the distance between their positions. CK2a and CK2a' are surrounded in red. Illustration reproduced with the courtesy of Cell Signaling Technology, Inc. (www.cellsignal.com).

Notably, protein kinases are present in all living organisms but with structural differences, as examples:

- Eukaryotic Protein Kinases (EPK) in eukaryotes, probably more than 28,000 different EPK, exist,

- EPK-Like Kinase (ELK) are present in prokaryotes, 18,699 ELKs have been identified,
- Histidine kinases are also present in bacteria but they are structurally different to EPK or ELK.^{8,9}

1.2.5 Protein Kinase structures

Protein kinase A (PKA) was the first protein kinase structure resolved by crystallization and X-ray diffraction in 1991.¹⁰ Rapidly, a large number of protein kinase structures have been determined and all share the same structural core features (Fig 5a). All of them are composed of two lobes. The N-terminal lobes are mainly composed of five β strands, and one crucial and well conserved α C-helix, which is very important for the overall structure organization. Indeed, it has been reported that displacement of the α C-helix is the major way for allosteric kinase inhibition (see paragraph 1.4.3). The C-terminal lobe is mainly composed of helices rendering it more rigid than the N-terminal lobe. The ATP binding site is localized at the interface of the two lobes, in a very well conserved pocket. The adenosine moiety of ATP binds in a hydrophobic pocket and makes special H-bonds with the hinge region. Close to the adenosine binding site, a "gatekeeper" residue controls the access to a second pocket used by several marketed inhibitors to improve their selectivity (Fig 5b,c). The triphosphate moiety of ATP binds with the help of two magnesium ions between the glycine-rich loop (also called P-loop) and the magnesium-binding loop. Therefore, the third phosphate group is exposed and ready to be transferred to a protein substrate. The catalytic loop is an important regulator of kinase activity and, in the majority of kinases, this loop can adopt two conformations: open or closed. The closed conformation is the basal and inactive position. This conformation could be switched to the open or active conformation by a specific event, such as a phosphorylation in the catalytic loop or an activating-protein binding.¹¹

(a)

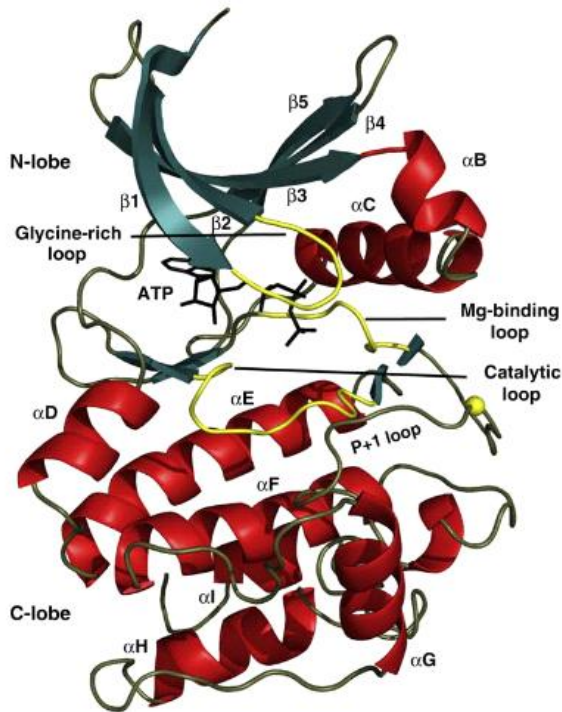


Fig 5: Structure of the conserved protein kinase core. (a) General bilobal kinase structure based on PKA (Reprinted from Taylor, S. S. et al.¹², Copyright (2016), with permission from Elsevier).

Study of the spatial conservation of residues among kinases revealed that two groups of amino acid are spatially very well conserved. Due to their spine pattern going through the catalytic site and the key elements of kinase regulation, they were called catalytic spine and regulatory spine, respectively (Fig 6). Both of them are anchored on the αF -helix. Based on the protein kinase A sequence: the catalytic spine is composed of 8 amino-acids, V57, A70, M128, L172, L173, I174, L227, M231 and the regulatory spine is composed of 5 amino-acids, L95, L106, F185, Y164, D220.¹⁵ In contrast to active kinase structures, these residues were not found to be well positionned in inactive kinase structures, underlining the relevance of these two spines in kinase regulation.¹⁶

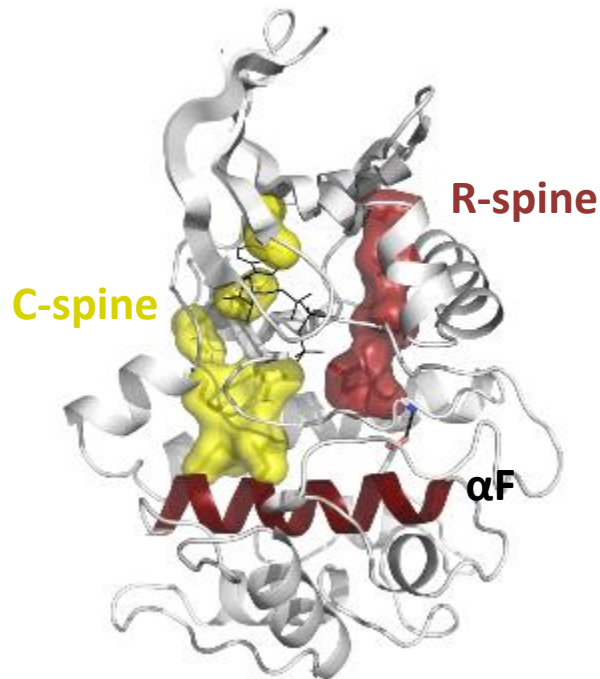


Fig 6: Structural representation of the Catalytic spine (C-spine) and Regulatory spine (R-spine) anchored on the αF -helix (based on PKA) (From Kornev, A. P. *et al.*¹⁵, Copyright (2016) National Academy of Sciences, USA).

1.2.6 Protein Kinases as therapeutic targets

The 518 protein kinases of the human kinome represent less than 2% of the whole human genome⁷ but there are considered to represent 22% of the druggable genome.¹⁷

Because of their crucial roles in cell signaling, protein kinases are considered as the second major drug target after G-Protein-Coupled Receptors. However, since the seminal discovery of R. Erikson, showing that the transforming factor of Rous sarcoma virus was a protein kinase (v-Src),¹⁸ it took more than twenty years for the approval in 2001 by the authorities of the first selective small molecule kinase inhibitor targeting Bcr-Abl and called imatinib (Fig 7).¹⁹

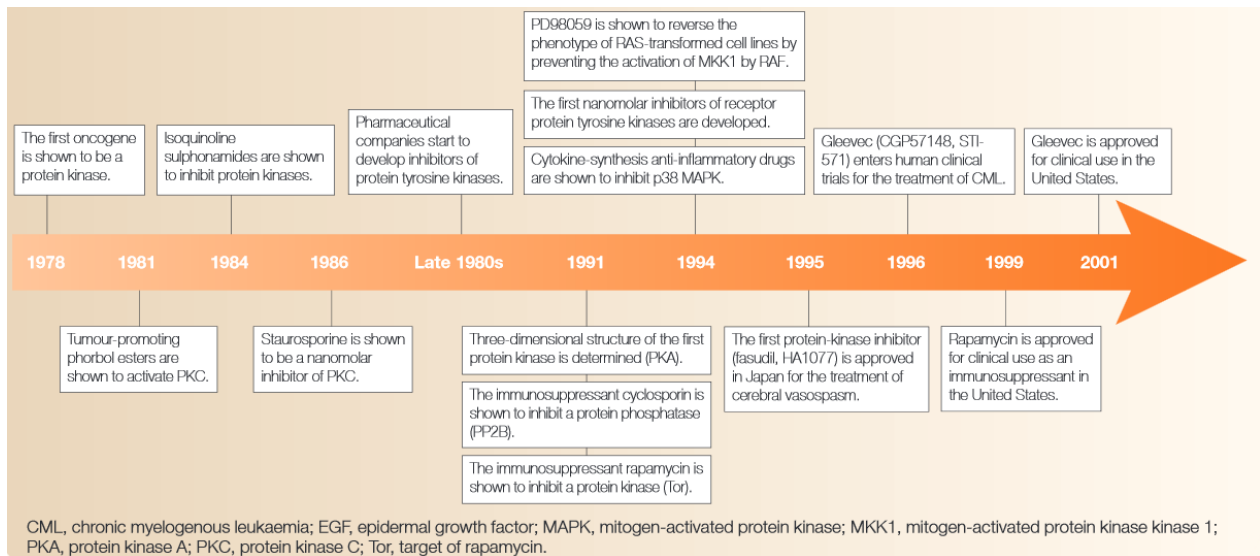


Fig 7: Key events in the development of protein-kinase inhibitors (Reprinted by permission from Macmillan Publishers Ltd: [Nat. Rev. Drug Discov.] from Cohen, P.¹⁹ copyright (2016))

Imatinib (Gleevec[®], Novartis) is an orally available inhibitor of Bcr-Abl and the first kinase inhibitor approved by the FDA and EMA for the treatment of chronic myelogenous leukaemia. Since, tremendous efforts of many laboratories have been focused on the identification of new kinase inhibitors and an increasing number of these inhibitors has been approved to treat several diseases (Table1). In 2013, imatinib was elected as the most innovative drug in oncology in the last 25 years, based on a physicians' survey.²⁰

Table 1: Small molecule kinase inhibitors approved by EMA, classified by approval year until 2013.^{21,22}

Target	Molecule name	Trade name	Year of EMA approval	Company
Bcr-Abl	imatinib	Gleevec®	2001	Novartis
EGFR	erlotinib	Tarceva®	2005	Roche
Bcr-Abl, Src, c-KIT	dasatinib	Sprycel®	2006	Bristol-Myers Squibb
VEGF	pegaptanib	Macugen®	2006	OSI/Pfizer
VEGFR, PDGFR, BRAF, c-Kit...	sorafenib	Nexavar®	2006	Bayer
VEGFR, PDGFR	sunitinib	Sutent®	2006	Pfizer
HER2	lapatinib	Tyverb®	2008	GlaxoSmithKline
Bcr-Abl	nilotinib	Tasigna®	2009	Novartis
EGFR	gefitinib	Iressa®	2009	AstraZeneca/Teva
VEGFR, PDGFR, c-Kit	pazopanib	Votrient®	2010	GlaxoSmithKline
VEGFR, PDGFR, c-KIT	axitinib	Inlyta®	2012	Pfizer
ALK, HGFR, c-MET	crizotinib	Xalkori®	2012	Pfizer
JAK	ruxolitinib	Jakavi®	2012	Novartis
VEGFR, EGFR, RET, BRK	vandetanib	Caprelsa®	2012	AstraZeneca
BRAF	vemurafenib	Zelboraf®	2012	Roche
Bcr-Abl	bosutinib	Bosulif®	2013	Pfizer
ErbB	afatinib	Giotrif®	2013	Boehringer Ingelheim
Bcr-Abl, BEGFR, PDGFR, FGFR, EPH, Src, c-KIT, RET, TIE2, FLT3	ponatinib	Iclusig®	2013	ARIAD Pharmaceuticals
RET, VEGFR, PDGFR	regorafenib	Stivarga®	2013	Bayer

1.3 Protein kinase CK2

1.3.1 Overview

Protein Kinase CK2 was discovered in 1954 during a study conducted by G. Burnett and E. Kennedy.²³ CK2 activity was revealed by the ability of the soluble extract of rat liver mitochondria to phosphorylate a protein, the casein, rather than small metabolites. In consequence, they suspected the presence of a possible protein phosphokinase.

In 1979, G. Hathaway and J. Traugh²⁴ purified two kinases from rabbit reticulocytes. Due to their ability to phosphorylate casein *in vitro*, they named them Casein Kinase 1 and Casein Kinase 2. Casein Kinase 2 was able to use either ATP ($K_m = 10 \mu\text{M}$) or GTP ($K_m = 40 \mu\text{M}$) as phosphate donors. Moreover, a highly purified preparation of CK2 analyzed by denaturing gel electrophoresis showed proteins of molecular weights of 42, 38 and 24 kDa. This finding suggests a heterogeneous subunit structure of CK2.

In the 80's, several groups worked on other kinases such as the dog cardiac Troponin-T kinase by C. Villar-Palasi and A. Kumon in 1981²⁵ or as the Glycogen Synthase Kinase 5 (GSK-5) by the group of P. Parker in 1982²⁶. Later, researchers realized that these two supposed kinases were however one, the protein kinase CK2.

At that time, the confusion came from two points. First, based on its ability to phosphorylate α -casein *in vitro*, Casein Kinase 2 was misnamed at its discovery since casein is not an *in vivo* substrate of CK2. Second, CK2 phosphorylates a pleiotropic number of substrates and cumulative literature described more than 300 *in vivo* substrates of CK2, involved in all aspects of the cell signaling network.²⁷ Consequently, several questions rise from these findings: How CK2 could be a good therapeutic target with so many substrates? What does make protein kinase CK2 a "special" kinase?

1.3.2 Structural specificities

1.3.2.1 The holoenzyme (CK2 $\alpha_2\beta_2$)

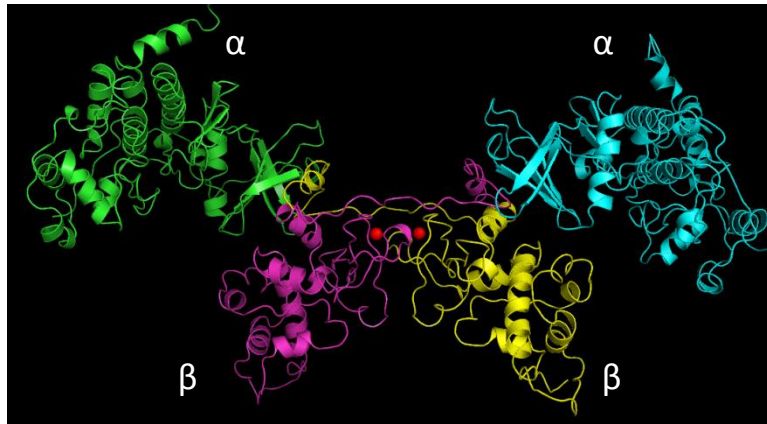


Fig 8: Structure of the holoenzyme form of the protein kinase CK2 (1JWH).^{28,29} In green and in blue: the two catalytic subunits (α). In magenta and in yellow: the dimer of regulatory subunits (β) linked by a “zinc finger binding motif” (the two red spheres).

CK2 is a multimeric kinase (Fig 8). The CK2 holoenzyme complex (125 kDa) is composed of a dimer of two β -subunits (regulatory subunits) and two α - or α' -subunits (catalytic subunits). The α -subunit (40 kDa) shares general features of protein kinases but the β_2 -subunit (45 kDa) is a unique protein with no sequence similarity with any other proteins.

In contrast to the majority of multimeric kinases like PKA or CDKs, that requires the binding/or unbinding of their regulatory subunit for activity, the β subunit does not turn on/off the kinase activity but instead, modulates its substrate selection of CK2 in a complex and not fully understood manner.

1.3.2.2 The CK2 α catalytic subunit

The catalytic subunit shares general features of human kinases such as a large C-terminal lobe mainly composed of α -helix and a smaller N-terminal lobe mainly composed of β -sheets. Nevertheless, CK2 α exhibits some structural specificities (Fig 9):^{30,31}

- An activation segment locked in an active state, responsible of the constitutive activity of CK2 α ,
- A good plasticity of the hinge/ α D region,
- An unusual “DWG” motif instead of the usual “DFG”.

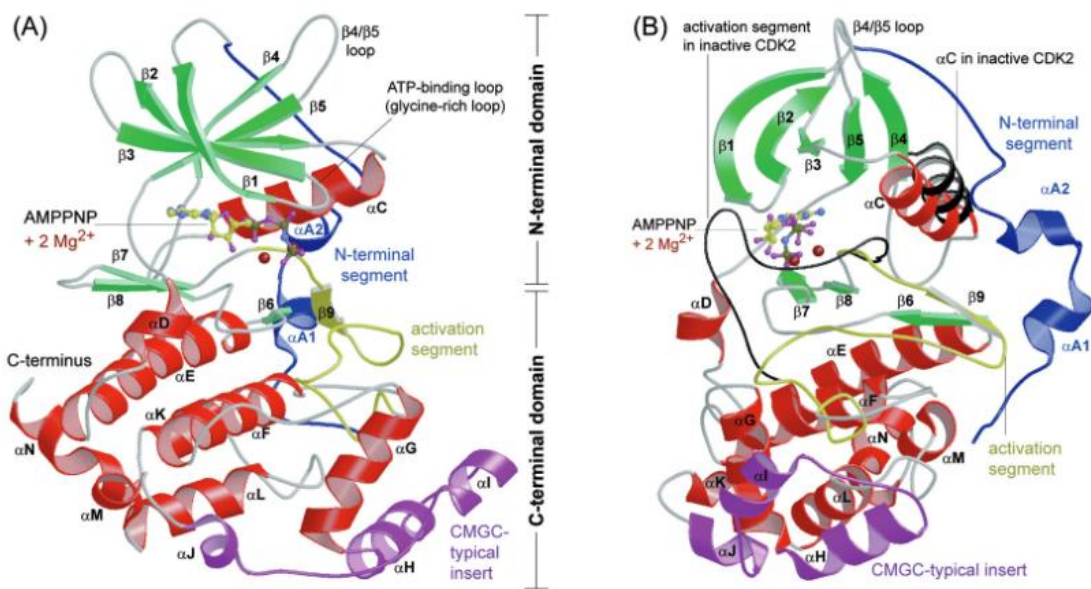


Fig 9: Structure of the catalytic subunit of CK2 from *Zea mays* in complex with AMPPNP and magnesium ions^{31–33} (From Niefind, K. *et al.*³¹, with permission of Springer). (B) represent the same than (A) but after a 90° rotation around a vertical axis. The activation segment and the α C-helix drawn in black are from the inactive conformation of CDK2 to show a possible inactive state of CK2.

A global comparison of X-ray structures of CK2 with the structures of CDK2 (Fig 10) revealed some interesting differences in their structural flexibility. Indeed, the N-terminal segment, the α C-helix, the catalytic loop and the activation segment of CK2 α are rigid and always observed in the same conformation whereas flexibility of these regions was observed in CDK2 structures. In the other hand, the glycine-rich loop, the β 4/ β 5 loop, the hinge region and the α I-helix are the main flexible part of CK2 α whereas these regions are rigid in CDK2 structures. The

complete different flexibility profile obtained for CK2 and CDK2 supports the specificity of CK2 regulation, in comparison with other kinases.³¹

The activation segment (Mg-binding loop, $\beta 9$, activation loop, P+1 loop) of CDK2 is very flexible. Upon cyclin binding, the positions of these key regulatory elements change and so, induce CDK2 activation. In the opposite, the activation segment of CK2 α is rigid and is not modified upon CK2 β binding. Indeed, in contrast to the majority of other protein kinases,³⁴ the activation segment of CK2 α is locked in the active conformation. No phosphorylation event is required to switch this activation segment in the active state because specific interactions of the N-terminal segment with the activation loop lock it in the fully productive conformation.³⁰

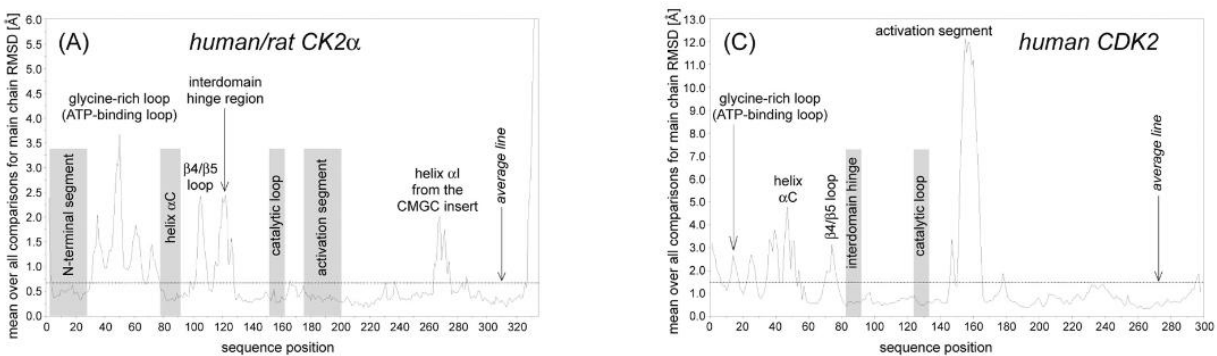


Fig 10: Representation of structural invariable and variable region for human CK2 in comparison with CDK2 (From Niefind, K. *et al.*³¹, with permission of Springer). All possible 3D structures were superposed and an average structure was determined. Then, average deviation represented by RMSD shows the structural variability of each part of the kinase structure. Specific rigid region are represented in grey and variable regions are represented by a peak.

The hinge region (H115-D120) connects the two lobes of CK2 α . This region plays a central role in ATP/GTP binding by forming several hydrogen bonds with adenine or guanine.³² The hinge region is closely connected to the αD -helix and two different conformations can be observed: open or closed and the amino acid Phe121 is the flag used to determine the conformation. Indeed, Phe121 can be observed “in” the C-spine making it complete (closed form) or “out” the C-spine (open form) (Fig 11). The equivalent residue of Phe121 in PKA catalytic spine is the residue Met128. But, on the contrary of PKA spines, in CK2 structures, ATP seems to favor the open conformation of the hinge/ αD region, making the catalytic spines uncompleted. Therefore, based on X-ray structures, CK2 α seems to be active with an uncomplete C-spine.^{35–37}

The DFG motif is composed of three amino-acids (Aspartic acid 175, Phenylalanine 176, Glycine 177 in PKA). This motif is very well conserved in EPKs. The aspartic acid is crucial for magnesium binding but the most important residue of this motif is the central phenylalanine. Indeed, the phenylalanine can twist from the “in” or active conformation to the “out” or inactive conformation.³⁸ In drug design, this special feature is a frequent strategy to target the ATP pocket in an inactive state. For example, imatinib targets the ATP pocket of Bcr-Abl in the DFG-out conformation.^{39,40} In the entire human kinome, CK2 α (and α') is the only kinase that does not have the DFG motif but instead a DWG one. The presence of a large residue tryptophan in position 176 instead of a phenylalanine induces stronger contacts and interactions with other residues of the environment. In consequence, the DWG-motif is stabilized in the “in” (active) conformation. The “out” conformation was never observed in X-ray structures of CK2 α . However, kinetic experiments with CK2 α mutant (W176F) and CK2 α wild type revealed that they both have the same V_{max} value. This result is not consistent with the fact that Trp176 is responsible of the fully active state of CK2 α and that the mutated CK2 α to Phe176 supports the release of ADP as expected.^{41,42}

1.3.2.3 The CK2 α' catalytic subunit isoform

A second isoform of CK2 α was identified and named CK2 α' . Both isoforms coexist in cells but CK2 α' is present in a larger quantity in the brain and testicles.⁴³ On the contrary of CK2 α , mice with CK2 α' knockout are viable, but sterile.⁴⁴ Overall comparison of amino-acid sequences revealed only very few differences, mainly in the C-terminal segment (Fig 12).⁴⁵ The affinity between CK2 α' and CK2 β is, of note, weaker (about 12-fold) than the affinity between CK2 α and CK2 β .⁴⁶

Bischoff *et al.*⁴⁵ shown that the differences in C-terminal segment and the affinity for CK2 β are linked. In CK2 α' , the prolongation of the N-terminal β -sheet by a β -strand and the presence of a tryptophan residue (Trp34) in a conserved hydrophobic cavity (localized between the β 4/ β 5 loop and the helix- α C) stabilized the β 4/ β 5 loop in the open conformation. This conformation is required for CK2 β binding but authors proposed that the rigidity of the β 4/ β 5 loop in CK2 α' could prevent adaptation under β -binding, and is consequently responsible for the lower affinity. The second important point underlined in their study is that the “in” conformation of the hinge/ α D

region observed for CK2 α' whereas the “out” conformation is observed in the large majority of CK2 α structures. Nevertheless, more crystallization experiments are required to conclude if this observation is a generality or a rare case.⁴⁵

numb. <i>hsCK2α'</i> :	1	10	20	27	Pro32	Trp34	41	50	60	70
<i>hsCK2α'</i>	mpgpaagSRA	RVYaeVNsLR	sREYWDYEaH	VpsWGNQDDY	QLVRKLGRGK	YSEVF EAINI	TNNErVVVKI			
<i>hsCK2α</i>	~msgpvpSRA	RVYtdVNthR	pREYWDYEsH	VveWGNQDDY	QLVRKLGRGK	YSEVF EAINI	TNNEkVVVKI			
numb. <i>hsCK2α'</i> :	71	80	90	100	110	120	130	140		
<i>hsCK2α'</i>	LKPVKKKKIK	REvKILENLR	GGtNIIkLiD	tVKDPVSkTP	ALVFEyiNNT	DFKQLYQiLT	DfDIRFYMYE			
<i>hsCK2α</i>	LKPVKKKKIK	REiKILENLR	GGpNIItLaD	iVKDPVSRtP	ALVFEhvNNT	DFKQLYQtLT	DyDIRFYMYE			
numb. <i>hsCK2α'</i> :	141	150	160	170	180	190	200	210		
<i>hsCK2α'</i>	lLKALDYCHS	kGIMHRDVkP	HNVMIDHqqk	KLRLIDWGLA	EFYHPaQEYN	VRVASRYFKG	PELLVDYQMY			
<i>hsCK2α</i>	iLKALDYCHS	mGIMHRDVkP	HNVMIDHehr	KLRLIDWGLA	EFYHPgQEYN	VRVASRYFKG	PELLVDYQMY			
numb. <i>hsCK2α'</i> :	211	220	230	240	250	260	270	280		
<i>hsCK2α'</i>	DYSLDMWSLG	CMIASMIfrR	EPFFhGqDNY	DQLVRIAKVL	GTEeLYgYlk	KYhIdLDPhF	NDILGqHSRK			
<i>hsCK2α</i>	DYSLDMWSLG	CMIASMIfrk	EPFFhGhDNY	DQLVRIAKVL	GTEdLYdYid	KYnIeLDPrF	NDILGrHSRK			
numb. <i>hsCK2α'</i> :	281	290	300	310	C-terminus of 3E3B: Gln334 Cys336			350		
<i>hsCK2α'</i>	RWEnFiHSEN	rHLVSPEALD	lLDKLLRYDH	QqRLTAkeAM	EHPYFYpVVK	eQsqpcadna	vlssgltaar			
<i>hsCK2α</i>	RWErFvHSEN	qHLVSPEALD	fLDKLLRYDH	QsRLTAReAM	EHPYFYtVVK	dQarmgsssm	pggstpvrsa			
numb. <i>hsCK2α'</i> :										
<i>hsCK2α'</i>	~~~~~	~~~~~	~~~~~	~~~~~	~~~~~	~~~~~	~~~~~			
<i>hsCK2α</i>	nmmsgissv	ptpsplgpla	gspviaaanp	lgmpvpaaag	aqq					

Fig 12: Sequence alignment of CK2 α and CK2 α' . Lower case letters are used to underline non-identical position and the C-term structurally non-determined region (Reprinted from Bischoff, N. et al. ⁴⁵, Copyright (2016), with permission from Elsevier).

1.3.2.4 The CK2 β regulatory subunit

The regulatory subunit of CK2 (β_2) is a unique protein composed of a dimer of β protein linked by the strong interaction of two zinc chelating fingers motif (Fig 13). The zinc-binding motif (F106-P146) is only composed of β -sheets and loops whereas the other part of the protein also harbors α -helix.⁴⁷ Each CK2 β subunit of the dimer is able to bind to one α -subunit through an interaction with the loop (L187-H193) of the CK2 β tail (Fig 13).

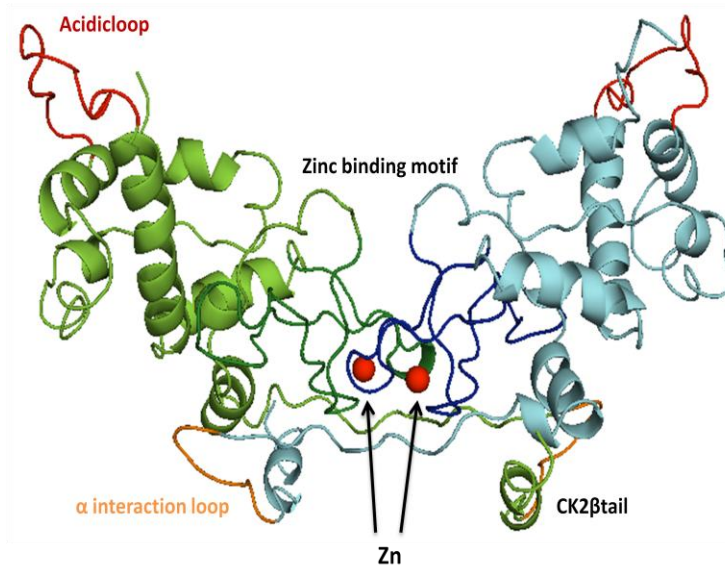


Fig 13: Schematic representation of a β -subunit dimer (1JWH).^{28,29} One β monomer is represented in green and dark green for its zinc-binding motif and the second one in blue and dark blue, respectively. The two zinc ions are represented by red spheres. Acidic loop is represented in dark red. The α -interacting loops with the two α -interaction hot-spots (Y188 and F190) are represented in orange.

The α/β interface has been well studied to understand the mode of formation of the holoenzyme and, in particular, if it is a permanent or a transient complex. The identification of α/β interaction modulators would be the Grail that will enable scientists working on protein kinase CK2 to understand the cellular role of this protein/protein interaction.

Since the first crystal structure of CK2 holoenzyme was solved,²⁸ several studies have pointed out important features of the α/β interface. The size of this interface is between 771 \AA^2 and 1099 \AA^2 , depending on the crystal structure and interface type (symmetric or asymmetric).⁴⁸ The affinity between CK2 α and CK2 β is very high, with a dissociation constant measured between 4 and 13 nM.^{48,49}

CK2 β stabilizes CK2 α as shown by the Differential Scanning Calorimetry experiment (Fig 14, A). The CK2 α melting point increased from 45.6°C to 54.7°C in presence of the β dimer. On the other side, the melting point of the β -subunit is only slightly decreased from 60.6°C to 60.2°C.⁴⁹

The interaction between the two subunits of CK2 is mainly directed by the “interaction loop” or “CK2 β tail” (L187-H193) of β -subunit and the “remote cavity” or “ α/β interaction pocket” defined by the strands β 1 to β 5 of the α -subunit (Fig 14, B and D).

In the regulatory subunit, the two hot spots responsible for a substantial part of the affinity are Tyr188 and Phe190. Thus, mutations of these residues to alanine induce a strong decrease in α/β affinity.⁵⁰ CK2 β tail is preformed to bind to CK2 α , as the conformation of the β tail is identical in the bound or unbound state (Fig 14, C).⁴⁹

In the catalytic subunit, the hot spots are Leu41 and Phe54, localized on the β 1 and β 2 strands. In the bound form, these residues are in close interaction with the β -hairpin loop of the β -subunit. The β 4/ β 5 loop is another key element of the α/β interaction and this loop can adopt different conformations, depending of the α/β interaction pocket occupancy (Fig 14, D). The β 4/ β 5 loop is closed in the absence of the β subunit but an “open” conformation was observed in presence of the β subunit^{28,48} or in presence of a cyclic peptide that mimics the β tail.⁵¹

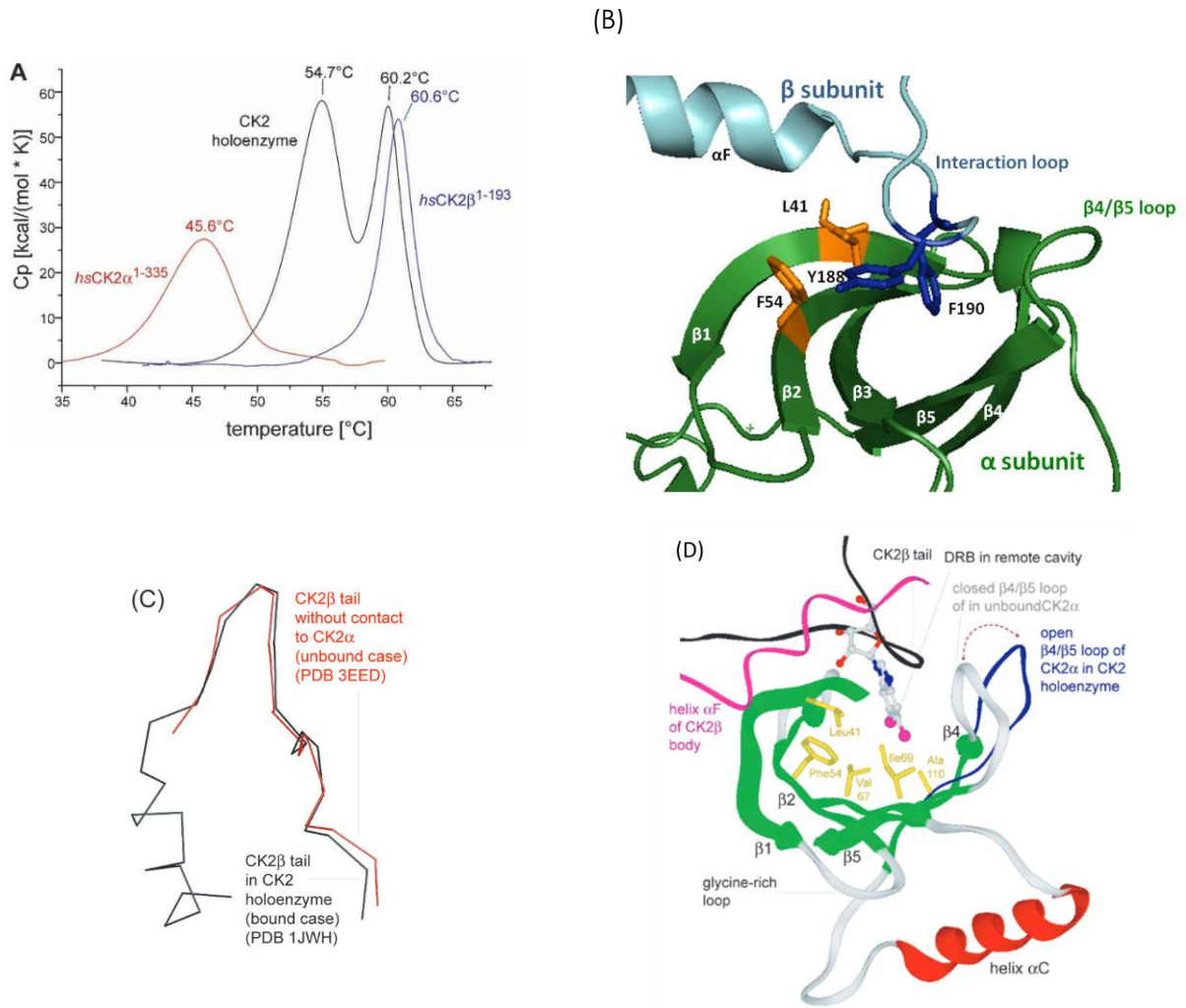


Fig 14: Key elements of the CK2 α/β interaction. (A) DSC curves of $hsCK2\alpha^{1-335}$ (red), $hsCK2\beta^{1-193}$ (blue), and the corresponding holoenzyme (black) (From Raaf, J. *et al.*⁴⁹, with the permission of John Wiley and Sons). (B) Structural overview of the α/β interface. CK2 α is represented in green and the hot spots (L41 and F54) in orange. CK2 β is colored in blue and the two hot spots (Y188 and F190) in dark blue (based on 4DGL⁵²) (C) Superposition of the CK2 β tail bound or unbound to CK2 α (From Niefind, K. *et al.*³¹, with permission of Springer). (D) Structural overview of the α/β interaction with a focus on the two conformations of the $\beta4/\beta5$ loop (From Niefind, K. *et al.*³¹, with permission of Springer).

1.3.3 CK2 implication in pathophysiology

1.3.3.1 CK2 α overexpression in cancers

As a multifunctional/multi-substrates enzyme, CK2 occupied a central position in cell signaling. Therefore, CK2 role in cancer development has been extensively investigated. The expression level and activity of CK2 have been widely studied in diverse tumor types and it has been determined that CK2 is globally a marker of poor survival prognosis for patients.

Indeed, in 2004, CK2 α overexpression has been shown to be a marker of poor prognosis in squamous cell carcinoma of the lungs. A survey on 16 patients shown that after 90 months, only 10% of patients with a high CK2 α level survive whereas 50% of patients with a normal CK2 α expression were alive (Fig 15, A).⁵³

In 2007, a survey on 131 patients with prostate cancer has shown that CK2 α is overexpressed in prostate cancer cells in comparison with normal prostate cells. Moreover, nuclear localization of CK2 α is correlated with high-grade tumors and poor prognostic factors.⁵⁴

The same year, a second implication of CK2 α was found in Acute Myeloid Leukemia (AML) as a survey on 48 patients has shown that CK2 α overexpression is correlated with a poor survival prognosis (Fig 15, B).⁵⁵

In 2010, CK2 α expression was studied in breast carcinoma and revealed that CK2 α is individually a poor prognosis marker. Moreover, CK2 α was chosen together 11 other markers to bring an accurate classification for 86% of the tumors on 905 patients.⁵⁶

In 2011, overexpression of CK2 α in nuclei of colorectal tumor tissues have been correlated to bad prognosis for patients and as an independent prognostic marker for human colorectal cancer (Fig 15, C).⁵⁷

In 2013, the analysis of 537 glioblastomas has demonstrated that CSNK2A1 gene encoding CK2 α was overexpressed in 33.7% of glioblastomas and even in more than 50% of classical glioblastomas whereas CK2 α ' expression was not changed. Only a slight modification was observed in CK2 β expression (7.3% of gene deletion). Moreover, downregulation of CK2 α , by siRNA or inhibitors, counteracted glioblastoma development.⁵⁸

In 2014, 187 patients with gastric carcinoma were studied and CK2 α expression was a marker of survival prognosis (Fig 15, D). CK2 α was involved in phosphorylation of DBC1 and the inhibition of both CK2 α and DBC1 decreased proliferation of cancer cells.⁵⁹

In 2015, a small cohort study revealed that CK2 α was upregulated in Renal Cell Carcinoma tumor samples. Moreover, 786-O cells were used as model of RCC and CK2 inhibition by CX-4945 treatment underlined the potential of CK2 as a target to cure RCCs.⁶⁰

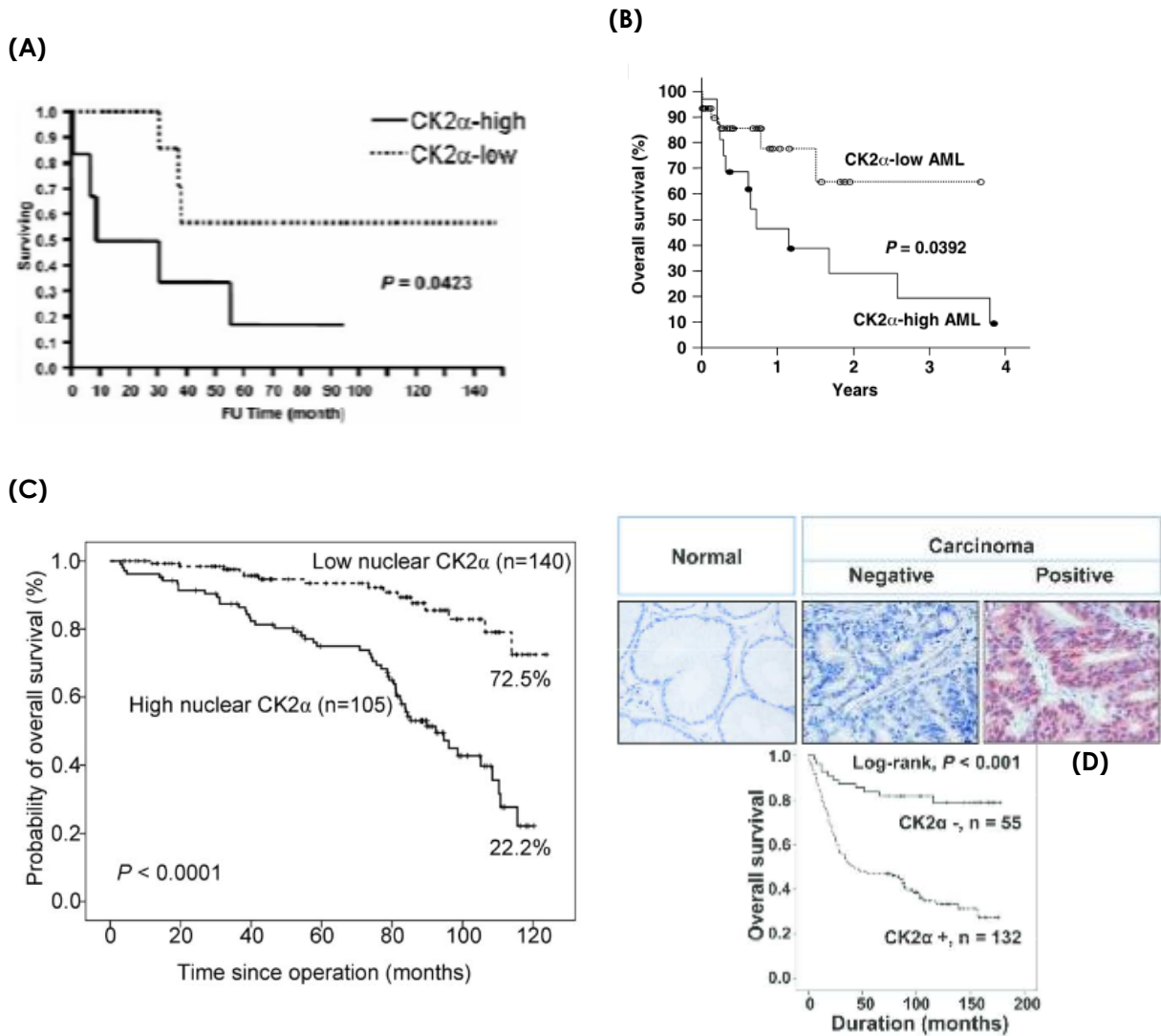


Fig 15: Clinical implication of the protein kinase CK2. (A) Survival rate in function of the expression level of CK2 α in squamous cell carcinoma (Reprinted from O-charoenrat, P. *et al.*⁵³, with permission from AACR). (B) Survival rate of patient with Acute Myeloid Leukemia (AML) depending of their CK2 α expression level (Reprinted from Kim, J. S. *et al.*⁵⁵, with permission from AACR). (C) Survival analysis of patients with human colorectal cancer. Low nuclear CK2 α means labeling index $\leq 40\%$ for nuclear CK2 α by immunoreactivity and high nuclear CK2 α means $>40\%$ (From Lin, K.-Y. *et al.*⁵⁷, with the permission of John Wiley and Sons). (D) Implication of CK2 α in gastric carcinoma, immunohistochemical expression of CK2 α in normal tissue, low and high

CK2 α gastric carcinoma and patient survival depending of the expression level of CK2 α (From Bae, J. S. et al.⁵⁹, with the permission of John Wiley and Sons).

1.3.3.2 CK2 α implication in cell signaling

The correlation between CK2 α overexpression and prognosis in a large number of cancers is in relation with the multiple consequences of this overexpression in cells (Fig 16).⁶¹

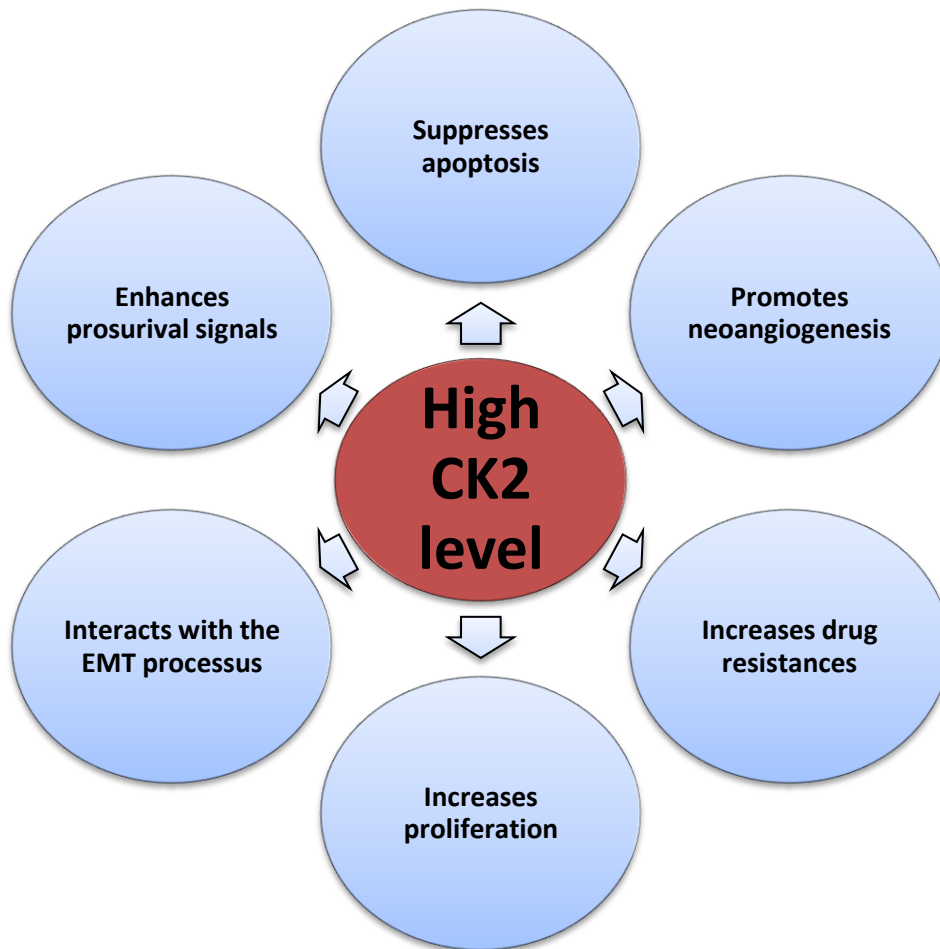


Fig 16: Consequences of a high CK2 expression.

CK2 α overexpression induces favorable conditions for tumor development by acting on several cell signaling pathways implicated in cancer.

CK2 is involved in the regulation of NF- κ B pathway at multiple levels. CK2 phosphorylates I κ B leading to its degradation and the release of NF- κ B.⁶² Moreover, CK2 can directly

phosphorylate NF- κ B p65 subunit, inducing the augmentation of the transcriptional activity of NF- κ B *in vivo*.^{63,64}

CK2 is able to promote the Wnt signaling by several actions. CK2 phosphorylates Disheveled (Dvl), β -catenin on Thr393 and LEF-1 on Ser42 and Ser61. These events lead to the stabilization of β -catenin and to the promotion of β -catenin/LEF-1 complex formation (Fig 17, B).^{61,62} In parallel, CK2 phosphorylates α -catenin (Ser641), thus destabilizing the α -catenin/ β -catenin complex that inhibits β -catenin. Therefore, CK2 favors the transcription of survival genes.⁶⁵

CK2 activates the PI3K/Akt pathway by a direct phosphorylation of Akt in position Ser129 and Ser473. Moreover, CK2 also acts upstream by a negative control on PTEN, which is a natural blocker of the PI3K/Akt pathway. Laterally, CK2 enhances the protection of Akt by HSP90 activation/stimulation. Thus, CK2 favors survival signals.⁶¹

Consequently, CK2 inhibition has been proved to be a valuable way to treat cancer cells. Indeed, CK2 acts as a major support to prosurvival and antiapoptotic signals by acting on the NF- κ B, Wnt and Akt pathway (Fig 17). CK2 is not directly involved in these pathways but acts as a side regulator through activation or inhibition of key enzymes.⁶⁶

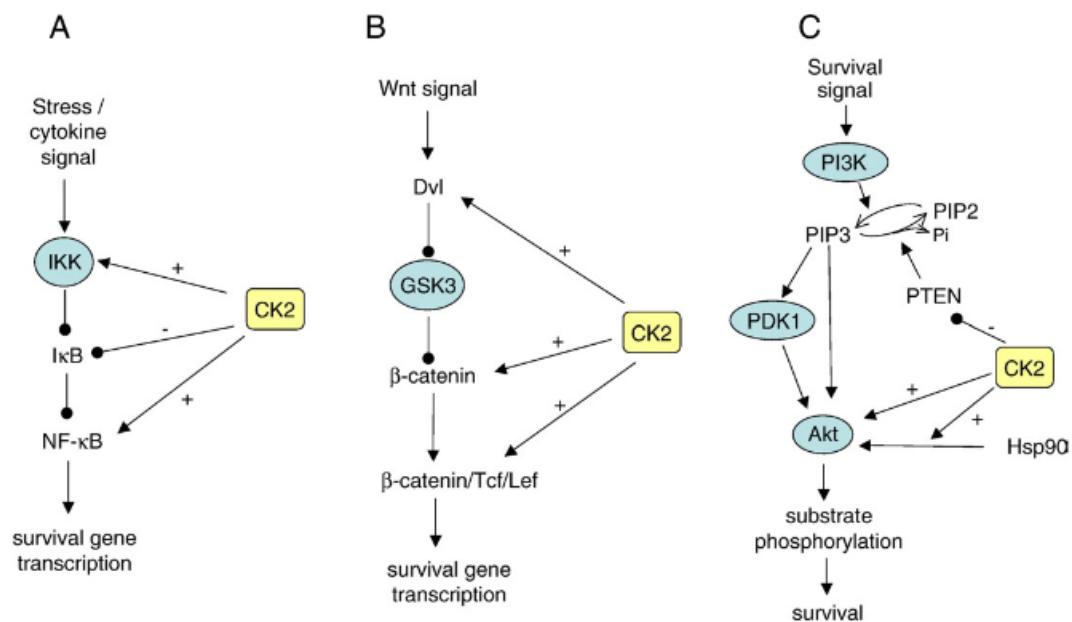


Fig 17: Role of CK2 in regulation of NF- κ B (A), β -catenin (B) and Akt (C) signaling (Reprinted from Ruzzene, M. *et al.*⁶⁶, Copyright (2016), with permission from Elsevier).

In addition, CK2 is involved in the multidrug resistance phenomenon.⁶⁷ CK2 inhibition has been demonstrated to be efficient to restore sensitivity toward imatinib of imatinib-resistant LAMA84 cells⁶⁸, as well to induce apoptosis in various drug resistant cell lines.⁶⁹ Moreover, a large-scale proteomic study on the phosphorylation stoichiometries in lung cancer cells and gefitinib-resistant lung cancer cells has recently demonstrated that CK2 and EGFR are the two kinases with wider implication in drug resistance pathway.⁷⁰ Thus, CK2 appears to be an interesting target to counteract drug resistance phenomena.

1.3.3.3 Functional role of CK2 β

CK2 β knockout experiments have been used to determine the role of the regulatory subunit in different models.

In *Saccharomyces cerevisiae*, the knockout of one or the two different regulatory subunits (CK2 β 1 and CK2 β 2) induces only salt sensitivity and a partial blockage in the adaptation to the G₂/M checkpoint arrest but no difference in growth or viability was observed, so showing that yeasts can survive in the absence of CK2 β .^{71,72}

CK2 β deletion in mice leads to early embryonic lethality, leading to mutant embryos with a reduced size. A decrease in cells proliferation was observed but not in apoptosis markers. Thus, in contrast to yeast, mammals require a normal level of CK2 β to survive.⁷³ Moreover, conditional CK2 β knockout in embryonic central nervous system led to defects in proliferation and differentiation, the latter underlining the major role of CK2 β in central nervous system development.⁷⁴

CK2 β deletion in mammary epithelial cells (MCF10A) leads to phenotypic changes. Indeed MCF10A epithelial cells transfection with siRNA targeting CSNK2B gene induces a mesenchymal phenotypes. Immunofluorescence images have shown a decrease in E-Cadherin expression, an increase in the N-Cadherin level and a reorganization of the actin filaments. These observations are characteristics of an increase in cell mobility (Fig 18).^{75,76}

Moreover, unbalanced level of CK2 subunits (lower expression level of β -subunit) in breast tumour samples has been correlated with EMT markers such as decrease in E-Cadherin and Occludin expression and increase in N-Cadherin, Vimentin, α SMA and Snail1 expression.⁷⁶

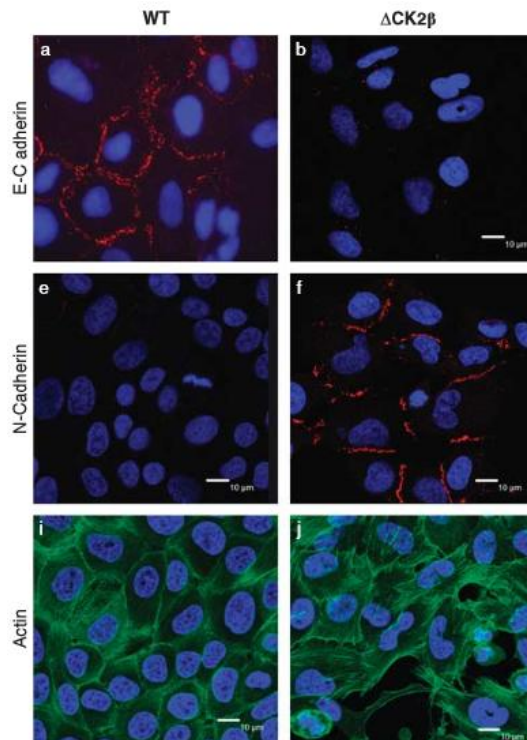


Fig 18: Immunofluorescence images of MCF10A WT and Δ CK2 β with E-Cadherin, N-Cadherin or Phalloidin antibodies in combination with Hoechst-33342 (Reprinted by permission from Macmillan Publishers Ltd: [Oncogene] from Deshieri, A. *et al.*⁷⁶, copyright (2016)).

Biochemical approaches have been used to identify proteins interacting with CK2 β . CK2 β partners could be classified in two categories:

- CK2 α dependent partners which bind specifically to CK2 β ,
- CK2 α independent partners which bind specifically to CK2 β only when CK2 α is not bound to the regulatory subunit.

Several CK2 α dependent binding partners of CK2 β were characterized, some of them only *in vitro* such as p90^{Rsk}, PKC ζ , topoisomerase II, p27^{KIP1}, CD5, FGF-2, Nopp 140 and L41 but few of them were also characterized as CK2 β binding partners *in vivo* (Table 2). Interestingly, four serine/threonine kinases, c-Mos, Chk1, A-Raf and AMPK α 2 were characterized as CK2 α independent binding partners of CK2 β . The β -subunit binding site on these kinases is localized in the same area than on CK2 α . Moreover CK2 β is able to modulate their activity like the one of CK2 α .⁷⁷ As a remark, activation of AMPK α 2 by CK2 β suppressed EMT.⁷⁸

Table 2: *In vivo* CK2 β binding partners.

Interaction partner	Function	Reference
CK2α dependent binding partners of CK2β		
p53	Tumor supressor	79-81
p21 ^{WAF1/CIP1}	CDK inhibitor	81,82
Cdc25B	Phosphatase, CDK activator	83
L5	Ribosomal protein	81,84
HHV-6IE2	Human herpesvirus 6 immediate-early protein	85
CK2α independent binding partners of CK2β		
c-Mos	Serine/Threonine protein kinase, MAPK activation	81,86,87
Chk1	Serine/Threonine protein kinase, regulator of DNA damage, induced G2 arrest	88
A-Raf	Serine/Threonine protein kinase, mitogenic signaling, cell proliferation	81,84,89
AMPK α 2	AMP-activated protein kinase, heterotrimeric serine/threonine kinase, cellular energy homeostasis, EMT	78

A possible consequence of the multiple interactome of CK2 β is proposed in Fig 19. If the amount of CK2 α (or/and CK2 α') in one cell compartment is equal or higher to the quantity of CK2 β , the holoenzyme form ($\alpha_2\beta_2$) is predominant and CK2 mainly interacts with proteins that could bind to the holoenzyme form. In the contrary, if the regulatory subunit is present in excess, free β dimer could bind to other kinases such as c-Mos, Chk1, A-Raf and regulate them (Fig 19, b), or to other proteins such as p53, p21, p27 (Fig 19, c)... In consequence, the equilibrium between CK2 α and CK2 β expression has to be very well controlled in subcellular compartments and any dysregulation may lead to dramatical alteration in cell signaling pathways.⁹⁰

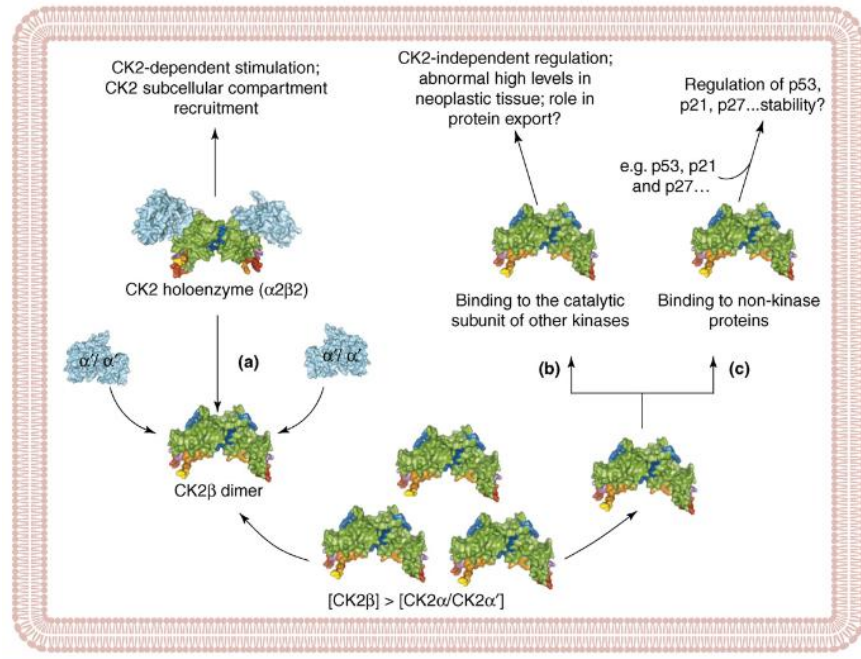


Fig 19: Possible mechanisms of cell signaling modulation by CK2 as a function of CK2β expression (Reprinted from Bolanos-Garcia, V. M. *et al.*⁹⁰, Copyright (2016), with permission from Elsevier). (a) In the presence of an excess of CK2β, CK2 is preferentially in the holoenzyme form and interacts with holoenzyme's substrate. (b) Free CK2β could interact and modulate other kinases (such as c-Mos, A-Raf, Chk1...) in the same way than for CK2α. (c) CK2β could bind to other proteins independently of CK2α and maybe modulates them by activation/inactivation, stabilization...

1.3.4 Known CK2 inhibitors

For a long time, CK2 was considered as an “undruggable kinase”.⁹¹ Indeed, despite the long period since the discovery of CK2 in 1954²³, its full characterization in 80s and the first x-ray structure of CK2 solved in 1998³⁰, only one potent ATP competitive inhibitor, CX-4945, underwent clinical trials.⁹²

Various chemical structures have been identified as CK2 inhibitors, through various approaches⁹³⁻⁹⁶ and the majority of them could be classified in several general families (Fig 20):

- Benzimidazole derivatives including TBB, TBI and DMAT,
- Anthraquinone derivatives based on the natural product emodin,
- Coumarin derivatives such as ellagic acid,
- Indolo-quinazoline derivatives such as IQA,
- Benzo-naphthyridine derivatives, with CX-4945 in phase II clinical trial,
- Atypical inhibitors such as GIGB-300 (also in clinical trials), POMs, azonaphthalenes, peptide-like α/β interaction inhibitors and bi-substrate inhibitors.

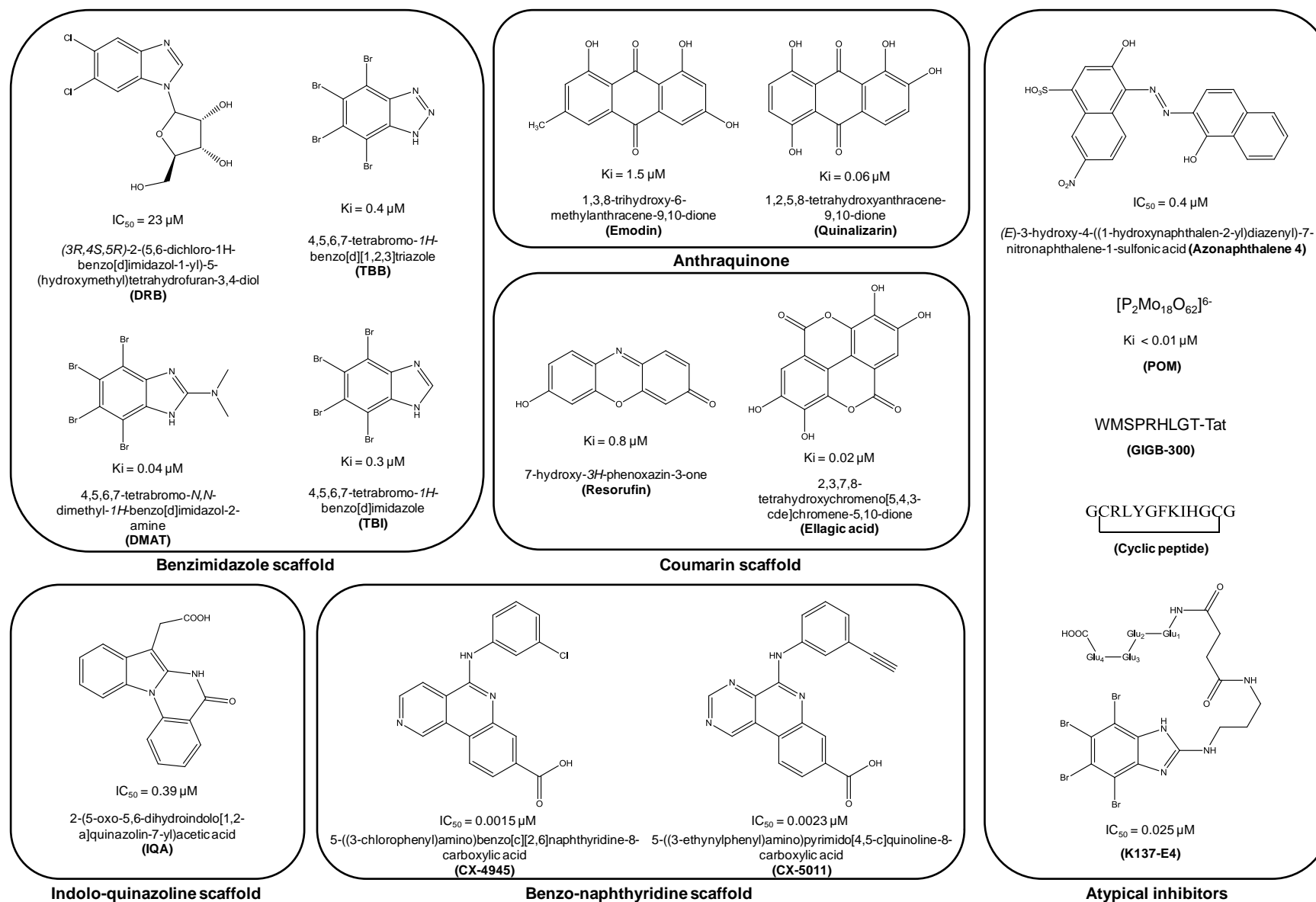


Fig 20: Selected examples of CK2a modulators based on their chemical scaffold or mechanism of action.

The following discussion will focus on CX-4945, which is the most developed CK2 inhibitor and some of the atypical inhibitors will be discussed in paragraph 1.4.4 and 1.5.4.

1.3.4.1 CX-4945 and *in vitro* selectivity

CX-4945 is the prototype of CK2 inhibitor and is in clinical Phase II for the treatment of several cancers. This molecule, developed by Cylene Pharmaceuticals®, belongs to the family of benzo-naphthyridine. It is a very potent inhibitor of CK2 ($IC_{50} = 14.7$ nM) and one of the most selective.⁹⁷ Indeed, CX-4945 has a Gini coefficient⁹⁸ of 0.667 on a panel of 235 protein kinases. In comparison, other CK2 inhibitors have lower Gini coefficient, 0.612 for quinalizarin, 0.60 for TBCA, and even lower than 0.4 for TBB, DMAT or TIBI (Table 3).⁹⁷

However, an off-target inhibitory activity of Cdc2-like kinases (Clks) was recently reported for CX-4945.⁹⁹ The Clk family of kinases is involved in the regulation of alternative splicing through the phosphorylation of serine/arginine rich (SR) proteins: CX-4945 is actually more potent on Clk-2 ($IC_{50} = 3.8$ nM) than on CK2 α ($IC_{50} = 14.7$ nM). Furthermore, CX-4945 causes the inhibition of cellular SR protein phosphorylations at low micromolar concentrations in a CK2 independent manner.⁹⁹ Although the consequences of this off-target remain to be clearly understood, this recent result underlines the fact that potent and selective CK2 α inhibitors are difficult to obtain through targeting the ATP binding pocket. Another study describes several CX-4945 off-targets with the respective IC_{50} of 1 nM on CK2 α and CK2 α' , 17 nM on DAPK3, 35 nM on FLT3 and on TBK1, 41 nM on Clk3, 45 nM on HIPK3, 46 nM on Pim-1 and 56 nM on CDK1/cyclinB.⁹²

Table 3: Selectivity of CK2 inhibitors expressed with Gini coefficients in comparison with some approved kinase inhibitors.⁹⁸

Target	Inhibitor	Number of PK tested	Gini coefficient
CK2α	CX-4945 (0.5 μ M) ¹⁰⁰	102	0.62
	CX-4945 (0.5 μ M) ¹⁰⁰	235	0.67
	Quinalizarin (1 μ M) ¹⁰¹	78	0.62
	TBCA (0.5 μ M) ¹⁰²	300	0.60
	TBB (10 μ M) ¹⁰³	70	0.38
	DMAT (10 μ M) ¹⁰³	70	0.34
	TBI (10 μ M) ¹⁰³	70	0.31
Bcr-Abl	Imatinib (0.5 μ M) ¹⁰²	300	0.77
Bcr-Abl	Dasatinib (0.5 μ M) ¹⁰²	300	0.74
PDGFR/VEGFR	Sunitinib (0.5 μ M) ¹⁰²	300	0.52

1.3.4.2 Cellular effects of CX-4945

CX-4945 induces cell death in various cell lines with an average EC₅₀ of 5.5 μ M in 43 cell lines originated from different cancers (Fig 21). Moreover, extensive studies in breast cancer cell lines have shown an apparent correlation between the efficacy of CX-4945 and the level of CK2 α expression. Cell lines with a higher level of CK2 α (mRNA and protein) are more sensitive toward CX-4945;⁹² this last point underlined the importance of CK2 α inhibition to treat cancers that are dependent on abnormal high CK2 α level.

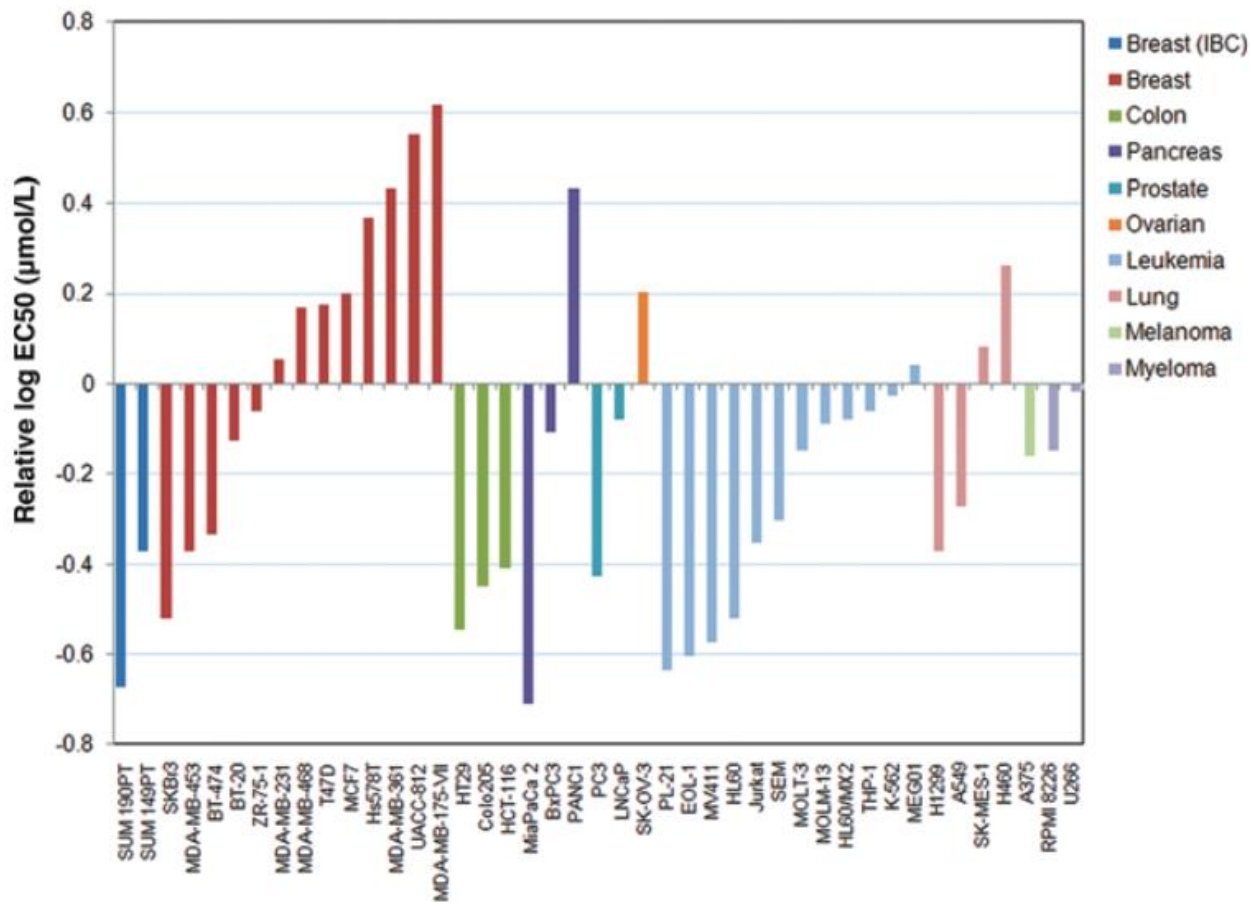


Fig 21: Cell viability assay results on a panel of 43 cancer cell lines. The baseline represents the average EC₅₀ (5.5 µM), cell lines with a negative logEC₅₀ are more sensitive than average, and positive less sensitive (Reprinted from Siddiqui-Jain, A. *et al.*⁹², with permission from AACR).

CX-4945 inhibits CK2 activity in various cell lines in the micromolar range. A decrease of Akt phosphorylation (Ser129, specific to CK2) was observed. Moreover, CX-4945 induces a decrease in phosphorylation of p21(Thr145), PTEN (Ser370 and Ser380) but at a concentration about 10-fold higher.^{69,92,104}

Xenograft model experiments were conducted and showed CX-4945 efficiency to induce breast and pancreatic tumor regression without any weight loss for mice (Fig 22).

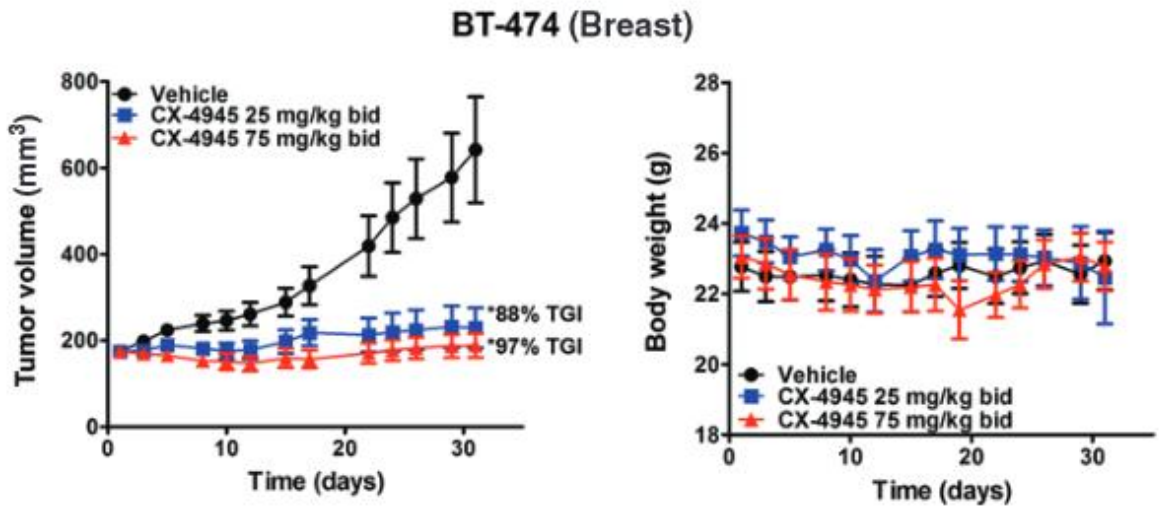
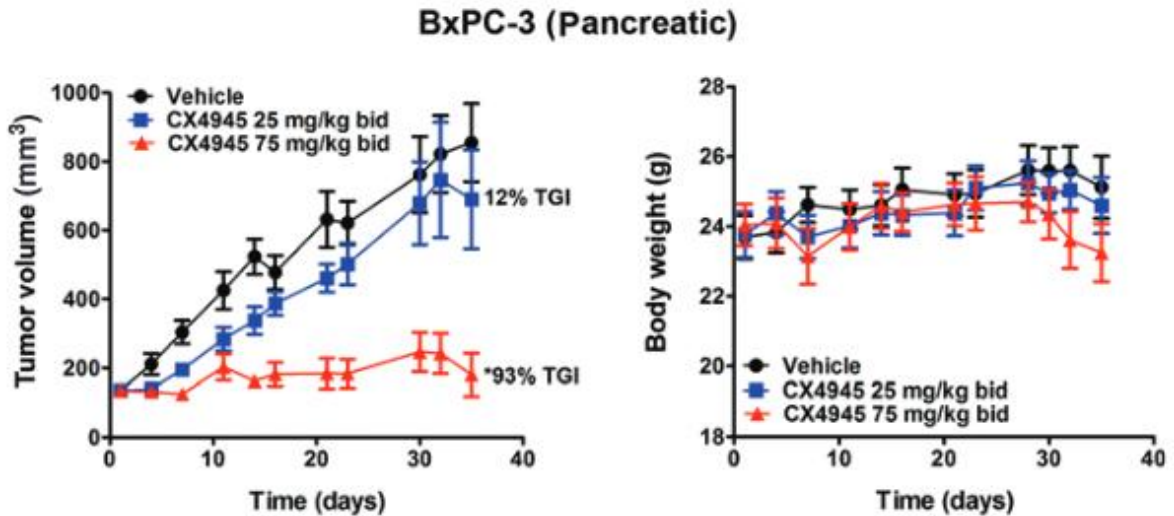
A**B**

Fig 22: Effect of CX-4945 in BT-474 (A) and BxPC-3 (B) xenograft models. CX-4945 or Sodium Phosphate Buffer (vehicle) were administrated by oral gavage twice a day (Reprinted from Siddiqui-Jain, A. *et al.*⁹², with permission from AACR).

Recently, a study dealing with human head and neck squamous cell carcinomas revealed a possible resistance mechanism to CX-4945 treatment, both in cellular-based assay and in xenograft models. Resistance to CX-4945 involved an increase in the reporter gene activity of p21, p53, AP-1 and IL-8, as well as an increase of Ki67. The resistance is, of note, clearly dependent on the cell lines.¹⁰⁵

To date, CX-4945 remains the most promising CK2 inhibitor efficient *in vitro*, in cell-based assay and *in vivo*. Nevertheless, the recently described off-targets (Clk, for example) and resistance pathways could be a serious drawback in clinical development. Notwithstanding, CX-

4945 validates CK2 as a target of interest to treat several cancer types. Consequently, new potent and more selective CK2 inhibitors are still required to make CK2 inhibition a success story in cancer treatment.

1.3.4.3 Overview of CK2 inhibitors binding sites

The major part of the described CK2 modulators bind to the ATP cleft (Fig 23) but several compounds have been characterized as non-ATP competitive modulators of CK2 and they can be classified in four groups:

- Allosteric inhibitors of CK2 α including azonaphthalene class of compounds, POMs, CFTR fragment peptide...
- α/β interaction inhibitors which are Protein Protein Interaction Inhibitors (PP2I) more than kinase inhibitors. This group includes DRB (5,6-dichlorobenzimidazole 1- β -D-ribofuranoside) and a cyclic peptide (Pc) derived from the C-terminal tail of CK2 β .
- Substrate inhibitors represented by one small peptide named CIGB-300, nowadays in phase II clinical trials. CIGB-300 does not interact directly with CK2 but with its substrates. Indeed, this small peptide is able to bind selectively to a CK2 phosphorylation site of CK2 substrate, thus preventing CK2 phosphorylation *in vitro*. The main target of CIGB-300 *in vivo* is B23/nucleophosmin.¹⁰⁶⁻¹⁰⁸
- The last class aim to develop a dual site inhibitor, by coupling TBBi to an amino-acid sequence rich in aspartate residues. This molecule is able to bind simultaneously in the ATP pocket and in the substrate binding site, as shown by a very high affinity for CK2 ($K_i = 0.5$ nM).¹⁰⁹

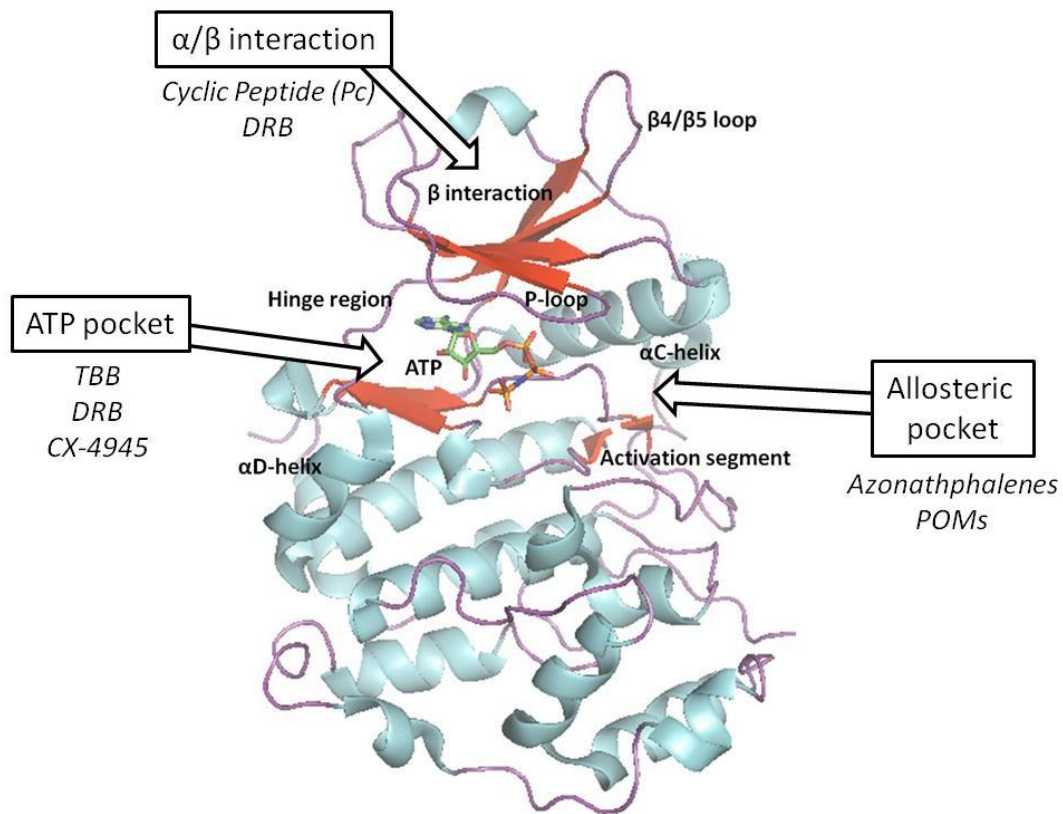


Fig 23: Schematic representation of the different inhibitors binding sites on CK2 α structure (based on 2PVR cristallographic file¹¹⁰).

1.4 Allostery and non-ATP competitive inhibitors

1.4.1 Allostery definition

The word "allosteric" was first described in 1961, after the 26th Cold Spring Harbor Symposium on Quantitative Biology dedicated to "cellular regulatory mechanisms". The word allosteric was used in the report of this conference by Monod and Jacob.¹¹¹ This statement followed years of research on feedback inhibition of biosynthetic pathway in bacteria by the end product of the synthetic chain¹¹²⁻¹¹⁵ and on the hemoglobin subunit cooperation to bind oxygen molecules. These two authors proposed to call "allosteric inhibition" the phenomenon of end-product inhibition "where the inhibitor is not a steric analogue of the substrate": they guessed that this statement implied a different binding site.

Following this seminal research, the first model describing the allostery concept was proposed in 1965 and was called Monod-Wyman-Changeux (MWC) by the name of its inventors.¹¹⁶ The MWC model tried to define the main criteria of allosteric inhibition in multimeric proteins. A part of the new concepts focused on the change of protein conformation that induced the inhibition. They supposed that the protein could exist in both active and inactive form and that an allosteric inhibitor favors the inactive conformation whereas the natural substrate favors the active conformation.¹¹⁷ One year later, a second model was proposed by Koshland, Nemethy and Filmer (KNF model). The major difference with the MWC model is that monomers of the oligomer structure are not connected to each other and so, each monomer could have a different conformation. The binding of one ligand induced a conformational modification favorable to the binding of the ligand in the adjacent subunit.¹¹⁸ In 1984, the first model describing allosteric regulation without conformational change was proposed by Cooper and Dryden.¹¹⁹

Allosteric regulations of proteins are very interesting, due to the opportunity to modulate with increased selectivity previously targeted enzyme and to target some of the previously "non-druggable" proteins. This last point is very similar to what researchers try to achieve with Protein-Protein Interactions Inhibitors (PP2Is), as they wish to bring new targets in drug discovery.¹²⁰

1.4.2 Kinase inhibitor classes and allostery

The first kinase inhibitors were ATP-competitive. They targeted the canonical ATP cleft but soon, the poor selectivity of these inhibitors was discovered (eg for staurosporine). Indeed, a good selectivity is very difficult to achieve through ATP-site targeting because of the numerous proteins that binds ATP molecules. On the other hand, high potency was obtained with ATP competitive inhibitors because of the easy targeting of the large hydrophobic ATP pocket. In addition, by exploiting specific features, several well potent and selective ATP-competitive inhibitors are already in clinical use, such as imatinib (Bcr-Abl)¹²¹, gefitinib (EGFR)¹²², sunitinib (VEGFR, PDGFR)¹²³ or dabrafenib (B-Raf)¹²⁴. To efficiently target some refractory kinases, allosteric inhibitors were considered and several out-of-the-box inhibitors were identified and will be discussed thereafter.

Researchers defined four categories (Fig 24) to classify the different kinase inhibitors, depending on their mechanisms of action:

- ✓ Type I: ATP-competitive inhibitors that strictly bind into the ATP pocket and maintain the kinase in an active conformation but prevent the ATP-Mg complex binding are defined as class I inhibitor. Staurosporine and dasatinib are two examples of this class.
- ✓ Type II: encompass the inhibitors that bind to the ATP cleft and simultaneously to a hydrophobic pocket located between the DFG motif in the "out" position and the α C-helix. The binding to this double pocket enable a greater selectivity. Imatinib and sorafenib are type II inhibitors. Recently, a new special class named 1/2 was added for the molecules that bind to the same pockets than type II inhibitors but with the DFG in the "in" position.
- ✓ Type III: inhibitors that do not compete with ATP and bind to a true allosteric pocket, inducing an inactive conformation. Most of them act through α C-helix displacement or by locking the DFG motif in an inactive conformation.
- ✓ Type IV: compounds that are also "type III-like" allosteric inhibitors but which bind to a pocket distant from the ATP cleft.

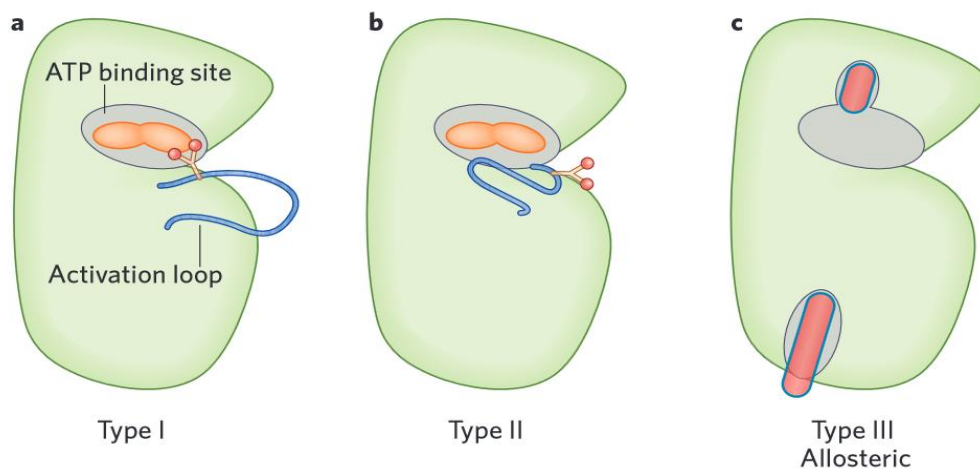


Fig 24: Schematic representation of kinase inhibitor types (Reprinted by permission from Macmillan Publishers Ltd: [Nat. Chem. Biol.] from Foda, Z. H. *et al.*¹²⁵, copyright (2016). (A) Type I: small molecule (orange) binds to ATP pocket (grey) with the DFG motif on the activation loop (blue) in the “in” position. (B) Type II: small molecule binds to the ATP pocket but with the DFG motif in the “out” position. (C) Type III (and IV): allosteric inhibitor (red) binds in a different pocket near the ATP pocket or far from it.

1.4.3 Examples of non-ATP competitive inhibitors of protein kinases

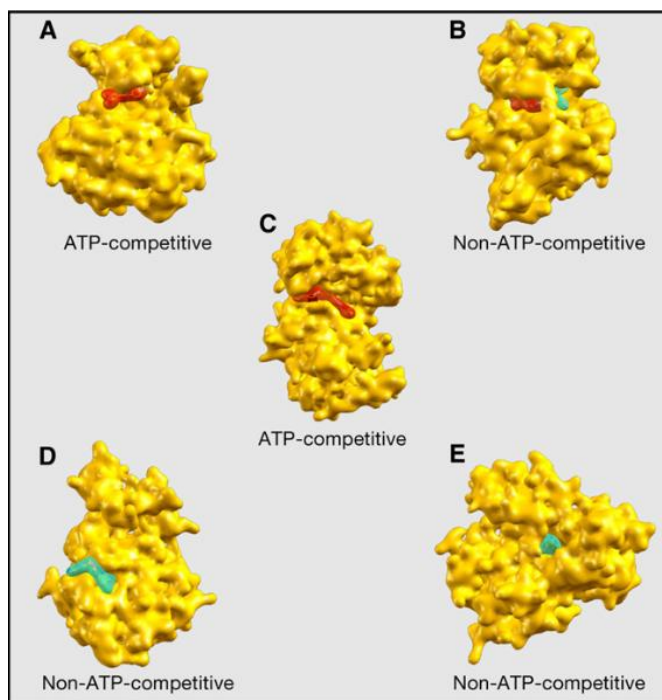


Fig 25: Few examples of kinase inhibitors in their binding sites (Reprinted from Nussinov, R. *et al.* ¹²⁶, Copyright (2016), with permission from Elsevier). (A) Orthosteric inhibitor (Gefitinib in red) bound to active EGFR kinase (PDB ID: 3UG2). (B) Allosteric inhibitor (PD318088 in cyan) and ATP (in red) bound to inactive MEK1 (PDB ID: 1S9I). (C) ATP competitive inhibitor (imatinib in red) bound to inactive p38 (PDB ID: 3HEC). (D) Allosteric inhibitor (in red) bound to CHK1 (PDB ID: 3JVR). (E) Allosteric inhibitor bound to the interface of Akt and PH domain (PDB ID: 3O96).

1.4.3.1 ANS pocket

Cyclin-Dependent Kinases (CDKs) are key regulators of the cell cycle and they are deregulated in numerous pathologies. Despite numerous efforts to find good CDK inhibitors, and several of these molecules that underwent into clinical trials, research groups did not succeed to develop an efficient compound. All of the developed molecules were ATP-competitive inhibitors and one of their major drawbacks was their selectivity. Recently, a new pocket was identified on CDK2 and named ANS pocket, as this compound (8-anilino-1-naphthalene sulfonate) was the only molecule described to bind into this pocket.

ANS is a commonly used fluorescent probe. In the process of searching for new compounds able to compete with cyclins for CDK2 binding, Betzi *et al.* have set up an assay based on ANS displacement. They realized later that ANS specifically binds to CDK2 with a K_d of $37 \mu\text{M}$ and X-ray structures revealed a specific pocket able to bind two ANS molecules (Fig 26). ANS inhibits CDK2 through αC -helix displacement, thus locking the inactive state of CDK2.^{127,128}

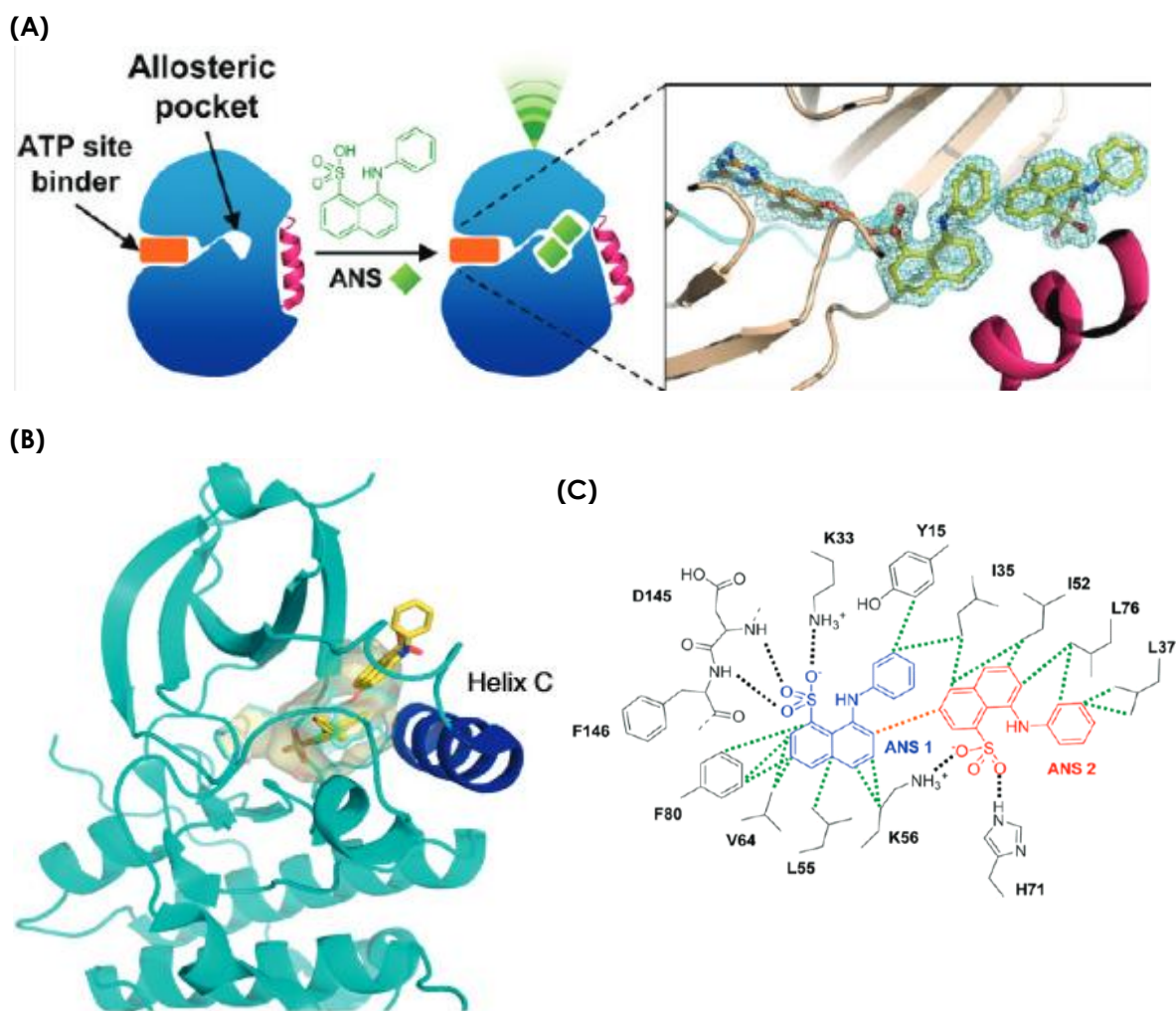


Fig 26: ANS pocket in CDK2. (A) Schematic representation of the ANS pocket without or in presence of the two ANS molecules. A small ATP competitive compound can bind in the same time than ANS without any competition (Reprinted with permission from Betzi, S. *et al.*¹²⁸, Copyright (2016) American Chemical Society). (B) CDK2 X-ray structure with two ANS molecules bound (PDB ID: 3PXF) (Reprinted from Palmieri, L. *et al.*¹²⁹, Copyright (2016), with permission from Elsevier). (C) Schematic representation of the ANS interactions into their binding sites in CDK2 (Reprinted with permission from Betzi, S. *et al.*¹²⁸, Copyright (2016) American Chemical Society).

1.4.3.2 PIF pocket

The AGC protein kinase family is one of the most evolutionary conserved groups that represents 12% of human kinome (61 kinases and 2 pseudo kinases).¹³⁰ The C-terminal segment of AGC kinases presents a unique hydrophobic motif which fold back in a hydrophobic pocket localized between $\beta 4$, $\beta 5$ loop and α -B-, α -C-helix. This pocket, named PIF pocket, played a central role in AGC protein kinases regulation (Fig 27, A).¹³¹ Despite the general presence of the PIF pocket in AGC kinases, PDK1 is the kinase in which the PIF pocket has the most crucial role. Indeed, in PDK1, binding of the C-terminal segment does not only turn on/off the kinase activity but modulates the protein kinase substrate selection.

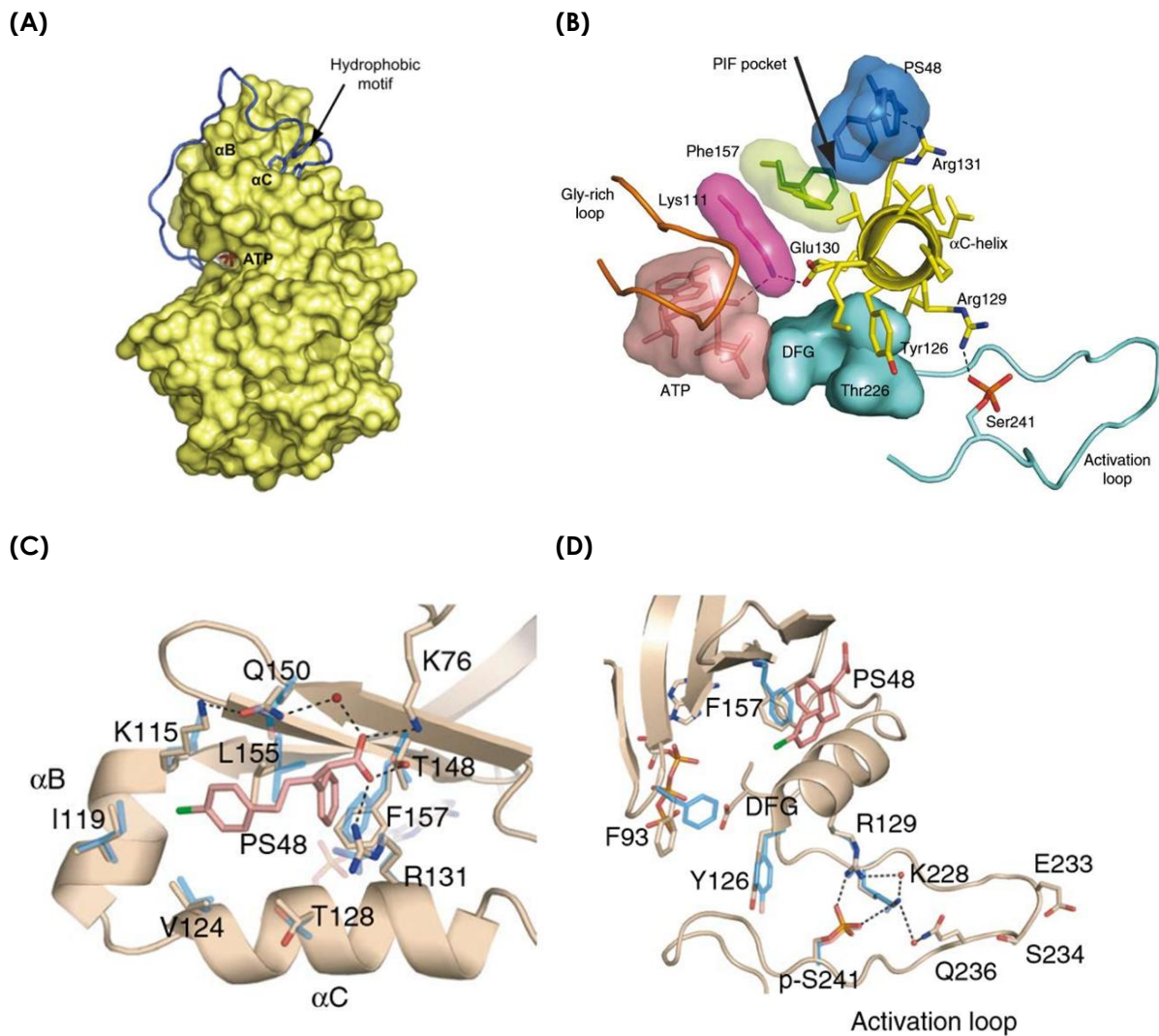


Fig 27: PIF pocket in PDK1. (A) General X-ray structure of AGC kinases (from PKA, PDB ID: 1ATP) with the C-terminal extension in blue and the two hydrophobic residues bound to the PIF pocket

(Reprinted from Arencibia, J. M. *et al.*¹³⁰, Copyright (2016), with permission from Elsevier). (B) General view of the α C-helix central role between the active site, the PIF pocket of PDK1 and the activation loop (Reprinted by permission from Macmillan Publishers Ltd: [Nat. Chem. Biol.], From Hindie, V. *et al.*¹³², copyright (2016)). (C) and (D) Superimposition of PDK1-ATP (blue) and PDK1-ATP-PS48 (off-white) showing key interacting amino-acids (Reprinted by permission from Macmillan Publishers Ltd: [Nat. Chem. Biol.], From Hindie, V. *et al.*¹³², copyright (2016)).

The crucial role of the PIF pocket in PDK1 makes it a promising target for therapeutic drugs. 2-(3-Oxo-1,3-diphenylpropyl)malonic acid and its derivatives were identified as small molecules targeting the PIF pocket of PDK1. They act as *in vitro* activators of PDK1 and selective substrate inhibitors in cell assays.^{133–135} These molecules selectively bind to the hydrophobic pocket localized behind the α C-helix and stabilize key residues implicated in kinase activity (Fig 27).

The PIF pocket is also present in PKC ζ and 4-benzimidazolyl-3-(4-chloro-phenyl)butanoic acid family of compounds targets this pocket. Compounds of this class are allosteric inhibitors of PKC ζ with a very good selectivity whereas they are weak activator of PDK1.¹³⁶

1.4.3.3 Akt pocket

Another member of the AGC group has interesting features for allosteric inhibition, the protein kinase Akt (also named Protein Kinase B, PKB). Akt plays a key role in survival and proliferation regulation. All three human isoforms (Akt1, Akt2 and Akt3) of Akt share an N-terminal Pleckstrin Homology (PH) domain which takes part in Akt regulation. Indeed, the kinase in its PH “out” form is ready to be activated by phosphorylation whereas the PH “in” form is inactive.

The importance of Akt makes this kinase a promising target for cancer treatment. One of the compound screenings undergone to find Akt inhibitors revealed two molecules with a mixed-competitive effect toward ATP. These molecules inhibit Akt in a PH-dependent manner. Indeed, the IC₅₀ of these compounds are in the micromolar range in the presence of the PH domain whereas they are completely inactive in the absence of the PH domain. This effect is opposite to the one observed with staurosporine, which is active in both cases but with preference for Akt in the absence of the PH domain.¹³⁷

Medicinal chemistry and structural optimization drove researchers to find improved compounds with nanomolar potency and high selectivity (Fig 28, B and C).^{138,139} X-ray structures revealed a new pocket formed in the presence of the PH domain. Furthermore, a disorganization of the α C-helix was observed in presence of small molecules bound in this pocket. The Akt pocket is localized at the interface of the kinase domain and of the PH-domain making the presence of the PH-domain a strict requirement for inhibitor binding (Fig 28, A).¹⁴⁰

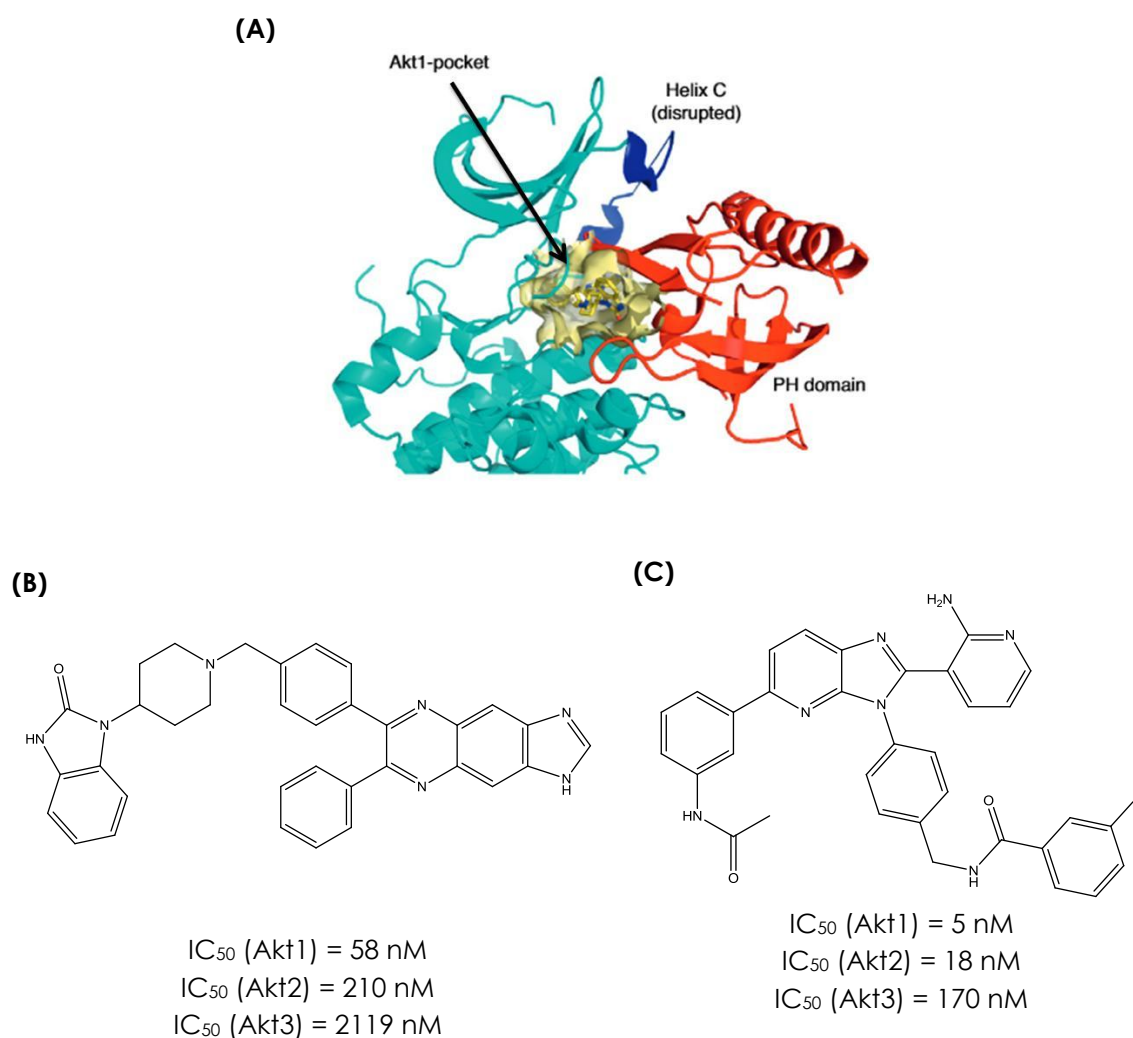


Fig 28: Overview of Akt1 pocket. (A) Structural overview of Akt1 pocket with the Pleckstrin Homology (PH) domain in red (Reprinted from Palmieri, L. *et al.*¹²⁹, Copyright (2016), with permission from Elsevier) (B) Chemical structure of the allosteric Akt inhibitor VIII¹³⁹. (C) Chemical structure of the allosteric Akt inhibitor described by Ashwell *et al.*¹³⁸.

1.4.3.4 P-loop pocket

The P-loop pocket (or MEK pocket) is localized between the P-loop (Mg-binding loop) and the α C-helix in Mitogen-activated protein kinase kinase (MEKs). Several small molecules have been found to bind to the MEK pocket: the first one PD184352 was described in 1999.¹⁴¹ Based on mutation experiments, a putative binding site was considered¹⁴² and later confirmed by X-ray structure determination (Fig 29).¹⁴³

Interestingly, all of the type III inhibitors of MEKs have been crystallized in presence of an ATP analog. Hydrogen bonds could be observed between inhibitors and phosphates of the nucleotide and synergetic effect for binding was observed for some of these type III inhibitors.¹⁴⁴

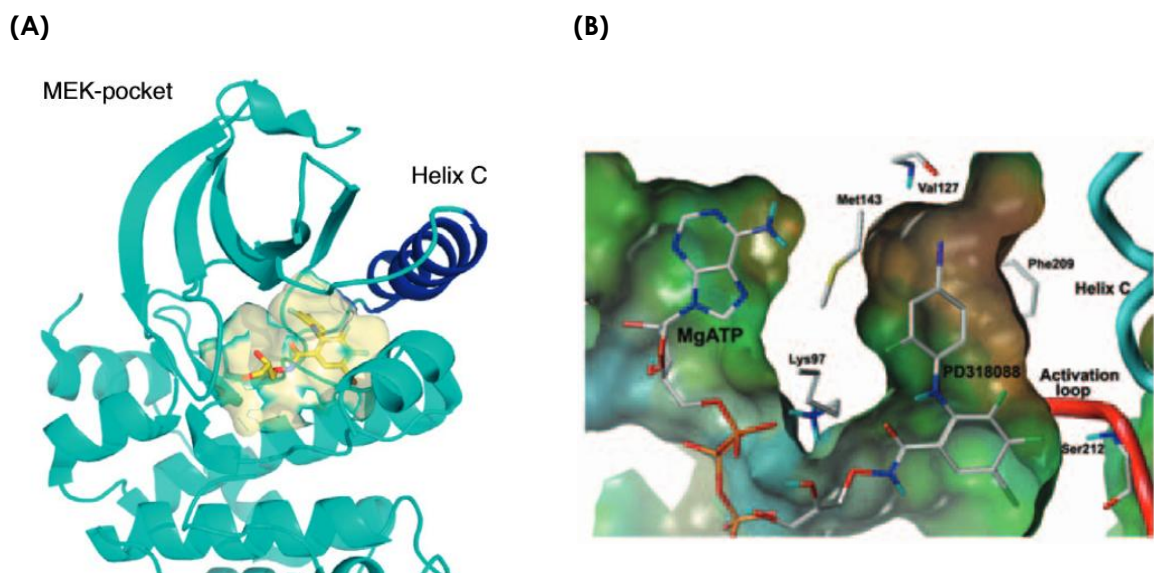


Fig 29: Structural view of the MEK-pocket localized between the DFG-motif and the α C-helix. (A) General 3D view of the MEK-pocket (PDB ID: 1S9J) (Reprinted from Palmieri, L. *et al.*¹²⁹, Copyright (2016), with permission from Elsevier). (B) View, from the N-terminal lobe, of the ATP molecule bound to the catalytic site and of PD318088 compound bound to the allosteric MEK pocket. Brown surface represents the most hydrophobic residues and green the most hydrophilic

(Reprinted by permission from Macmillan Publishers Ltd: [Nat. Struct. Mol. Biol.] from Ohren, J. F. *et al.*¹⁴³, copyright (2016)).

Following these results, several highly selective MEK1/MEK2 inhibitors were discovered and one of them, trametinib¹⁴⁵(Fig 30) was approved by FDA in 2013 for the treatment of patients with BRAF V600E mutated metastatic melanoma. Nowadays, trametinib is used in combination with dabrafenib to overcome resistances.¹⁴⁶

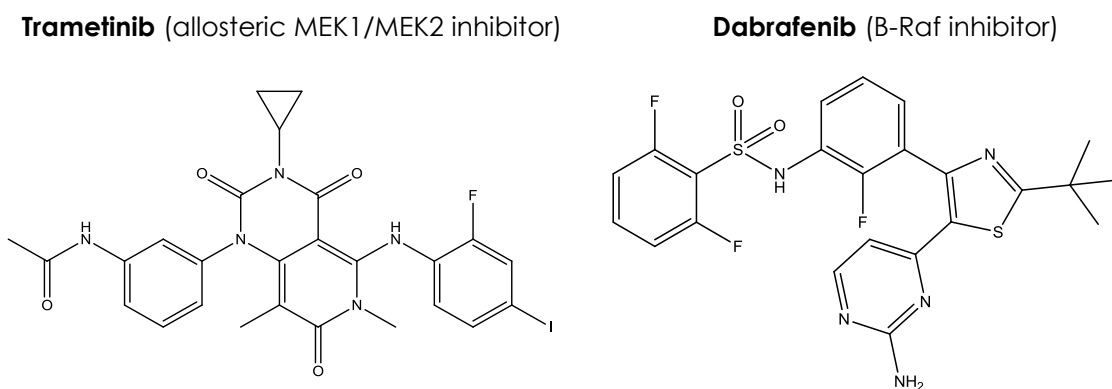


Fig 30: Chemical structure of trametinib and dabrafenib.

Recently, findings about the binding mode of an ERK inhibitor named SCH772984 revealed that it shares some features with MEK Type III inhibitors. SCH772984 was firstly described as a potent and selective ERK inhibitor but its mechanism of action remained unknown.¹⁴⁷ Then, Chaikuad *et al.* supposed that a Type II mechanism of action could be the reason of the overall good efficacy of this inhibitor. Experiments enabled them to determine the exact and unique binding mode of this molecule. Indeed, SCH772984 binds to the ATP pocket and, at the same time, to the P-loop pocket providing specific properties such as slow binding kinetics. Piperazine-phenyl-pyrimidine moiety of this compound binds to the specific P-loop pocket near the α C-helix with the P-loop Tyr36 shifted to the “in” position whereas the indazole moiety binds classically in the ATP pocket (Fig 31). Interestingly, SCH772984 binding mode is different in off-targeted kinases such as Haspin where it binds with a classical type I mechanism.¹⁴⁸

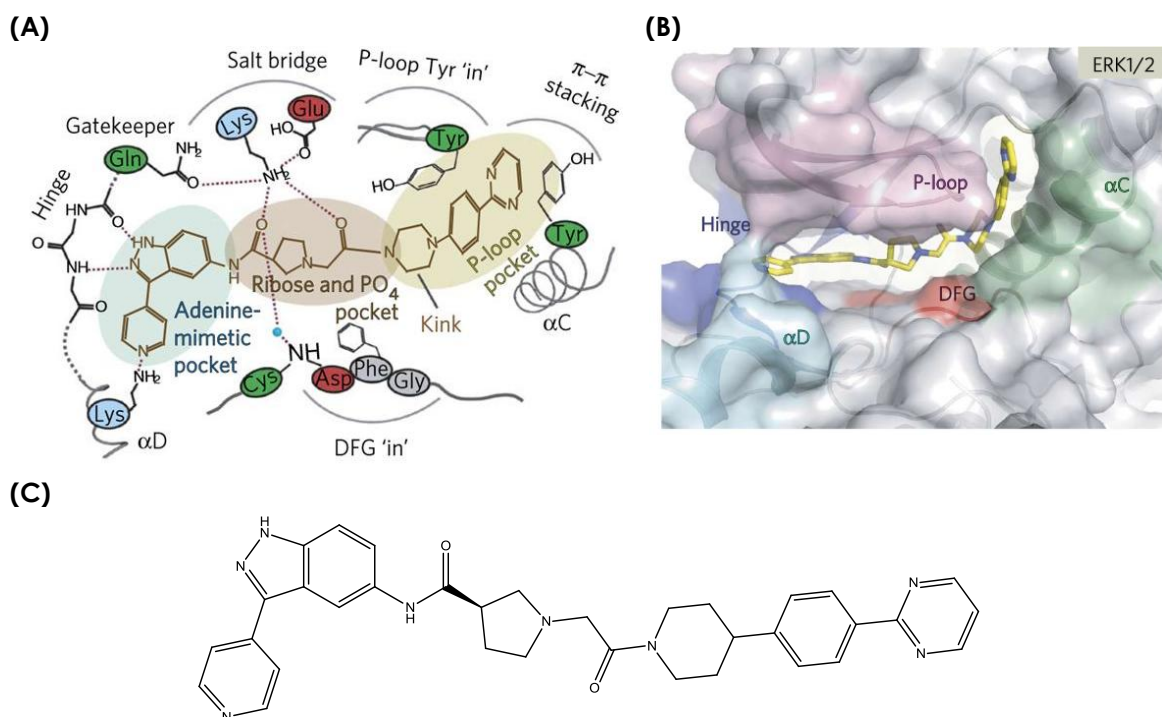


Fig 31: SCH772984 binding mode to ERK1/2 using the dual ATP/P-loop pocket. (A) Schematic representation of SCH772984 bound to ERK1/2. Adenine pocket is underlined with a blue shadow, ribose and phosphates pocket with a red shadow and the P-loop pocket with a brown shadow (Reprinted by permission from Macmillan Publishers Ltd: [Nat. Chem. Biol.] from Chaikuad, A. *et al.*¹⁴⁸, copyright (2016)). (B) ERK1/2 surface representation with SCH772984 (PDB ID: 4QTA) (Reprinted by permission from Macmillan Publishers Ltd: [Nat. Chem. Biol.] from Chaikuad, A. *et al.*¹⁴⁸, copyright (2016)). (C) Chemical structure of SCH772984.

1.4.4 Allosteric inhibitors and CK2

As described in paragraph 1.3.2.2, CK2 is considered as always active.³⁰ This statement is based on the observation of the same active conformation in all X-ray structures of CK2 α . Moreover, no regulation mechanisms such as phosphorylation are required for CK2 α activity. Nevertheless, during attempts to crystallize CK2 α in the presence of small molecule (DRB or glycerol) in the α/β interaction pocket, Raaf *et al.* obtained the first CK2 α structure in an inactive conformation. In this structure, the conformation of the ATP-binding loop (or glycine-rich loop, or P-loop) differs from the canonical one. Indeed, Tyr50 of the P-loop collapses in the ATP pocket, preventing ATP binding, instead of making interaction with Lys74 and Lys77 of the α C-helix (Fig 32).¹⁴⁹ This structure opens the question about the “always active conformation” and it is fair to expect that specifically designed small molecules could favor this inactive conformation and act as allosteric inhibitors. Moreover, by looking at the β -factor of the CK2 α structures, it is clear that the ATP-binding loop is one of the most flexible parts of CK2 α , together with the β 4/ β 5 loop. This point is confirmed by the global overview of CK2 α structures, already discussed in paragraph 1.3.2.2 (Fig 10).³¹ A displacement of the ATP-binding loop by a small molecule seems to be a likely event.

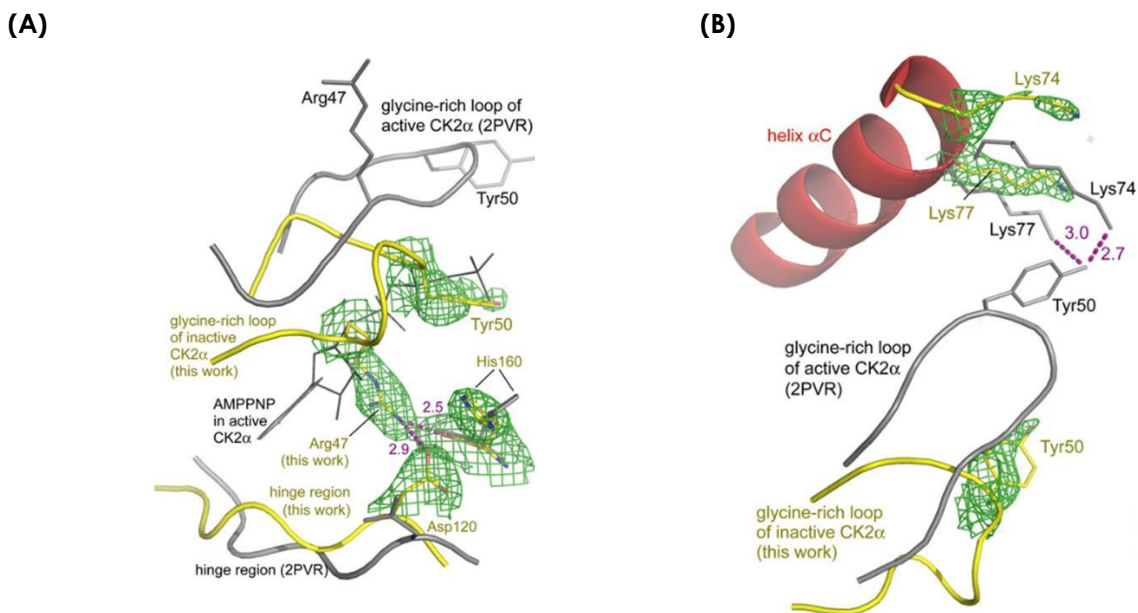
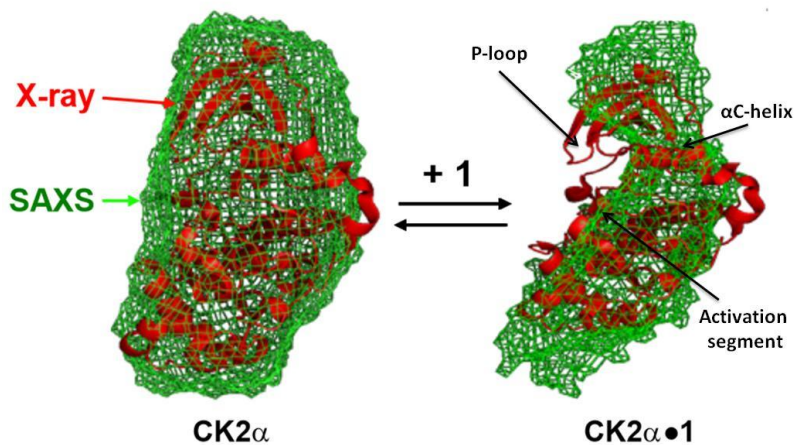


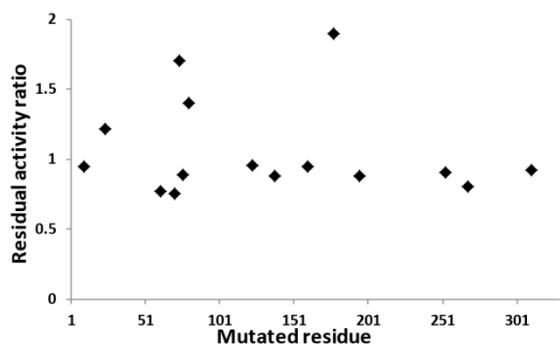
Fig 32: Glycine-rich loop conformation in active CK2 α (PDB ID: 2PVR) and in inactive CK2 α (PDB ID: 3FWQ) (Reprinted from Raaf, J. *et al.*¹⁴⁹, Copyright (2016), with permission from Elsevier). (A) Representation of the ATP binding pocket occupied by ATP (grey) in active CK2 α and by Arg47 and Tyr50 (yellow) in inactive conformation. (B) Specific interactions of Tyr50 with Lys74 and Lys77 in active conformation (grey) and absence of interactions in inactive CK2 α (yellow).

As already mentioned, almost all CK2 inhibitors described until now target the ATP pocket and are ATP-competitive inhibitors (TBB, TBI, CX-4945...). Nevertheless, one exception, the azonaphthalene class of compounds, is particularly interesting, even if the binding site was not precisely determined (Fig 33). Indeed, this family of small molecules has been described as non ATP-competitive inhibitors of CK2 α . SAXS experiments disclosed that, in the presence of an azonaphthalene derivative (Fig 33, C), a striking deformation of the kinase structure takes place in the region near the P-loop, α C-helix and activation segment has been observed (Fig 33, A). Moreover, three CK2 α mutants Lys71A, Lys76A and Leu178A were found less sensitive toward azonaphthalene inhibition than WT-CK2 α (Fig 33, B).¹⁵⁰ Lys71 and Lys76 residues are localized in the α C-helix and they make interactions with the P-loop. Leu178 is located at the beginning of the activation segment, close to the ATP pocket. These results support the concept that the binding site of azonaphthalene series is localized in the area between α C-helix and the activation segment.

(A)



(B)



(C)

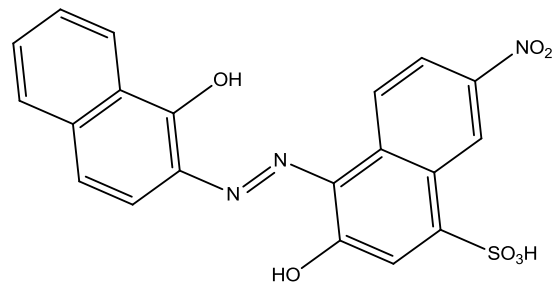


Fig 33: Overview of the azonaphthalene class of compounds. (A) Surimposition of X-ray structure (PDB ID: 1PJK) in red ribbon and SAXS ab initio shape restoration for CK2 α and CK2 α + azonaphthalene (From Moucadel, V. *et al.*¹⁵⁰, with the permission of Impact Journals, LLC). (B) Inhibitory effect of 0.4 μ M azonaphthalene on CK2 α mutated in the residues: 10, 24, 61, 71, 74, 76, 80, 123, 138, 160, 178, 195, 253, 268, 308, 311 to alanine (From Moucadel, V. *et al.*¹⁵⁰). (C) Chemical structure of the lead compound azo of the azonaphthalene class.

Few other non ATP-competitive inhibitors have been described such as polyoxometalates (POMs).¹⁵¹ Studies also supported their binding site to be located in the same region of CK2 α than azonaphthalenes but, as POMs could not be classified as drug-like small molecules, the following discussion will not deal with this class of compounds.

A last class of dual site inhibitors is of particular interest. They were obtained by coupling the commonly used TBBi (ATP competitive inhibitor) to a small acidic peptide containing multiple aspartate residues. As the result, they were able to interact both with the ATP-site and with the substrate binding site of CK2 α , leading to very potent compounds. The most potent inhibitor ARC-1502 showed a tremendous affinity for CK2 α with a K_i of 0.5 nM, more than 2500-fold better than the initial ATP competitive inhibitor ($K_i = 1.34 \mu\text{M}$). As expected, the acidic peptide part of ARC-1502 binds to the substrate binding region of CK2 α (PDB ID: 4FBX) but the low resolution of this part of the molecule in the X-ray structure prevents a better understanding of its the binding mode.¹⁰⁹ Following this work, novel dual-site inhibitors were obtained by coupling the ATP-competitive inhibitor K137 to small peptide sequences. The most potent compound (K137-E4) was linked to four glutamic acid residues and exhibited an IC_{50} of 25 nM for CK2 $\alpha_2\beta_2$. The glutamic acid residues interact with the residue involved in binding of n+1 (R191, R195, K198) and n+3 (K74, K77) of the substrate proteins. Interestingly, K137-E4 was lacking cell membrane permeability: this molecule was therefore able to inhibit selectively the ecto-CK2 activity. In consequence, K137-E4 appears to be a valuable tool to understand the physiological role of the ecto-CK2.¹⁵²

In conclusion, previous studies support the potential interest of the P-loop, the αC -helix and the activation segment to be targeted by small molecules to induce CK2 α inactivation. Nevertheless, up to now, no precise allosteric pocket has been defined on CK2 α and allosteric drug-like inhibitors have not been identified yet.

In this part of the manuscript, α/β interaction inhibitors that could be considered as allosteric modulators of CK2 have not been discussed. Information about this strategy for CK2 modulation will be detailed in paragraph 1.5.4.

1.5 Protein-Protein Interaction Inhibitors

1.5.1 Definitions and importance

Protein-Protein Interactions (PPI) have been extensively studied because of their crucial role in protein regulation. Indeed, a simple interaction between two proteins is the most common way to regulate their activity through protection toward degradation, translocation, activation, inactivation, degradation... Human protein-protein interaction network, also called interactome, consists of the whole set of interactions between proteins that could occur in a given organism.¹⁵³ The size of the human interactome is estimated to have 130,000 binary interactions and, consequently, 130,000 possible targets to modulate cell signaling.¹⁵⁴ A web database called "Interactome Database"¹⁵⁵ reports all described binary interactions.

Protein-protein interaction enables scientists to target proteins that were considered undruggable such as p53/mdm2, EphA4/ephrinB, HPV E2/E1...

1.5.2 Specific difficulties in PP2I discovery

Protein-protein interaction inhibitors (PP2Is) faced different difficulties compared to "usual" orthosteric enzyme inhibitors. In contrast to enzyme inhibitors, there are no natural small molecule which could act as ligands as starting scaffolds, nor well-defined pockets, nor convenient enzymatic assays to evaluate these small molecules... Large and flat interfaces, lack of cavities, competition with large protein, smooth interface are the main difficulties for the design of new PP2Is.

Most of the proteins interact through the intermediate of a large surfaces,^{156,157} with a common surface size of about 1,500 to 3,000 Å². To the opposite, interactions between proteins and small molecules are much smaller, with an average surface interaction equals from 300 to 1,000 Å². However, alanine scanning mutagenesis of residues located in protein interfaces revealed that, despite the large number of residues implicated in the interaction, only few of them are responsible of the major part of the affinity. Most of the time, one to three hydrophobic residues located at the center of the interactions are responsible of the majority of the affinity, and so, they are called hot spots.¹⁵⁸ In consequence, small molecules targeting only these key elements could be sufficient to modulate the protein-protein interaction.¹⁵⁹⁻¹⁶¹

Another important feature of protein-protein interfaces is their global flatness. Nevertheless, surface flexibility allows adaptation to small molecule binding. Indeed, side chain or loop movements can reveal small pockets that are not observable at a first glance on the protein structure. Transient pockets could be revealed in flat protein surface during 10 ns molecular dynamic simulation, as shown with Bcl-X_L, IL-2 and MDM2. In these three examples, transient pockets opened during simulation, confirming the situation obtained in crystal structures of these proteins with small molecules inhibitors. This statement underlined the drugability of the “apparently flat” protein interfaces.¹⁶²

Most of PP2Is come from compound library screenings. Nevertheless, screenings for PP2Is are considered arduous, due to the low hit rate that is generally obtained from large library screening. One source of this problem could be that compound libraries have been designed to target classical enzyme active sites whereas protein-protein interfaces required different chemical structures properties. In consequence, specific libraries have been designed to target protein interactions.^{163,164} In addition to screenings, fragment-based approaches using various methods such as NMR, SPR or enzymatic assays are often used to identify PP2Is.¹⁶⁵ Since the success of the molecule ABT-737, discovered by NMR fragment screening and now in clinical trials,^{166,167} several other protein-protein interactions such as ZipA/FtsZ,¹⁶⁸ pVHL/HIF-1 α ¹⁶⁹ and Bcl-X_L¹⁷⁰ have been studied by NMR. Elisa Barile *et al.* have recently published a very interesting review which described in details all the NMR methods used for the identification and optimization of PP2Is.¹⁷¹

Lipinski's “rule of five” ($H_{\text{Donor}} < 5$, $H_{\text{Acceptor}} < 10$, $MW < 500$, $\text{LogP} < 5$) is a global feature leading to a good absorption and so, to a good *in vivo* efficiency. These rules are commonly accepted as general guidelines to follow in drug discovery programs.¹⁷² However, for PP2Is, a consensus is generally accepted: due to the size of protein-protein interfaces, larger molecules are required. A comparison between molecular descriptors of PP2Is and a subset of classical drugs enables a verification of this statement (Fig 34):¹⁷³

- Molecular weight: the average molecular weight of PP2Is is bigger than for other drugs but most of PP2Is have a molecular weight under 500 g/mol.
- logP: none of the described PP2Is has a negative logP and they have a general logP greater than classical drugs (75% of PP2Is have a logP under 5).
- Hydrogen bond formation: both subsets of molecules respect Lipinski's rules concerning the number of hydrogen bond acceptors and the number of hydrogen bond donors.

- Topological Polar Surface Area (TPSA): TPSA is considered to be less than 140 Å² and both families of molecules respect this statement, even if PP2Is share a larger TPSA than classical drugs.

This comparison confirms the global need of larger molecules to address protein-protein interfaces but most of the PP2Is still respect the Lipinski's rule of five and in consequence could be promising candidates.

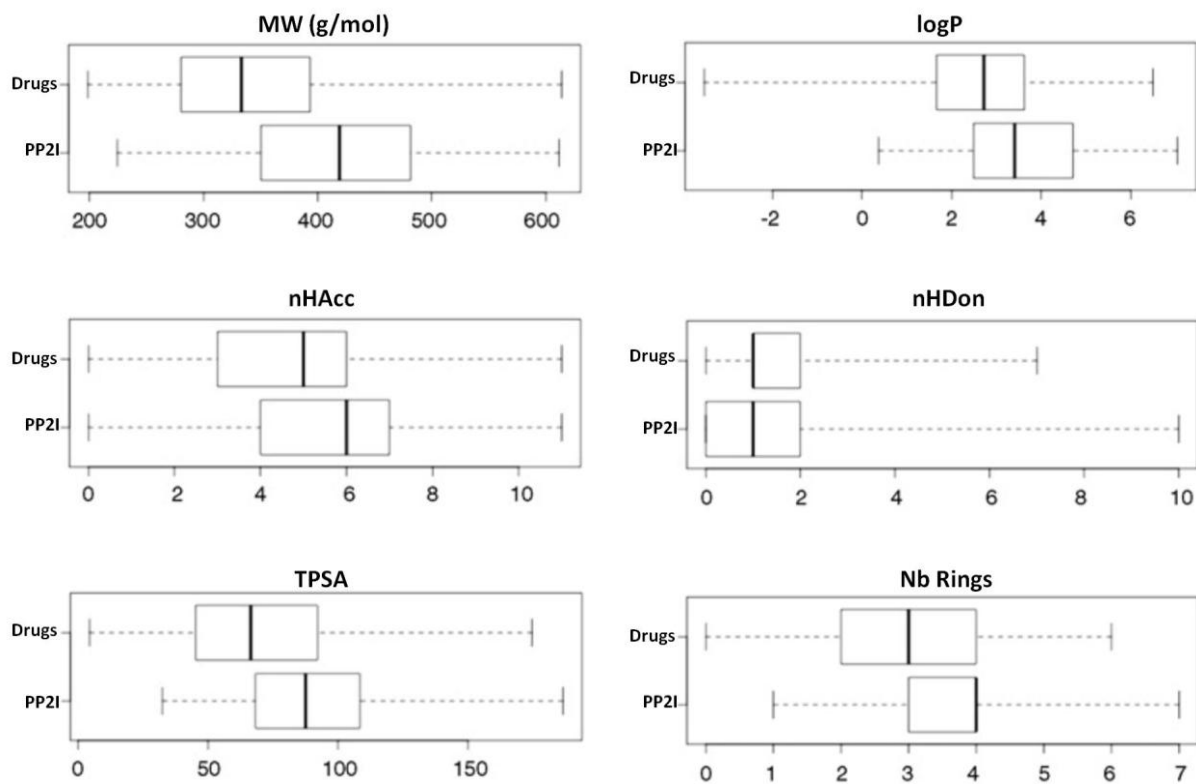


Fig 34: Distribution of several molecular descriptors calculated on a family of 66 PP2Is and 557 drugs. Minimum value, first quartile, median, third quartile and maximum values are represented (Reprinted from Sperandio, O. et al.¹⁷³, Copyright (2016), with permission from Elsevier).

1.5.3 Successful stories

Protein-protein interactions can be classified in two subtypes depending of the natural secondary structure type:

- Helix-mediated interaction: an α -helix is the natural binder of the targeted protein,

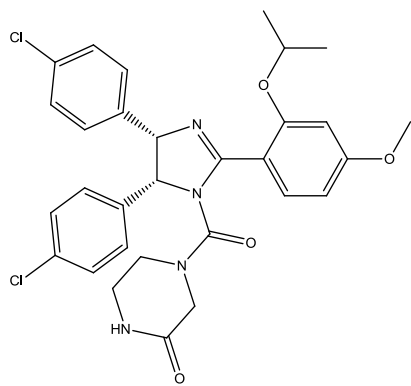
- Loop-mediated interaction: a loop, often more flexible and related to macrocycles, is the natural binder of the protein.

1.5.3.1 Helix mediated interaction inhibitors

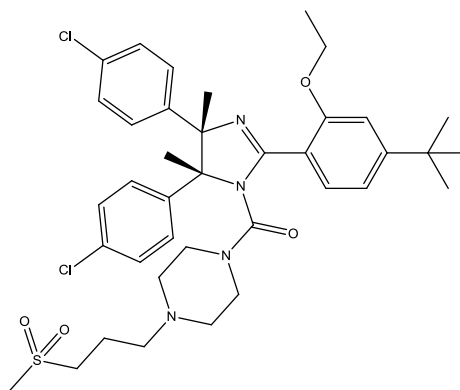
A survey on all PDB structures shows that only 15% of PDB entries consist of multiprotein complexes and, in this subgroup, 62% of the interactions have an helix at the interface.¹⁷⁴ Naturally, helix mimetics are the best option to find inhibitors of such interactions¹⁷⁵ and this could be obtained:

- From helix stabilization, using side-chain cross links by covalent bonds or hydrogen bonds,
- From β -foldamers, composed of amino-acid analogs able to adopt an helix conformation,
- From small molecule scaffolds which are helical surface mimetics. This category is advantageous because they are composed of small organic molecules and not of peptide derivatives.¹⁷⁶

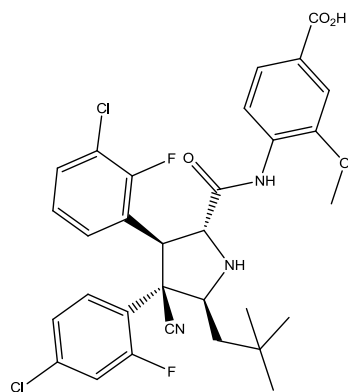
Several successful molecules have been developed as helix competitors. One of the most famous cases of protein-protein interaction, the p53/MDM2 interaction, is mediated by an helix. Indeed, one α -helix of the N-terminal transactivation domain of p53 binds to MDM2, thus preventing p53 tumor suppressor effect. In 2004, Vassilev *et al.* published the first *in vivo* effective small molecule inhibitor of the p53/MDM2 interaction: Nutlin-3a.¹⁷⁷ These results were the proof-of-concept that inhibition of this interaction in a murine model restored the p53 tumor suppressor activity. Following this result, researchers focused their works to find other efficient chemical structures targeting this interaction.^{178,179} Nowadays, 5 molecules are already in clinical trials and some more are going to enter such trials (Fig 35).¹⁸⁰



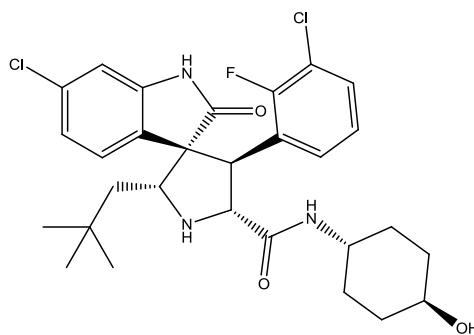
Nutlin-3a¹⁷⁷
 HTRF IC₅₀ = 88 nM
 MTT IC₅₀ = 1.5 μM



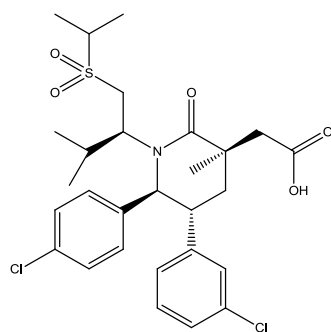
RG7172¹⁸¹
 HTRF IC₅₀ = 18 nM
 MTT IC₅₀ = 0.4 μM



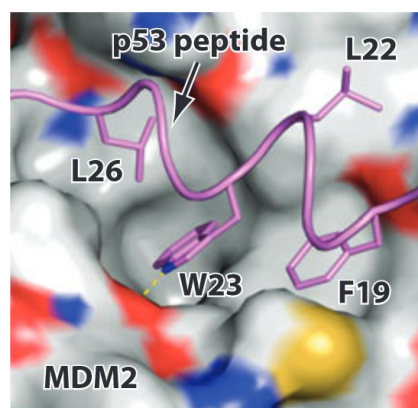
RG7388¹⁸²
 HTRF IC₅₀ = 6 nM
 MTT IC₅₀ = 0.03 μM



SAR405838¹⁸³
 Ki = 0.88 nM



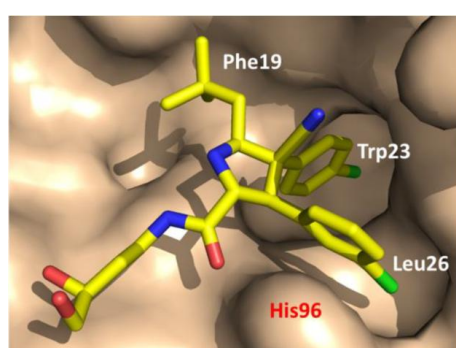
AMG-232¹⁸⁴
 SPR K_d = 0.045 nM



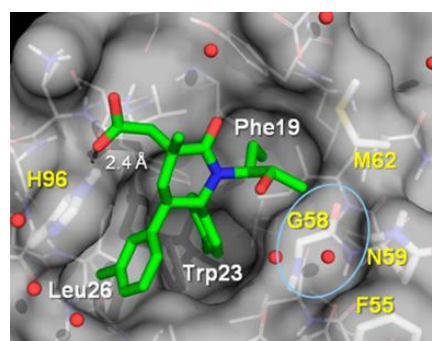
p53 peptide bound to Mdm2¹⁷⁹ (PDB ID: 1YCR) K_d = 60 nM¹⁸⁵

Fig 35: Examples of p53/MDM2 inhibitors and representation of the natural residues involved in the interaction (From Shangary, S. *et al.*¹⁸⁶, with the Annual Review of Pharmacology and Toxicology).

Small molecule inhibitors of p53/MDM2 interaction mimic the key residue (Phe19, Trp23, Leu26) of the p53 helix which binds to MDM2 (Fig 36). Medicinal chemistry optimization has led to small molecules with stronger affinities for MDM2 than p53 (60 nM).



RG7388



AMG-232

Fig 36: Structure of RG7388 (Reprinted with permission from Ding, Q. *et al.*¹⁸², Copyright (2016) American Chemical Society) and AMG-232 (Reprinted with permission from Sun, D. *et al.*¹⁸⁴, Copyright (2016) American Chemical Society) bound to MDM2 protein. Amino-acid names written in white correspond to the position of the key residue of p53 binds to MDM2.

Even if p53/MDM2 is probably the most well studied protein-protein interaction and with the greatest number of drugs in development, some other inhibitors have been successfully developed for other interactions (Bcl-X_L/BAK or BAD, HPV E2/E1, ZipA/FtsZ, IL-2, α -tubulin/ β -tubulin...). Extensive and recent reviews concerning PP2Is have been published by Tracy L. Nero *et al.*¹⁸⁷, Madhu Aeluri *et al.*¹⁷⁸, Lech-Gustav Milroy *et al.*¹⁸⁸

1.5.3.2 Loop-mediated interaction inhibitors

Despite the fact that α -helix interactions composed the major part of protein-protein interactions described in the PDB databank, non-helical and non-strand loops are the drivers of many protein-protein interactions.¹⁸⁹ A computational approach was described by Jason

Gavenonis *et al.* to identify loops ("hot loops") which are important for affinity in protein interfaces. Among all identified loops, computational alanine scanning was used to determine hot spots and loops that include more than one hot spot. Using this method, 1407 hot loops were identified in the PDB databank, which represents 5.6% of all interface loops. Among this subgroup, 19% of the hot loops represent more than 75% of the predicted energy of the all interface, 36% more than 50% of the predicted energy interface and 67% more than 25%. This study highlights the importance of these hot loops in protein-protein interactions. Interactions mediated by loops can also be targeted for drug development¹⁹⁰ and some examples are presented below.

EphA4 protein belongs to the Eph family of tyrosine kinase, composed of 16 members, which can bind to different glycosylphosphatidylinositol-anchored ephrin-A or transmembrane ephrin-B to regulate various biological responses.¹⁹¹ Modulation of EphA4/ephrin interaction is a promising target to cure several diseases such as cancers or amyotrophic lateral sclerosis.

The interaction between EphA4 and ephrin-B is mediated by a loop of ephrin-B that binds to a groove of EphA4.¹⁹² As frequently observed, the first modulator of EphA4/ephrin-B interaction was a small peptide. Actually, three different peptides were discovered by phage display screening as EphA4 binders.¹⁹³ Further investigations led to the identification of the binding site of these peptides and revealed their competition with ephrin for EphA4 binding. Moreover, these peptides are selective for EphA4 among Eph receptors (Fig 37, A and B).¹⁹⁴

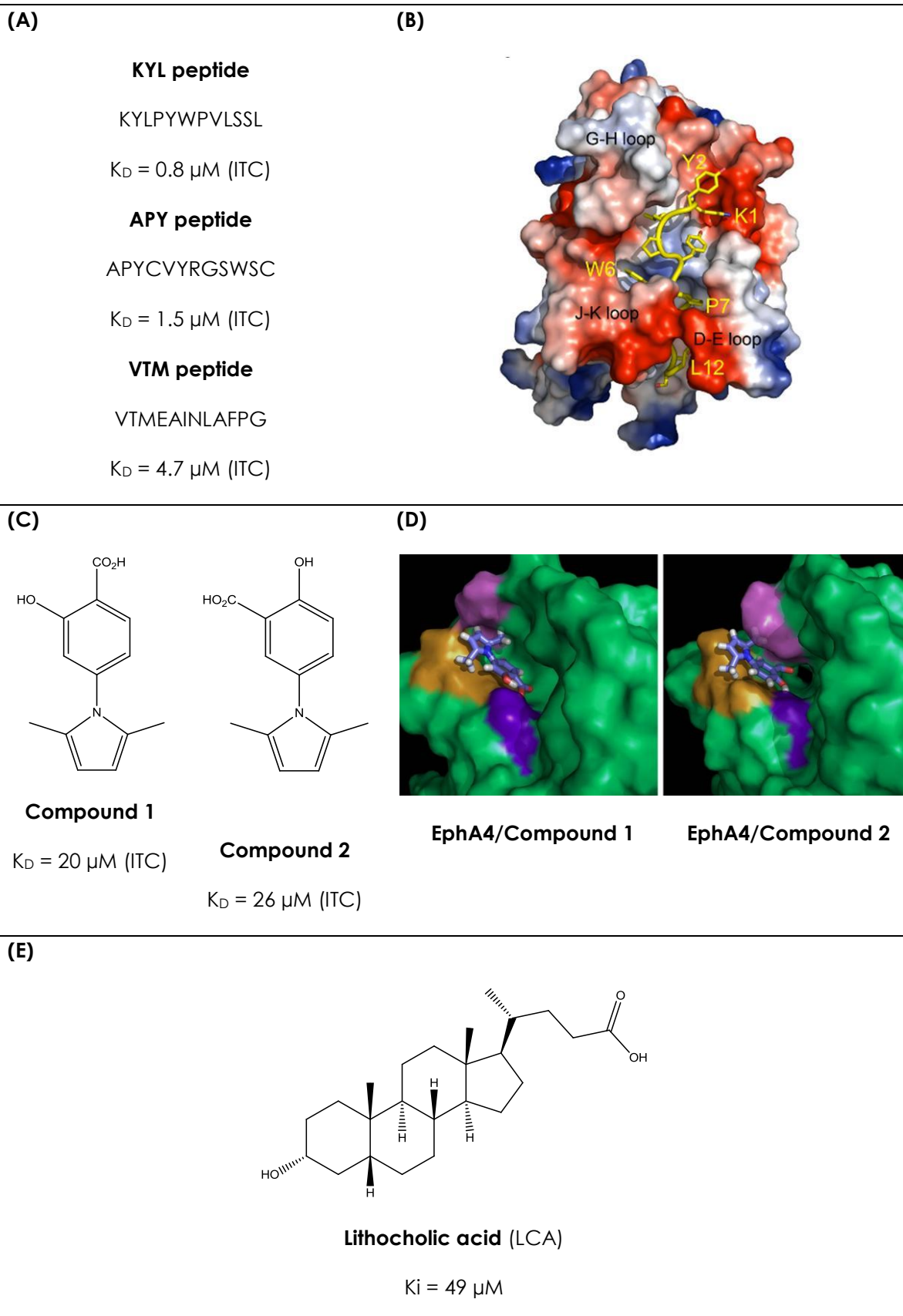
Two small molecules were later identified as inhibitors of EphA4/ephrin interaction by using an ELISA-based screening for the interaction between EphA4 and Biot-KYL peptide.¹⁹⁵ These small molecules have moderate affinity (about 20 μ M) for EphA4, probably because of the absence of an interaction with the complete interface of EphA4/ephrin. Nevertheless, they remain good starting point for further drug optimization. Competition experiments, combined with NMR experiments and docking simulations, enabled the determination of a putative binding site consistent with affinity and ability to prevent ephrin binding (Fig 37, C and D).¹⁹⁶

By using the same screening approach, another structurally unrelated compound was discovered as EphA4/ephrin inhibitor: lithocholic acid. This compound has a moderate affinity for EphA4 ($K_i = 49 \mu$ M), despite a higher molecular weight. Other bile acids such as cholic acid, deoxycholic acid and chenodeoxycholic acid did not show any effect on EphA4/ephrin interaction. However, lithocholic acid showed an effect on all EphA and EphB proteins, which was consistent with a lack of selectivity and a common mechanism to bind ephrins (Fig 37, E).¹⁹⁷

Another example is brought by compound 76D10, which was characterized as an inhibitor of EphA/ephrin interaction with a better potency (4.4 μM) but with an irreversible mechanism. Moreover, the instability of 76D10 prompted Roberta Noberini *et al.*¹⁹⁵ to suppose that the degradation product of 76D10 was the true active compound. They were not able to identify this product but speculated about an oxidation mechanism (Fig 37, F).

Bainan Wu *et al.*¹⁹⁸ used a high-throughput screening by using a NMR approach to find inhibitors of the EphA4/ephrin-B interaction. From a library of fragments related to peptide structure, few weak inhibitors were identified. Afterwards, structural improvements through medicinal chemistry strategies led them to a potent and specific inhibitor of EphA4/ephrin-B interaction. Compound 22 is able to inhibit the interaction between EphA4 and ephrin-B with an IC_{50} of 3.7 μM and a good selectivity among Eph receptors. They speculated that a smaller molecule even less potent than compound 22 could be obtained by setting aside amino acid derivatives for more effective compound.¹⁹⁸

All the studies dealing with EphA4/ephrin-B interaction represent a good overview of the strategy to find potent and selective PP2Is, from the characterization of the interaction (the first active peptides) and the difficult translation to small molecules by classical screening. The use of innovative methods, adapted to the identification of potent and active PP2I, was most of the time necessary.



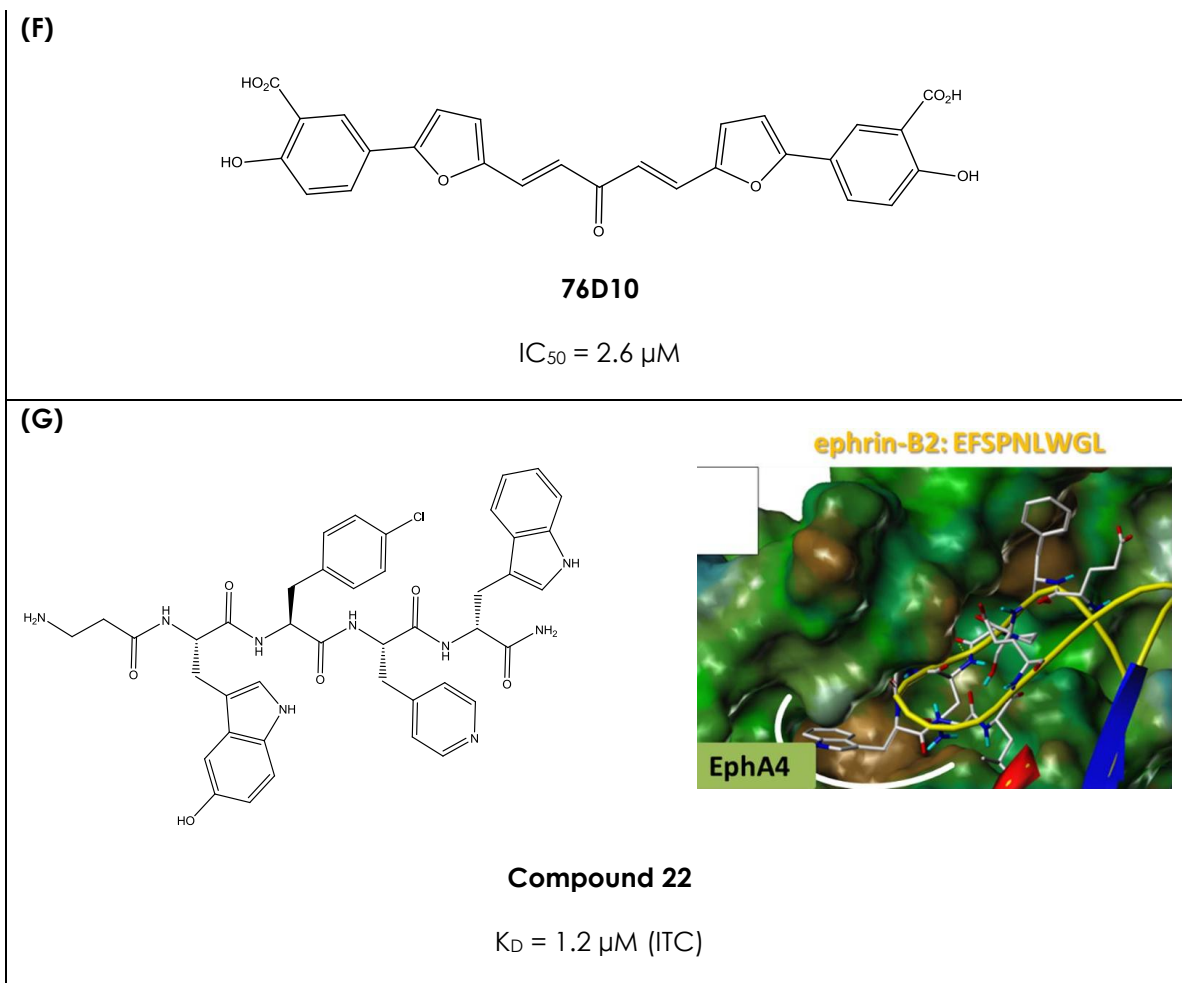
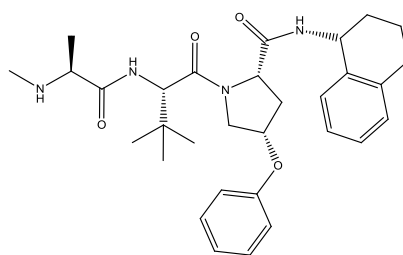


Fig 37: EphA4 interaction. (A) Amino acid sequences of the three peptides active on EphA4/ephrin-B interaction. (B) Docking model of KYL peptide in EphA4, based on NMR and mutagenesis experiments (From Lamberto, I. *et al.*¹⁹⁴, with the permission of Portland Press journals). (C) Chemical structures of two small molecule inhibitors of the EphA4/ephrin-B interaction. (D) Docking model of EphA4 binding site of the two small molecules (from (C)), based on NMR experiments. Residues Ile31 & Met32 in the D-E loop are represented in brown, Ile131 & Gly132 of the J-K loop are represented in violet and Gln43 in the β -strand is colored in blue (From Qin, H. *et al.*¹⁹⁶ with the permission of Portland Press journals). (E) Chemical structure of lithocholic acid, a moderate inhibitor of Eph/ephrin interaction. (F) Chemical structure of a putative irreversible inhibitor of EphA4/ephrin interaction. (G) Chemical structure of the peptide derivative 22, inhibitor of the EphA4/ephrin-B interaction and docking model of compound 22 and EphA4. Ephrin-B2 loop is represented by a yellow ribbon (From Barile, E. *et al.*¹⁷¹, with the permission of ACS Publication).

XIAP antagonists target another loop-mediated interaction and exhibited interesting results. Inhibitors of Apoptosis Proteins (IAPs) are overexpressed in many cancers and they prevent apoptosis by caspase inhibition. XIAP antagonists could reverse caspases inhibition and induce apoptosis. Smac is a natural XIAP antagonist and the nature of the interaction between Smac and XIAP was determined by NMR.¹⁹⁹ Later, synthetic molecules with nanomolar inhibitory activities were obtained, based on tripeptide derivatives (Fig 38).²⁰⁰ A combinatorial screening strategy based on tri-phenylurea scaffold was also used to successfully find cellular effective XIAP antagonists.²⁰¹



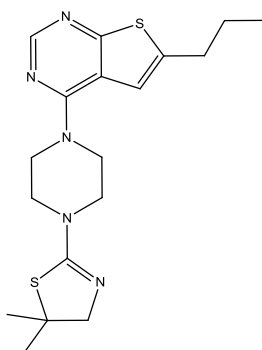
XIAP antagonist

$K_D = 5 \text{ nM}$

Fig 38: Structure of tripeptide-based small molecule with XIAP antagonist properties.

Menin/MLL interaction is also a successful example to find potent inhibitors of loop-mediated interactions. Mixed Lineage Leukemia (MLL) fusion protein requires the interaction with Menin protein to promote oncogenic activity. Inhibitors of this interaction will induce apoptosis and block proliferation. Initial PP2I hits were found by HTS and then developed by medicinal chemistry optimization to lead to several compounds with sub-micromolar IC_{50} (Fig 39).²⁰²

MI-2



$IC_{50} = 0.45 \mu\text{M}$

LE = 0.35

Fig 39: Chemical structure of a small molecule inhibitor of Menin/MLL interaction.

Research firstly focused on α -helix mediated interaction and a lot of protein-protein interaction inhibitors which mimic α -helix have been identified.^{175,178,188} However, a large proportion of protein-protein interaction is mediated by loops and only several examples of inhibitors targeting loop mediated interaction have been identified. Without any doubt, the number of PP2Is that interact with loop interactions will increase in the near future.

1.5.4 PP2I and CK2

As described in paragraph 1.3.2.1, CK2 is a multimeric protein, composed of a dimer of regulatory subunit (β subunit) that could bind two catalytic subunits (α and/or α' subunit). The regulatory subunit changes the substrate selection of CK2 α . Moreover, *in vitro* experiments have shown that the regulatory subunit activates and stabilizes CK2 α . Association and dissociation of the catalytic subunit to beta dimer (β_2) is an *in vivo* dynamic process but the driver of this phenomenon has not been identified yet.²⁰³

Interactions between CK2 α and CK2 β have been well characterized and already described in paragraph 1.3.2.4. The first crystal structure of CK2 holoenzyme (PDB ID: 1JWH) was published in 2001. The interface between α and β subunit was described as asymmetric, *id* the two α/β interactions in the holoenzyme are not identical, with an average interaction surface of

860Å².²⁸ More recently, a new structure of α/β interaction was resolved (PDB ID: 4DGL), showing a symmetric interaction with a surface about 1000Å² and a K_D of 4 nM.⁴⁸ The interaction is mediated by the interaction loop of the regulatory subunit which binds to the N-terminal lobe of CK2 α . The main two hot spots of the interaction loop are Tyr188 and Phe190.⁵⁰ In the other side, the two corresponding hot spots of the α -subunit for β binding are Leu41 and Phe54 (Fig 40, A).²⁰⁴ Despite the strong affinity between CK2 α and CK2 β , the fact that α/β complex is transient make it a good target for protein-protein interaction inhibitors design.

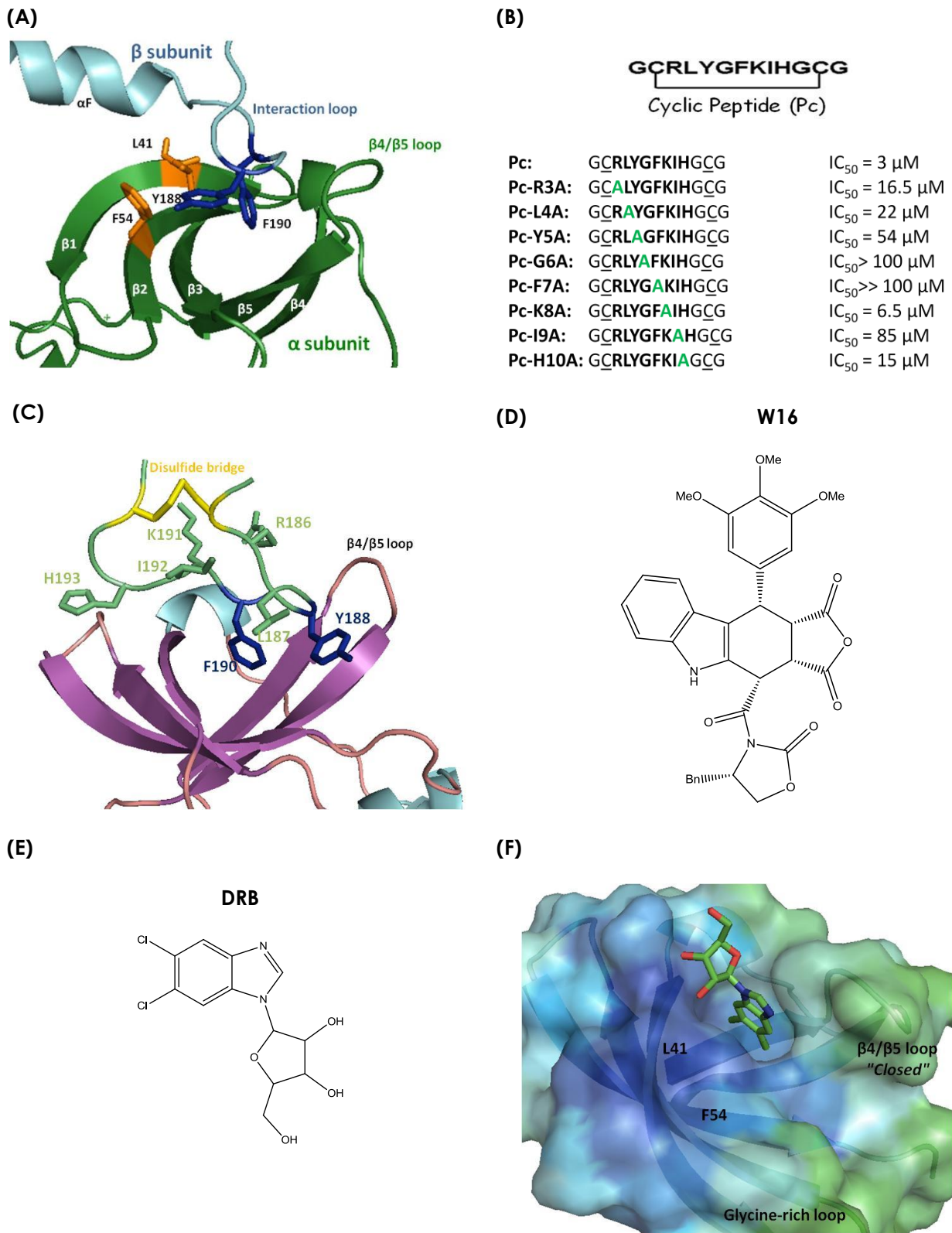


Fig 40: Modulators of CK2 α / β interaction. (A) Structural overview of the α / β interface. CK2 α is represented in green and the two hot spots (L41 and F54) in orange. CK2 β is colored in blue and

the two hot-spots (Y188 and F190) in dark blue (based on PDB ID: 4DGL²⁹). (B) Chemical structure of Pc and results of alanine mutagenesis scanning on Pc affinity for CK2 α . (C) Pc is represented in green except for the hot spots in blue and the disulfide bridge between the two cysteines in yellow. Amino-acid numbering is based on CK2 β sequence, glycine residues are not labeled (based on PDB ID: 4IB5).^{29,51} (D) Chemical structure of W16 compound. (E) Chemical structure of 5,6-dichlorobenzimidazole 1- β -D-ribofuranoside (DRB). (F) DRB in the α/β interaction pocket. Surface is colored depending of the β -factor, blue for rigid and green for flexible. Positions of the CK2 α hot spots are underlined by their labels (based on PDB ID: 3H30²⁹).

In 2007, Béatrice Laudet *et al.*⁵⁰ described a small cyclic peptide derived from a loop localized in the C-terminal part of CK2 β . This peptide competes with CK2 β to bind on CK2 α . This small peptide, called Pc, was designed after mutagenesis experiments that revealed the key residues (Tyr188 and Phe190) involved in α/β interaction. These two hot spots are located at the extremity of a 90° β -hairpin loop formed by residues R¹⁸⁶LYGFKIH¹⁹³: Pc mimics this sequence. Then, glycine and cysteine residues were added to cyclize the peptide, and by this way, to lock the peptide conformation. The resulting cyclic peptide inhibited the phosphorylation of CK2 β -dependent peptide substrate with an IC₅₀ of 3 μ M whereas no inhibition was observed on CK2 β -independent substrates. Moreover, Pc is able to disrupt the CK2 $\alpha_2\beta_2$ complex with the same potency. Alanine scanning mutagenesis experiments were conducted with Pc and confirmed the crucial role of YGF motif, which binds deeper inside the α/β pocket (Fig 40, B).⁵⁰ In 2013, Jennifer Raaf *et al.* were able to co-crystallize CK2 α and Pc (PDB ID: 4IB5). The structure confirmed the expected binding mode and underlined the importance of the YGF motif in Pc binding.⁵¹ Recently, during the development of an HTS assay to identify inhibitor of α/β interaction, the Pc peptide was improved. Based on docking experiments, central phenylalanine was replaced by *para*-iodo-phenyl alanine and the K_D of the novel I-Pc was improved: 0.24 μ M, measured by ITC, instead of 0.56 μ M for the initial Pc.²⁰⁵

In 2008, two small molecules were published as α/β interaction modulators. Béatrice Laudet *et al.* published indolo analogs of podophyllotoxine, also named the W family of compounds, with the W16 as the hit compound. This molecule was described as an α/β interaction inhibitor but CK2 α is inhibited by W16 with the same potency, probably by protein aggregation. In consequence, this compound was not suitable for further optimizations (Fig 40, D).²⁰⁶ In 2008, Jennifer Raaf *et al.*²⁰⁷ published the first crystal structure of CK2 α with a small molecule in the α/β interaction pocket (also called remote pocket). In attempts to crystallize CK2 α and 5,6-dichlorobenzimidazole 1- β -D-ribofuranoside (DRB, Fig 40, F) known as CK2 α

inhibitor, they obtained a crystallographic structure with two molecules of DRB: one in the ATP pocket and one in the α/β interaction pocket (Fig 40, F). Biochemical assays have confirmed the dual binding mode of DRB but despite the binding of DRB in the α/β interaction pocket, no significant effect on the association or dissociation of the holoenzyme was observed in presence of DRB. This lack of efficiency is probably due to the weak affinity of DRB for CK2 α (Fig 40, E, F).²⁰⁷

Several groups have put a lot of efforts to find a cellular efficient inhibitor of CK2 α /CK2 β interaction that will enable a deeper understanding of the role of this interaction in living organism. Nonetheless, such an inhibitor has not been published yet.

2. Aim of the thesis

Cancer cell growth relies on activated oncogenes as well as on deregulated non-oncogenes.²⁰⁸ The Protein Kinase CK2 is one of the deregulated non-oncogenic proteins which supports cancer development through activation of pro-survival, anti-apoptotic and proliferative signals (See Introduction 1.3.3.1-2. for further details).^{61,66} CK2 is an ubiquitous Ser/Thr protein kinase, composed of a dimer of regulatory subunit (β) and two catalytic subunits (α and/or α').²⁸ The catalytic subunit of CK2 is constitutively active, while the regulatory subunit modulates the selectivity toward a subset of substrate proteins.⁷⁷ The central position of CK2 in the control of various cell signaling pathways requires a fine internal control of CK2 activity. However, little is known about the cellular regulation of CK2 and the role of the regulatory subunit in the substrate selection. Additionally, previous studies promoted the interest of targeting CK2 to counteract cancer development, and one ATP-competitive inhibitor is currently in clinical trial, CX-4945, (5-(3-chlorophenylamino)benzo[c][2,6]naphthyridine-8-carboxylic acid, silmitasertib).²⁰⁹ Nevertheless, off-targets and resistances to CX-4945 have been recently revealed (see Introduction 1.3.4.1-2. for further details).⁹⁹

In contrast to ATP-competitive inhibitors, only few small molecules were reported to target allosteric binding sites on the catalytic domain of kinases, which can be explained by the fact that these allosteric inhibitors exploit unique binding sites and isoform-specific regulatory mechanisms.²¹⁰ Besides the fact that allosteric kinase inhibitors usually present higher selectivity, these molecules do not compete with the high cellular ATP concentration. Indeed, for kinases with relatively high ATP binding affinities ($K_m = 1\text{--}20\ \mu\text{M}$), it could be difficult to develop ATP-competitive inhibitors, which could be selective and, at the same time, potent enough to exhibit cellular activity.²¹¹

The aim of this work was:

A) to develop novel non ATP-competitive inhibitors of CK2. Two distinct hit compounds from previous *in silico* screening campaigns (Fig 41) had to be optimized using

different medicinal chemistry approaches. Series of analogs had to be designed, also supported by molecular docking. Finally the inhibitory activity and binding affinity toward CK2 had to be determined;

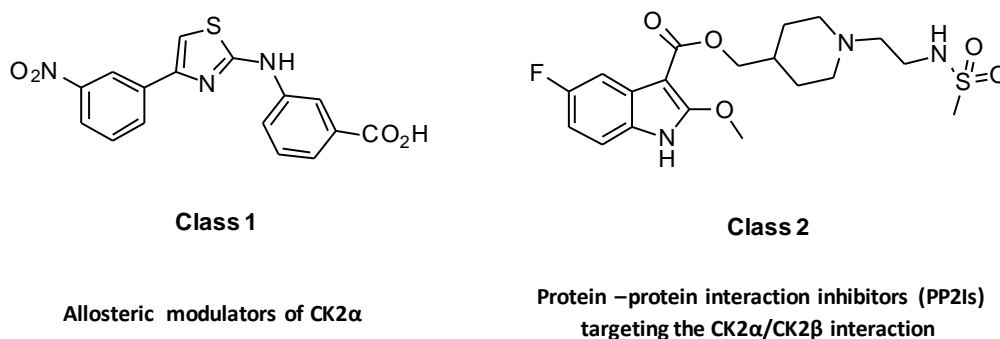


Fig 41: Class 1 and class 2 hit compounds from previous *in silico*-screening campaigns.

- B) to confirm and further investigate the mechanism of action of the optimized non-ATP competitive inhibitors. Based on the original hits, two distinct chemical classes (1 & 2) of compounds had been developed in part A, and were supposed to modulate CK2 activity by different mechanisms. The following modes of action were postulated and had to be investigated using diverse cell-free and cell-based assays:
- Allosteric modulators of CK2 α** could overcome the selectivity issues observed in the case of CX-4945 and we believed that they could exert a better *in vivo* potency than ATP-competitive inhibitors. It was hypothesized that compounds deriving from class 1 (Fig 41) might bind to a novel allosteric site, outside the ATP binding pocket and could lock the “always active” CK2 α conformation into an inactive state. The goal of our study was to verify the allosteric mechanisms of our optimized inhibitors and eventually identify the binding site using a combination of single-alanine mutagenesis, temperature-dependent circular dichroism, saturation-transfer difference NMR experiments and molecular

modeling. Finally, consequences of the novel mechanism of action on the regulation of CK2 in cells were to be investigated.

- ii. **Protein–protein interaction inhibitors (PP2Is) targeting the CK2 α /CK2 β interaction:** compounds deriving from class 2 (Fig 41) were supposed to block the interaction between the regulatory subunit (β) and the catalytic subunit (α) because the β binding pocket had been used as a template for the *in silico* screening from which the class 2 secondary hit was identified. Since the α/β subunit interaction is dynamic²¹², optimized derivatives of this compound might be useful to obtain a deeper understanding of the mechanisms that control this interaction and their physiological consequences in cells and whole organisms. The goal was to synthesize a small library of class 2 analogs and to evaluate their activity in biochemical and cell-based assays. Another objective was the characterization of the effects of optimized compounds. Moreover, a complementary study of the CK2 activity in cells of a previously described cyclic peptide was planned, in order to assess whether the novel and unique approach of modulating CK2 by small PP2Is could have potential therapeutic applications.

3. Results

3.1 Modulation of protein kinase CK2 activity in cells through novel non-ATP competitive inhibitors

CK2 is an ubiquitous Ser/Thr protein kinase involved in the control of various signaling pathways and is thought to be constitutively active. In the present study, we identified a novel class of CK2 inhibitors, which displayed a non ATP-competitive mode of action and stabilized an inactive conformation of CK2 in solution. Single mutation scanning, CD spectrometry and STD-NMR experiments demonstrated that the compounds bind in an allosteric pocket outside the ATP-binding site. Our data strongly suggested that the putative binding site was located at the interface between the α C helix and the flexible glycine-rich loop. The optimized compound **7** showed a micromolar potency to reduce CK2 substrate phosphorylation both in enzymatic assays and in cell-based experiments. Furthermore, a substrate-dependent CK2 inhibition as well as modulation of the CK2 α subcellular localization was observed upon compound **7** treatment. Thus, compound **7** is a novel tool to investigate conformation-dependent mechanisms of CK2 regulation in cells and may be further developed into anti-cancer drugs exploiting a novel mode of CK2 inhibition.

3.1.1 Scientific rationale

The protein kinase CK2 has an exceptional position within the human kinome due to the significant proportion of the cellular phosphoproteome that can be attributed to this kinase.²⁷ This ubiquitously expressed protein kinase is involved in the activation of several pro-oncogenic pathways that are critical for cell proliferation, differentiation and survival.^{21,3} Numerous reports underlined the relationship between CK2 overexpression and poor survival rates in lung carcinoma, prostate cancer, acute myeloid leukemia, breast carcinoma, colorectal tumors, glioblastomas and gastric carcinoma.^{6,7} The crucial role of CK2 as a cancer driver makes it an interesting target in cancer therapy, and CK2 inhibition proved to be an effective method to induce tumor regression.^{9,2}

CK2 is a tetrameric enzyme composed of a dimer of regulatory subunits (β) and two catalytic subunits, CK2 α and/or CK2 α' .²⁸ The catalytic subunit of CK2 is considered as constitutively active³⁰ and can phosphorylate more than 300 substrates²⁷ while the regulatory subunit modulates the selectivity toward a subset of substrate proteins.^{7,7}

Most of the known CK2 inhibitors bind to the ATP pocket and show an ATP-competitive behavior in enzymatic assays^{9,1} CX-4945 (5-(3-chlorophenylamino)benzo[c][2,6]naphthyridine-8-

carboxylic acid, silmitasertib) is one of the most potent CK2 inhibitors ($IC_{50} = 14$ nM) and is currently in phase II clinical trials.²⁰⁹ X-ray crystallographic analysis revealed that CX-4945 binds to the ATP-binding pocket of CK2 α in the active conformation.²¹⁴ Although CX-4945 is rather selective, it was recently reported to be actually more potent against Clk (Cdc2-like kinase) 2 ($IC_{50} = 4$ nM), a kinase involved in the regulation of alternative splicing.⁹⁹ This recent result underlines the fact that potent and selective CK2 α inhibitors are difficult to obtain through targeting the ATP binding pocket. Therefore, research efforts are spent to identify inhibitors that exploit specific regulatory mechanism to suppress the catalytic activity of the kinase. Besides the potential pharmacological benefit, such allosteric ligands are often invaluable tools to investigate the underlying allosteric mechanism that allows the catalytic domain to switch between the active and the inactive state. It was previously reported that azonaphthalene dye-derived compounds inhibit the catalytic activity of CK2 α in a non-ATP-competitive manner, however, the exact binding site and a potential mechanism of inhibition remained elusive¹⁵⁰. Besides, inorganic PolyOxoMetalate complexes (POMs), e. g., $[P_2Mo_{18}O_{62}]^{6-}$, were described as potent allosteric inhibitors of CK2 α , exhibiting nanomolar IC_{50} s and great selectivity in a panel of 29 kinases.¹⁵¹ However, POMs lack cellular activity and there is little perspective to develop them further as *in vivo* active agents.

In the present study, we describe the identification of a novel, cellularly active class of non ATP-competitive CK2 inhibitors. Using different methodologies, we provide evidence that the compounds target an alternative binding pocket distinct from the ATP binding site.

3.1.2 Hit compound 1 is a non-ATP competitive inhibitor of CK2

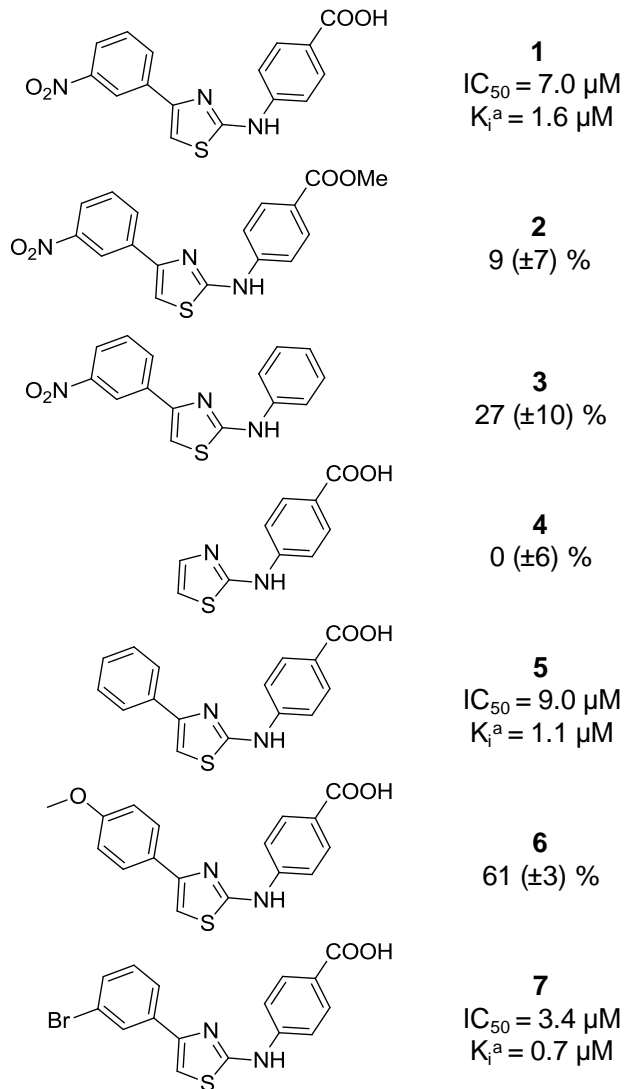


Figure 1. Chemical structures of compounds **1-7**. IC_{50} (S.D. < 20 %) and K_i are depicted for compound **1**, **5** and **7**. For the others, CK2a inhibition percentages in presence of 10 μM of respective compound are depicted with S.D. values given in brackets. aK_i values were determined from graphical plotting of the Lineweaver-Burk plot slopes.

Compound **1** (Figure 1) was identified as a part of a Virtual Ligand Screening (VLS) campaign against non-ATP binding sites on CK2.^{215,216} Michaelis-Menten kinetic experiments were performed on top ranking VLS hits in order to confirm the non-ATP-competitive mechanism of their action. Despite its relatively weak potency ($IC_{50} = 7 \mu M$ on CK2a), this evaluation sparked

our interest in compound **1** because it exhibited an unusual mixed-type mechanism of inhibition (Figure 2A) and a constant potency in the presence of increasing ATP concentrations (Figure S1A). Moreover, raising the concentration of the peptide substrate did not impair CK2 inhibition by **1**, ruling out that the compound competed with substrate binding (Figure S1B). Furthermore, monomeric CK2a showed the same sensitivity toward inhibition by compound **1** as the preformed tetrameric complex CK2 $\alpha_2\beta_2$ (Figure 2B). In addition, CK2 inhibition by compound **1** was not affected by increasing concentrations of CK2 β (Figure 2C). These results clearly demonstrated that the regulatory β -subunit did not influence the inhibition by compound **1**, suggesting that **1** does not bind in the α/β interaction pocket on the α -subunit. Next, the selectivity of **1** was evaluated against a panel of 44 selected kinases. The selectivity profile was encouraging: besides CK2a, only three other kinases from the panel were inhibited by more than 50 % in the presence of 50 μM of compound **1**: EGFR (74 % inhibition), EphA4 (55 %) and Pim-1 (54 %). Two additional kinases, MuSK (38 %) and PDGFR α (35 %) were inhibited by more than 30 % (Table S1).

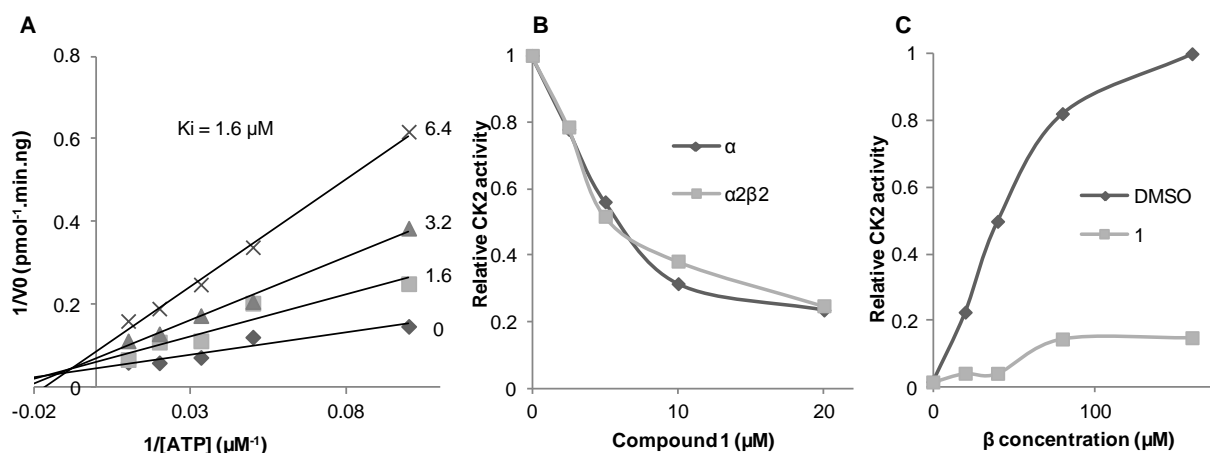


Figure 2. Analysis of the mode of inhibition of compound **1**. **A.** Lineweaver-Burk inhibition plot of human recombinant CK2a by compound **1** at various ATP concentrations. The K_i was determined by plotting the slopes at varying inhibitor concentrations. **B.** CK2a and CK2 $\alpha_2\beta_2$ activity in the presence of increasing concentrations of compound **1**. **C.** Effect of increasing CK2 β concentrations on the inhibition of fixed amounts of CK2a by compound **1** (20 μM).

3.1.3 Structural requirements of the new inhibitors for CK2 α affinity

Based on these promising results, a small set of compound **1** derivatives was synthesized (Scheme S1) to establish preliminary structure–activity–relationships (SAR) and possibly optimize the potency toward CK2 α . The compound structures are depicted in Figure 1. Conversion of the carboxylic acid function in compound **1** to an ester, or deletion of it, resulted in a strong decrease in affinity for CK2 α (Figure 1, compounds **2** and **3**), suggesting that the binding involved ionic interactions with a basic residue. The presence of a phenyl group at position 4 of the aminothiazole core was also found to be crucial, as indicated by the complete lack of activity of the truncated analog **4** (Figure 1). While modulation of the electron density of this 4-phenyl did not change the inhibitory activity compared with that of the unsubstituted congener **5** (cf. **1**, **2** and **6** in Figure 1), increasing the lipophilicity by a bromo-substituent significantly enhanced the affinity to reach the sub-micromolar range ($K_i = 0.7 \mu\text{M}$, compound **7**, Figure 1). Thus, the SAR obtained with the 4-phenyl ring suggested that binding of this moiety to CK2 α was driven by hydrophobic interaction with a lipophilic pocket (Figure 1).

The selectivity of the most potent compound **7** was then evaluated against a panel of 32 selected kinases, specifically enriched by closely related kinases from the CMGC family but also including kinases from other branches of the kinome (Table S2). In addition to CK2 α , six others kinases were inhibited by more than 60 % in the presence of 50 μM of compound **7**: EphA4 (73 %), GSK3 β (71 %), CK1 γ 1 (69 %), ACVR1 (66 %), Clk4 (61 %) and MLCK (61 %). Notably, Clk2, the main off-target of the ATP-competitive compound CX-4945, was inhibited by only 33 %.

3.1.4 Identification of a putative allosteric pocket

Enzyme kinetic experiments (Figure 2 and Figure S1) suggested an alternative mechanism of action relying on a potential binding site outside the ATP pocket. To find a clue about the potential location of an alternative binding pocket for small molecules, we analyzed the available CK2 α crystal structures. A study by Niefind *et al.*³¹ suggested that the glycine-rich loop is one of the most variable regions in X-ray structures of CK2 α , suggesting a putative flexibility of this loop in solution. This feature was also supported by metadynamics studies simulating conformational transitions²¹⁷ and by recent structural studies.²¹⁸ In most CK2 α crystal structures, the glycine-rich loop conformation is maintained by two hydrogen bonds linking the Tyr50 of this loop and two lysine residues (Lys74, Lys77) of the basic cluster (compare e.g., PDB entries 3PE1 and 3Q9Z). In order to find alternative conformations of the glycine-rich loop, we analyzed all 72

crystal structures (and individual chains within these structures) of the human enzyme available in the PDB as of November 2014. Two crystal structures (PDB entries: 3FWQ and 3JUH) were identified, in which the key hydrogen bonds fixing Tyr50 are lacking. In consequence, Tyr50 has fully collapsed in the ATP binding site of the 3FWQ structure.¹⁴⁹ The second structure (PDB code: 3JUH), also presents Tyr50 turned away from its usual location to an intermediate position toward the ATP binding site (Figure 3A).³³ Thus, it can be assumed that CK2 exists in conformational states that allow a movement of the glycine-rich loop. Further examination of the X-ray structures in PDB entries 3FWQ and 3JUH revealed a hydrophobic pocket, large enough to accommodate a small molecule, which, in the active conformation, is partially occluded by Tyr50 and the glycine-rich loop (Figure 3B). This putative allosteric pocket was located between the glycine-rich loop and the α C-helix, delimited by residues Tyr50, Lys71, Val73, Lys74 and Lys77. To investigate if this region might be targeted by our compounds, nine GST-CK2 α single-point alanine mutants covering this area were tested in enzymatic assays in the presence of a fixed concentration of **7**. All CK2 α mutants displayed reasonable catalytic activity, which was at least 30 % of that of the wild type. Three mutants (Lys74Ala, Lys77Ala and His160Ala) were found to be more resistant to inhibition by compound **7** than the wild type, and therefore selected for dose–response experiments. These studies showed that the IC₅₀ values of compound **7** were significantly increased for the Lys74Ala (1.8-fold), the Lys77Ala (3.2-fold), and the His160Ala mutant (2.3-fold) (Figure 4). It is reasonable to assume that the lysine residues interact with the carboxylate of **7**, and that in each lysine mutant, the remaining nearby lysine residue can compensate in part for the loss of electrostatic interactions, thus attenuating the drop in binding affinity. Taken together, our results from enzyme inhibition kinetics, site–directed mutagenesis and SAR analysis were consistent with the binding of our new compounds to an allosteric site, composed of a carboxylate coordination site formed by the basic cluster containing Lys74/77, and an adjacent hydrophobic cavity which accommodates the 4-phenyl moiety. As suggested by the 3D structures (PDB entries 3JUH and 3FWQ, see above), the hydrophobic pocket was most likely located between the α C helix, 3rd β -strand of the N-terminal lobe, the activation loop and the glycine-rich loop of the kinase (Figure 3).

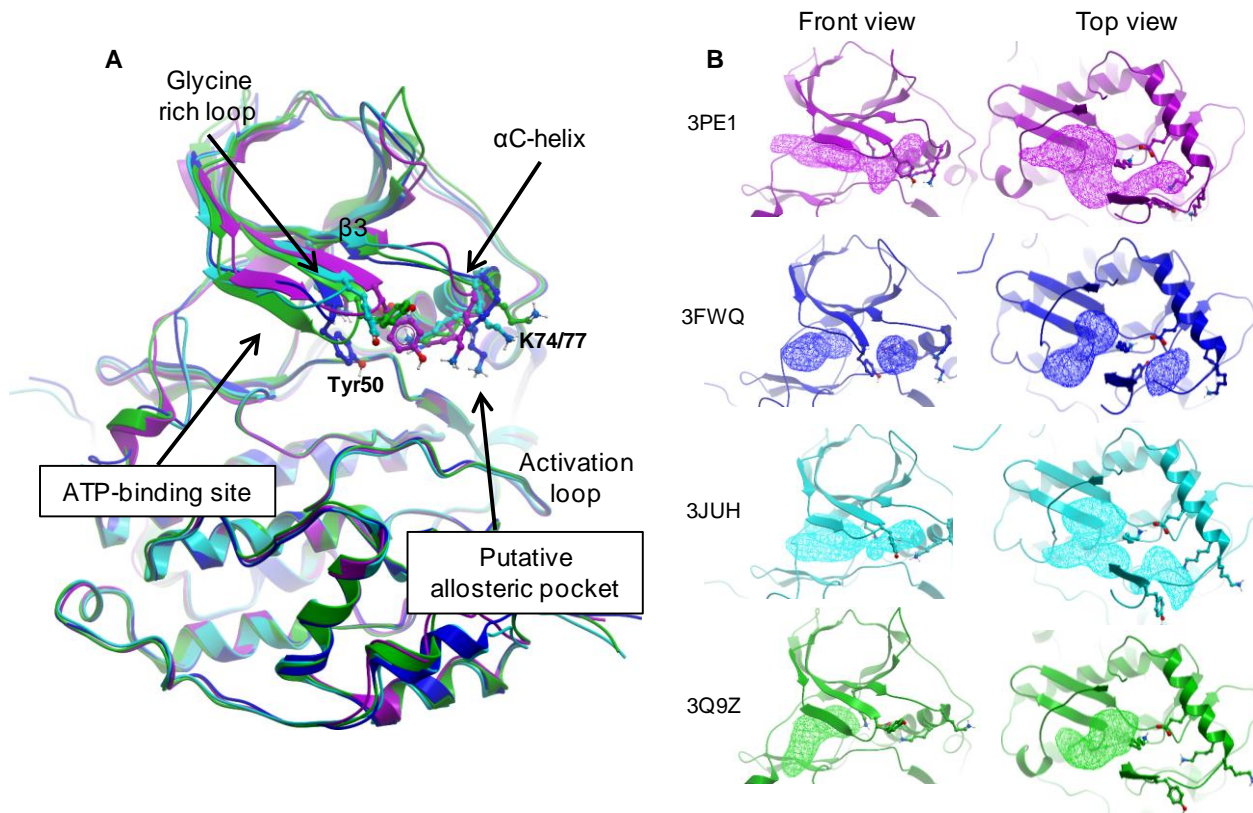


Figure 3. A. Superposition of four CK2 α structures (3PE, magenta; 3FWQ, blue; 3JUH, cyan; 3Q9Z; green). The ATP-binding site is occupied by CX-4945 in 3PE1 and by AMPPNP in 3JUH and 3Q9Z (not shown for clarity). **B.** A separated view from front or top of each structure is depicted. The pockets were identified using ICM pocket finder and represented with a mesh surface. The putative allosteric pocket is partially available in 3PE1, fully accessible in 3FWQ and 3JUH but completely absent in the conformation crystallized in 3Q9Z.

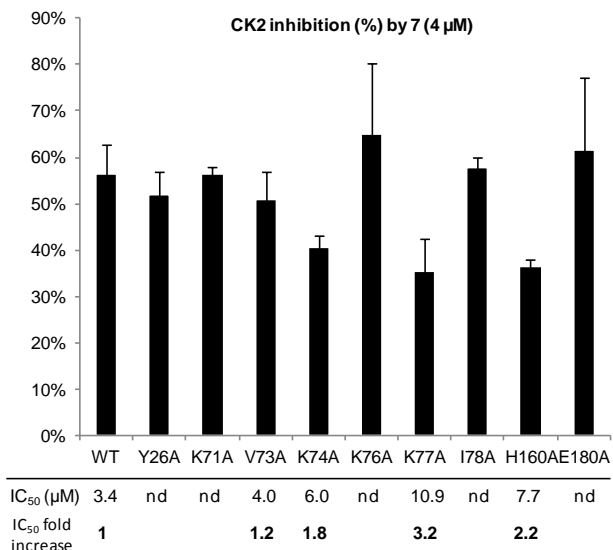


Figure 4. Percentage of inhibition of GST-CK2 α wild-type and single alanine mutants in the presence of compound **7** (4 μ M). IC₅₀s were determined for GST-CK2 α wild-type and mutants with reduced sensitivity toward inhibition (S.D. < 20 %). The fold increase in the respective IC₅₀ over that of the wild-type is indicated at the bottom. nd: not determined.

3.1.5 Compounds **5** and **7** induce a thermal destabilization of CK2 α

Binding of the allosteric inhibitor was expected to stabilize a conformation in which the interactions between Tyr50 and Lys74/77 do no longer link the glycine-rich loop with the α C-helix, thereby leading to an increase in the glycine-rich loop flexibility. Hence we hypothesized that the inactive conformation stabilized by our inhibitors might be less protected against thermal denaturation than the apo enzyme or the complex with ATP binding site-directed compounds. Indeed, using CD spectroscopy to monitor the transition to the unfolded state, we observed a clear reduction of the melting temperature (T_m) in the presence of compounds **5** or **7** compared with the enzyme alone (Table 1). In contrast, the ATP-competitive reference compound CX-4945 stabilized the protein structure, resulting in an increased T_m . An enhancement of the thermal stability was consistently reported for small ligands targeting the ATP binding site, comprising the classical ATP-competitive inhibitors but also the so-called type II inhibitors, which induce a local conformational change involving the DFG-motif – although not many thermal shift assay data are available in the latter case.^{219,220} Hence, the differential effect of our compounds was a further hint that they were not directed to the ATP-binding site.

Table 1. Unfolding temperatures of CK2 α in the presence of compound **5**, **7** or CX-4945 as monitored by TdCD.

Sample	T_m (°C)
CK2 α	53.2 (\pm 0.3)
CK2 α + 5 (50 μ M)	50.3 (\pm 0.3)
CK2 α + 7 (6.25 μ M) ^a	52.0 (\pm 0.2)
CK2 α + CX-4945 (6.25 μ M) ^a	55.4 (\pm 0.2)

The midpoint unfolding temperatures (T_m) shown are averages of three independent experiments (\pm S.D.). The CK2 α concentration was 5 μ M. ^aConcentrations were limited by the compound solubility in methanol.

3.1.6 The binding sites of compound **5** and the ATP-competitive inhibitor CX-4945 do not overlap

To provide further evidence for a binding of our compounds to an alternative, allosteric pocket, we performed binding NMR experiments, which permit to analyze binding events in solution. Compound **5** was chosen for Saturation Transfer Difference (STD) experiments²²¹ due to its good solubility in water. Competition experiments between compounds **5** and CX-4945 revealed that they could bind simultaneously to CK2 α , proving that they were addressing two distinct binding sites (Figure 5A). By comparison, further STD experiments showed that the 7-azaindole, a fragment substructure known to bind the ATP-site of kinases, did not interact with CK2 α in the presence of CX-4945 (Supplementary Figure S2).

STD experiments can also discriminate protons of the inhibitor buried in the protein structure from protons of the compound exposed to the solvent, permitting the so-called STD-based epitope mapping.²²¹ Hence, STD factors were calculated for the different protons of compound **5**. Clearly, the benzoic acid moiety was found to be exposed to the solvent, as indicated by weak STD factors, while the remaining proton of the thiazole and the proton at position 10 of the adjacent phenyl ring displayed larger STD factors, indicating that these molecule parts were fully buried in the CK2 α structure (Figure 5B-C).

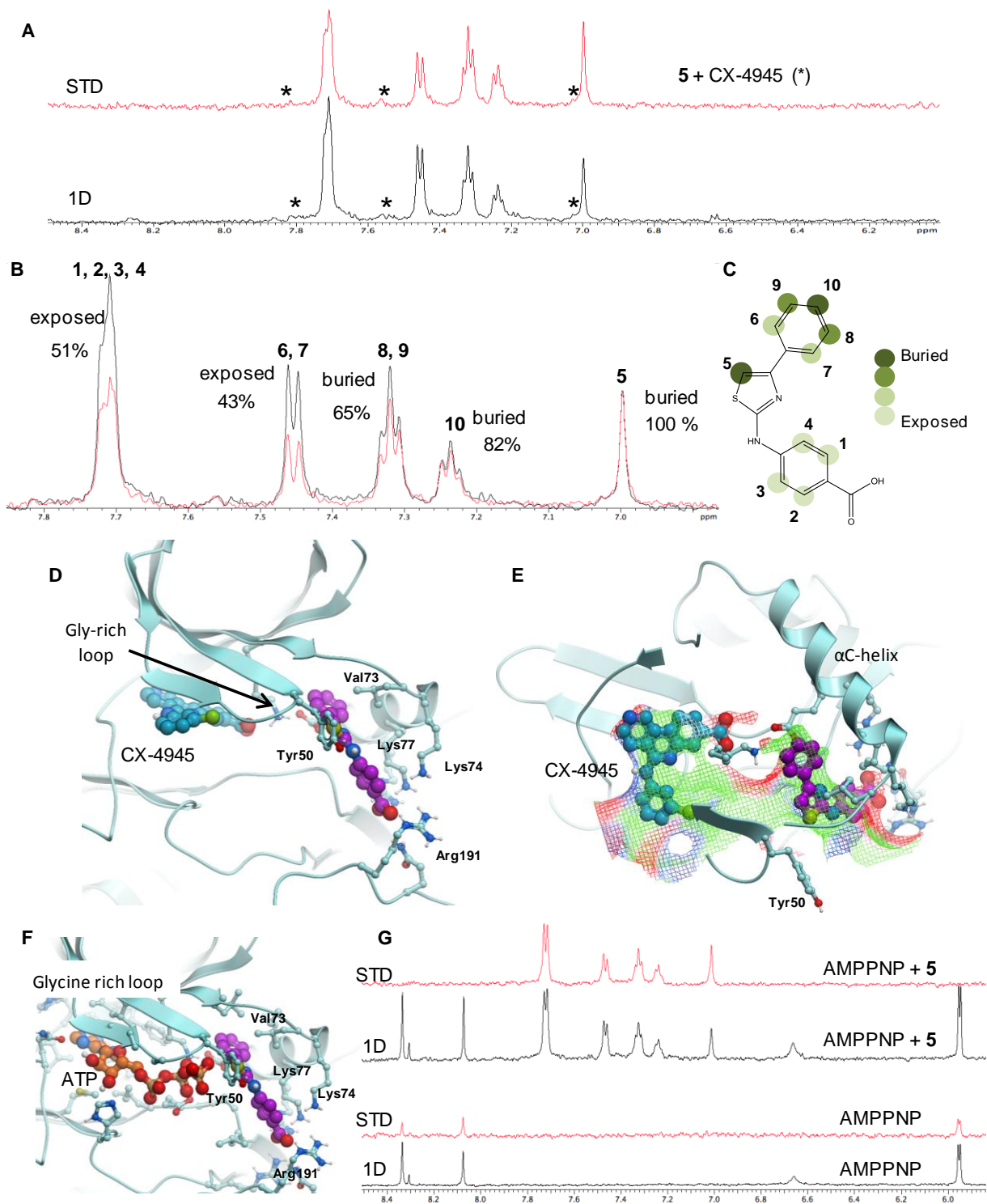


Figure 5. STD-based evidence for the simultaneous binding of compounds **5** and CX-4945, epitope mapping for compound **5** and correlation with the docking model. **A.** 1D (black) and STD (red) NMR experiments of compound **5** (500 μM , approx. $700 \times K_i$) recorded in the presence of the kinase inhibitor CX-4945 (100 μM , approx. $10^5 \times K_i$) with 5 μM CK2 α , showing that CX-4945

does not displace compound **5** binding. **B.** The STD factors measured for compound **5** upon binding to CK2 α are indicated for the different protons as observed in the $^1\text{H-NMR}$ spectrum. **C.** Representation of the STD factors with a green scale on the chemical structure of **5**. **D.** Double docking poses of compound **5** (magenta, in the putative allosteric pocket) and CX-4945 (blue, in the ATP-binding pocket). Residues interacting with compound **5** are depicted and named, except for Arg80, which is hidden by compound **5**. **E.** Top view of the double docking poses of compound **5** and CX-4945. The mesh represents the so-called Lee-Richards surface ²²²: the imaginary surface where ligand atom centers should be placed for optimal interactions with the receptor; it is colored by preferred ligand atom properties, with green, white, red, and blue standing for aliphatic, aromatic, H-bond acceptor and H-bond donor, respectively. **F.** 3D docking model of ATP and **5** simultaneously bound to CK2 α (PDB: 1JUH). The proximity between ligands is energetically unfavorable. Accordingly, the docking score for compound **5** in the presence of bound ATP (-28.64 ICM score units) was much less favorable than its score in the absence of ATP (-37.42 ICM score units). **G.** Binding of AMP-PNP to CK2 α . 1D (black) and STD (red) NMR experiments of AMP-PNP (500 μM) is shown in the absence and in the presence of compound **5** (500 μM) with 5 μM CK2 α . The binding of compound **5** prevents the interaction of AMP-PNP with CK2 α .

3.1.7 *In silico* prediction of the binding mode

To obtain more detailed insight in the binding mode of the CK2 inhibitors, we performed docking simulations using the coordinates of PDB entries 3JUH and 3FWQ. The backbone conformation of the CK2 α structure in 3JUH³³ was found to be most compatible with the proposed mode of interaction. Hence, the final docking model was prepared from this structure by reverting Val66Ala and Met163Leu mutations in the ATP binding pocket of the crystal structure back to their wild-type amino-acids, followed by a conformational refinement of the side chains near the proposed pocket in the presence of the docked compounds.

Compounds **1–7** were docked into this final model, alone and in combination with either ATP or CX-4945. A representative docking pose for compound **5** is depicted in Figure 5D-E. Interestingly, the predicted binding modes of all compounds **1–7** did not differ between the apo- and CX-4945-bound CK2 α . In all cases, basic residues in the $\alpha\text{C-helix}$ (Lys74, Lys77 and Arg80) and the activation segment (Arg191) were found to coordinate the carboxyl-substituted phenyl ring of the compounds *via* a network of favorable hydrogen bonds and salt bridges. The overall binding model was consistent with the SAR and the pattern of exposed/buried protons as determined by the STD-NMR (cf. Figure 5B-C). Furthermore, the decreased sensitivity of the K74A

and K77A mutants toward the inhibitor (Figure 4) was in full accordance with a role for the α C-helix and the activation segment in binding the carboxylate; however, the decreased sensitivity of the H160A mutant could not be explained by a direct contact with the inhibitor. It is conceivable that, in this mutant, the formation of the allosteric pocket might be impeded, thus increasing the energetic barrier for inhibition by our compound.

While the conformation of the protein structure model based on PDB entry 3JUH was compatible with a simultaneous docking of CX-4945 and either of the compounds **1-7**, docking of ATP was only successful with the apo-model; when attempted in the presence of either of the docked compounds **1-7**, a minor steric clash occurred with the terminal phosphate group of ATP (Figure 5F). The latter was consistent with the prevention of AMP-PNP binding in the presence of **5** as observed in the STD-NMR (Figure 5G).

3.1.8 Compound 7 retains its cell-free potency in cell-based CK2 inhibition assays

As mentioned above, dysregulated CK2 is considered as pro-oncogenic and was validated as a pharmaceutical target for anti-cancer therapies ⁶⁶. Specifically, the importance of CK2 activity for the development of clear-cell renal cell carcinomas (ccRCCs) has been described recently ⁶⁰. Therefore, the ccRCC cell line 786-O was chosen as an *in vitro* model to evaluate the anti-cancer activity of compounds **1-7**. In the cytotoxicity assay, all of the compounds affected the cell viability after a 24 h treatment. The most potent inhibitor **7** also effected the strongest reduction in 786-O cell viability (EC_{50} : 25 μ M). This cellular efficacy was remarkable since in the same assay, the canonical ATP-competitive inhibitor CX-4945 exhibited an EC_{50} of 6.1 μ M, reflecting only a 4-fold higher activity than **7** (Figure S3), in spite of its much higher cell-free potency (IC_{50} : 5 nM).

Next, we performed Western Blot analyses to investigate whether CK2 α activity was indeed inhibited by our compounds in living cells. CK2 is responsible for the phosphorylation of α -catenin on residue Ser641,²²³ and Akt1 on residue Ser129.²²⁴ Therefore, these two phospho-acceptor sites were chosen as selective reporters of CK2 cellular activity. After a 24 h treatment of 786-O renal carcinoma cells with compound **7**, a strong decrease in both α -catenin (Ser641) and Akt1 (Ser129) phosphorylation was observed (Figure 6A), confirming that CK2 was a cellular target of this inhibitor. Subsequent dose-response experiments showed that **7** inhibited the phosphorylation of α -catenin (Ser641) and Akt1 (Ser129) with EC_{50} s of 6 μ M and 16 μ M, respectively (Figure 6B). These EC_{50} s were in good agreement with the concentration required to reduce the viability of 786-O cells by half (25 μ M), also arguing that the inhibition of the CK2-dependent signaling was functionally linked to the observed cell death induction. Interestingly,

we noted only a modest 5-fold drop in potency for **7** between the cell-free assay (IC_{50} : 3.4 μ M) and the suppression of Akt phosphorylation in living cells (EC_{50} : 16 μ M). In comparison, the reference compound CX-4945 exhibited a cell-free potency of 5 nM and a cellular efficacy of 1 μ M for both substrates (Figure S6), indicating a striking 200-fold drop in potency. This finding was in accordance with the distinct mechanism of action identified for **7**. As indicated by its observed mixed-type of mechanism for CK2 inhibition, this compound did not directly compete with ATP. Therefore the high cellular ATP concentration should not affect the binding of **7** to CK2 α to the same degree as would be expected for CX-4945.

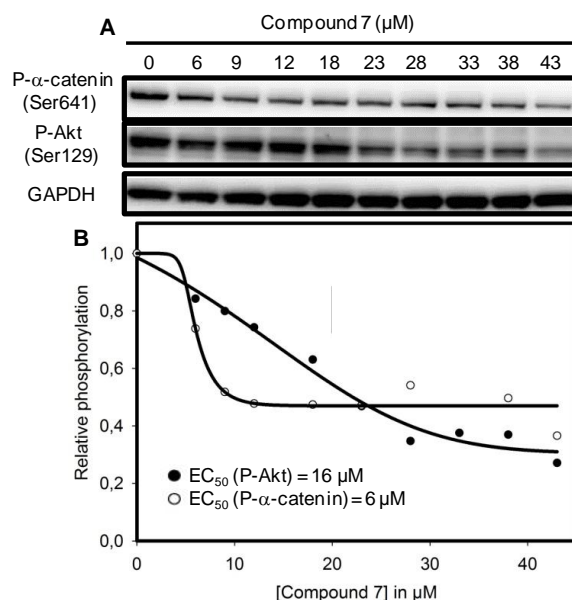


Figure 6. Inhibition of cellular CK2 activity by compound **7**. **A.** 786-O cells were incubated with various concentrations of **7** for 24h, and the phosphorylation status of two protein substrates of CK2 was measured by Western Blot analysis of the cell extracts. GAPDH was probed as loading control. **B.** Western Blot quantification was performed using ImageJ and fitted to a sigmoid equation using SigmaPlot to determine the EC_{50} s.

3.1.9 The inhibition of CK2 activity by compound **7** is substrate-dependent

It was intriguing that compound **7** exhibited a small but reproducible difference in the potency to inhibit the substrate phosphorylations of α -catenin (IC_{50} : 6 μ M) vs. Akt1 (IC_{50} : 16 μ M), a feature which was not seen in the case of CX-4945. Hence we aimed at corroborating this observation by analyzing the phosphorylation of further known CK2 protein substrates, using defined cell-free conditions (Figure 7A). Compound **7** inhibited Six1 phosphorylation and CK2 β

autophosphorylation with the same efficacy as the canonical peptide substrate used in the previous dose–response assay (IC_{50} : 3.4 μ M). However, a striking 10-fold difference was observed for the phosphorylation of nucleolin (IC_{50} : 42 μ M). In contrast, CX-4945 inhibited the phosphorylation of nucleolin with about the same potency as that of other protein substrates and the peptide substrate (IC_{50} : 5 nM). This result suggested that the efficacy of compound **7** to inhibit CK2 activity depends on the protein substrate.

Nucleolin is an abundant nucleolar protein known to bind to CK2 α with very high affinity.²²⁵ Due to this complex formation, a significant portion of CK2 α in growing cells is usually concentrated in the nucleoli²²⁶. CK2 phosphorylates the bipartite nuclear localization signal near the N-terminus of nucleolin, thus promoting its nuclear translocation.²²⁷ In consequence, the phosphorylation status of the CK2 phospho-acceptor site in nucleolin is expected to determine the subcellular localization of the high-affinity complex, which can be monitored by a fluorescent label. Using an EGFP-CK2 α construct, we analyzed whether compound **7** and CX-4945 differently influence the subcellular localization of CK2 α in 786-O renal cancer cells. Indeed, we found that CX-4945 induced a significant translocation of EGFP-CK2 α from the nucleoli to the nuclear matrix and the cytoplasm compartments (Figure 7B), whereas compound **7** was without visible effect. These results were consistent with the observed potency differences of compound **7** and CX-4945 with respect to the inhibition of nucleolin phosphorylation. Thus, the alternative mode of action of **7**, that rendered its potency substrate–dependent, further translated to a different impact on the subcellular localization pattern of high affinity CK2 α /substrate complexes when compared with the ATP-competitive inhibitor CX-4945.

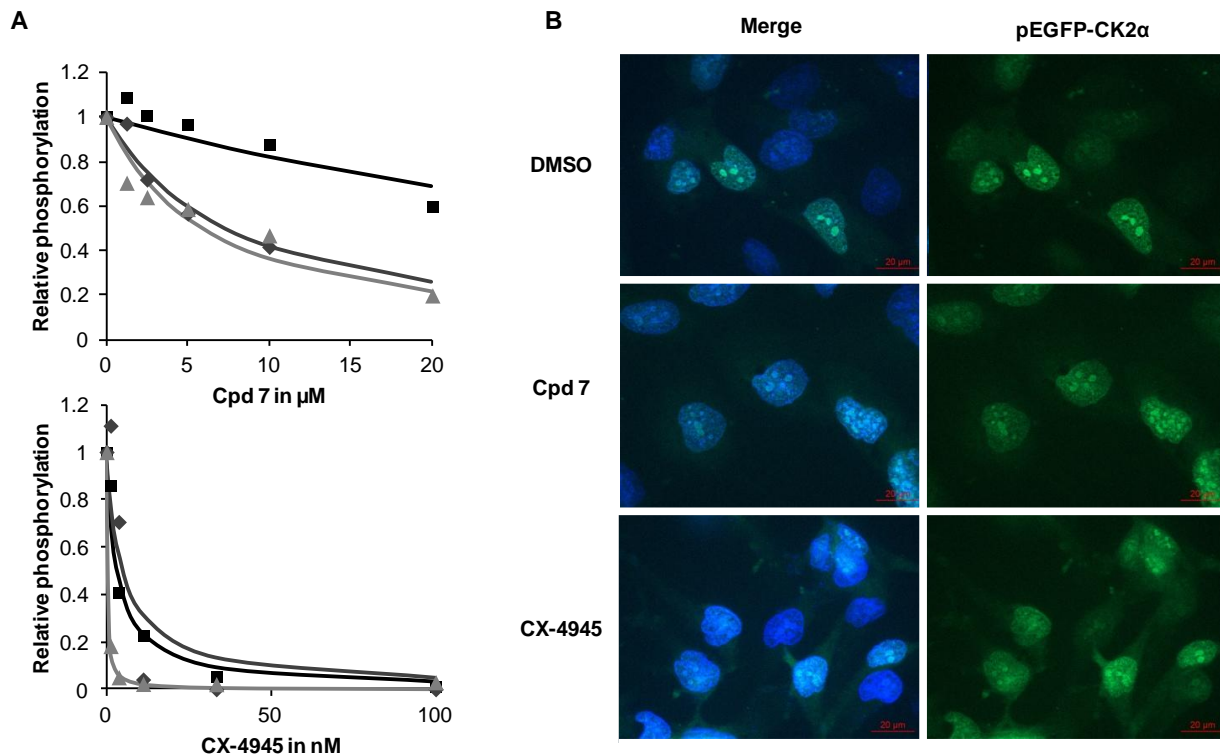


Figure 7. Cellular consequences of the stabilization of the CK2 α inactive conformation. **A.** Protein substrates phosphorylation (■ nucleolin, ▲ Six1, ◆ CK2 β auto-phosphorylation) by CK2 $\alpha_2\beta_2$ in presence of various concentration of compound **7** (upper panel) or the ATP-competitive inhibitor, CX-4945 (under panel). Graphs represent the average of two measurements. **B.** 786-O pEGFP-CK2 α cell imaging showing the subcellular localization of CK2 α after 12h treatment with DMSO, compound **7** (40 μM) or CX-4945 (8 μM). Nuclei were stained with Hoechst-33342 and merged images as well as GFP single channel were depicted for clarity.

3.1.10 Conclusion

CK2 is of main interest in cancer treatment because of its implication in promoting cancer development,⁶⁶ in drug resistances⁷⁰ and in epithelial plasticity.²²⁸ However, only one CK2 inhibitor, CX-4945, entered clinical trials up to now.⁹² The vast majority of CK2 inhibitors developed so far was directed against the ATP binding site, entailing insufficient selectivity and cellular activity in many cases.^{103,229} Even with CX-4945, selectivity issues arise⁹⁹. To date, very few studies described alternative strategies for the pharmacological inhibition of CK2, and none of them presented drug-like small molecules.^{150–152,230} Herein, we have provided first evidence for the existence of an alternative binding pocket, distinct from the conserved ATP-site, which can

accommodate small drug-like molecules. We have also proven that binding affinities sufficient to impart efficient CK2 inhibition can be achieved. Based on single mutation scanning and STD-NMR experiments, also supported by *in silico* studies, the small molecules described in this paper were predicted to bind to an allosteric pocket localized at the interface between the glycine-rich loop and the α C-helix. Notably, the position of the allosteric pocket described here partially superimposes with that of the previously discovered alternative binding pocket in the MAP kinases MEK1 and -2 (data not shown)¹⁴³. However, an α C-helix displacement was clearly observed upon allosteric inhibitor binding in the MEK pocket whereas the rigidity of this helix in CK2a prevents a significant displacement. In the case of CK2a, it is more likely that the glycine-rich loop is the mobile part during pocket opening. Nevertheless, based on structural similarities, the identification of this allosteric pocket on the constitutively active CK2a supports the possible existence of a comparable pocket in other related kinases.^{148,231}

Our STD-NMR experiments revealed that binding of the ATP analog AMP-PNP was prevented in the presence of the 2-aminothiazole derivative **5**. This might be explained by a partial direct competition of AMP-PNP – and analogously of ATP as well – with the small ligand. The docking result depicted in Figure 5F demonstrates that compound **5** would come rather close to the terminal phosphate moiety of theoretically bound ATP. Alternatively, the available crystal structures 3JUH and 3FWQ support the idea that upon binding of the 2-aminothiazole derivatives, the glycine-rich loop might switch to a conformation not compatible with binding of the terminal ATP phosphate moiety.^{149,218} The resulting allosteric down-regulation of ATP binding is also in keeping with the data from the STD-NMR and, importantly, also from the enzyme kinetics analysis. The latter showed a mixed-type of inhibition toward ATP with an increase in K_m and a decrease in V_{max} , suggesting that the inhibitors stabilize a less productive conformation, thus causing a decrease in the apparent affinity for ATP. In consequence, a truly allosteric mechanism of inhibition is more likely to be the prevailing mechanism of action of our compounds (Figure S5). This view also supported by the cellular experiments, which revealed for compound **7** only a low drop of potency in cells (EC_{50} (α -catenin phosphorylation): 6 μ M) compared with the cell-free assay (IC_{50} : 3.4 μ M). Considering the high intracellular levels of ATP in the mM range, the noticeable retention of activity of **7** suggests that at least in cells, (partial) ATP competitive mechanisms cannot play a major role. It is noteworthy that a similar outcome had been observed with CI-1040, a highly selective and non-ATP competitive inhibitor of MEK1/2, that showed a ratio of about 5 to 6-fold between enzymatic potency (IC_{50} = 17 nM) and cellular efficacy (EC_{50} = 100 nM).^{141,232} For classical ATP-competitive inhibitors, the commonly observed ratio is much higher (in the 100-fold range), depending on the K_m of the respective kinase for

ATP.¹¹ Hence, the alternate mechanism of inhibition may provide an advantage for *in vivo* applications of future optimized derivatives of **7**.

Proteins and among them protein kinases are regulated through various conformational changes. In solution, an equilibrium between various conformations is observed and some of them could be stabilized by ligand binding, leading to a conformational selection.^{233,234} CK2 α was considered as a constitutively active protein kinase since decades.³⁰ Given that more than 300 proteins were identified as potential substrates of this kinase, it is fair to ask how the catalytic activity towards these numerous substrates is regulated.²⁷ Although CK2 β was found to modulate substrate specificity of the catalytic subunit upon complex formation,⁷⁷ it is unlikely that this is the only physiological mechanism of controlling the CK2 activity.²¹² Raaf et al. (2009) solved by X-ray crystallography an inactive conformation of CK2 α , which displayed a putative allosteric pocket in the region we mapped as the interaction site; however, no evidence could be provided that such an inactive state exists *in vivo*.¹⁴⁹ Altogether, the results presented herein provide evidence that CK2 α does not exclusively exist in a "switch on" state but can adopt an inactive conformation, which can be stabilized by binding of our compounds, and which may resemble the inactive state of CK2 α observed in the mentioned crystal structure. Furthermore, our results obtained both in cell-free and cellular assays demonstrated that the inhibitory efficacy of our allosteric modulators was substrate-dependent, suggesting that some substrates may affect - by physical interaction with CK2 α - the compound's ability to stabilize a catalytically inactive conformation. Therefore, the compounds described herein could be considered as the first substrate-selective modulators of cellular CK2 activity, clearly differing from the common total CK2 inhibitors. Nevertheless, compound **7** effected growth inhibition of tumor cells *in vitro*, even though - in contrast to CX-4945 - its potency to suppress specific phosphorylations may vary depending on the protein substrate.

In conclusion, our compounds are useful as probes to investigate how the modulation of CK2 conformational states may contribute to the regulation of the kinase's activity in specific contexts. Also supported by the results from such experiments, our inhibitors may be further developed into drugs targeting pathogenic signaling pathways in specific tumor entities.

Supplementary Figures, Tables and Scheme

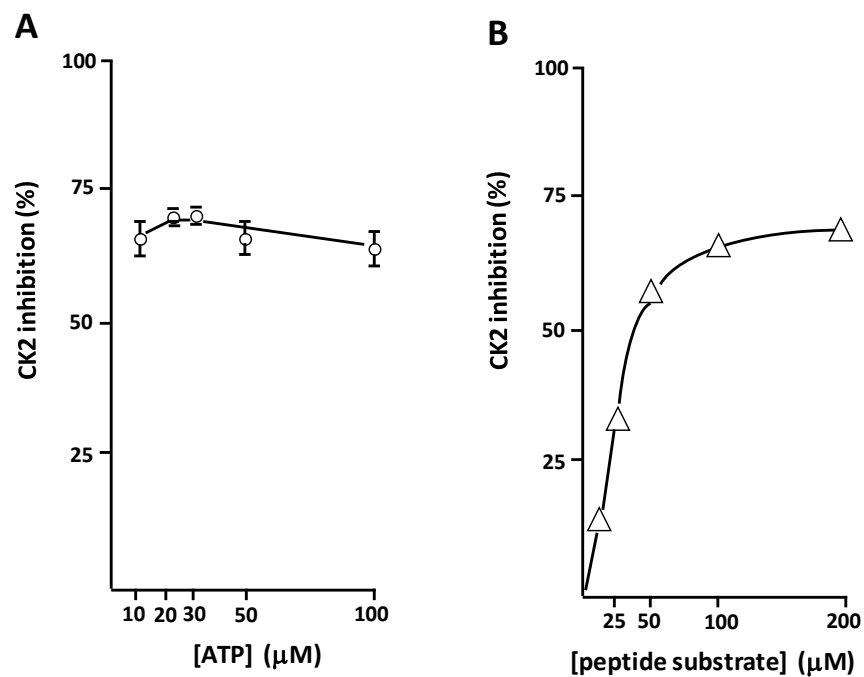


Figure S1. A. Effects of increasing ATP concentrations on the inhibition of CK2a activity by compound **1**. CK2a (20 ng) was incubated with or without 15 μM of **1** after which its activity was assayed with 200 μM of CK2 β -independent peptide substrate in the presence of increasing ATP concentrations. **B.** Effects of increasing peptide substrate concentrations on the inhibition of CK2 activity by **1**. CK2a (20 ng) was incubated with or without 15 μM of **1** after which its activity was assayed with 100 μM ATP in the presence of increasing concentrations of CK2 β -independent peptide substrate.

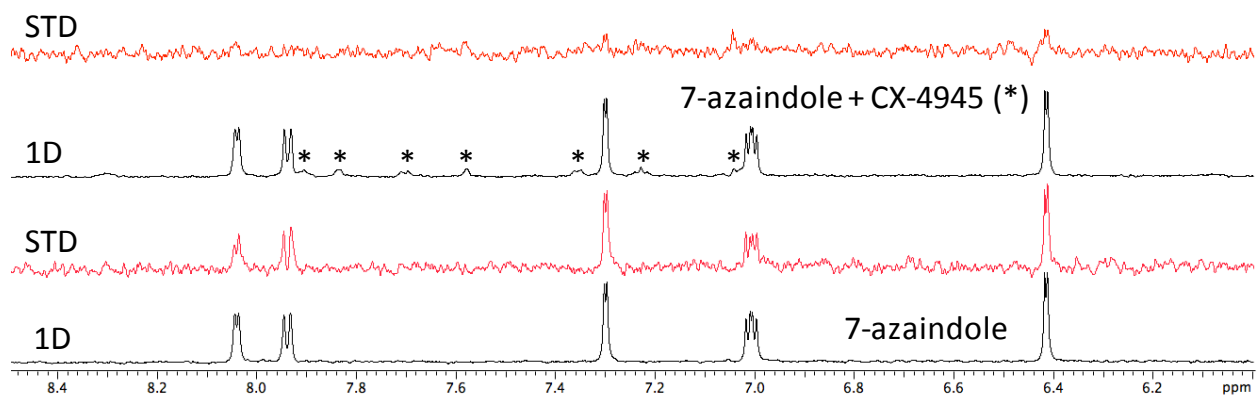


Figure S2. STD NMR experiments for CK2a. 1D (black) and STD (red) NMR experiments of the compound 7-azaindole (500 μM), a small molecule known to target the ATP-binding site of kinases (STD signals with CK2a alone are displayed at the bottom), is displaced by the kinase inhibitor CX-4945 (100 μM) (STD spectrum at the top).

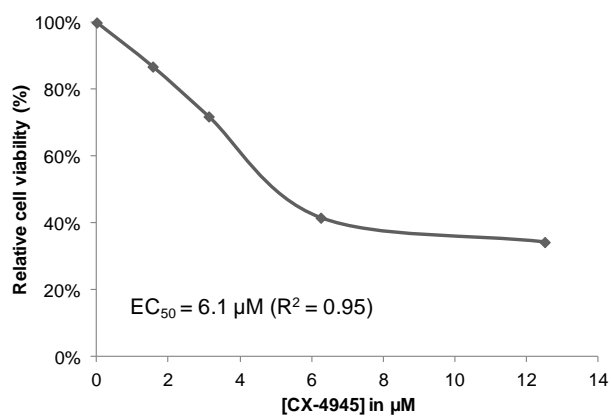


Figure S3. 786-O cells viability in presence of various CX-4945 concentrations. EC_{50} was determined by linear interpolation after transformation to $\log[c]$ scale.

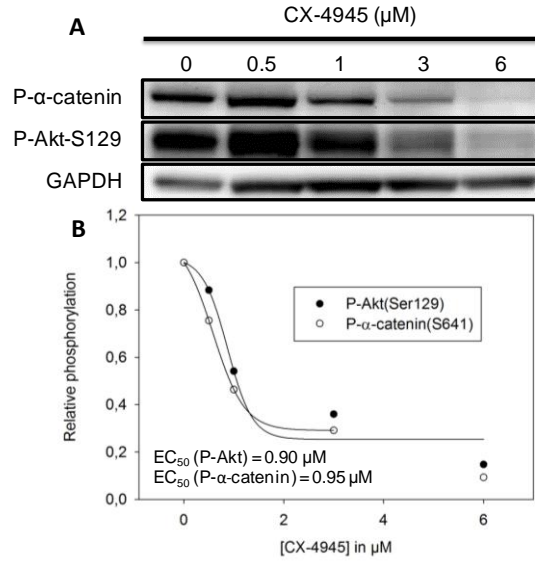


Figure S4. Inhibition of cellular CK2 activity by CX-4945. **A.** 786-O cells were plated and incubated for 24 h with various concentrations of CX-4945. The phosphorylation status of two protein substrates of CK2 was then measured by Western Blot analysis of the cell extracts. Anti-GAPDH was used as loading control. **B.** Western Blot quantification was performed using ImageJ and fitted to a sigmoid equation using SigmaPlot to determine the EC₅₀s.

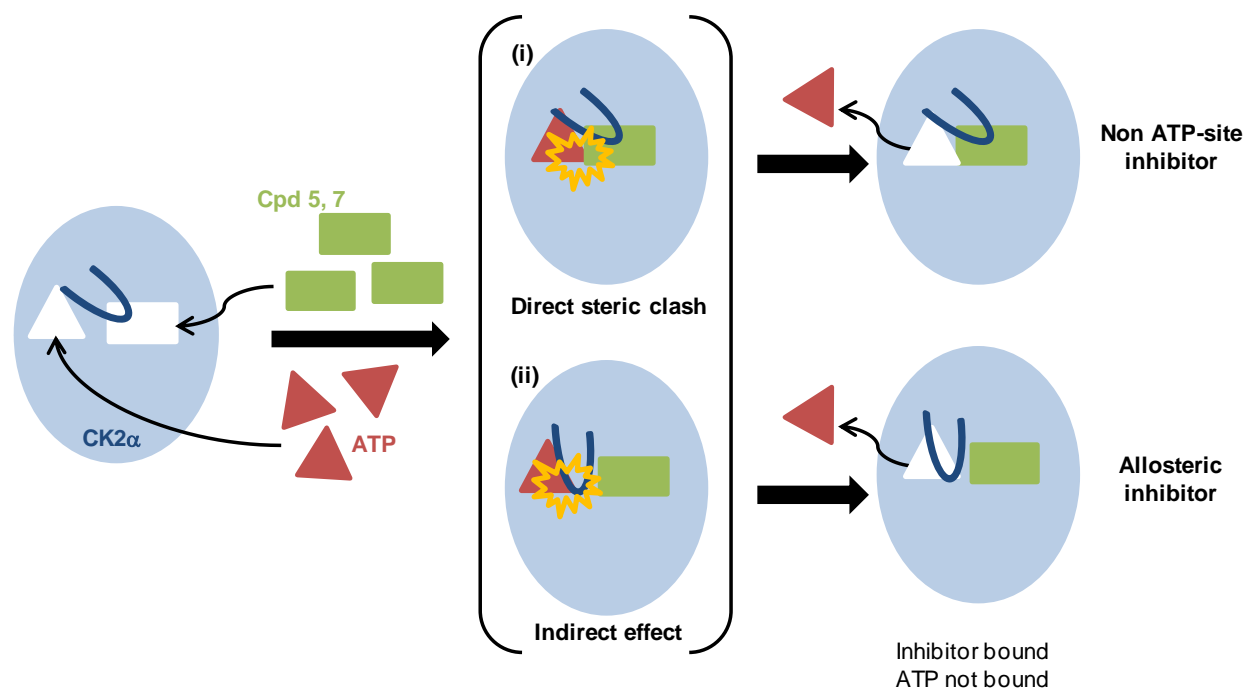


Figure S5. Proposed models of the mechanism of CK2 α inhibition by compounds **5** and **7**. On the left, compounds **5** and **7** bind to CK2 α prior to or after ATP binding. Binding of the small ligands induces a decrease in the V_{max} and an increase in the K_m for ATP (cf. Lineweaver-Burk plot, Figure 2). Also considering the results from the STD-NMR experiments (cf. Figures 5), two alternative mechanisms are consistent with this mixed-type inhibition, as illustrated in the middle: (i) a direct, but limited steric clash between ATP and the new compounds, adding a minor competitive proportion to the non-ATP competitive mechanism ("non ATP-site inhibitor"); (ii) binding of new compounds stabilize a conformational deformation of the ATP-binding pocket, which involves a larger movement of the glycine-rich loop (in blue), inducing a decrease in affinity for ATP (indirect effect); this represents a truly allosteric mechanism.

Table S1. Residual kinase activity in the presence of compound **1** at 50 μ M.

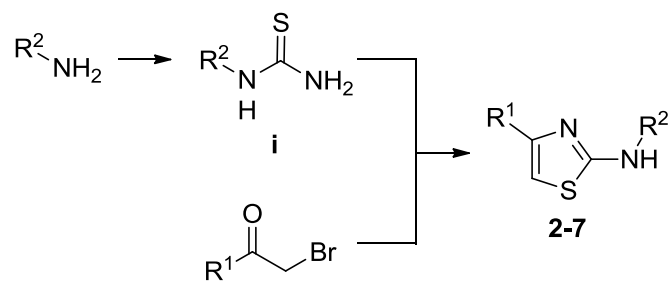
Protein Kinase	Residual activity (%)	Protein Kinase	Residual activity (%)	Protein Kinase	Residual activity (%)	Protein Kinase	Residual activity (%)
CK2 α (h)	0	HIPK2(h)	83	IR(h), activated	93	CaMK1(h)	101
EGFR(h)	26	MAPK1(h)	84	CDK6/cyclinD3(h)	95	CDK2/cyclinE(h)	101
EphA4(h)	45	LKB1(h)	85	cSRC(h)	97	Met(h)	102
Pim-1(h)	46	PKB α (h)	85	FGFR1(h)	97	PAK2(h)	102
MuSK(h)	62	CDK2/cyclinA(h)	86	Fyn(h)	97	IKK α (h)	103
PDGFR α (h)	65	PKC α (h)	86	HIPK1(h)	97	MEK1(h)	103
AMPK α 1(h)	71	cKit(h)	87	HIPK3(h)	98	Abl (h)	104
Aurora-B(h)	74	PKA(h)	87	CDK9/cyclinT1	99	CDK7/cyclinH(h)	104
DYRK2(h)	78	CDK1/cyclinB(h)	89	Rsk1(h)	99	JAK2(h)	104
Aurora-A(h)	79	CHK2(h)	89	ROCK-1(h)	100	Lyn(h)	104
GSK3 β (h)	79	c-RAF(h)	92	Yes(h)	100	mTOR(h)	104

Results were obtained from kinase profiler service offered by Life Technologies with ATP concentration adjusted to the respective K_m of each kinase. Duplicate values did not differ by more than 15 % in all assays.

Table S2. Residual kinase activity in presence of compound **7** at 50 μ M.

Protein Kinase	Residual activity (%)	Protein Kinase	Residual activity (%)	Protein Kinase	Residual activity (%)
EphA4(h)	27	CLK2(h)	67	PKC α (h)	92
GSK3 β (h)	29	Abl(h)	69	MEK1(h)	95
CK1 γ 1(h)	31	CHK2(h)	72	JAK2(h)	98
ACVR1 (ALK2)	34	TBK1	75	MKNK1 (MNK1)	101
CLK4(h)	39	CDK1/cyclinB(h)	78	PDGFR α (h)	102
MLCK (MLCK2)	39	DYRK1a	79	DAPK3	104
STK17A (DRAK1)	48	CLK1(h)	80	EGFR(h)	106
CK2a2	48	HIPK3	82	CDK2/cyclinE(h)	107
GSG2 (HASPIN)	55	CLK3(h)	86	ROCK-1(h)	107
Pim-1(h)	57	RIPK2	86	cKit(h)	116
HIPK2	57	MuSK(h)	90		

Results were obtained from kinase profiler service offered by Life Technologies with ATP concentration adjusted to the respective K_m of each kinase. Duplicate values did not differ by more than 17 % in all assays.



Scheme S1. Synthesis of the aminothiazole **2-7** compounds. Reagents and conditions: a) CS_2 , Et_3N in THF/ H_2O , RT, 24 h, then I_2 in THF, $0\text{ }^\circ C$ to RT, 3 h b) NH_4OH 30 %, RT, 6 h c) EtOH, reflux, 3-12 h.

3.2 2-Aminothiazole derivatives as potent and selective allosteric modulators of the protein kinase CK2

Protein kinase CK2 is an ubiquitous protein Ser/Thr kinase involved in cancer development. Based on the 4-(4-phenylthiazol-2-ylamino)benzoic acid scaffold, extensive Structure Activity Relationship studies were carried out and led to significant improvement of potency. The non-ATP competitive mechanism of action of the leading compound, 2-hydroxy-4-((4-(naphthalen-2-yl)thiazol-2-yl)amino)benzoic acid (**8e**) was confirmed. In addition, cellular experiments have shown interesting effects for cellular CK2 inhibition and apoptosis induction, in comparison with CX-4945, a phase II clinical trial ATP-competitive CK2 inhibitor. Thus, targeting CK2 in a non-ATP competitive manner leads to *in cellulo* highly efficient compounds with interesting perspectives for further *in vivo* developments.

3.2.1 Scientific rationale

Tumor development could rely on deregulated oncogenes but also on deregulated non-oncogenes.²⁰⁸ Indeed, several proteins sustain tumor development, even if they are not the primary cause of the cancer. In this context, CK2 plays a central role as several studies revealed its implication as a cancer driver.⁶⁶ CK2 overexpression has been widely correlated with a poor prognosis for patient in prostate cancer⁵⁴, breast carcinoma⁵⁶, glioblastoma⁵⁸, gastric carcinoma²³⁵ or renal cell carcinoma.⁶⁰ Indeed, CK2 acts as a major support to pro-survival and anti-apoptotic signals by interfering with NF- κ B, Wnt and Akt pathways.⁶⁶ Thus, CK2 overexpression supports a favorable environment for cancer development described as the "hallmarks of cancer".^{4,5,236}

CK2 is a ubiquitous Ser/Thr protein kinase composed of a dimer of regulatory subunits (β) and two catalytic subunits, CK2 α and/or CK2 α' .²⁸ The catalytic subunit of CK2 is constitutively active, while the regulatory subunit modulates the selectivity toward a subset of substrate proteins.⁷⁷

CK2 inhibition has been proved to be a valuable strategy to fight cancer and several inhibitors have been developed, among which CX-4945 (5-(3-chlorophenylamino)benzo[c][2,6]naphthyridine-8-carboxylic acid, silmitasertib).²⁰⁹ This ATP-competitive inhibitor of CK2 is the most promising molecule. Developed by Cylene Pharmaceuticals, this compound is a highly potent (IC_{50} = 14 nM) and selective (Gini coefficient⁹⁸

= 0.67) inhibitor of CK2 α with a good efficiency in cellular experiments. Besides, in mice xenografts models, tumor regression was observed upon CX-4945 treatment.^{92,97} Looking for splicing regulation through phosphorylation of serine/arginine rich (SR) proteins, Kim *et al.* revealed a special CK2-independent implication of CX-4945 in cellular regulation of SR protein phosphorylation.⁹⁹ Indeed, this compound was found to be a strong inhibitor of Cdc2-like kinase-2 (Clk-2) (IC₅₀ = 4 nM), almost four-fold more potent than on CK2 α (IC₅₀ = 14 nM).⁹⁹ Although the consequences in splicing regulation remain elusive, this off-target activity of silmitasertib underlines the need for potent and more selective CK2 inhibitors.

Recently, 2-aminothiazole derivatives **1-3** (Figure 1) were identified as non-ATP competitive inhibitors of CK2 α . A complete study allowed us to determine the allosteric mechanism of action of these molecules: (i) A simultaneous binding of compound **2** and of the ATP-competitive inhibitor CX-4945 was observed by STD-NMR experiments; (ii) The unfolding temperature of GST-CK2 α monitored by CD spectrometry decreased upon compound **2** or **3** binding whereas an increase was observed in the presence of CX-4945; (iii) Single mutation scanning coupled with extensive molecular modeling studies have led to the identification of an 2-aminothiazole binding site, at the interface of the flexible glycine-rich loop, the α C-helix, the third β -strand of the N-terminal lobe and the activation loop. The allosteric pocket was defined by residues Tyr50, Leu70, Val73, Lys74, Lys77, Arg80 and Arg191. These findings emphasize the specificity of such mechanism of CK2 inhibition by this class of compounds.

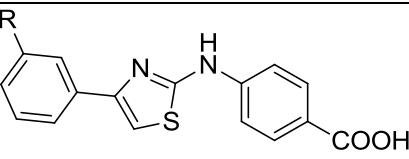
		
Cpd	R	IC ₅₀ (CK2 α) in μ M
1	NO ₂	7
2	H	9
3	Br	3.4

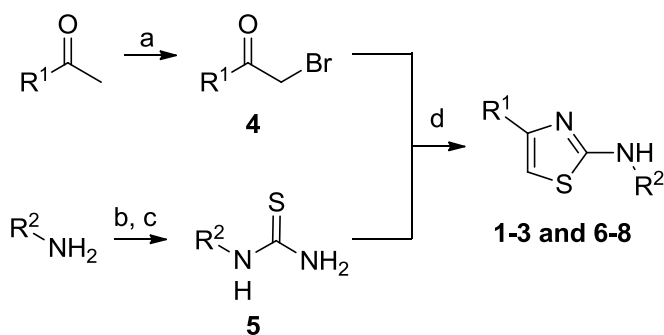
Figure 1. Chemical structures of three allosteric inhibitors previously described (S.D. < 20 %). (chapter 3.1)

3.2.2 Chemistry

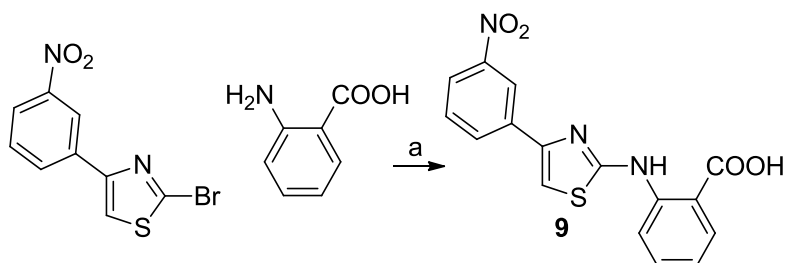
Aminothiazoles core were prepared according to Hantzsch-type syntheses from 2-bromoacetophenones and thiourea intermediates (Scheme 1). Most of the 2-bromoacetophenones **4** were commercially available or easily prepared (**4a-c**) from commercially available acetophenones through a bromination step, as described in the literature.^{237,238} Thioureas **5** were obtained after reaction of isothiocyanate intermediates with ammonia solution. The latter were synthesized after reaction of the primary amine of aniline derivatives with carbon disulfide, in presence of triethylamine, followed by iodine oxidation.²³⁹ Hantzsch syntheses were carried out in ethanol and the resulting products were directly obtained as solids, after their precipitation with water. Semi-preparative HPLC, recrystallization, or washing procedures led to the final products with a LC-UV (254 nm) purity higher than 95%. In some cases, ethyl ester derivatives were obtained instead of the free carboxylic acids. Then, a saponification step with NaOH was carried out to obtain the desired products **6c** and **7g**.

Compound **9** could not be obtained through Hantzsch-type synthesis, maybe due to the spatial proximity between the primary amine and the carboxylic acid of 2-aminobenzoic acid, which prevents the formation of the isothiocyanate intermediate. Consequently, a nucleophilic substitution between 2-bromo-4-(3-nitrophenyl)thiazole and 2-aminobenzoic acid in hydrochloric acid was performed to obtain the desired 2-((4-(3-nitrophenyl)thiazol-2-yl)amino)benzoic acid (**9**) albeit in a low 2% yield (Scheme 2).

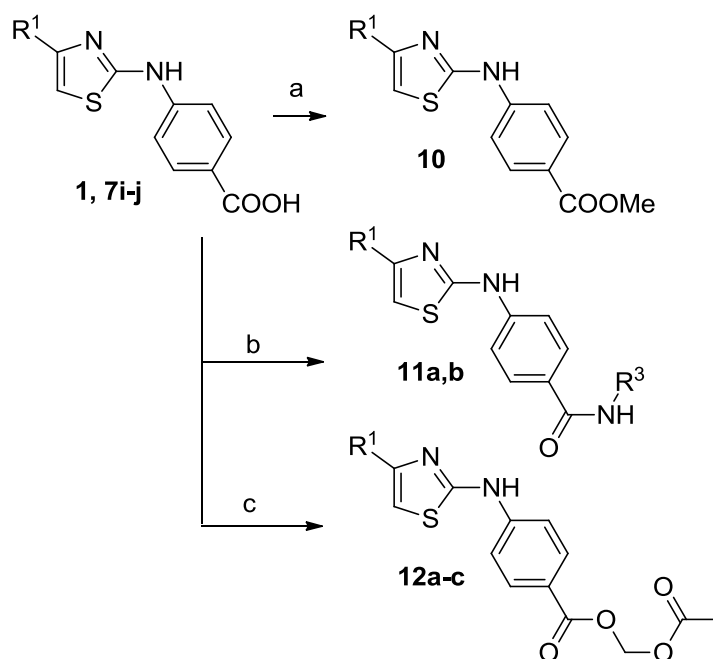
Several modifications were considered on the carboxylic acid function (Scheme 3). Methyl ester derivative **10** was easily obtained through a classical acidic esterification step. Sulfonamide derivatives **11a-b** were obtained according to amino-acid coupling procedures whereas acetoxymethyl prodrugs **12a-c** were accessed from carboxylic acid derivatives (**1** or **7i-j**) and bromomethyl acetate through a previously described method.²⁴⁰



Scheme 1. Hantzsch-type synthesis. Reagents and conditions: a) Br₂, CHCl₃, 40°C, 5 min or Br₂, HBr 32% in AcOH, MeOH, 60°C, 4h. b) CS₂, Et₃N in THF/H₂O 1/1, RT, 24h, then I₂ in THF, 0°C to RT, 3h. c) NH₄OH 30%, RT, 6h. d) EtOH, reflux, 3-12h.



Scheme 2. Preparation of compound **9** through aromatic nucleophilic substitution. Reagents and conditions: a) HCl_(aq) 37%, 1,4-dioxane, 90°C, 48h.



Scheme 3. Syntheses of esters and amides **10-12**. Reagents and conditions: a) H₂SO₄ 95% 3 drops, MeOH, reflux, 2h. b) **11a**: HATU, DIPEA, dry DMF, 30 min; NaH, RSO₂NH₂, dry THF, RT, 30 min; then RT, 4h. **11b**: EDC, HCl, DMAP, RSO₂NH₂, CH₂Cl₂, RT, 36h. c) Bromomethyl acetate, Et₃N, dry DMF, RT, 12h.

3.2.3 Structure-Activity Relationships

The preliminary Structure-Activity Relationships (SAR) revealed the importance of key features of our diaryl aminothiazole derivatives for CK2 α inhibition (chapter 3.1). Indeed, attempts to remove or to hide (as a methyl ester) the acid function led to totally inactive compounds (Table 1; compounds **6a** and **10**, respectively), underlying the importance of such functional group on the aromatic ring. Consequently, we envisaged the evaluation of several analogs sharing the 3-nitrophenyl moiety but with variations of the carboxylic acid part (Table 1). Compound **6b** having this group at position 3 was 4-fold less potent than its *para* regioisomer **1**. However, when the carboxylic acid functional group was displaced in position 2 (derivative **9**) we observed a similar range of efficiency than the parent compound **1**. Compound **6c** with two carboxylic acid functions in *meta* positions was also prepared but its very low solubility prevented any biological evaluation. Compound **6d** with a phenyl acetic acid moiety was, by far, less efficient on CK2 α than compound **1**, underlining the fact that benzoic acid in position 4 is the best moiety for protein inhibition.

We tried thereafter various modulations on the second aromatic ring while conserving the 4-benzoic acid group for the first one (Table 2). Starting from compound **1** with a 3-nitro substitution on the phenyl moiety, we modulated the electron density of this ring using various substitutions: 3-bromo **3**, 3-methoxy **7a**, 4-methoxy **7b**, 2,4-methoxy **7c**, 2,4-hydroxy **7d**, 2-hydroxy-4-bromo **7e**, pyridin-2-yl **7f** and without any substitution **2**. In these cases, no significant improvement of IC₅₀ was observed, even though hydrophobic substituent such as a bromine atom at position 3 or 4 improved CK2 α inhibition, with IC₅₀ values of 3.4 μ M and 5 μ M (**3** and **7e**, respectively).

The small differences in IC₅₀ values of compounds **1-3** and **7a-f** with these various substitutions prompted us for more drastic structural modifications of the phenyl moiety. Removal of the phenyl ring (**7g**) or its replacement by a non-aromatic bulky *tert*-butyl moiety **7h** resulted in a strong decrease of CK2 α inhibition. On the other hand, replacement of the phenyl ring by a 3-thiophene **7i** improved twice the inhibition of CK2 α (IC₅₀= 5 μ M for **7i**). Moreover, we have observed that a naphthyl ring substitution resulted in a better protein inhibition, with an IC₅₀ value of 3 μ M for compound **7j**. This latter finding is consistent with the requirement of a hydrophobic moiety in this part of the inhibitors, as already noticed with compound **3**.

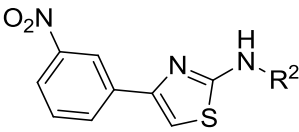
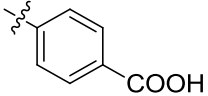
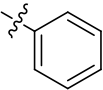
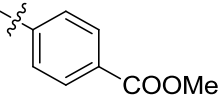
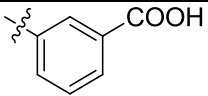
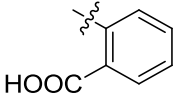
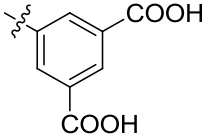
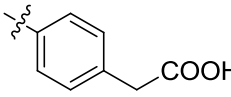
In consequence, several benzoheterocyclic derivatives **7k-m** were synthesized and evaluated. Compound **7k** with a chromene instead of the naphthyl group and compound **7l** containing a 2-benzofuran moiety were less potent than compound **7j**. The promising result obtained with a thiophene substitution (**7i**) suggested us to introduce a 5-benzothiophene substituent, but in this case, no significant improvement of the inhibition of CK2 α was noticed.

Preliminary docking experiments conducted on compounds **1** and **7j** suggested that the size of the naphthyl moiety induces a more constraint binding mode in the allosteric pocket than for compound **1**. In consequence, it seems promising to have a new look on the carboxylic acid substitution on a 4-naphthalen-2-yl-thiazol-2-yl-arylamines. Several derivatives **8a-e** were synthesized (Table 3) and evaluated for their CK2a inhibitory properties. Compounds **8a** without acid function and **8b** with a 4-cyano substitution definitely lacked for CK2a inhibition. However, with the naphthyl substitution in R¹, the carboxylic acid function appears to better increase the potency in position 3 (**8c**) than in position 4 (**7j**). The opposite result was observed in the presence of the 3-nitrophenyl group for R¹ (Table 1; compounds **1** and **6b**). The 6-methoxy-3-benzoic acid analog **8d** exhibited a potency on CK2a similar than the parent compound **8c**. So, results from the SAR studies underlined the need of an acid group in position 3/4 of the phenyl ring and docking results suggested that more interactions between the basic residues (Lys74, Lys77, Arg80 and Arg191) of CK2a and this acidic function could be possible. To increase these interactions, we tried to add on this ring another functional group and a salicylic acid derivative **8e** was considered. This structural modification provided a very good result as the inhibitory properties was five-fold higher (compound **8e** compared to **7j**), as shown by the sub-micromolar IC₅₀ value (IC₅₀ = 0.6 μM for compound **8e**, see Table 3).

Carboxylic acid derivatives could sometimes be a source of troubles for *in vivo* experiments with cell permability issues. To continue the structural exploration, we considered bioisosteric modifications and a prodrug approach. Several compounds were synthesized, deriving from **1**, **7i,j** (Table 4) and compared with *para*-substituted acids **7j** and **8e**. These derivatives might not exhibit better *in vitro* potency but better physicochemical properties, suitable with cellular experiments. Thereby, cell viability experiments were considered as the easiest way to evaluate compound efficiency as CK2 inhibitors induce a decrease in cell viability.^{92,101} Acylsulfonamide derivatives are well known carboxylic acid bioisosteres as they preserve the acidic properties (pK_a ≈ 4-5) but with improved bioavailability.²⁴¹ In our case, two acylsulfonamide derivatives were synthesized and evaluated: methylsulfonamide **11a** and 4-methylbenzenesulfonamide **11b** both exhibited similar *in vitro* potency with a respective 41% and 54% inhibition of CK2a at 10 μM. However, looking at their ability to reduce cell viability, compound **11b** (87% decrease at 25 μM) was by far better than compound **11a** (23% decrease at 25 μM). Moreover, tosyl derivative **11b** was more efficient than the parent compound **7j** (43% decrease in cell viability at 25 μM) and as efficient as the best compound of this series (**8e**, 87% decrease at 25 μM). In order to discriminate these compounds, the Percentage Efficiency Index

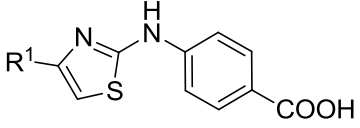
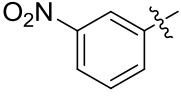
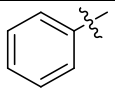
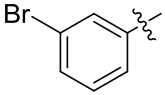
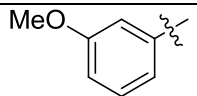
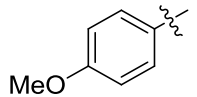
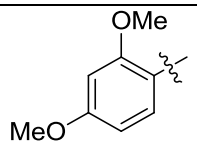
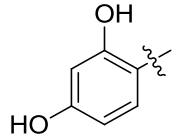
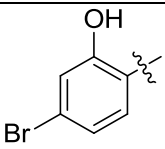
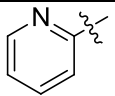
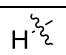
(PEI), which render ligand efficiency as a function of molecular weight,²⁴² was calculated for each molecule (Table 4). This index underlined the predominance of compound **8e** (PEI = 2.6) in comparison with compound **11b** (PEI = 1.1). For two structures having the same cellular efficiency, the one with the lowest molecular weight (**8e**) was considered as the best candidate for further developments. A prodrug strategy using acetoxymethyl ester groups was considered.²⁴⁰ Among the three evaluated derivatives **12a-c**, none of them led to improvement in cellular efficiency (Table 4). Further experiments evaluating the stability of these prodrugs have to be carried out before envisaging new derivatives.


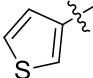
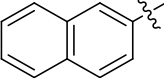
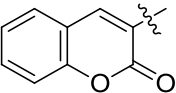
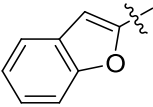
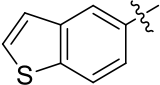
Table 1. Importance of the benzoic acids function on R².

		
Cpd	R ²	IC ₅₀ ^a (μM)
1		7
6a		>25
10		>25
6b		30
9		8
6c		^b
6d		>50

^aIC₅₀ values are the mean of ≥2 experiments with errors within 40% of the mean. ^bSolubility troubles prevent IC₅₀ determination.

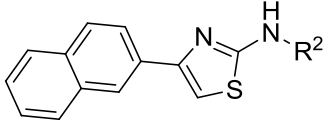
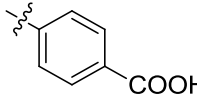
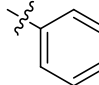
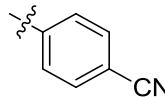
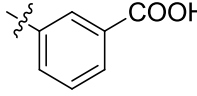
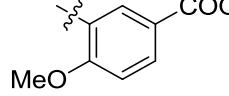
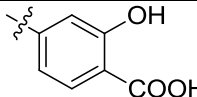
Table 2. SAR studies on hydrophobic ring R¹.

		
Cpd	R ¹	IC ₅₀ ^a (μM)
1		7
2		9
3		3.4
7a		12
7b		6
7c		13
7d		7
7e		5
7f		14
7g		>50

7h		>50
7i		5
7j		3
7k		8
7l		14
7m		4

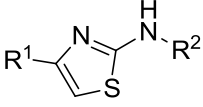
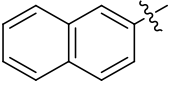
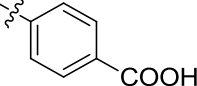
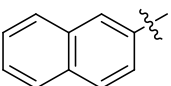
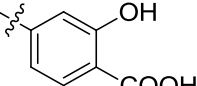
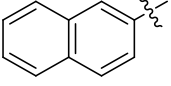
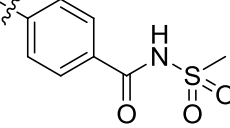
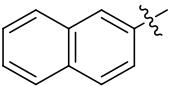
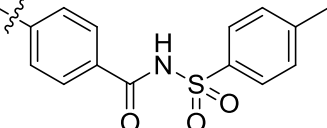
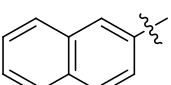
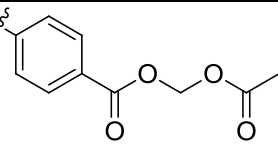
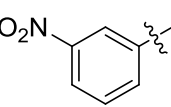
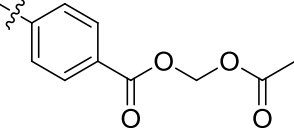
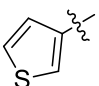
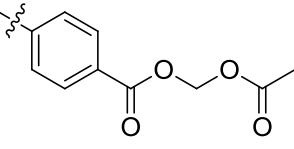
^aIC₅₀ values are the mean of ≥2 experiments with errors within 40% of the mean.

Table 3. Pharmacomodulation studies on 4-naphthalen-2-yl-thiazol-2-yl-arylamine derivatives.

		
Cpd	R ²	IC ₅₀ ^a (μM)
7j		3
8a		>50
8b		>50
8c		2
8d		8
8e		0.6

^aIC₅₀ values are the mean of ≥2 experiments with errors within 40% of the mean.

Table 4. *In vitro* and cellular effects of selected carboxylic acid bioisosteres and prodrugs.

					
Cpd	R ¹	R ²	CK2a inhibition (%) at 10 μM ^a (IC ₅₀ ^b)	PEI ^c	Cell toxicity (% from DMSO) at 25 μM ^d
7j			67 (3)	1.9	43
8e			96 (0.6)	2.6	87
11a			41	1	23
11b			54	1.1	87
12a			41	1	45
12b			7	0.2	42
12c			37	1	48

^aRecombinant CK2a inhibition percentage in presence of 10 μM of corresponding compound.

^bIC₅₀ values are the mean of ≥2 experiments with errors within 40% of the mean. ^cPEI = (%).

inhibition as fraction (0 – 1.0) in presence of 10 μM of corresponding compound) / (molecular weight, kDa).²⁴² d786-O cell toxicity, 24h, 25 μM of respective compound.

3.2.4 Enzymatic characterization of compound **8e** effects on CK2

With this efficient CK2 α inhibitor **8e** in hand, we then wanted to know if its mechanism of action was similar to that of initial compounds described in Figure 1, ie through binding to an allosteric site.

So, to evaluate if this compound exhibits non-ATP competitive behaviors in enzymatic assays, we have performed a Lineweaver-burk plot analysis of CK2 α inhibition by compound **8e**. As illustrated in Figure 2A, a non-ATP competitive mechanism of action, similar to compounds **1-3**, was observed, with a K_i value of 0.18 μM . Then, the effect of compound **8e** was evaluated on CK2 α and on the holoenzyme CK2 $\alpha_2\beta_2$, with a β -independent peptide substrate (peptide 29) and a β -dependent peptide substrate (peptide M) as well. These three experimental conditions displayed similar results, as the potency of **8e** remained constant (Figure 2B): this thereby underlines the ability of **8e** to inhibit CK2 α and the holoenzyme complex with the same potency.

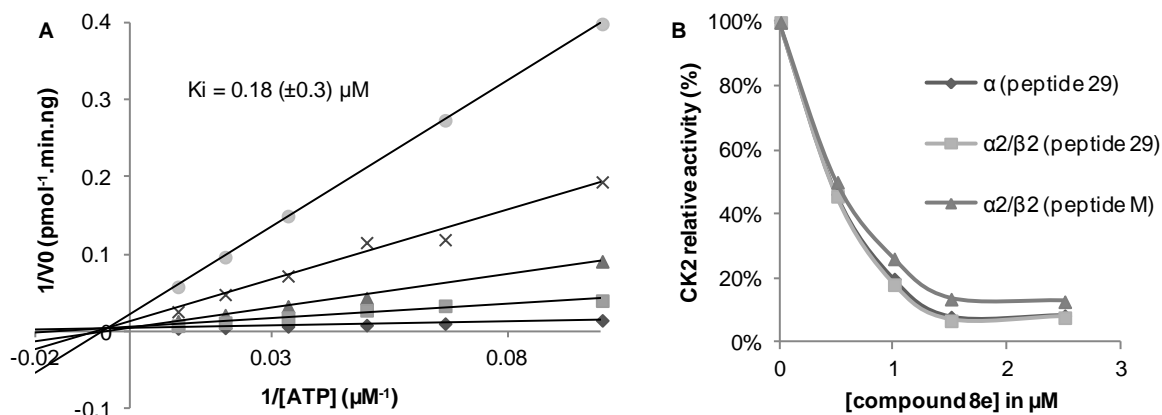


Figure 2. Enzymatic characterization of compound **8e**. **A.** Lineweaver-Burk inhibition plot of human recombinant CK2 α by compound **8e** at various concentrations: 0, 0.5, 1, 1.5, 2.5 μM . K_i was determined by plotting the slopes at varying inhibitor concentration from three independent experiments. **B.** CK2 α and CK2 $\alpha_2\beta_2$ activity with various peptide substrates in presence of increasing concentration of compound **8e**.

3.2.5 Compound **8e** binds to an allosteric pocket of CK2 α

Compound **8e** was screened on a panel of 13 GST-CK2 α mutants, mainly located in the area of the putative binding site described in chapter 3.1. Three mutants were significantly less sensitive toward inhibition by **8e**: Val73Ala, Lys77Ala and His160Ala (Figure 3) and therefore selected for dose response experiments. Compound **8e** IC₅₀ was strongly increased in comparison with the wild-type GST-CK2 α (IC₅₀ = 0.6 μ M), a 2.8-fold increase for Val73Ala (1.7 μ M) was observed, a 4.3-fold increase for Lys77Ala (2.6 μ M) and a 1.7-fold increase for His160Ala (1 μ M).

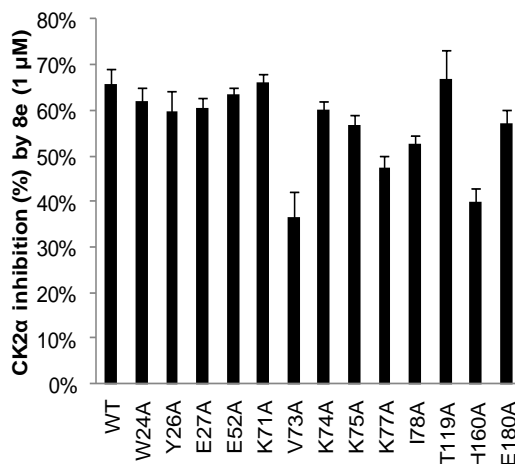


Figure 3. Percentage of inhibition of GST-CK2 α (WT or single alanine mutant) in presence of compound **8e** (1 μ M).

3.2.6 Compound **8e** is a selective inhibitor of CK2

Selectivity among human kinome is an important feature for kinase inhibitors to avoid side effects.^{102,243} Using the Gini coefficient as a reporter of the overall selectivity, it is clear that allosteric inhibitors such as PD184352 (MAPKK1 optimized inhibitor), is more selective (Gini coefficient = 0.91)⁹⁸ than quinalizarin, an optimized ATP-competitive inhibitor of CK2 (Gini coefficient = 0.61).¹⁰¹ Targeting the less conserved allosteric binding site of kinases could be a solution to have a higher selectivity. For our study, compound **8e** was evaluated against a selected panel of 53 kinases (Supplementary Table S1) and only four other kinases, in addition to CK2 α , were inhibited by more than 50%: ErbB2 (70%), Aurora-B (62%), Pim-1 (60%) and PI3K (53%). It was noteworthy that the main off-target of the CX-4945, Clk2, was not inhibited by **8e** and, among the four isoforms of cdc2-like kinases, only Clk4 (23%) was weakly inhibited. Moreover, compound **8e** overall selectivity (Gini coefficient = 0.78) was higher than for CX-4945 (Gini

coefficient = 0.67) and than for other CK2 inhibitors described in the literature.^{97,103}

3.2.7 Inhibition of CK2 cellular activity and apoptosis induction by **8e**

CK2 inhibitors are known to decrease the cell viability^{92,101} and, consequently, the most active compound **8e** was selected for a cell viability screening on nine cell lines, originated from various tissues (Table 5). Among cancer cells, aminothiazole **8e** exhibited GI_{50} values from 5 μM in clear cell renal cell carcinoma (ccRCC) cell line 786-O to 20 μM in prostate cancer cell (DU145). Interestingly, compound **8e** is by far less toxic in non-cancerous (benign) kidney cells (RPTEC) with a GI_{50} 5-fold higher (27 μM) than in kidney cancer cells (786-O). This latter result is consistent with the dependence of cancer cells to a high level of CK2 α expression for their development, as already described.⁶⁶ Of note, CX-4945, the canonical ATP-competitive inhibitor of CK2 α exhibited a GI_{50} of 6 μM in 786-O cells (Supplementary Figure S1), so in the same range than **8e**.

786-O cells are known to be resistant to classical chemotherapy.²⁴⁴ Moreover, the potential of CK2 α as a relevant target to treat 786-O cells has been already described.⁶⁰ Therefore, the 786-O cell line was selected as a cellular model for further evaluation of compound **8e** efficiency, by using Western Blot analysis.

First, inhibition of CK2 activity within living cells was evaluated. Two protein substrates, Akt and α -catenin, known to be phosphorylated by CK2 on residue Ser129²²⁴ and Ser641²²³, respectively, were used as reporter of CK2 cellular activity. A strong decrease in phosphorylation of Akt (Ser129) and α -catenin (Ser641) was observed after a 24h treatment with compound **8e** (Figure 5A). We can conclude that compound **8e** inhibited CK2 cellular activity and decreased cell viability, also observed macroscopic observations during cell viability experiments (presence of numerous dead cells).

Then, we were interested in apoptosis markers. Two of them, the apparition of cleaved PARP and the decrease in survivin protein level, were investigated by Western Blot. Both apoptosis markers appeared simultaneously after 24h treatment by compound **8e** (Figure 5B). The concentration of **8e** needed for apoptosis induction (about 6 μM) is consistent with the GI_{50} (about 5 μM) and the cellular inhibition of CK2 activity (about 5 μM) supporting that CK2 inhibition is responsible for cell death.

Table 1. Effect of compound **8e** on various cell lines.

Tissue	Cell name	Cmpd 8e GI ₅₀ in μM
Kidney	786-O	5 (\pm 2)
	RPTEC	27 (\pm 5)
Breast	MCF7	10 (\pm 2)
	MCF10A	10 (\pm 3)
Lung	H1299	9 (\pm 4)
	A549	12 (\pm 3)
Prostate	PC3	7 (\pm 2)
	DU145	20 (\pm 6)
Glioblastoma	U138	13 (\pm 3)

Cells were grown as described in the experimental part and GI₅₀ values were determined by linear interpolation after transformation to log[c] scale. Standard deviations from minimum two independent experiments are depicted between brackets.

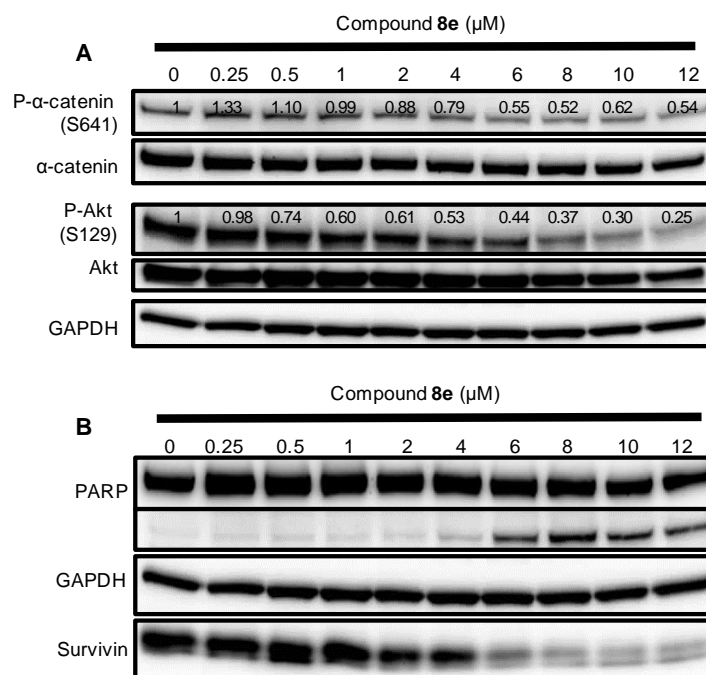


Figure 5. Cellular effect of compound **8e**. **A.** Cellular inhibition of CK2 by compound **8e**. 786-O cells were plated and incubated 24h in the presence of various concentrations of **8e**. Phosphorylation statuses of two protein substrates of CK2 were measured by Western Blot analysis

of cell extracts. Band intensities were quantified using ImageJ and Anti-GAPDH was used as loading control. **B.** Apoptosis induction upon compound **8e** treatment. 786-O cells were plated and incubated 24h in the presence of various concentrations of **8e**. Apparition of cleaved PARP and decrease of survivin was observed by Western Blot analysis of cell extracts. Anti-GAPDH was used as loading control.

3.2.8 Conclusion

From the allosteric inhibitor of CK2 α described in chapter 3.1, compound **3**, we investigated new pharmacomodulation studies based on the 2-aminothiazole scaffold. SAR studies have led to potent and selective allosteric inhibitors of CK2 α . The SAR demonstrated clearly that a hydrophobic and aromatic substitution in position 2 of the 2-aminothiazole core had a positive effect on CK2 α inhibition; as well as an acid function at the opposite side, on the aromatic linked to the amino group of the thiazole. The binding site of the optimized compound **8e** was confirmed in the allosteric pocket by single mutation scanning and docking studies. The allosteric binding pocket of **8e** is located at the interface delimited by the flexible glycine-rich loop, the α C-helix, the 3rd β -strand of the N-terminal lobe and the activation loop. A good selectivity was achieved with a Gini coefficient of 0.78 against a panel of 53 selected kinases. In comparison, the clinical phase II inhibitor, CX-4945 exhibited a Gini coefficient of 0.67. Moreover, Clk2, the main off-target of CX-4945 was not inhibited by **8e**, neither the other kinase of the Clk family. In addition of an interesting selectivity, the mechanism of action of compound **8e** may be responsible for the advantageous efficiency in cellular-based assay. Indeed, **8e** exhibited an very good potency to inhibit CK2 α cellular activity, in the same ranges than the clinical phase II inhibitor, CX-4945. This latter result has to be linked with the important difference of potency on recombinant CK2 α (0.6 μ M for **8e** and 0.014 μ M for CX-4945). As a potent CK2 α inhibitor, **8e** induced apoptosis after 24h treatment at a concentration of 6 μ M and lead various cancer cell lines to death. In summary, the optimized allosteric inhibitor of CK2, **8e**, exhibited a cell efficiency comparable with the clinical phase II inhibitor, CX-4945 and it is a promising molecule for further *in vivo* studies.

3.3 Identification of the first cellular efficient modulator of the protein kinase CK2 subunit interaction

CK2 is a tetrameric protein kinase composed of two catalytic subunits (α and/or α') and a dimer of regulatory subunit (β). CK2 β interaction changes the substrate selection of the catalytic moiety. Previous studies demonstrated that a deregulation of the dynamic interaction between CK2 α and CK2 β induced major alterations in cell signaling leading to phenotype modifications. However, cellular efficient CK2 β -competitive inhibitors are required to understand this complex mechanism. In the present study, a cellular efficient inhibitor of the CK2 subunit interaction was obtained through biomolecular engineering of a small cyclic peptide previously described as a CK2 α antagonist. This fusion peptide exhibited a micromolar potency to interfere with the CK2 α/β interaction in cell-based assay leading to striking modifications of the CK2 subunits subcellular localization as well as to a significant modification in p21 phosphorylation, coupled with EGFR down-regulation. In addition of its potential to investigate the dynamic regulation of the CK2 α/β interaction in living-cell, the remarkable decrease in cell viability observed upon disruption of α/β interaction makes it as a valuable cell death-inducing tool.

3.3.1 Scientific rationale

CK2 exhibits an heterotetrameric quaternary structure in which a central dimer of regulatory subunits (CK2 β) bridges two catalytic subunits, CK2 α and/or CK2 α' .²⁸ The plethora of CK2 substrates²⁷ that are involved in the promotion of cell survival, proliferation and differentiation²¹³ shows the complexity of the CK2 cellular signaling network and supports the view that this enzyme participates to the regulation of many of the same cellular responses that characterize the "hallmarks of cancer" originally described by Hanahan and Weinberg^{4,5}. Thus the crucial role of CK2 in tumorigenesis makes it an attractive pharmacological target in cancer therapy, and CK2 inhibition proved to be an effective method to induce tumor regression.⁹² Most of chemically diverse CK2 inhibitors bind to the ATP pocket⁹¹ such as, for example, CX-4945 (5-(3-chlorophenylamino)benzo[c][2,6]naphthyridine-8-carboxylic acid, silmitasertib, IC₅₀ = 14 nM) which is currently in phase II clinical trials.²⁰⁹

Both the isolated CK2 α subunits and the holoenzyme are endowed with constitutive activity. However, the regulatory subunit modulates the substrates preference of the catalytic subunit.⁷⁷ Previous studies demonstrated that the CK2 subunits interactions are dynamic and that each subunit could be independently found in different subcellular compartment.^{203,245} It is

assumed that a dynamic rather than a static interaction of the CK2 subunits may help adjust the kinase specificity to ensure that the relevant form of the catalytic subunit is present at each of these locations. Moreover, several studies^{75,228} revealed the role of the regulatory subunit in the control of the epithelial to mesenchymal transition (EMT). Indeed, CK2 β down-regulation in epithelial breast cells is sufficient to promote EMT through Snail1 upregulation.⁷⁶ However, despite the great importance of the α/β interaction in the regulation of cell polarity and cell morphology, the cellular effectors responsible of its fine control remain unknown. Furthermore, perturbing the prominent CK2 α /CK2 β interaction with artificial compounds might suppress specific CK2 holoenzyme functions.

Very few potential inhibitors of this interaction have been published^{50,51,206,207}. Using a structure-based design approach⁵⁰ and a random screening strategy,²⁰⁶ we previously identified a CK2 β -competitive lead compound: Pc, a cyclic peptide that could actually counteract the holoenzyme formation in cell-free assays.⁵⁰ In the CK2 holoenzyme structure, a segment located in the N-terminal region of CK2 β (L187-H193) forms a β -hairpin loop which inserts deep into a remote hydrophobic groove present in the β 4/ β 5 sheets of CK2 α .²⁸ Two residues, Tyr188 and Phe190 were characterized as the hot-spots and therefore, the peptide Pc was designed from the structure of the CK2 β -tail encompassing these two hot-spots. Thus, Pc represents a unique CK2 β -based small molecule fully capable of interacting with CK2 α and to disrupt the α/β interaction in cell-free assays at 3 μ M concentration. Moreover, Pc was shown to disturb the CK2-holoenzyme-catalyzed phosphorylation of CK2 β -dependent CK2-substrate proteins.⁵⁰ The hot-spots mutations (Tyr5Ala, Phe7Ala; equivalent to Tyr188 and Phe190 in CK2 β structure) were sufficient to impair the *in vitro* efficiency of Pc.⁵⁰ Later on, both X-ray crystallography data and thermodynamic signatures demonstrated that Pc and CK2 β binding to CK2 α are similar.⁵¹ Thus, Pc represents the first effective CK2 β -competitive compound derived from the C-terminal CK2 β segment. However, this peptide antagonist lacks cellular efficiency and its optimization through structural modifications, such as attachment to cell-permeable adducts was required.

In the present study, we described biomolecular engineering of the Pc peptide to promote its cellular activity. Using this peptidic tool, we provide the first evidence of the consequences of a specific disruption of CK2 α /CK2 β interaction in living cells.

3.3.2 Design of a cell permeable chimeric TAT-Pc

We synthesized a chimeric Pc analogue termed TAT-Pc composed of both active Pc in which the disulfide bond used for cyclization have been replaced by an amide linking the side chain of K1 and to the C-term of G13 (KGGRLYGFKIHGG) and a 13-mer peptide (GRKKRRQRRRPPQ) derived from TAT protein of the human immunodeficiency virus 1.^{246,247} This

TAT sequence is a cell-penetrating peptide which can carry element such as drugs, small peptide or nucleic acid into the cells.²⁴⁸ Thus, the covalently linked TAT-Pc chimeric construct in which the TAT sequence is placed at the N-terminal side of Pc was expected to be cell-permeable (Figure 1). In order to assess the cell penetration, a TAMRA fluorescent probe was added to the construct which could then be located by fluorescence microscopy. The TAT sequence enabled a remarkable uptake of the TAMRA-TAT-Pc construct into the cells as the majority of the peptide was located into the cells in less than 4h (data not shown). We also synthesized a cyclic peptide (TAT-Pc-rand) in which the Pc residues were in a random position was obtained as well as a cyclic peptide (TAT-Pc-mut) with the two Pc hot spots residues (Tyr5 and Phe7) mutated to alanine (Figure 1).

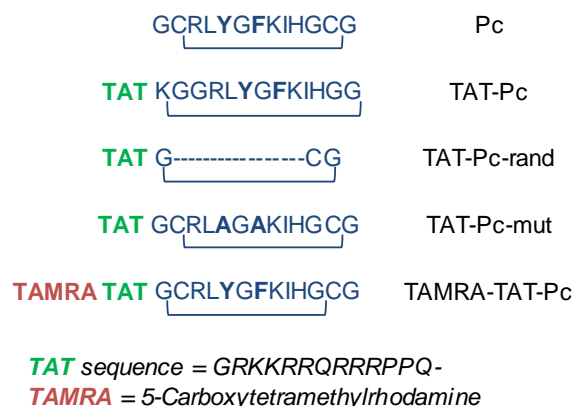


Figure 1: Sequences of the Pc, TAT-Pc, TAT-Pc-rand, TAT-Pc-mut, TAMRA-TAT-Pc. The two spots, Y5 and F7 (corresponding to Y188 and F190 in CK2 β sequence) or mutated residues are depicted in bold for clarity.

3.3.3 TAT-Pc suppresses the CK2 α /CK2 β interaction in living cells

Previous studies have demonstrated that Pc peptide is an efficient CK2 β -competitor in cell-free assay.^{50,51} Consequently, we were interested in the cellular observation of the CK2 α /CK2 β interaction upon treatment with the cell-permeable TAT-Pc. Proximity ligation assay is a method of choice to evaluate a protein-protein interaction in living cells as it enables the direct observation of proteins interactions in unmodified cells.²⁴⁹ Thus, we applied this methodology in HeLa cells. In untreated cells, CK2 $\alpha_2\beta_2$ complexes were observable as dots with an average 5.5 interactions per cell (Figure 2). Confirming literature data,²⁴⁵ the CK2 $\alpha_2\beta_2$

complexes were transient as only few sporadic complexes were detected and as they did not overlap with the large CK2 α and CK2 β expression observed by immunostaining experiments (data not shown). In TAT-Pc treated cells, a striking decrease of the overall number of complex formation was observed with an average number of interactions lower than 2 per cell for a concentration of TAT-Pc equal or greater than 40 μ M (Figure 2). These observations suggest that TAT-Pc translocates through cell membranes and behaves as a cell-efficient inhibitor of the CK2 α /CK2 β interaction.

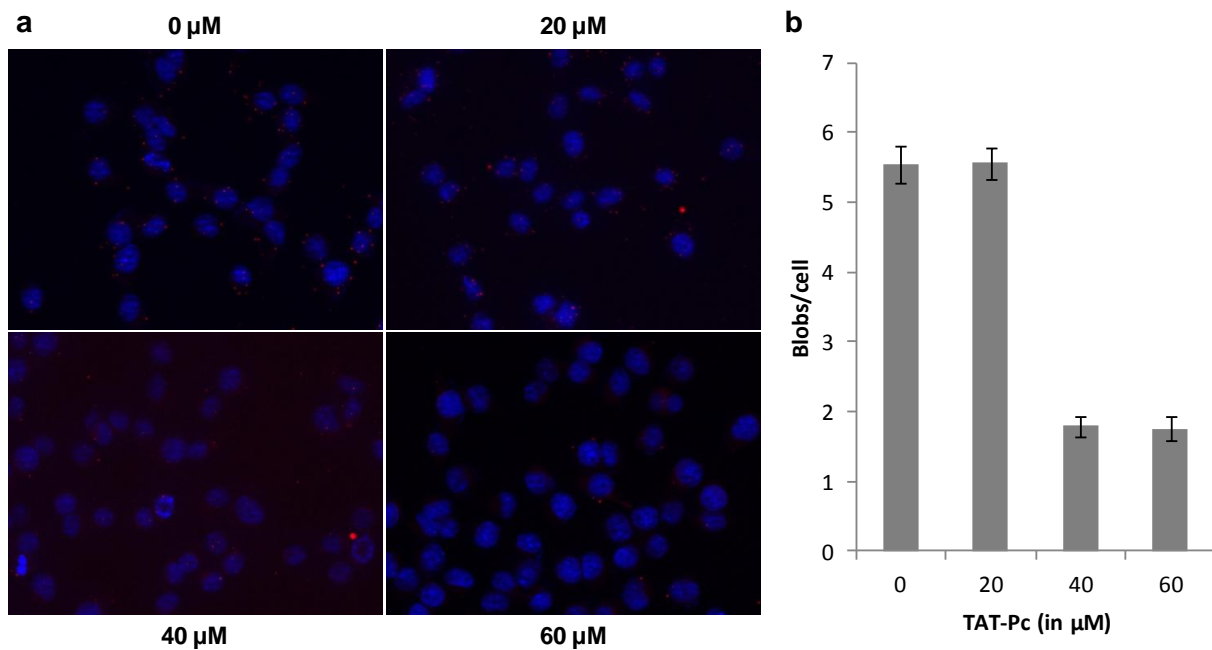


Figure 2: Inhibition of the CK2 subunit interaction in HeLa cells. **(a)** PLA images of HeLa cells treated for 6h with 0, 20, 40 or 60 μ M of TAT-Pc. Red blobs represents CK2 α /CK2 β interaction. Nuclei were stained with Hoechst-33342. **(b)** Quantification of the average blobs per cell using BlobFinder.²⁵⁰ More than 150 Cells were analyzed for each condition. Error bars represent S.E.M.

3.3.4 CK2 subunits subcellular localization is altered by TAT-Pc

Previous studies demonstrated that CK2 subunits have the capacity to translocate independently from the nucleus to the cytoplasm.²⁴⁵ We hypothesized that the inhibition of the CK2 α /CK2 β interaction might affect/disturb the CK2 subunits localization. Indeed, we observed a striking translocation of CK2 α and CK2 α' from the nucleus to the cytoplasm upon TAT-Pc

treatment (Figure 3), whereas the catalytic subunits remained mostly nuclear in presence of DMSO or in the presence of the ATP-competitive CX-4945 inhibitor. In contrast, CK2 β was mainly located in the cytoplasm in controls as well as in the presence of TAT-Pc. These observations are in agreement with the independent and dynamic regulation of CK2 subunit subcellular localization and highlight the influence of the holoenzyme formation on CK2 subunit translocations.

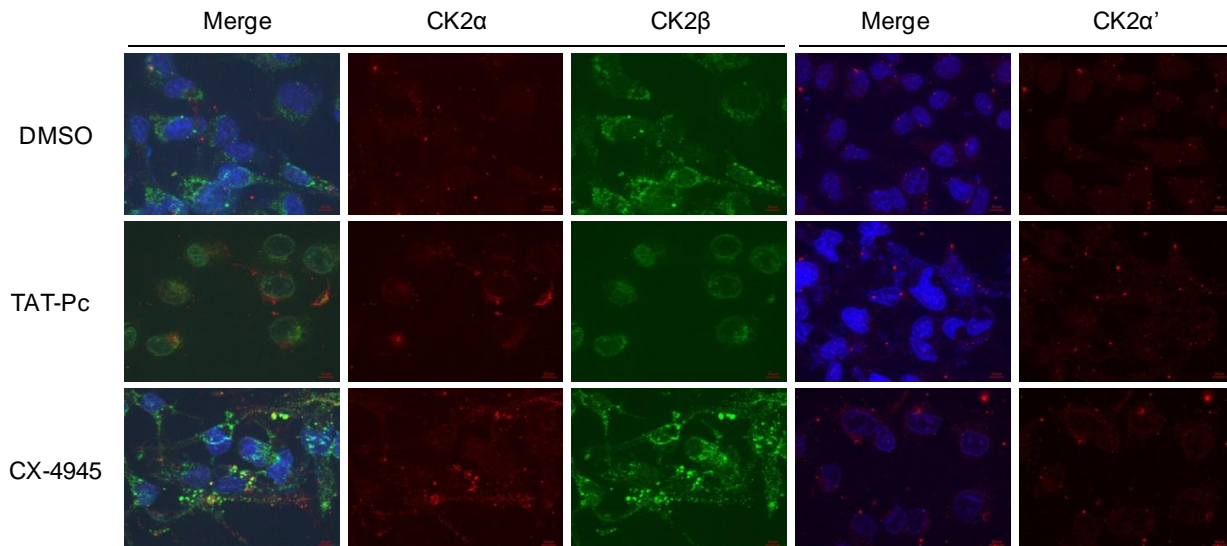


Figure 3: Subcellular localization of CK2 subunits in 786-O renal carcinoma cells. Cells were treated with DMSO as control, TAT-Pc (30 μ M) or CX-4945 (12 μ M) for 12h before fixation.

3.3.5 Epidermal growth factor receptor (EGFR) down-regulation upon TAT-Pc treatment

Upon stimulation, the EGFR can initiate several downstream signaling cascades leading to cell proliferation.²⁵¹ Autophagosome-mediated EGFR down-regulation induced by CK2 inhibition has been documented.²⁵² As we observed a decrease in cell proliferation after TAT-Pc treatment, we investigated the EGFR status in presence of TAT-Pc or CX-4945. Using immunostaining methods, we observed a striking translocation from the cell membrane to the cytoplasm associated with a down-regulation of EGFR after TAT-Pc or CX-4945 treatments in mammary epithelial cells (MCF10A) (Figure 4). Moreover, these observations were correlated with an increase of endosomal activity attested by the LAMP1 marker. Interestingly, stable silencing of CK2 β expression in these epithelial cells (MCF10A- $\Delta\beta$) led to a similar translocation of

EGFR from the cell membrane to the cytoplasm (Figure 4). Thus, the previously described implication of CK2 in EGFR regulation²⁵² is dependent on the CK2 α /CK2 β interaction and its perturbation could lead to a decrease in cell proliferation. This finding may provide a new strategy to target the EGFR signaling pathways and to overcome resistance to EGFR inhibitors.²⁵³

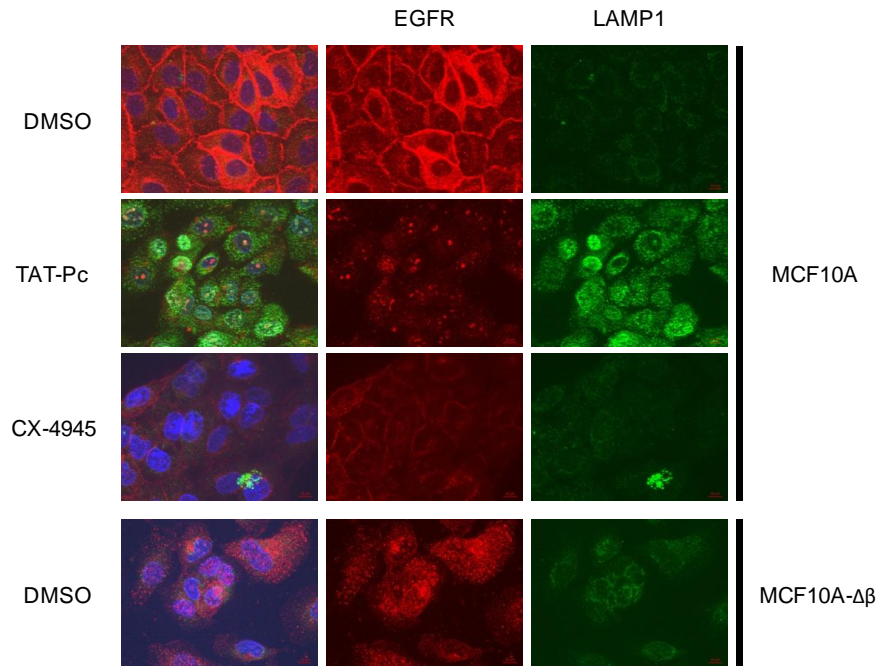


Figure 4: EGFR degradation through lysosomal activity upon TAT-Pc treatment. MCF10A cells were treated for 12h with DMSO as control, TAT-Pc (30 μ M) or CX-4945 (12 μ M). MCF10A- $\Delta\beta$ cells were used as additional reference. Cells were immunostained with anti-EGFR (red), anti-LAMP1 (green), chemically stained with DAPI (blue), and then analyzed by confocal microscopy.

3.3.6 p21 phosphorylation is increased by TAT-Pc

p21^{CIP1/WAF1} is an universal inhibitor of cyclin-dependent kinases such as CDK1, CDK2 and CDK4/6 playing a key role in cell cycle regulation.^{254,255} It has been reported that p21 is phosphorylated by CK2 $\alpha_2\beta_2$ and interacts with the CK2 β N-terminal end *in vitro*.²⁵⁶ A decrease of p21 (T145) phosphorylation was systematically observed upon treatment with ATP-competitive inhibitors of CK2,^{92,257} suggesting that status of p21 phosphorylation could be used as a reporter of CK2 activity. However, in contrast of these previously described results, we did not observe the phosphorylation of recombinant p21 protein by CK2 $\alpha_2\beta_2$ in our *in vitro* assay (data not shown). Nevertheless, as p21 phosphorylation seems to be related to CK2 activity in cellular-based assays,

we evaluated this feature by Western Blot analysis of cell extracts. Indeed, a striking dose-dependent increase of p21 (T145) phosphorylation was observed upon treatment with TAT-Pc (Figure 5a-b). Additionally, this effect was not observed upon treatment with the cell-permeable but inactive versions of Pc (TAT-Pc-rand and TAT-Pc-mut) (Figure 5a-b). In contrast, the ATP-competitive inhibitor, CX-4945, promoted a decrease of p21 (T145) phosphorylation (Figure 5a). The TAT-Pc dependent increase of p21 phosphorylation was, of note, a general effect as it was observed in several cell lines (786-O, MCF10 and HeLA).

Interestingly, previous studies showed that the C-terminal segment of p21 (p21⁽¹⁴⁵⁻¹⁶⁴⁾) could adopt different secondary conformations regulating proteins PCNA, CaM and SET binding²⁵⁸ and the phosphorylation of p21 on the residue T145 prevents PCNA binding.²⁵⁹ Since the nuclear localization signal of p21 (RKR⁽¹⁴⁰⁻¹⁴²⁾) is located near T145,²⁶⁰ we hypothesized that phosphorylation on T145 could impact the C-terminal structure leading to significant modification of protein binding and of the subcellular localization of p21. Indeed, TAT-Pc treatment triggered a striking nuclear localization of p21 whereas a homogeneous localization in the cytoplasm and in the nucleus was observed in DMSO controls or upon treatment with the ATP-competitive inhibitor, CX-4945 (Figure 5c-d).

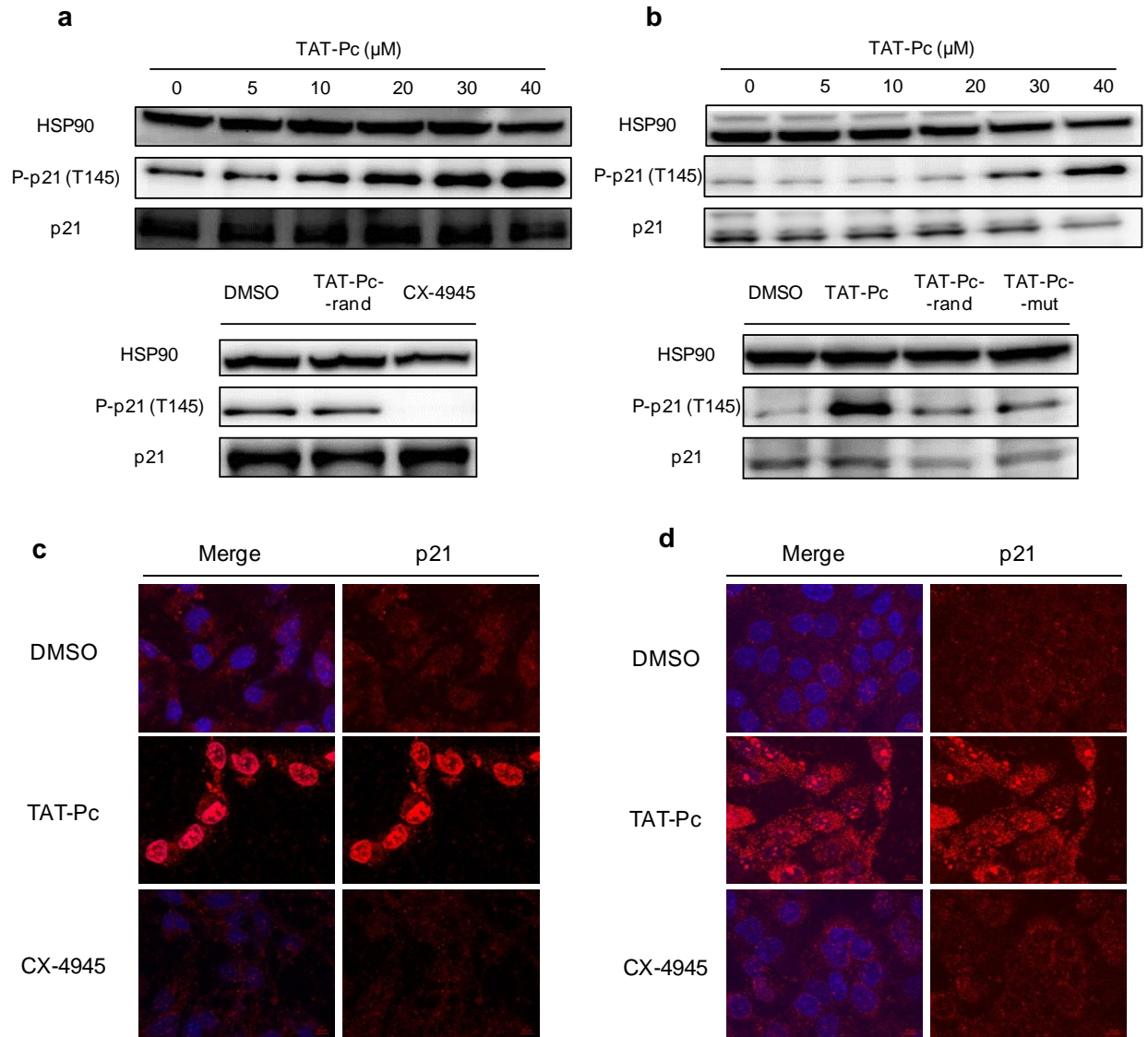


Figure 5: Effect on p21. **(a)** Phosphorylation status of p21 in 786-O renal carcinoma cells. Cells were treated for 48h with TAT-Pc (various concentrations, see upper panel), DMSO, TAT-Pc-rand (40 μM) or CX-4945 (6 μM) (see lower panel). **(b)** Phosphorylation status of p21 in MCF10A cells. Cells were treated for 48h with TAT-Pc (various concentration, upper panel), DMSO, TAT-Pc (40 μM), TAT-Pc-rand (40 μM) or TAT-Pc-mut (40 μM) in the lower panel. **(c)** Subcellular localization of p21 in 786-O renal carcinoma cells treated for 12h with DMSO as control, TAT-Pc (30 μM) or CX-4945 (12 μM). **(d)** Subcellular localization of p21 in MCF10A cells treated for 12h with DMSO as control, TAT-Pc (30 μM) or CX-4945 (12 μM).

3.3.7 Differential effects of CK2 α /CK2 β interaction inhibition and CK2 β knockdown

Previous studies demonstrated that CK2 β has a key role in epithelial plasticity and that shRNA-mediated silencing of CK2 β expression in epithelial MCF10A led to Epithelial-to-Mesenchymal Transition (EMT) through upregulation of SNAIL1.⁷⁶ Therefore, we investigated the effect of TAT-Pc on SNAIL1 expression as well as on two CK2 activity reporters (α -catenin-phospho-S641 and Akt1-phospho-S129). Surprisingly, no changes in Snail1 expression or in reporter phosphorylation level were observed whereas p21 phosphorylation was strongly increased upon TAT-Pc treatment (Figure 6). The latter support the concept that, in contrast to CK2 β silencing, inhibition of CK2 α /CK2 β interaction alters CK2 functions in a different manner that conveys in different cell phenotypes. Indeed, both approaches induced the degradation of EGFR (Figure 4) whereas EMT induction was only observable in the case of CK2 β silencing.

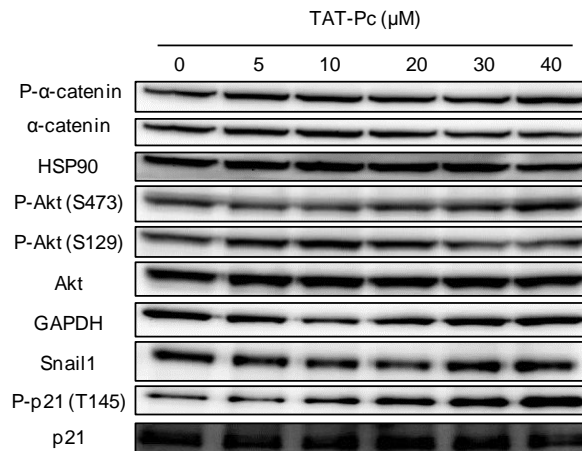


Figure 6: Western Blot analysis of TAT-Pc effects on CK2 activity markers (P- α -catenin, P-Akt), on EMT (Snail1 expression) and on p21 phosphorylation. 786-O renal carcinoma cells were treated with TAT-Pc for 48h prior to Western Blot analysis.

3.3.8 TAT-Pc decreases cancer cell viability

The observation that TAT-Pc induced the EGFR down-regulation and p21 translocation into the nucleus suggested that these two events could respectively lead to a decrease of cell viability and to cell cycle inhibition. Indeed, we observed a significant decrease of HeLa cell viability upon TAT-Pc treatment whereas the inactive TAT-Pc-rand did not exhibit any effect

(Figure 7). Therefore, this effect on cell viability as well as other cellular consequences triggered by TAT-Pc treatment are likely to be related to its ability to inhibit the CK2 α /CK2 β interaction.

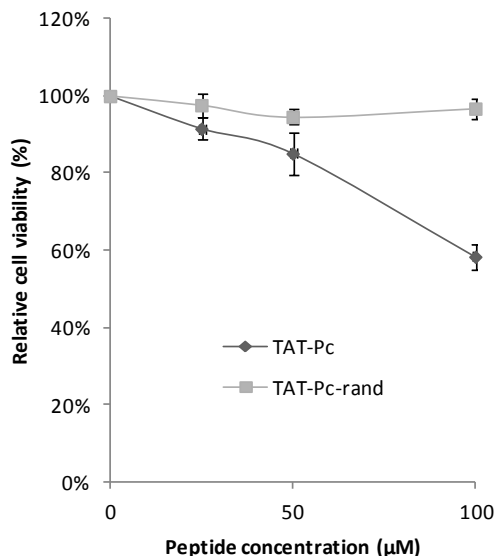


Figure 7: TAT-Pc decreased cell viability. HeLa cells were treated with TAT-Pc or TAT-Pc-rand for 48h before evaluation of cell viability in comparison with DMSO treatment.

3.3.9 Conclusion

Molecules that selectively inhibit the CK2 subunit interaction would be useful in determining the importance of CK2 β in the control of the many cellular processes that are governed by this multifunctional kinase. In particular, such inhibitors would provide more rapid and reversible tools than siRNA or overexpression methods for correctly identifying relevant CK2 β -dependent substrates. They will also serve as leads for the rational design of function-specific chemical drugs that disrupt some actions of CK2, but leave others intact, allowing the deregulation of specific intracellular pathways. Furthermore, selective disruption of the CK2 α -CK2 β interaction could find important applications to test pharmacologically the importance of this interaction in tumor cell growth.

3.4 Structure-Based discovery of a small chemical scaffold targeting the CK2 Subunits interface

The small cyclic peptide described in the chapter 3.3 demonstrated the therapeutic interest of the CK2 α /CK2 β interaction inhibition. However peptides are more difficult to transform into therapeutics than small molecules. Therefore, a virtual ligand screening was considered to identify small molecules able to bind in the α/β interaction pocket.

3.4.1 Virtual Screening and hit validation

A Virtual Ligand Screening directed on fumigated pocket at the interface of CK2 α /CK2 β subunit was realized by Irina Kufareva and Ruben Abagyan (Skaggs School of Pharmacy, La Jolla, USA). The hundred top scoring compounds were selected and their ability to inhibit the phosphorylation of CK2 β -dependent substrate *in vitro* was evaluated. After hit validation and removal of the promiscuous binders, one compound remained, the hit compound **1** (Figure 1). A parent compound (**2**) was commercially available and thus, was purchased.

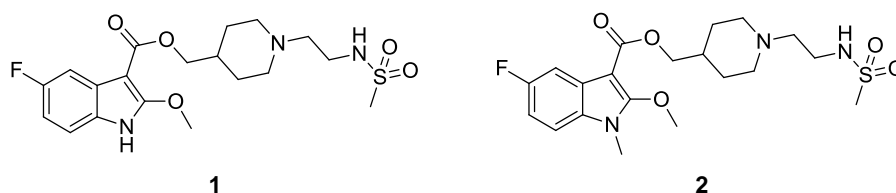


Figure 1. Chemical structures of the hit compound (**1**) from the *in silico*-screening and the parent inactive compound **2**.

Interestingly, compound **1** was able to inhibit the phosphorylation of CK2 β -dependent peptide substrate whereas compound **2** was not efficient (Figure 2a). CK2 β -independent peptide substrate phosphorylation was only slightly impacted by **1** and independently of CK2 β concentration (Figure 2b) whereas the inhibition of the CK2 β -dependent peptide substrate depends on CK2 β .

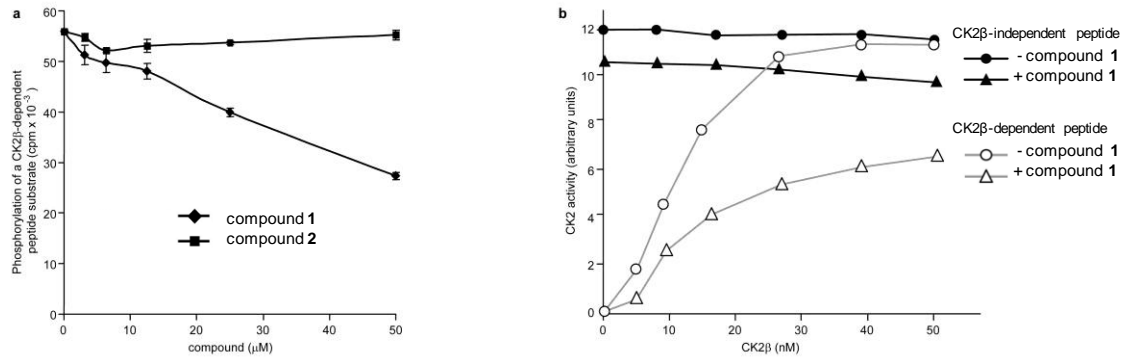


Figure 2. (a) Compound **1** inhibits phosphorylation of a CK2β-dependent substrate (eIF2-derived peptide) by the CK2 holoenzyme in a dose-dependent manner. Under the same conditions, compound **2** has no effect; **(b)** Compound **1** affects CK2β-independent peptide phosphorylation to a smaller degree than CK2β-dependent peptide phosphorylation. CK2α (40 nM) was incubated without or with 100 μM compound **1**, in the presence of increasing concentrations of CK2β and assayed for phosphorylation of CK2β-independent and CK2β-dependent peptide substrates (133 and 600 μM, respectively) and 100 μM ATP.

In addition, inhibition of CK2β-dependent phosphorylation by compound **1** can be antagonized by increasing CK2β concentrations (Figure 3a). This result indicates that **1** and CK2β are likely to bind to CK2α in a mutually exclusive mode. Steady-state kinetic analysis of compound **1** was performed by incubation of CK2α with increasing concentrations of CK2β in the presence of different concentrations of the compound (Figure 3b). This experiment suggests a mixed competitive inhibition towards CK2β; K_i was estimated to 66 μM.

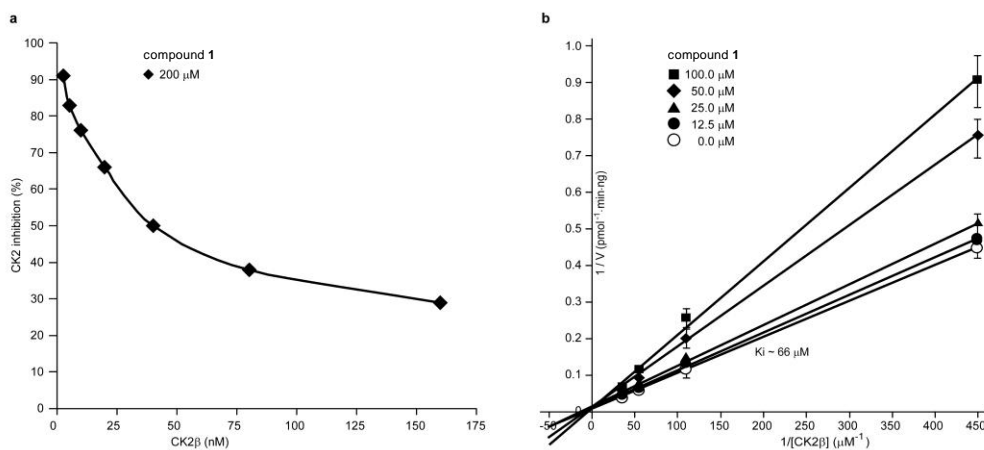


Figure 3. Inhibition of CK2β-dependent phosphorylation by compound 1 is reversed by CK2β. (a) CK2α (50 nM) was incubated in the presence of 200 μM compound **1**, saturating concentrations

of the CK2 β -dependent peptide substrate (600 μ M) and ATP (100 μ M), and increasing concentrations of CK2 β ; **(b)** Steady-state kinetic analysis of CK2 complexation showed a K_i of 66 μ M. The data represent the average of three experiments performed in duplicate.

Docking of compound **1** in the β -interaction pocket (Figure 4) is consistent with the preliminary results obtained. Moreover, the reason of the inactivity of compound **2** is easy to understand as the N-methyl substitution on the indole will prevent the hydrogen bond between the amino function and the backbone of Tyr39. Furthermore, we can postulate that the size of the methyl prevents the entry of the indole core into the hydrophobic pocket.

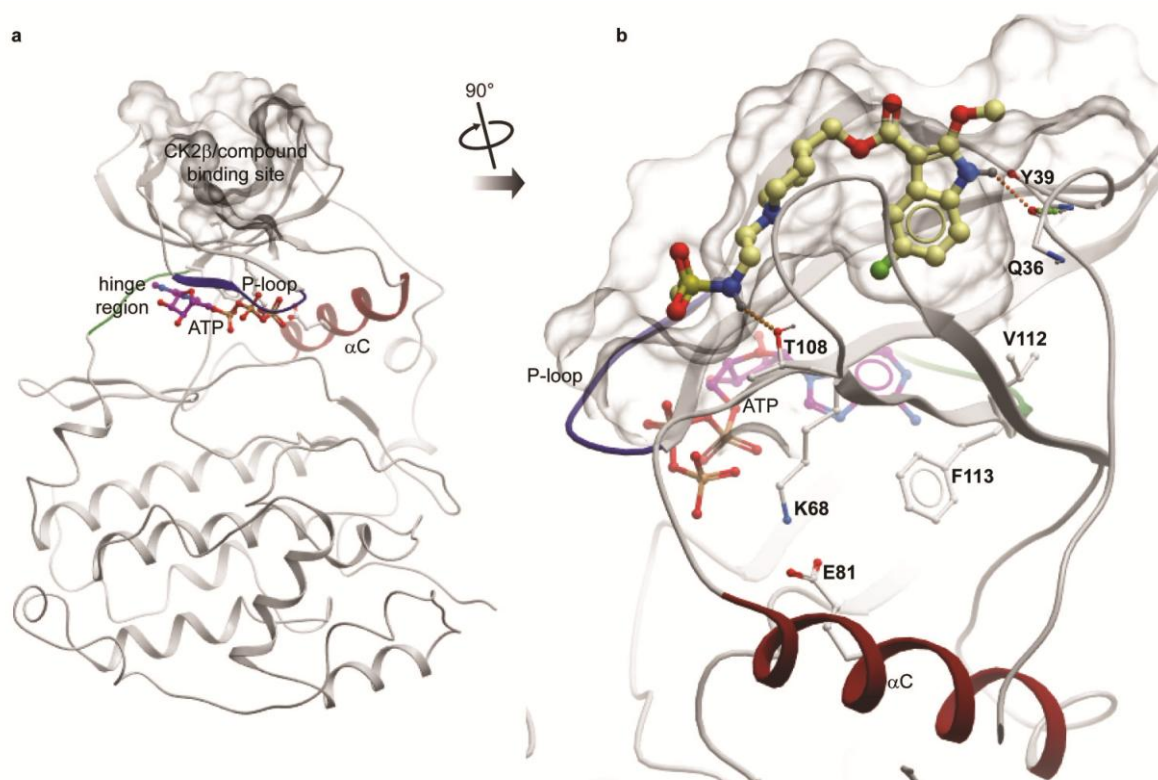


Figure 4. Compound binding mode predicted by ICM virtual docking: **(a)** Overall architecture and compound/CK2 β binding site; **(b)** Predicted pose of compound **1**.

The two compounds described above exhibited interesting *in vitro* properties to inhibit the CK2 α /CK2 β interaction and they demonstrated the druggability of the CK2 α / β interaction pocket. Therefore, we considered the development of a small library of compound **1** analogs to

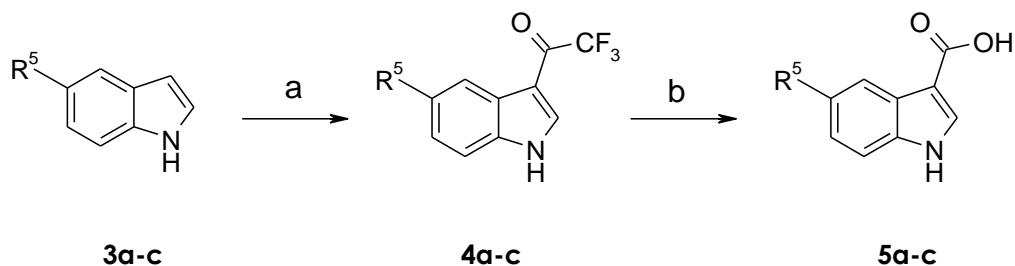
improve their potency and study the structure-activity relationships. A small selection of compounds and their syntheses are presented in the next paragraphs.

3.4.2 Chemical synthesis

3.4.2.1 Linear synthetic approach for the grafting of the lateral chain

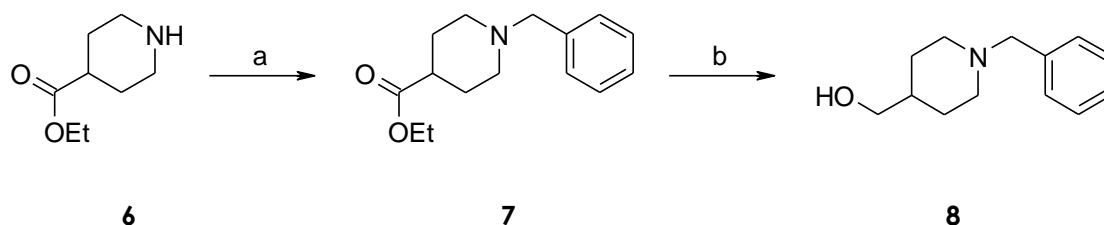
A linear synthetic approach was first investigated by Dr. Mohamed Ettaoussi (EA 4446 B2C): three intermediates were required for this strategy.

First of all, the acid function had to be introduced on the C3 indole position. Several methods have been tried and the most effective one had a global yield up to 80 % on 5-nitro-1H-indole, with an easy work up and no additional purification was needed (Scheme 1).^{261,262}



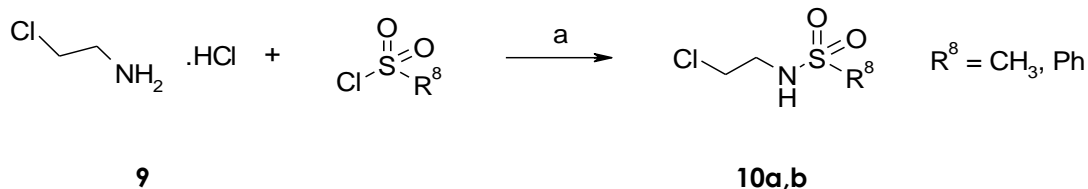
Scheme 1. Acid functionalization in position 3 of the indole. Reagents and conditions: a) TFAA (2.25 eq), anhydrous DMF, 0°C to 150°C, 12h; b) NaOH (10 eq), H₂O, 100°C, 2 h.

Compound **8** was also required and was obtained as described in Scheme 2 from the commercially available ethyl isonipecotate **6** in two steps. First, the amino function was protected with a benzyl group. The ester function was then reduced into an alcohol using lithium aluminum hydride to give compound **8** with an excellent yield over the two steps (Scheme 2).



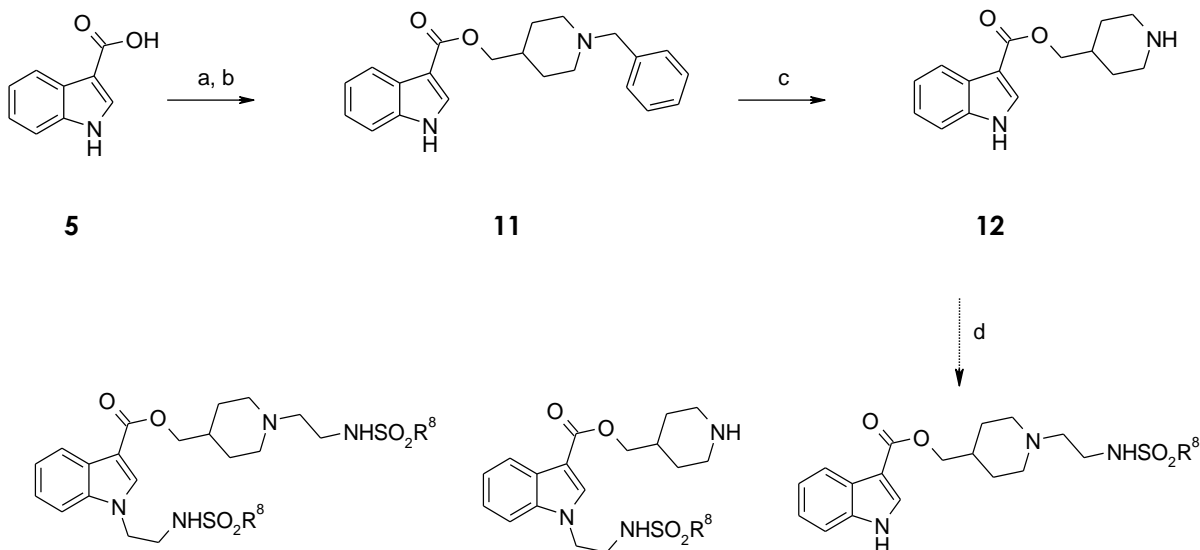
Scheme 2. Synthesis of (1-benzyl-piperidin-4-yl)methanol. Reagents and conditions: a) BnCl, K₂CO₃, EtOH, RT, 48h; b) LiAlH₄, THF, 0°C then reflux, 3h.

Chloro derivatives were used to graft the sulfonamide part of the target molecules. Compounds **10** (Scheme 3) were obtained by reaction between chloroethylamine **9** and methyl- or phenyl-sulfonylchloride, in the presence of triethylamine.



Scheme 3. Synthesis of *N*-(2-Chloroethyl)-methane/phenyl-sulfonylamide derivatives. Reagents and conditions: a) NEt_3 , THF, 5-10°C then RT.

The linear synthesis consists of 3 steps. From 3-carboxylic-1*H*-indole acid, an esterification reaction was carried out through acyl chloride intermediate to obtain compound **11** (Scheme 4). The second step was the deprotection of the amino function: the benzyl group was cleaved using a catalytic hydrogenation to give compound **12**. The last step was the amino alkylation with chloro derivatives **10**. The expected compounds were obtained and were isolated among a complex mixture of polysubstituted indoles. The purification of this crude mixture was very difficult to carry out (Scheme 4).



Scheme 4. Synthesis of *N*-(2-Chloroethyl)-methane/phenyl-sulfonylamide derivatives. Reagents and conditions: a) $(\text{COCl})_2$, THF, RT, 24h; b) (1-Benzyl-piperidin-4-yl)methanol (**8**), CHCl_3 , 0°C then

reflux for 24 h; c) H₂, Pd/C, MeOH, RT; d) N-(2-Chloroethyl)-methane or phenyl-sulfonylamide (**10**) K₂CO₃, acetone, reflux for 24 h.

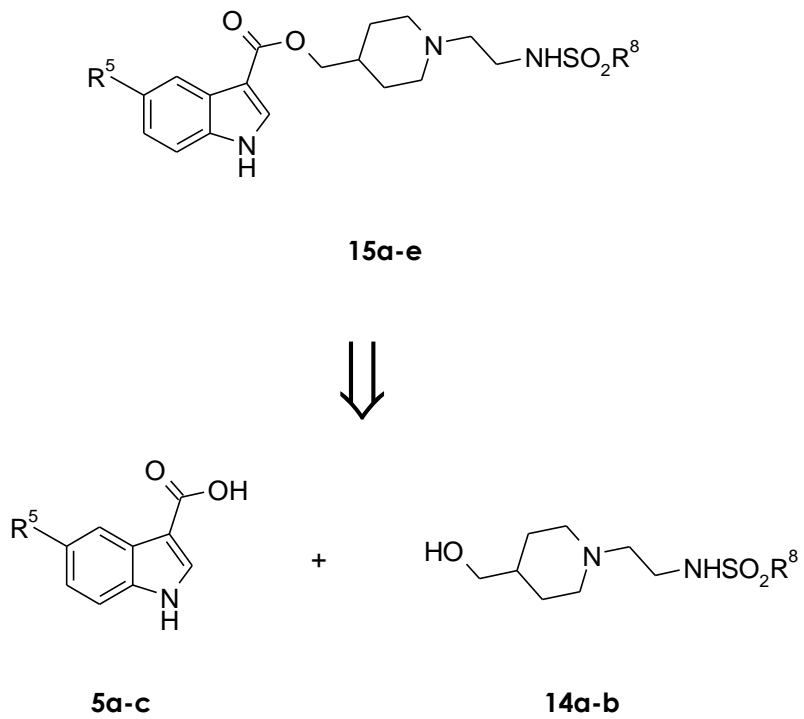
Two main solutions were considered to circumvent this problem:

- The N1 indole protection with a benzenesulfonyl group, for example.
- A new and more convergent synthesis pathway, with the esterification at last step.

The second solution seemed to be the most reliable one because it was well described on similar structures.²⁶³

3.4.2.2 *Convergent synthetic approach*

To circumvent the poly alkylation problem at the last step, a new synthetic pathway was applied. The key step was the esterification between an indole 3-carboxylic acid and a functionalized piperidinyl (Scheme 5). Furthermore, these two acid and alcohol precursors were easily obtained in large amounts.

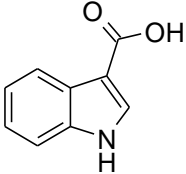
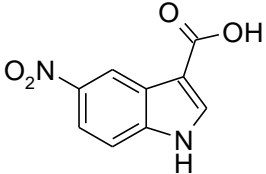
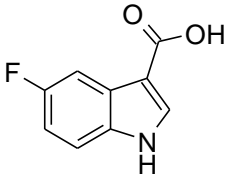


Scheme 5. Retrosynthetic convergent synthetic pathway.

a) Acid intermediates

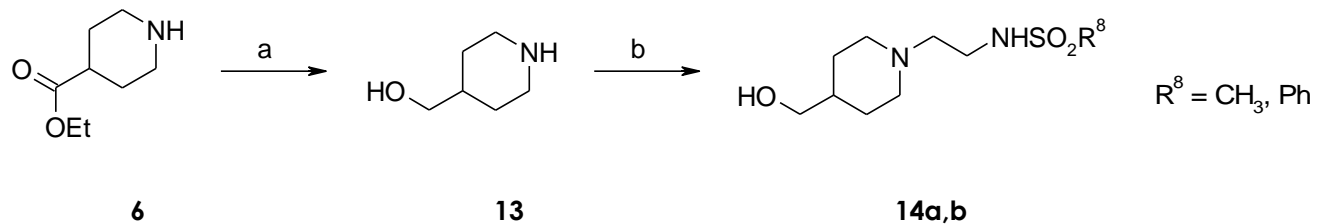
Acid building blocks **5b-c** were obtained by the TFAA method (Scheme 1) or, in the case of 3-carboxylic-1*H*-indole acid **5a**, from the 1*H*-indole-3-carbonitrile intermediate. With these two methods, six compounds were obtained in good yields (Table 1).

Table 1: Acid derivatives.

Structure/Name	Yield
 3-carboxylic-1<i>H</i>-indole acid - 5a	69 % <i>From 1<i>H</i>-indole-3-carbonitrile</i>
 5-nitro-1<i>H</i>-indole-3-carboxylic acid - 5b	91 %
 5-fluoro-1<i>H</i>-indole-3-carboxylic acid - 5c	90 %

b) Alcohol intermediates

Alcohol derivatives were obtained in two steps by a different method than in the linear pathway (Scheme 6).²⁶³⁻²⁶⁵ The difference in yields between the two analogues **14a** and **14b** (Table 2) could be explained by the products' solubility: precipitation in the last step of the sulfonamide with a phenyl group occurred, whereas it was not observed with the methyl sulfonamide. This precipitation facilitates the isolation of intermediate **14b**. The extraction of the methyl derivative ($R^8 = \text{Me}$) was more difficult leading to a lower yield (30%).



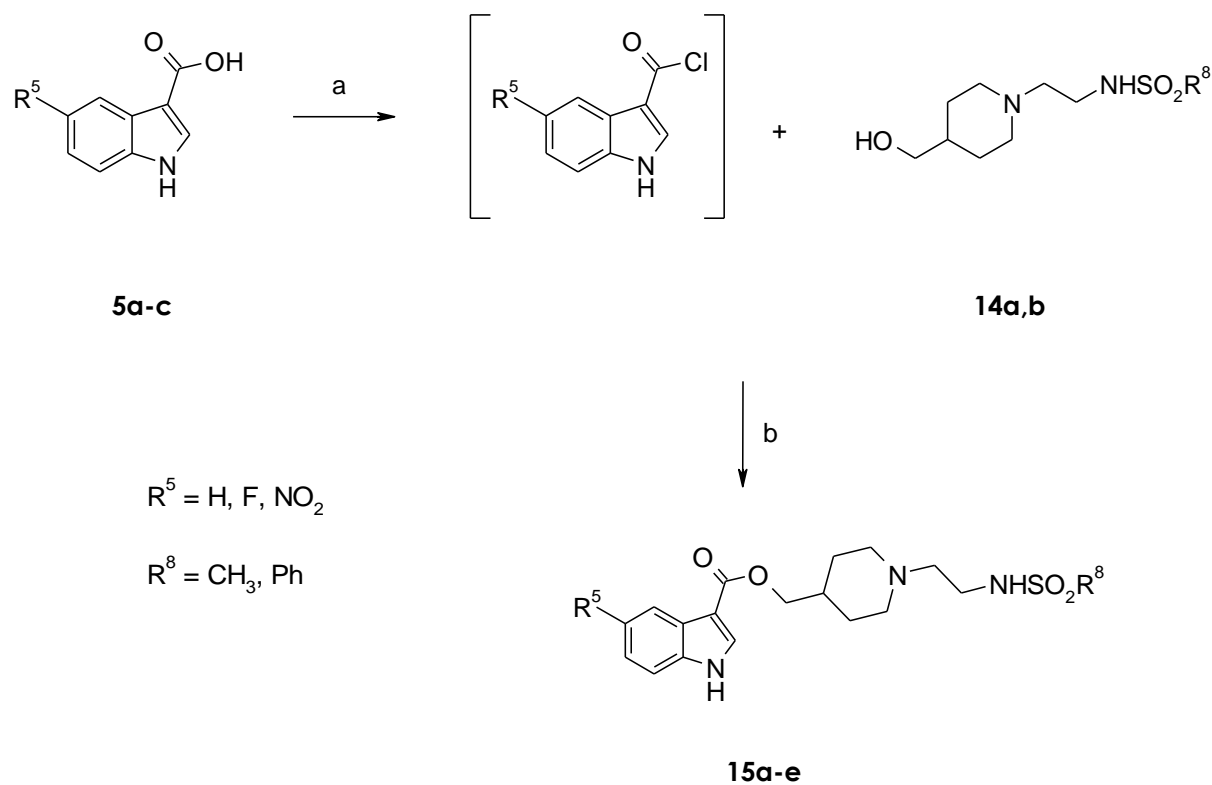
Scheme 6. Synthesis of alcohol intermediates. Reagents and conditions: a) LiAlH_4 , anhydrous THF, 0°C to RT, 20h; b) *N*-(2-Chloroethyl)phenylsulfonamide, DIPEA, MeCN, reflux, 2h; or *N*-(2-Chloroethyl)methylsulfonamide, MeCN, RT, 12h.

Table 2: Alcohol intermediates.

Structure/Name	Yield
 N-[2-[4-(hydroxymethyl)-1-piperidinyl]ethyl]methanesulphonamide - 14a	30 %
 N-[2-[4-(hydroxymethyl)-1-piperidinyl]ethyl]phenylsulfonamide - 14b	82 %

c) Coupling step

The esterification step described in Scheme 7 is exactly the same for all derivatives, which allowed the use of a Radleys® parallel reaction device.



Scheme 7. Coupling step through an esterification reaction. Reagents and conditions: a) SOCl₂, CH₂Cl₂, reflux, 24h; b) CH₂Cl₂, reflux, 24h.

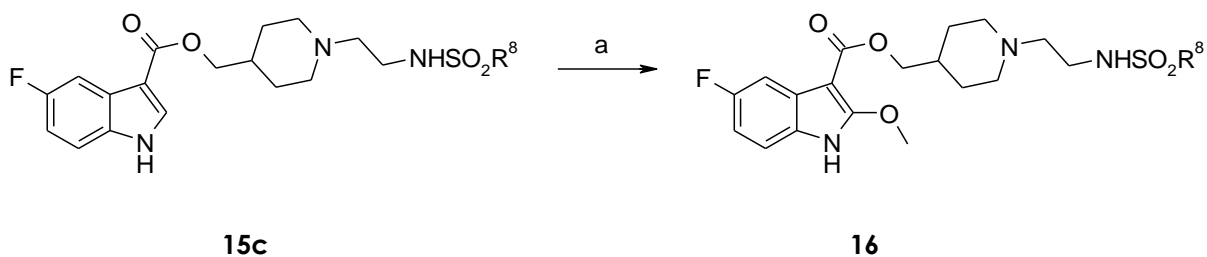
With this method, the small library of compounds **15a-e** was synthesized within few steps and with easily accessible building blocks.

d) Substitution in position 2 of the indole

The insertion of the methoxy in position 2 was also a key reaction because it allowed an additional functionalization on the indole core at the last step.

The method described in Scheme 8 consists of a two-step reaction: first a chlorination with *N*-chlorosuccinimide in dichloromethane followed by addition of the reaction mixture over an acidic methanol solution. This protocol was successfully adapted from literature^{263,266} for the

preparation of all ester derivatives, except with the 5-nitroindole core as LC/MS analyses showed that the reaction did not occur at all.



Scheme 8. Methoxy substitution at position 2 of the indole ring. Reagents and conditions: a) NBS, CH_2Cl_2 , 0°C , 10 min and then MeSO_3H , MeOH, 0°C to RT, 2h.

3.4.3 Cell-free biological evaluation

Compounds were evaluated in kinase activity assays and in SPR dose-response experiments to measure the affinity for CK2a.

Two different peptide substrates were used in these assays:

- peptide 29, phosphorylated either by CK2a or by the holoenzyme (β -independent),
- peptide M, only phosphorylated by the holoenzyme (β -dependent).

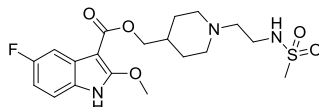
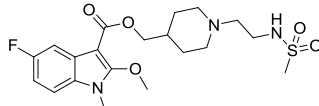
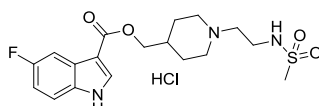
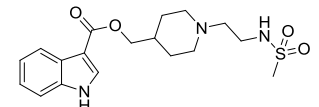
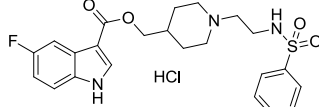
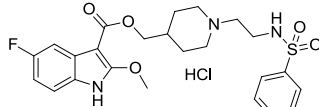
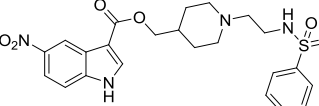
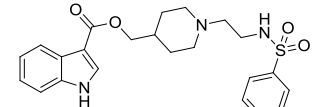
This assay was reliable and reproducible but it measured the kinase activity and not only the direct impact on the α/β interaction. It was performed in three different experimental conditions to evaluate the effect on the α/β interaction as well as the effects on α inhibition (Table 3):

- (a) with peptide 29 (β independent) and a $10\ \mu\text{M}$ ATP concentration,
- (b) with peptide M (β dependent) and a $10\ \mu\text{M}$ ATP concentration,
- (c) with peptide M and $100\ \mu\text{M}$ ATP concentration.

Results obtained from Surface Plasmon Resonance (SPR) and enzymatic experiments were consistent, though the CK2 inhibition was observed in every conditions (a, b and c) of the enzymatic assays. The latter was in opposite of our expectations for a strong inhibition, only in the presence of the β -dependent peptide substrate and independently of the ATP concentration.

A possible explanation relies on the close proximity of the CK2 α /CK2 β interaction with the ATP pocket. Indeed, the Tyr39 residue separates the ATP pocket to the bottom of the hydrophobic pocket, in which the indole core is binding. Therefore, binding of other compounds could partially impair the ATP binding according to an allosteric model. This hypothesis was supported by the mixed-type of inhibition observed toward ATP with compound **1**.

Table 3: Evaluation of CK2 α affinity and of CK2 inhibition in presence of 50 μ M of the corresponding inhibitor.

Compound	Structures	CK2 inhibition (%) in condition			SPR
		(a)	(b)	(c)	Kd (μ M)
1		37	55	29	100 (20)
2		nd	nd	15	nd
15a		29	49	13	87 (8)
15b		9	29	25	100 (20)
15c		53	67	44	61 (2)
16		68	80	52	37 (1)
15d		72	79	41	14 (1)
15e		45	49	57	33 (5)

The percentage inhibition is the average of duplicate experiments, performed in the presence of the respective inhibitor at 50 μ M and (a) peptide 29 (β -independent) (100

μM), ATP (10 μM); or (b) peptide M (β -dependent) (100 μM), ATP (10 μM); or (c) peptide M (100 μM), ATP (100 μM). K_d values represent the affinity for CK2 α and were determined from dose-response curve from SPR experiments. The error in affinity determination is represented between brackets. nd: not determined.

3.4.4 Structure-Activity Relationship Studies

The preliminary SAR study with compound **1** and **2** revealed the importance of the free nitrogen atom on the indole core: this structural motif was thus conserved in all the compounds. The suppression of the methoxy group at position 2 of the indole (compound **15a**) did not impact the affinity for CK2 α , the latter is consistent with the docking of compound **1**, in which the methoxy group was exposed to the solvent (Fig 4, b) and did not exhibit specific interaction with CK2 α . Next, we studied the influence of the fluoro substitution at position 5 of the indole: our attempt to remove it (**15b**) demonstrated significant effect of this substituent.

At this point, all the compounds (**1**, **15a,b**) exhibited more or less the same affinity for CK2 α . Consequently, we hypothesized that this absence of significant effects could be due to the too weak affinities of our compounds for CK2 α , which could prevent a good ranking among them. Looking for substantial modifications that could improve the activity of our compound, we envisaged the addition of a phenyl group on the sulfonamide part. Indeed, preliminary docking studies suggested that the phenyl could make a π -cation interaction with the Lys71 and therefore be an asset for CK2 α affinity. Indeed, compound **15c** exhibited a better inhibition of CK2 than the parent compound **15a**. Consequently, we studied further the effect of the methoxy group at position 2 of the indole as well as the substitution at position 5, while maintaining the phenylsulfonamide moiety. Interestingly, in this case, the methoxy group at position 2 (**16**) increased CK2 α affinity as well as the substitution of the indole in position 5 with a nitro function (**15d**). The fluoro substitution at position 5 (**15c**) was, of note, negative for the activity in comparison with an unsubstituted compound (**15e**).

3.4.5 Biological evaluation in living cells

In the chapter 3.3, CK2 α /CK2 β interaction inhibition by TAT-Pc led to a decrease in cell viability. Consequently, we considered to begin our evaluation by a cell viability screening of our small set of compounds in MCF10A cells (Figure 5). In accordance with the *in vitro* evaluation,

compound **1**, **15a,b** did not exhibited a good efficiency. However, almost all the cells were dead after a 48h treatment with compounds **15c,d** and **16**. As a remark, precipitation occurred with compound **15d** at a concentration inferior to its cell efficiency concentration, thus preventing further evaluation of this derivative.

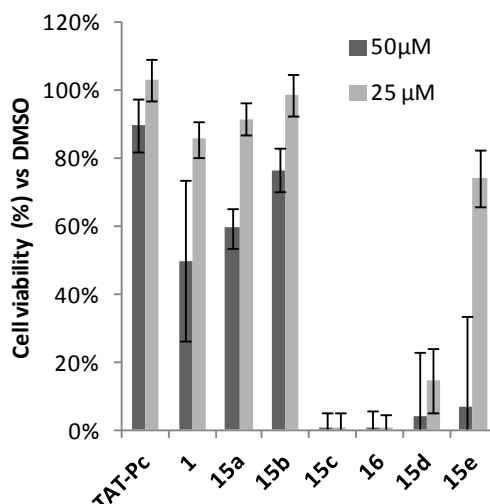


Figure 5. MC10A cell viability after 48h treatment with compounds **1**, **15a-e** and **16**.

In the chapter 3.3, p21 phosphorylation was proved to be a cellular marker of CK2 α /CK β interaction inhibition. Indeed, p21 phosphorylation was increased in a dose-dependent manner and correlated with the cell free potency of various TAT-Pc constructs. Therefore, after 48h cell treatment with compound **15b,e** and **16**, cell extracts were analyzed by western blot to evaluate the phosphorylation of p21 (Figure 6). The less potent compound **15b** exhibited a weak impact on p21 phosphorylation. Indeed, a concentration of 100 μ M was necessary to increase p21 phosphorylation. No effect was observed in the presence of 50 μ M of compound **15b**, the latter is consistent with the 80 % of living cell observed in the cell viability experiment at 50 μ M (Figure 5) and the 25 % of CK2 inhibition at 50 μ M measured in the enzymatic assay (Tab 3).

Whereas compound **15e** increased in a dose-dependent manner p21 phosphorylation in the same range than TAT-Pc, compound **16** exhibited a striking better efficiency than TAT-Pc to increase p21 phosphorylation. Indeed, a 20 μ M concentration of **16** is enough to reach the maximum level of p21 phosphorylation.

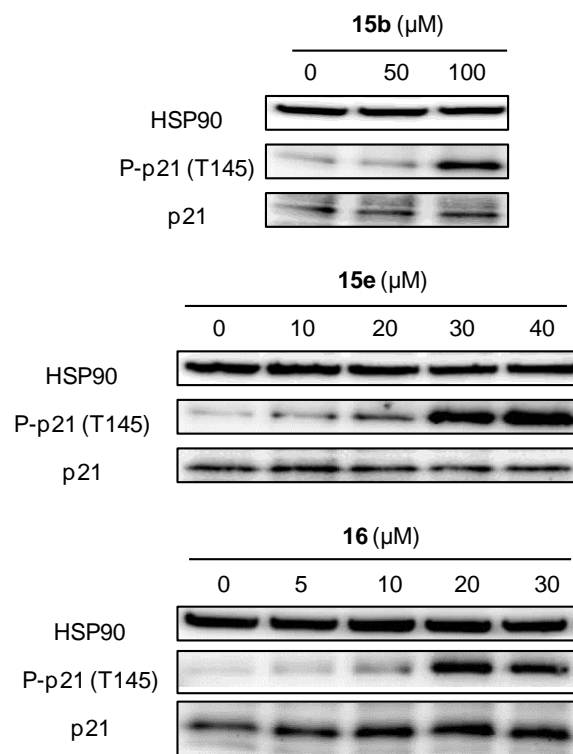


Figure 6. Phosphorylation status of p21 in MC10A after 48h treatment with compounds **15b**, **15e** and **16**.

3.4.6 Conclusion

In this chapter, we identified a small chemical scaffold which targets the CK2 α /CK2 β interaction after a virtual ligand screening. The effect of the hit compound **1** was *in vitro* characterized in several biochemical assays and demonstrated its ability to inhibit CK2 β -dependent substrate phosphorylation and to bind to CK2 α in a mutual exclusive mode with CK2 β . Then, a small set of compounds was synthesized using a convergent synthesis pathway and led to a first SAR study. Consequently, three compounds were evaluated in a cell-based assay and their ability to inhibit the CK2 α /CK2 β interaction was assessed through the western blot analysis of a marker of this inhibition. The best compound **16** exhibited a better efficiency than the reference TAT-Pc and could therefore be used as a relevant starting point for the development of new structures aiming to disturb the CK2 α /CK2 β interaction.

4. Final discussion

Identifying new mechanisms of protein regulation is of great interest as it opens the door to innovative strategies and new targets in therapeutic area. Two hit compounds with atypical mechanisms of action on protein kinase CK2 were identified during *in silico* screening campaigns. Thus, the aim of the present study was to develop these two classes of compounds and to characterize their effects in biochemical as well as in cellular-based assay. Therefore, their novel mechanism of CK2 regulation could be described accurately and the relevance of such approaches to target CK2 could be evaluated. The two classes of compounds could be defined as:

- (i) allosteric modulators of CK2 α (4.1)
- (ii) CK2 α /CK2 β interaction inhibitors (4.2)

4.1 Allosteric modulator of CK2 α

A weak hit was identified in a screening process for CK2 inhibitors and further characterization revealed its non-ATP competitive mechanism of action. Therefore, we developed a library of small molecules and obtained several compounds with good overall properties, as described in chapters 3.1 and 3.2.

4.1.1 CK2 specificities and allosteric inhibitors

The discovery of allosteric modulator of CK2 is challenging as CK2 was always observed in an active state.³⁰ Indeed, in previous studies, only few small molecules were proposed to inhibit CK2 α with a non-ATP competitive and non- β competitive mechanism (see Introduction of chapter 1.4.4).²³⁰ Derivatives of the azonaphthalen class of dyes were described to modulate the CK2 activity in a non-ATP competitive manner. However, the precise binding site of these compounds was not characterized. Nevertheless, the use of CK2 α mutants and SAXS experiments allowed to approximately localize the binding site near the α C-helix and the activation segment.¹⁵⁰ Unfortunately, these molecules could not be considered as drug-like and their development had to be stopped.

Besides small organic molecules, inorganic PolyOxoMetalates (POMs) have been described as potent allosteric inhibitors of CK2 and one of them, [P₂Mo₁₈O₆₂]⁶⁻, exhibited a nanomolar IC₅₀ and a great selectivity in a panel of 29 kinases.¹⁵¹ POMs are anionic complexes of early-transition metal ions and oxo ligands that lack cellular activity. Thus, there is few perspectives to develop them further into *in vivo* active agents. Biochemical analyses revealed that the mode of inhibition was mixed-type with respect to ATP and non-competitive toward the

peptide substrate. Partial proteolysis by trypsin followed by amino acid sequencing showed that two distinct fragments were protected from degradation by POM binding. One comprised of the N-terminal domain and three β strands (β 1, β 2 and β 3) encompassing the glycine-rich loop, whereas the other one consisted of the activation segment and the α F and α G-helices.¹⁵¹

Hence, the putative binding sites of the negatively charged azonaphthalenes and POMs molecules show an overlap in the region encompassed by α C-helix, glycine-rich loop and activation segment. This region plays a crucial role in kinase regulation, and several allosteric kinase inhibitors were demonstrated to act through α C-helix displacement.¹²⁹ The constitutive activity of Protein kinase CK2 is mainly due to the unique interaction between the N-terminal segment and the activation loop abolishing the necessity of any activating phosphorylation. In consequence, the activation loop is locked in the open-active conformation, and this region is one of the less flexible in CK2 α crystal structures, suggesting that any displacement by small molecules might be a tricky challenge.³⁰ On the other hand, the glycine-rich loop is one of the most flexible regions of CK2 α , which might facilitate a potential induced movement of this loop by small molecules.³¹ In most of the CK2 α crystal structures, the conformation of the glycine-rich loop is maintained by two hydrogen bonds linking the Tyr50 of the glycine-rich loop and two lysine residues (Lys74, Lys77) of the basic cluster. However, two crystal structures (PDB ID: 3FWQ¹⁴⁹, 4UB7²¹⁸) make exception by the lack of these key hydrogen-bonds and the collapse of Tyr50 in the ATP binding site. No explanations such as small molecule presence or crystallographic conditions were proposed as probable reason of the inactive conformation observed in 3FWQ.¹⁴⁹ However, in the case of 4UB7, they proposed that a specific halogen bond between an ATP-competitive inhibitor and the Tyr50 in presence of high salt concentration could be responsible of the glycine-rich loop displacement.²¹⁸ All the hints from the literature described above let us believe that CK2 could harbor an allosteric pocket in the region encompassing the activation segment, the glycine-rich loop (P-loop) and the α C-helix (Fig 42a). Therefore, preliminary docking experiments as well as single-alanine mutagenesis experiments were focused on this area and led to the determination of the precise interactions between our compounds and CK2 (Fig 42b).

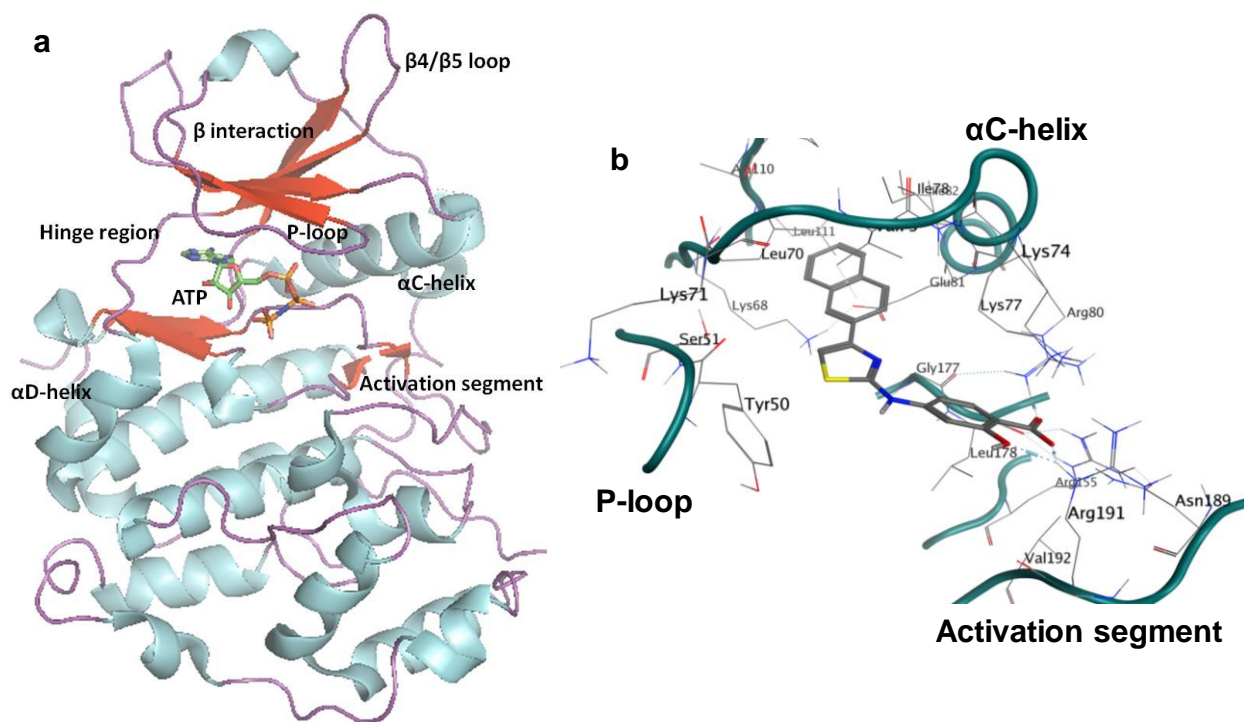


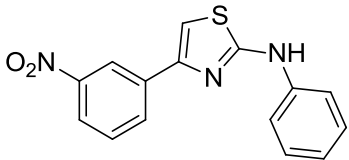
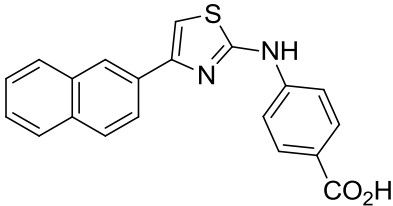
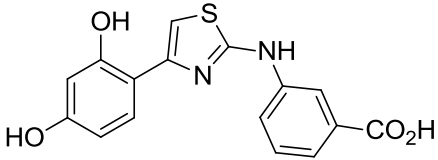
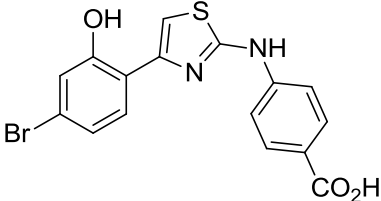
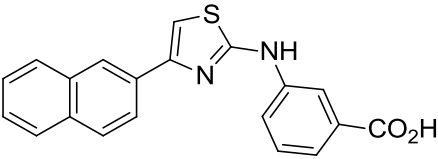
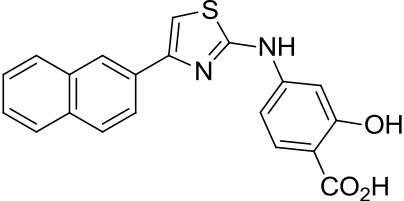
Fig 42: Key features of the structure of CK2 and of its allosteric pocket. (a) Key features of the structure of CK2 (based on 2PVR¹¹⁰). (b) Allosteric pocket of CK2 with 3.2-8e docked inside (based on PDB ID: 3JUH³³).

4.1.2 X-ray structures

Co-crystallization experiments in collaboration with Jean-Baptiste Reiser (Institut de Biologie Structurale, Grenoble) were envisaged to identify the binding site of our compounds. After several campaigns, suitable co-crystallization conditions were identified (based on PEG3350, pH 5.5, ammonium sulfate), and after a scale-up, diffracting crystals of CK2 α in the presence of several 2-aminothiazole derivatives were obtained (Table 4). Of note, the resolution obtained with the compound **3.1-3** was too low (superior to 3 Å) to lead to precise structure: its refinement was therefore not pursued. In addition, crystals obtained in the presence of compound **D3,35** (Table 4) were found without any ligand. However, electron density modification, representing compounds **3.2-7j**, **3.2-7e** and **3.2-8e** were identified: those compounds were located into the ATP pocket. The main interaction of our compounds with CK2 was between the carboxylic acid and the K68/D81 residues, with the cooperation of a water molecule (Fig 43). Of note, the same type of interaction is visible in CX-4945/CK2 α co-crystal structures (PDB ID: 3NGA and 3PE1).^{97,214} Moreover, the overall structure of CK2 α in the presence of our inhibitors is similar to those obtained in the presence of ATP-competitive inhibitors or

AMPPNP (PDB ID: 2PVR, 3MB6, 3MB7, 3NSZ).^{110,267} Therefore, based only on X-ray results, our class of compounds should exhibit an ATP-competitive mechanism of action. Consequently, we tried to answer to the key question: "How can we link the X-ray diffraction results with the whole set of our data?"

Table 4: Main parameters of the CK2 α X-ray structures obtained in the presence of various compounds.

Compound	Structure	Resolution	Electron density of the inhibitor
3.1-3		> 3 Å	-
3.2-7j		2.65 Å	Yes
D3,35		2.85 Å	No
3.2-7e		2.85 Å	Yes (partial)
3.2-8c		2.40 Å	partial
3.2-8e		2.20 Å	Yes

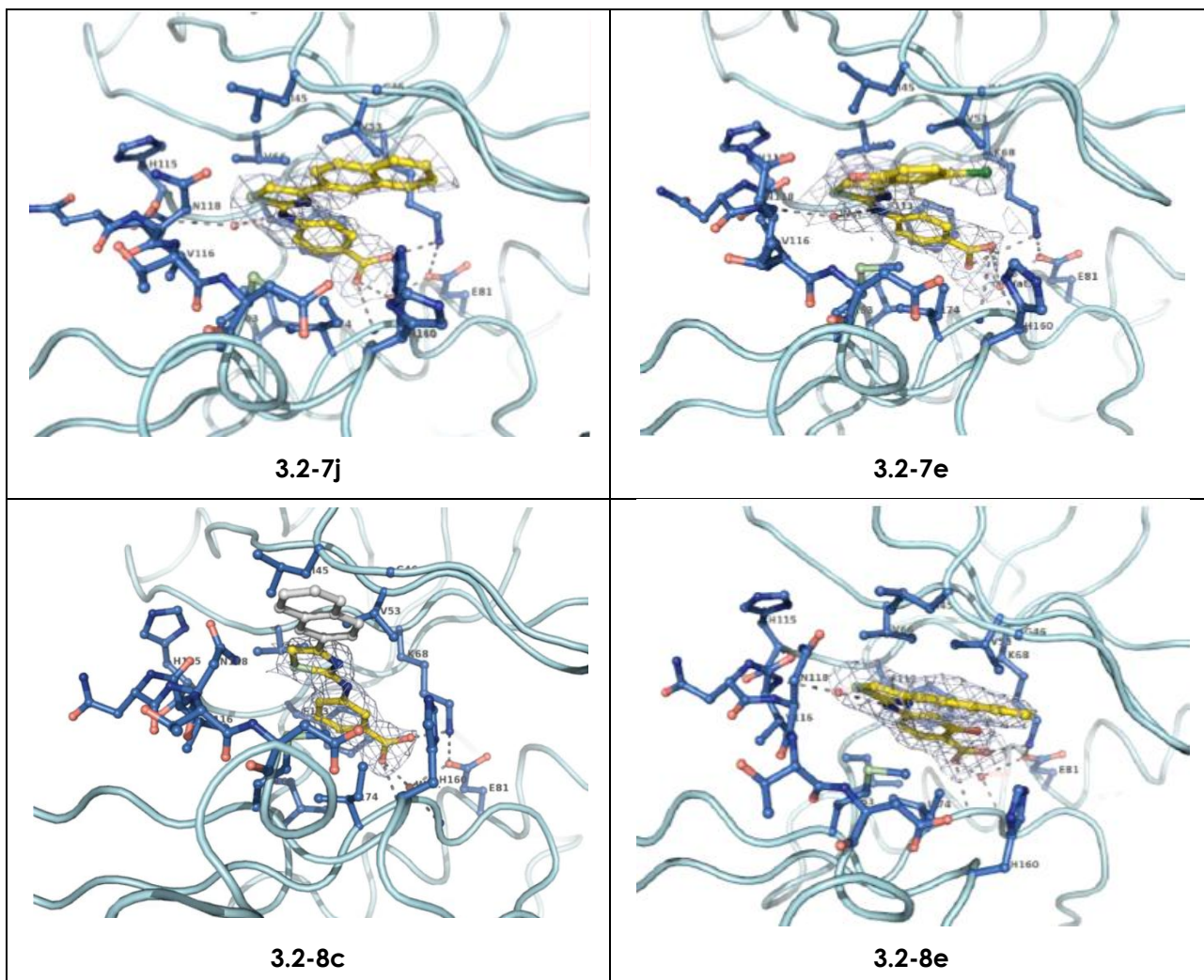


Fig 43: Representation of the ATP-binding pocket with several of our inhibitors, obtained from the X-ray structures.

The incompatibility of the results obtained from X-ray structures and the ones obtained from enzymatic kinetics, TdCD, STD-NMR and mutagenesis experiments (chapter 3.1) needed to be explained. Indeed, no information in the X-ray structures is in accordance with the mixed-type of inhibition, neither the lower thermal stability, nor the effects of V73A and K77A mutants. In addition, STD-NMR experiments clearly showed that 2-aminothiazole derivatives and CX-4945 could simultaneously bind to CK2 α . The latter is obviously impossible if 2-aminothiazole derivatives would bind into the same pocket than CX-4945, ie the ATP-site.

Crystal packing or crystallization conditions could be the source of the obtained incoherent structures. Indeed, co-crystals were obtained under special salt and pH conditions (pH = 5.5) in which CK2 α does not show any catalytic activity. In addition, X-ray structures are by definition obtained from a solid state which could block a specific conformation of the protein.

Due to their chemical structures, our compounds could certainly bind to the ATP-pocket, as seen in the X-ray structures. However, based on strong evidences, we have demonstrated that they could also bind to an allosteric pocket. Furthermore, the high cellular efficiency exhibited by compound **3.2-8e**, in comparison with ATP-competitive inhibitors, suggested that the cellular effects of our compounds relied on the allosteric mechanism of action.

Therefore, further co-crystallization campaigns are required to find the proper conditions to obtain new X-Ray structures consistent with the rest of our data. Additional attempts of co-crystallization, in presence of both CX-4945 and one of our inhibitor, will be considered.

4.1.3 Similarities and differences with others allosteric inhibitors

α C-helix displacement is a common method for allosteric inhibition of protein kinases¹²⁹ and several small molecules were described to bind near the α C-helix.^{128,140,148,268} Interestingly, as in the case of our allosteric inhibitors of CK2, the allosteric inhibitor of MEK1, PD318088,¹⁴³ and the allosteric inhibitor of ERK2, SCH772984¹⁴⁸ (Fig 44), bind at the interface of the α C-helix and of the glycine-rich loop, also called P-loop (Fig 45a).

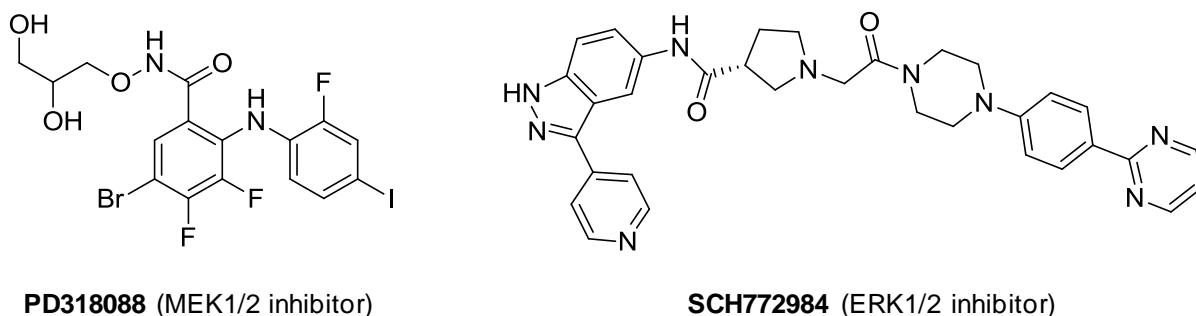


Fig 44: Chemical structures of PD318088 and SCH772984

The inactivation of MEK1 occurs through a small displacement (0.9 Å) of the α C-helix as well as a larger movement (2 Å) of the short helix present in the activation segment.²⁶⁹ The allosteric inhibitors of MEK1 (eg PD318088) stabilize this inactive conformation¹⁴³ and, interestingly, they bind to the protein in the presence of an ATP molecule or an ATP analog, with a synergistic effect.¹⁴⁴ Structure superimposition showed that the binding site of the allosteric MEK1 inhibitors (PD318088) and the allosteric CK2 inhibitor **3.2-8e** are in close proximity and share some similarities (Fig 45a,b). Nevertheless, the presence of the small helix in the activation segment of MEK1, and its flexibility combined with the one of the α C-helix, enable a deeper binding of the

allosteric MEK1 inhibitors in comparison with CK2 inhibitor **3.2-8e**. Moreover, the basic cluster of residues located in the α C-helix and in the activation segment of CK2, and necessary for **3.2-8e** binding, is absent in MEK1. Additionally, allosteric CK2 inhibitors and the ATP-competitive inhibitor, CX-4945, could bind together to CK2 (see chapter 3.1) but they could not bind in the presence of ATP or ATP analogs whereas MEK1 inhibitor can. Therefore, despite some similarities in their binding site, allosteric CK2 inhibitors and allosteric MEK1 inhibitors are very different and **3.1-7** and **3.2-8e** did not inhibit MEK1 (see the kinase panel, chapter 3.1 and 3.2).

SCH772984 is a potent and selective ERK inhibitor,¹⁴⁷ which acts through a simultaneous binding in the ATP-site and in the P-loop pocket.¹⁴⁸ The piperazine-phenyl-pyrimidine moiety of SCH772984 binds into the P-loop pocket near the α C-helix, with the P-loop Tyr36 shifted to the “in” position (Fig 45). The latter is similar to the binding of the naphthyl moiety of **3.2-8e** which also requires the switch to the “equivalent of Tyr36” in the CK2 structure, *ie* Tyr50. Interestingly, CK2 α and CK2 α' are strongly inhibited by SCH772984 but their mechanism of inhibition is not described.¹⁴⁸ However, SCH772984 also inhibits the kinase Haspin but in an ATP-competitive manner and the same mechanism could be suspected for CK2 as the residue Tyr64 of ERK1 necessary for SCH772984 binding is replaced by a lysine in the case of CK2.

Despite strong differences which enable to design highly selective inhibitors, the similarities in the binding pocket of these three compounds open the possibility to have similar pockets in other related kinases.

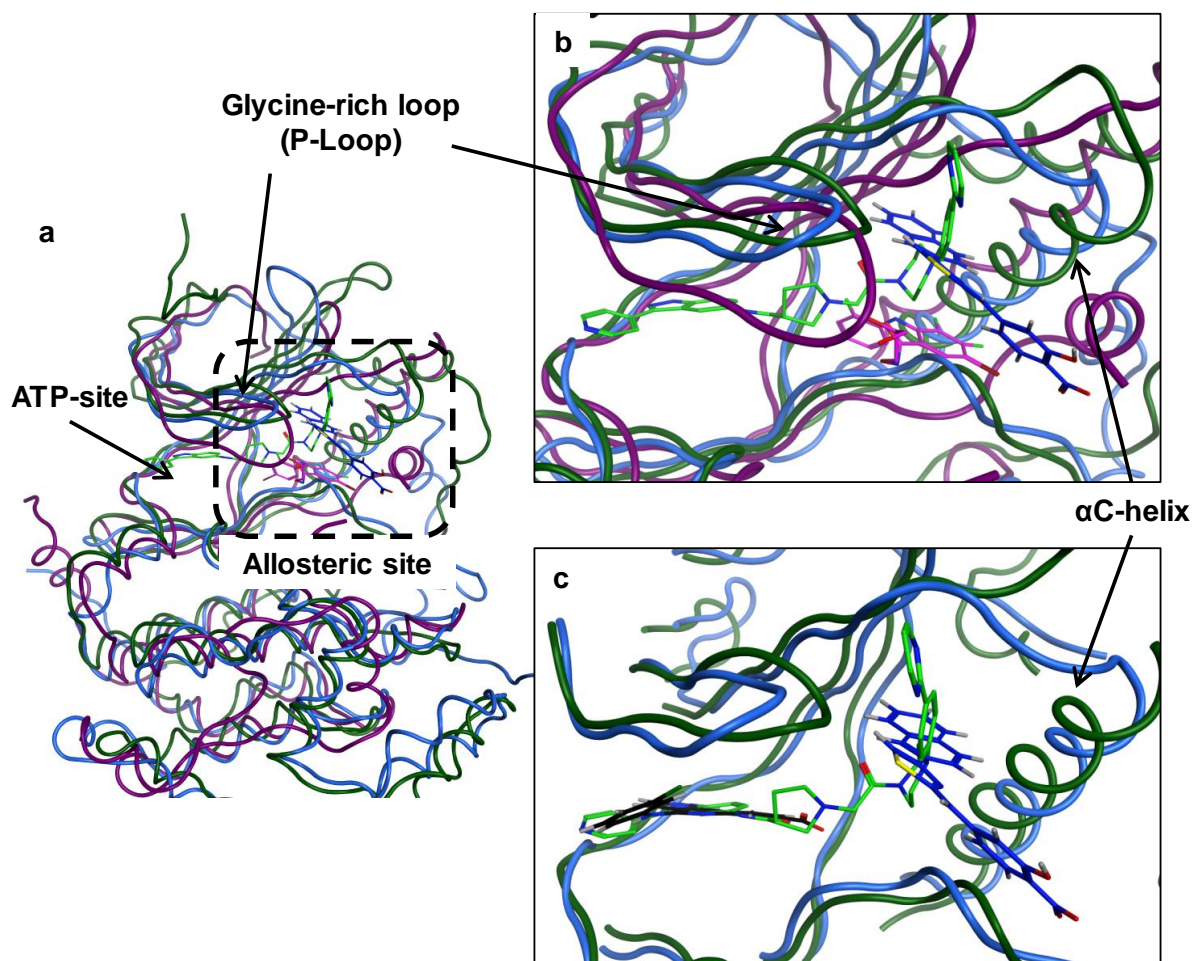


Fig 45: Allosteric binding site in CK2, MEK1 and ERK2. Structure from molecular modeling of CK2 (blue, based on PDB ID: 3JUH³³) and X-ray structures of MEK1 (magenta, PDB ID: 1S9J¹⁴³) and ERK2 (green, PDB ID: 4QTA¹⁴⁸) were superimposed. Respective allosteric inhibitors for each kinase, 3.2-8e for CK2, PD318088 for MEK1 and SCH772984 for ERK2 were depicted in dark blue, pink and bright green. (a) Overview of the kinase structures. (b) Overview of the allosteric pocket located between the α C-helix and the glycine-rich loop. (c) For clarity, only CK2/3.2-8e and ERK2/SCH772984 were conserved. The ATP-competitive inhibitor of CK2, CX-4945 (black), was docked in the ATP-pocket.

4.1.4 Indirect effect in the single-alanine mutagenesis experiments

In the single-alanine mutagenesis described in the chapter 3.1 and 3.2, we noticed an impact of the His160Ala mutation: a 2.2-fold increase of the IC_{50} was observed with **3.1-7**, and 1.7-fold for **3.2-8e**. Nonetheless, the His160 was not in direct interaction with our compounds in

the 3D structure models. Interestingly, an hydrogen bonding between Tyr50 and His160 was observed in the inactive structure (4UB7) described by Guerra, B. *et al.* (Fig 46)²¹⁸ Thus, we could hypothesize that the His160 residue is necessary to stabilize Tyr50 in the inactive conformation, and so for the efficient binding of our compounds.

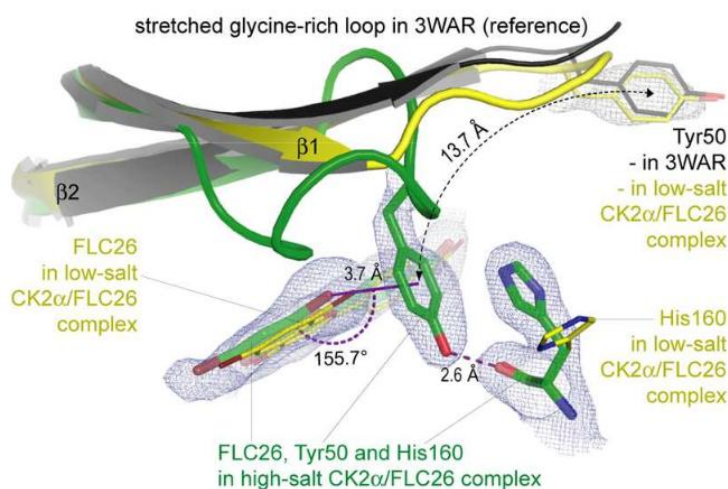


Fig 46: Glycine-rich loop displacement (from Guerra, B. *et al.*²¹⁸).

4.2 CK2α/CK2β interaction inhibitors

Different effects than with “classical” CK2 inhibitors were expected, as the regulatory subunit modulates the selectivity of CK2 toward a subset of substrate proteins.⁷⁷

Previously, a cyclic peptide (Pc) was identified as a potent *in vitro* modulator of CK2α but it was ineffective in cellular based assay.⁵⁰ Therefore, this peptide was conjugated to a viral TAT sequence and the resulting compound TAT-Pc was used in cellular-based assay. At the same time, a Virtual Ligand Screening (VLS) campaign was performed and several small molecules inhibitors of the α/β interaction were identified. After hit validation, one molecule **3.4-1** was selected as a true α/β interaction inhibitor. A small library of analogs was synthesized and then evaluated in biochemical assays and in cellular assays.

4.2.1 Structurale similarities with other related compound

Previously, 5,6-Dichlorobenzimidazole-1-β-D-ribofuranoside (DRB) was suggested to bind to two different sites: the ATP pocket and the “remote cavity” in the α/β interaction, although only CK2α inhibition through the interaction with the ATP pocket was proven.²⁰⁷ However,

interestingly structural similarities could be observed between DRB and our class of compounds **3.4-1** (Fig 47). Indeed, both compounds share hydrophobic moiety (benzimidazole or indole) which could deeply bind into the hydrophobic pocket, occupied by the Phe190 of CK2 β . In addition, the more polar moiety (ribofuranoside or ester/methoxy functions) are more exposed on the surface of CK2 α . Of note, active compounds from our library have an additional side chain composed of a piperidine linked to a methyl- or phenyl-sulfonamide. The latter function is responsible of the strict binding into the α/β interaction pocket, thus leading to a better observed affinity for CK2.

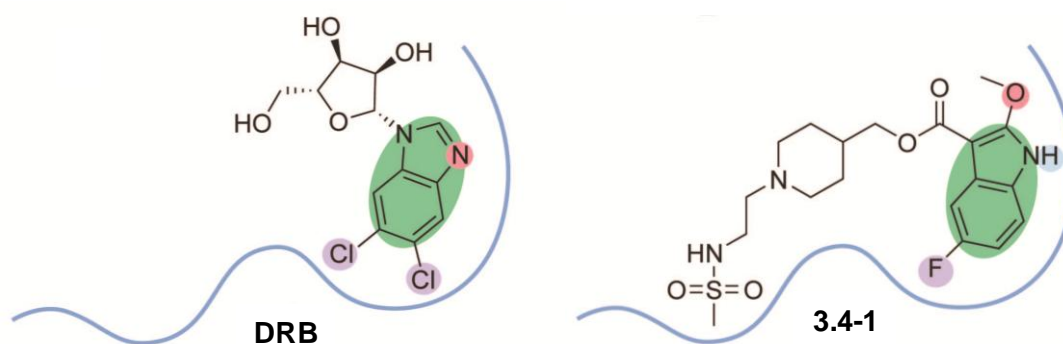


Fig 47: Schematic representation of the DRB (based on PDB ID: 3H30²⁰⁷) and compound 4.2-1 (based on docking experiments) in the α/β interaction pocket (blue line).

4.2.2 Effects in cell signaling

Both small molecules and the TAT-Pc construction induced different cellular effects than the ATP-competitive inhibitors or the allosteric inhibitors described in chapters 3.1 and 3.2. As described in Fig 48, CK2 α /CK2 β inhibitors led to degradation of EGFR which could block the MAPK, Akt and JNK pathways, therefore leading to a decrease of cell proliferation.²⁷⁰ An increase of p21 phosphorylation correlated with its translocation to the nucleus was also observed, the latter is likely to induce cell cycle arrest.^{260,271} In consequence, CK2 α /CK2 β interaction inhibitors seem to have a great potential in cancer therapy.

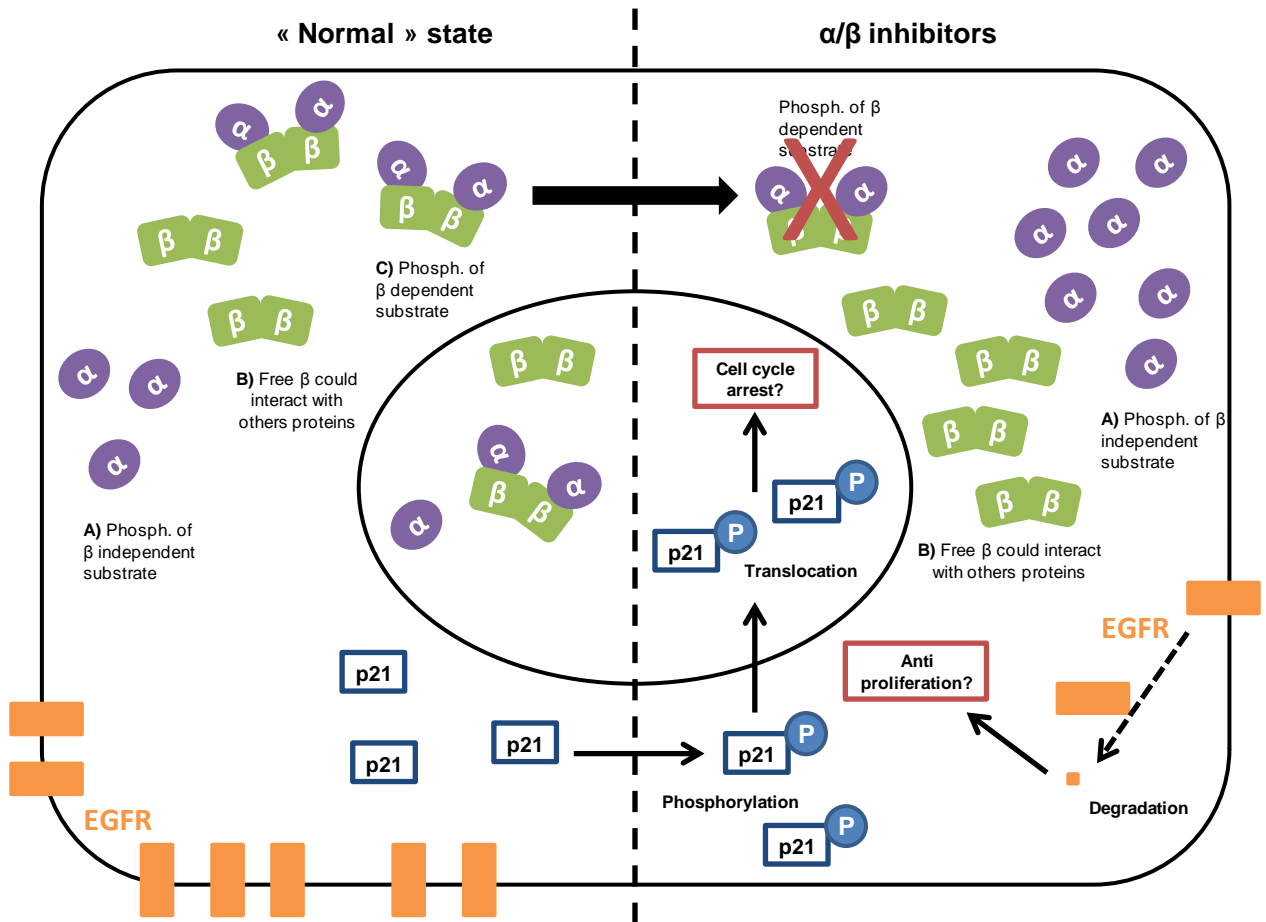


Fig 48: Schematic representation of the cellular consequences of the CK2α/CK2β interaction inhibition. “Normal” state represents the cell in absence of α/β interaction inhibitor and the dash line is the separation with the cell in presence of α/β interaction inhibitors.

4.3 Perspectives of further drug development

The two classes of compound described herein are of potential therapeutic interest. Therefore, the question of their further development into *in vivo* candidates emerged. Compound **3.2-8e** for the allosteric inhibitor and compound **3.4-16** for the protein-protein interaction inhibitor are the respective lead compound of each class (Fig 49).

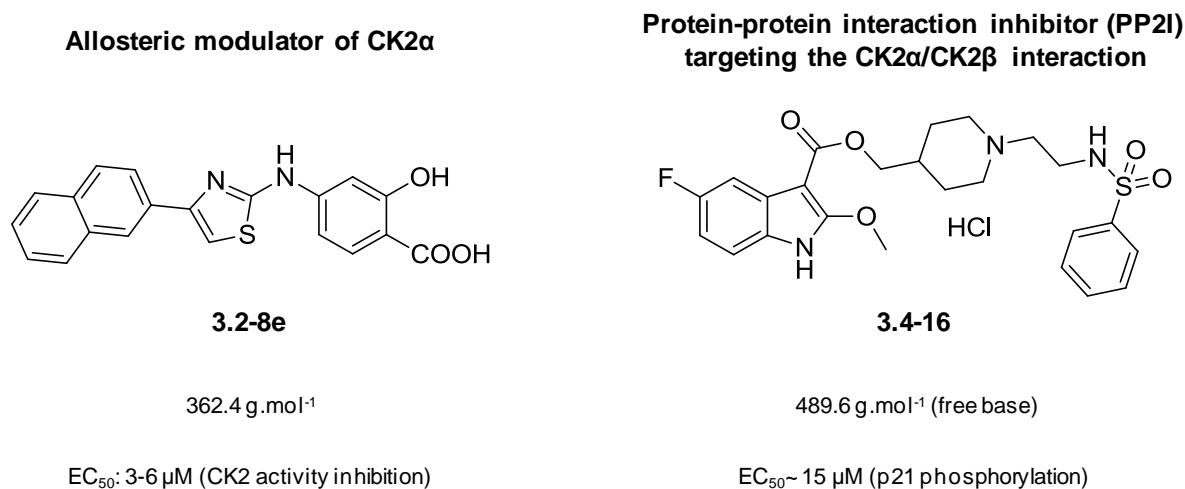


Fig 49: Overview of the lead compounds of each class.

4.3.1 Allosteric modulator of CK2 α

Compound **3.2-8e** demonstrated acceptable cell efficiency despite a strong binding to bovine serum albumin. Indeed, decrease of the serum concentration in the cell culture medium led to significant improvement of its cellular efficiency. This feature is in accordance with the chemical structure of **3.2-8e** whose acid function attached to a strong hydrophobic naphthyl part is the good pharmacophore for albumin binding.²⁷² The structural optimization of this compound in order to decrease the albumin binding is tempting, especially to modify the naphthyl ring, which is not really drug-like. And this appear to be feasible, thanks to the low molecular weight (362.4 g.mol⁻¹) of compound **3.2-8e**. However, literature reviewing demonstrated that 24% of the recently approved drugs have a plasma protein binding higher than 99% and that the low intrinsic clearance is the most important parameter to reach an acceptable *in vivo* unbound level of drug.²⁷³ Therefore, **3.2-8e** does not have to be optimized before further *in vivo* development in reason of its binding to albumin. Nevertheless, the sharp

SAR and the recent identification of the binding site could enable a quick optimization of compound **3.2-8e** in regard to potency and drug-like properties.

4.3.2 CK2 α /CK2 β interaction inhibitors

On the other hand, the optimized compound, **3.4-16**, belonging to the CK2 α /CK2 β interaction inhibitors is still in the preliminary development. Indeed, the SAR sample size appears to be relatively limited and further studies could lead to significant improvement of its affinity. Compound **3.4-16** demonstrated the feasibility of the CK2 α /CK2 β interaction inhibition and its therapeutic interest. Thus, the novelty of this class of compounds is remarkable. However, protein-protein interaction inhibition is highly challenging and requires large and long studies.^{178,187,188} Consequently, further STD-NMR, X-ray crystallography, SAR studies and cellular evaluations are necessary prior to consider *in vivo* development of this class of compounds.

4.4 Outlook

In conclusion, the present study aimed to describe two novel approaches to target CK2 (Fig 50):

- CK2 modulators which are able to block CK2 α into an inactive state, through a binding in an allosteric pocket located at the interface of the α C-helix and the P-loop.
- CK2 α /CK2 β interaction inhibitors which are able to counteract the formation of the holoenzyme through binding in the β interaction pocket in the N-terminal lobe of CK2 α .

We believe that the two new strategies described herein are of main interest because they could lead to more selective inhibitors with better *in vivo* efficiency. Moreover, a fine substrate-dependent modulation of CK2 activity instead of a complete inhibition could be achieved through both strategies, thus they could decrease the side effect inherent to cancer treatment. A precise mapping of the *in vivo* consequences of CK2 modulation with the inhibitors described herein will be required to understand completely their implications in cell signaling modulation.

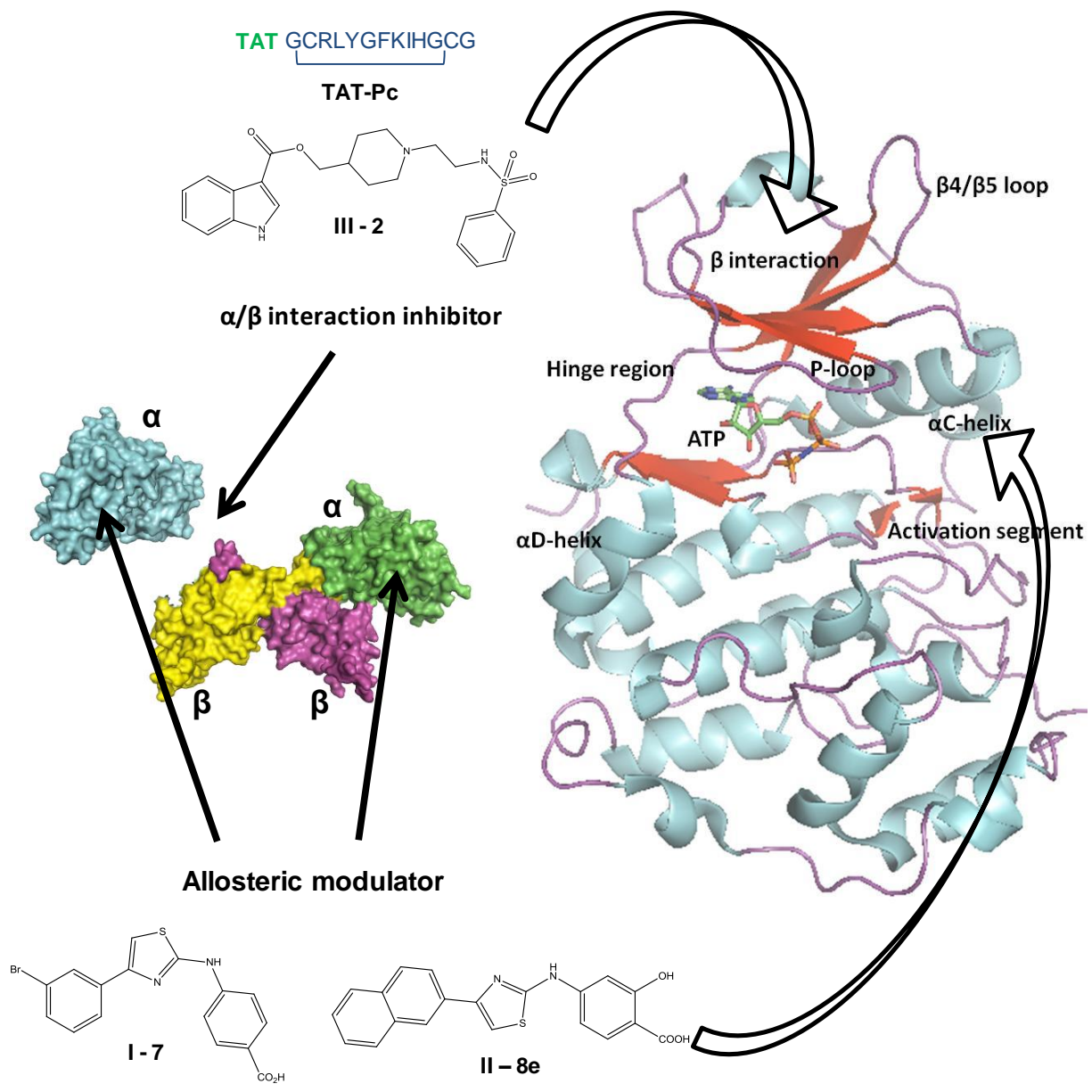


Fig 50: Schematic representation of the two novel strategies targeting CK2 presented in this work.

5. Experimental section

6.1 Chemistry

6.1.1 Synthesis of compounds of chapter 3.1

4-((4-(3-Nitrophenyl)thiazol-2-yl)amino)benzoic acid (**1**) was purchased from Sigma-Aldrich. All commercially available chemicals (phenylthiourea, 2-bromo-3'-nitro-acetophenone, 1,2-dichloro-1-ethoxyethane, 2-bromoacetophenone, 2-bromo-4'-methoxyacetophenone, 2-bromo-1-(3-bromophenyl)ethanone) and solvents were purchased from Sigma-Aldrich, Acros Organics, Fischer scientific or Alfa Aesar and were used without further purification. Reactions were monitored by Thin Layer Chromatography (TLC Silica gel 60 F254) purchased from Merck and observed under UV light (254 nm). Purification by semi-preparative HPLC was carried out on an Agilent 1200 series HPLC system (Agilent Technologies) using an Agilent C18 column (30 x 100 mm/10 μ m) as stationary phase and a gradient of water and acetonitrile as eluent. ^1H and ^{13}C NMR spectra were obtained in dimethylsulphoxide- d_6 on a Bruker DRX-500 instrument, operating at 500 MHz for the ^1H and at 125 MHz for the ^{13}C at 300 K, using residual signal of deuterated NMR solvent as internal reference ²⁷⁴. Chemical shifts are reported in parts per million (ppm), multiplicity of the signals are indicated by lower-case letters (singlet s, doublet d, triplet t, quadruplet q, multiplet m, broad singlet br s, or combination of letters). DEPT 135 was used to determine carbon valence. Analytical HPLC was performed using a SpectraSYSTEM™ (ThermoFisher) with a Macherey-Nagel C18 column (3 x 125 mm/5 μ m). HPLC purities were determined by UV absorption at 254 nm. ElectroSpray Ionisation (ESI) mass spectra were measured on a Finnigan Surveyor MSQ Plus mass spectrometer (ThermoFisher). Melting points (mp) of the solids were determined by SMP3 Melting Point Apparatus from Bibby Sterling.

4-Thioureidobenzoic acid (i). 4-Thioureidobenzoic acid was prepared according to the procedure already described ²³⁹. Carbon disulfide (22 mmol, 1.32 mL) was slowly added to a mixture of 4-aminobenzoic acid (7.3 mmol, 1 g), THF (5 mL), H_2O (5 mL) and Et_3N (18 mmol, 1.82 mL). The resulting mixture was stirred at RT for 24 h. Then iodine (7.7 mmol, 1.94 g) in THF (5 mL) was added dropwise at 0 °C and mixture was stirred for 3h. A 1 M HCl aqueous solution (7.5 mL) and Na_2SO_3 (1.46 mmol, 184 mg) were added and stirring was pursued for 15 min. The aqueous layer was extracted with EtOAc (3 x 50 mL). Combined organic layers were washed twice with brine, dried on Na_2SO_4 , filtered and concentrated to give the isothiocyanate intermediate as a slightly yellow solid, which was converted to the thiourea derivatives by stirring it at RT in NH_4OH

(30 %) for 6 h. After removal of the insolubles by filtration on a sintered-glass funnel, filtrate was concentrated to afford the *title* product as an off-white solid (7.3 mmol, 1.43 g). Yield = quantitative. LC-UV purity = 80 %. The compound was not ionized by ESI. ¹H-NMR (500 MHz, DMSO-d₆): δ (ppm) 7.56 – 7.58 (m, 2H), 7.80 – 7.82 (m, 2H). ¹³C-NMR (125.7 MHz, DMSO-d₆): δ (ppm) 116.9, 120.9, 129.3, 130.6, 169.2, 181.0. mp = 189-191 °C (in accordance with literature: 194 °C) ²⁷⁵.

Methyl 4-((4-(3-nitrophenyl)thiazol-2-yl)amino)benzoate (2). Three drops of 95 % H₂SO₄ were added to a mixture of 4-((4-(3-nitrophenyl)thiazol-2-yl)amino)benzoic acid (0.14 mmol, 46 mg) in MeOH (5 mL) and the mixture was then heated at reflux for 2 h. Na₂CO₃ 1 M was added until pH = 10-11 and MeOH was removed under *vacuo*. The obtained solid was filtrated and washed with water (2 x 5 mL) to afford the *title* product as a yellow solid (0.14 mmol, 49 mg). Yield = quantitative. LC-UV purity = 97 %. LCMS (ESI⁺) m/z = 356.01 for [M+H]⁺. ¹H-NMR (500 MHz, DMSO-d₆): δ (ppm) 3.82 (s, 3H), 7.79 (m, 4H), 7.96 (s, 2H), 8.17 (s, 1H), 8.40 (s, 1H), 8.71 (s, 1H), 10.84 (s, 1H). ¹³C-NMR (125.7 MHz, DMSO-d₆): δ (ppm) 51.7 (CH₃), 107.0 (CH), 116.1 (2 x CH), 119.9 (CH), 121.8 (C), 122.1 (CH), 130.3 (CH), 130.6 (2 x CH), 131.9 (CH), 135.7 (C), 144.9 (C), 147.8 (C), 148.3 (C), 162.6 (C), 165.8 (C). mp = 242-244 °C.

General procedure for the preparation of 2-aminothiazole analogs. An ethanolic solution of 2'-bromo-acetophenone derivative and aryl thiourea derivative at equimolar ratio adjusted with respect to LC-UV purity was heated at 80 °C for 3-12 h (reaction monitoring by TLC). The mixture was then cooled down to RT and water (twice more than EtOH v/v) was added. Mixture was stirred for 30 min and then filtrated. The obtained solid was washed twice with water to afford the product as a solid. When necessary, purification was performed (i) by recrystallization or washing with boiling MeCN (ii) by recrystallization or washing in H₂O/MeOH (iii) by HPLC preparative to obtain the product with LC-UV purity higher than 95 %.

4-(3-Nitrophenyl)-N-phenylthiazol-2-amine (3). The reaction was carried out according to the general procedure. Scale: 2-bromo-3'-nitro-acetophenone (0.66 mmol, 161 mg), phenylthiourea (0.66 mmol, 100 mg), absolute EtOH (5 mL). After removal of the solvents, water (10 mL) and MeOH (2 mL) were added. The pH of the solution was adjusted to 9 with solid Na₂CO₃ and then stirred for 1 h. After filtration and washing of the residual solid with water (3 x 5 mL), the product was obtained as a yellow solid (0.66 mmol, 196 mg). Yield = quantitative. LC-UV purity = 99 %. LCMS (ESI⁺) m/z = 298.06 for [M+H]⁺. ¹H-NMR (500 MHz, DMSO-d₆): δ (ppm) 6.99 (t, J = 6.9 Hz, 1H), 7.36 (t, J = 6.6 Hz, 2H), 7.65 (s, 1H), 7.71 (m, 3H), 8.14 (d, J = 7.3 Hz, 1H), 8.35 (d, J = 6.9 Hz, 1H), 8.69 (s, 1H), 10.39 (s, 1H). ¹³C-NMR (125.7 MHz, DMSO-d₆): δ (ppm) 105.6 (CH), 116.9 (2 x CH), 119.8

(CH), 121.4 (CH), 121.9 (CH), 129.0 (2 x CH), 130.1 (CH), 131.7 (CH), 135.9 (C), 140.9 (C), 147.6 (C), 148.2 (C), 163.5 (C). mp = 136-138 °C. (in accordance with literature: 122-124 °C)²⁷⁶.

4-(Thiazol-2-ylamino)benzoic acid (4). The reaction was carried out according to the general procedure. Scale: 1,2-dichloro-1-ethoxyethane (0.41 mmol, 50 μ L), 4-thioureidobenzoic acid (0.41 mmol, 80 mg), absolute EtOH (5 mL). Purification by semi-preparative HPLC (H₂O/MeCN/TFA: from 79/20/1 to 0/99/1 in 40 min) to afford ethyl 4-(thiazol-2-ylamino)benzoate as a white solid (0.09 mmol, 23 mg). Yield = 23 %. LC-UV purity = 96 %. LCMS (ESI⁺) m/z = 249.01 for [M+H]⁺. The ethyl 4-(thiazol-2-ylamino)benzoate (0.085 mmol, 21 mg) obtained was directly hydrolyzed in a mixture of THF (2 mL) and aqueous 0.5 M NaOH (1.15 mmol, 2.3 mL) at reflux for 4 h. Aqueous 1 M HCl was added until pH = 1 and then solvents were removed *in vacuo*. Crude product was purified by semi-preparative HPLC (H₂O/MeCN + 0.1 % TFA: from 90/10 to 10/90 in 40 min) to afford the *title* product as a white solid (0.07 mmol, 16 mg). Yield = 86 %. LC-UV purity > 99 %. LCMS (ESI⁺) m/z = 220.78 for [M+H]⁺. ¹H-NMR (500 MHz, DMSO-d₆): δ (ppm) 7.02 (d, J = 3.8 Hz, 1H), 7.33 (d, J = 3.8 Hz, 1H), 7.72 (d, J = 8.5 Hz, 2H), 7.88 (d, J = 8.8 Hz, 2H), 10.59 (s, 1H). ¹³C-NMR (127 MHz, DMSO-d₆): δ (ppm) 109.7 (CH), 115.7 (2 x CH), 122.5 (C), 130.7 (2 x CH), 138.8 (CH), 144.9 (C), 162.9 (C), 166.9 (C). mp = 270-272 °C (commercially available).²⁷⁷

4-((4-Phenylthiazol-2-yl)amino)benzoic acid (5). The reaction was carried out according to the general procedure. Scale: 2-bromo-acetophenone (0.51 mmol, 102 mg), 4-thioureidobenzoic acid (0.51 mmol, 100 mg), absolute EtOH (5 mL). Purification was performed by washing with boiling MeCN (5 mL) and hot filtration to afford the *title* product as a grey solid (0.24 mmol, 70 mg). Yield = 58 %. LC-UV purity = 95 %. The compound was not ionized by ESI. ¹H-NMR (500 MHz, DMSO-d₆): δ (ppm) 7.33 (t, J = 6.9 Hz, 1H), 7.44 (t, J = 6.9 Hz, 3H), 7.84 (d, J = 8.5 Hz, 2H), 7.95 (d, J = 7.9 Hz, 4H), 10.70 (br s, 1H). ¹³C-NMR (125.7 MHz, DMSO-d₆): δ (ppm) 104.1 (CH), 115.9 (2 x CH), 122.8 (C), 125.7 (2 x CH), 127.7 (CH), 128.6 (2 x CH), 130.8 (2 x CH), 134.3 (C), 144.9 (C), 150.2 (C), 162.2 (C), 167.0 (C). mp = 256-258 °C (in accordance with literature: 252 °C).²⁷⁸

4-((4-(4-Methoxyphenyl)thiazol-2-yl)amino)benzoic acid (6). The reaction was carried out according to the general procedure. Scale: 2-bromo-4'-methoxy-acetophenone (0.71 mmol, 163 mg), 4-thioureidobenzoic acid (0.51 mmol, 100 mg), absolute EtOH (10 mL). Purification was performed by washing with boiling MeCN (5 mL) and hot filtration to afford the *title* product as a grey solid (0.15 mmol, 49 mg). Yield = 29 %. LC-UV purity = 96 %. LCMS (ESI⁺) m/z = 327.09 for [M+H]⁺. ¹H-NMR (500 MHz, DMSO-d₆): δ (ppm) 3.80 (s, 3H), 7.00 (d, J = 7.3 Hz, 2H), 7.29 (s, 1H), 7.81 (d, J = 7.9 Hz, 2H), 7.87 (d, J = 7.9 Hz, 2H), 7.93 (d, J = 7.9 Hz, 2H), 10.65 (s, 1H), 12.54 (br s, 1H, O-H).

^{13}C -NMR (125.7 MHz, DMSO-d_6): δ (ppm) 55.1 (CH_3), 101.9 (CH), 114.0 (2 x CH), 115.9 (2 x CH), 122.7 (C), 127.1 (2 x CH), 127.2 (C), 130.8 (2 x CH), 145.0 (C), 150.1 (C), 158.9 (C), 162.1 (C), 167.0 (C). mp = 266-268 °C (commercially available).

4-((4-(3-Bromophenyl)thiazol-2-yl)amino)benzoic acid (7). The reaction was carried out according to the general procedure. Scale: 2-bromo-1-(3-bromophenyl)ethanone (0.36 mmol, 100 mg), 4-thioureidobenzoic acid (0.54 mmol, 106 mg), absolute EtOH (5 mL). Purification was performed by recrystallization in MeCN (5 mL) to afford the *title* product as a yellow solid (0.20 mmol, 75 mg). Yield = 56 %. LC-UV purity = 95 %. LCMS (ESI⁺) m/z = 374.62/376.65 for $[\text{M}+\text{H}]^+$. ^1H -NMR (500 MHz, DMSO-d_6): δ (ppm) 7.40 (t, J = 7.9 Hz, 1H), 7.51 (ddd, J = 7.9, 1.9, 0.9 Hz, 1H), 7.59 (s, 1H), 7.80 (d, J = 8.8 Hz, 2H), 7.94 – 7.97 (m, 3H), 8.11 (t, J = 1.9 Hz, 1H), 10.72 (s, 1H), 12.60 (br s, 1H). ^{13}C -NMR (125.7 MHz, DMSO-d_6): δ (ppm) 105.7 (CH), 115.9 (2 x CH), 122.1 (C), 122.9 (C), 124.7 (CH), 128.0 (CH), 130.3 (CH), 130.8 (2 x CH), 130.9 (CH), 136.5 (C), 144.7 (C), 148.4 (C), 162.4 (C), 166.9 (C). mp = 281-283°C.

6.1.2 Synthesis of compounds of chapter 3.2

4-((4-(3-Nitrophenyl)thiazol-2-yl)amino)benzoic acid (**1**) and 3-((4-(3-nitrophenyl)thiazol-2-yl)amino)benzoic acid (**6b**) was purchased from Sigma-Aldrich. All commercially available chemicals, 2-bromo-1-(3-nitrophenyl)ethanone (**4d**), 2-bromo-1-phenylethanone (**4e**), 2-bromo-1-(3-bromophenyl)ethanone (**4f**), 2-bromo-1-(2,4-dimethoxyphenyl)ethanone (**4g**), 2-bromo-1-(2,4-dihydroxyphenyl)ethanone (**4h**), 2-bromo-1-(4-bromo-2-hydroxyphenyl)ethanone (**4i**), 1-bromo-3,3-dimethylbutan-2-one (**4j**), 2-bromo-1-(thiophen-3-yl)ethanone (**4k**), 2-bromo-1-(naphthalen-2-yl)ethanone (**4l**), 3-(2-bromoacetyl)-2H-chromen-2-one (**4m**), 1-(benzofuran-2-yl)-2-bromoethanone (**4n**), 1-(benzo[b]thiophen-5-yl)-2-bromoethanone (**4o**), other starting materials and solvents were purchased from Sigma-Aldrich, Acros Organics, Fischer scientific or Alfa Aesar and were used without further purification. Reactions were monitored by Thin Layer Chromatography (TLC Silica gel 60 F254) purchased from Merck and observed under UV light (254 nm). Purification by semi-preparative HPLC was carried out on an Agilent 1200 series HPLC system (Agilent Technologies) using an Agilent C18 column (30 x 100 mm/10 μ m) as stationary phase and a gradient of water and acetonitrile as eluent. ^1H and ^{13}C NMR spectra were obtained in dimethylsulphoxide- d_6 , acetone- d_6 or CDCl_3 on a Bruker DRX-500 instrument, operating at 500 MHz for the ^1H and at 125 MHz for the ^{13}C at 300K, using residual signal of deuterated NMR solvent as internal reference.²⁷⁹ Chemical shifts are reported in parts per million (ppm), multiplicity of the signals are indicated by lower-case letters (singlet s, doublet d, triplet t, quadruplet q, multiplet m, broad singlet br s, or combination of letters). DEPT 135 was used to determine carbon multiplicity. Analytical HPLC was performed using a SpectraSYSTEM™ (ThermoFisher) with a Macherey-Nagel C18 column (3 x 125 mm/5 μ m). HPLC purities were determined by UV absorption at 254 nm. ElectroSpray Ionisation (ESI) mass spectra were measured on a Finnigan Surveyor MSQ Plus mass spectrometer (ThermoFisher). Melting points (mp) of solids were determined by SMP3 melting point apparatus from Bibby Sterling.

General procedure 1 for the preparation of 2'-bromo-acetophenone analogs from acetophenones (method A):²³⁷

Bromine (1 eq) was added dropwise over 5 min to a stirred and warmed (40°C) solution of acetophenone derivative (1 eq) in CHCl_3 . At the end of the addition, the mixture was cooled down at RT; Et_2O was then added, followed by a saturated aqueous solution of NaHCO_3 and the resulting mixture was then stirred for 30 min. The organic layer was separated, washed with a saturated aqueous solution of NaHCO_3 , dried with Na_2SO_4 and filtered. The volatiles were removed under reduced pressure to afford the product as a solid, which was used in the next step without further purification.

General procedure 2 for the preparation of 2'-bromo-acetophenone analogs from acetophenones (method B):²³⁸

Bromine (1 eq) was added dropwise to a solution of acetophenone derivative (1 eq) in a mixture of MeOH and HBr 32 % (2 eq) in AcOH. The mixture was then heated at 60°C for 4h. After removal of the volatiles *in vacuo*, the solid residue was washed 5 times with Et₂O and filtered to afford the product as a solid, which was used in the next step without further purification.

2'-bromo-3-methoxy-acetophenone (4a)

The reaction was carried out according to general procedure 1, scale: 3-methoxyacetophenone (3.33 mmol, 459 µL), bromine (3.33 mmol, 172 µL), CHCl₃ (10 mL), Et₂O (100 mL), to afford the *title* product as a yellow solid (3.33 mmol, 762 mg). Yield = quantitative. LC-UV purity = 75%. The compound was not ionized by ESI⁺. ¹H-NMR (500 MHz, CDCl₃) δ = 3.70 (s, 3H, CH₃-O), 4.3 (s, 2H, CH₂-Br), 6.99 (ddd, J = 1.0; 2.5; 8.2 Hz, 1H), 7.24 (t, J = 8.2 Hz, 1H), 7.34 (dd, J = 1.6, 2.5 Hz, 1H), 7.39 (ddd, J = 1.0, 1.6, 7.6 Hz, 1H). mp = 52-54°C, spectral data and melting point are in accordance with lit. data (61-62°C).²⁸⁰

2'-bromo-4-methoxy-acetophenone (4b)

The reaction was carried out according to general procedure 1, scale: 4-methoxyacetophenone (3.33 mmol, 500 mg), bromine (3.33 mmol, 172 µL), CHCl₃ (10 mL), Et₂O (100 mL), to afford the *title* product as a grey solid (3.33 mmol, 765 mg). Yield = quantitative. LC-UV purity = 78%. LC-MS (ESI⁺) m/z = 229.31 for [M+H]⁺. ¹H-NMR (500 MHz, CDCl₃) δ = 3.89 (s, 3H, CH₃-O), 4.40 (s, 2H, CH₂-Br), 6.95 – 6.97 (m, 2H), 7.96 – 7.98 (m, 2H). mp = 49-51°C, spectral data is in accordance with lit. data^{281,282}

2-bromo-1-(pyridin-2-yl)ethanone hydrogen bromide (4c)

The reaction was carried out according to general procedure 2, scale: 2-acetylpyridine (8.2 mmol, 930 µL), bromine (8.2 mmol, 430 µL), HBr 32 % in AcOH (16.5 mmol, 2.98 mL), MeOH (1 mL), to afford the *title* product as a slightly yellow solid (8.2 mmol, 2.3 g). Yield = quantitative. LC-UV purity = 85%. LC-MS (ESI⁺) m/z = 200.05/202.08 for [M+H]⁺. ¹H-NMR (500 MHz, CDCl₃) δ = 4.95 (s, 2H, CH₂-Br), 7.70 – 7.73 (m, 1H), 7.99 (td, J = 1.3, 7.9 Hz, 1H), 8.04 – 8.07 (m, 1H), 8.62 (br s, NH⁺), 8.70 – 8.71 (m, 1H). mp = 206-208°C, spectral data and melting point are in accordance with lit. data (200-205°C).²⁸³

General procedure 3 for the preparation of thiourea analogs from amines:

Carbon disulfide (3 eq) was slowly added to a mixture of aminobenzoic acid derivative (1 eq) in a 1/1 THF/H₂O (0.7 mol.L⁻¹) solvent mixture and Et₃N (2.5 eq). The resulting mixture was stirred at RT for 24h. Then iodine (1.05 eq) in THF (5 mL) was added dropwise at 0°C and the mixture was stirred for 3h. A 1M HCl aqueous solution (7.5 mL) and Na₂SO₃ (0.2 eq) were added and the stirring was continued for 15 min. The aqueous layer was extracted with EtOAc (3 x 50 mL). The combined organic layers were washed twice with brine (25 mL) and dried on Na₂SO₄. After filtration, the volatiles were removed under reduced pressure to give the isothiocyanate intermediate as a slightly yellow solid, which was converted to the thiourea derivative by stirring at RT in NH₄OH (100 mL) for 6h. NH₄OH refers to a 35% w/w ammonia solution in water. After removal of the solids by filtration on a sintered-glass funnel, the filtrate was concentrated to afford the thiourea product, which was used in the next step without further purification.

4-thioureidobenzoic acid (5a)

The reaction was carried out according to the general procedure 3, scale: 4-aminobenzoic acid (7.3 mmol, 1 g), to afford the *title* product as an off-white solid (7.3 mmol, 1.43 g). Yield = quantitative. LC-UV purity = 80%. The compound was not ionized by ESI⁺. ¹H-NMR (500 MHz, DMSO-d₆): δ = 7.56 – 7.58 (m, 2H), 7.80 – 7.82 (m, 2H). mp = 189-191°C, spectral data and melting point are in accordance with lit. data (194°C).²⁷⁵

3-thioureidobenzoic acid (5b)

The reaction was carried out according to the general procedure 3, scale: 3-aminobenzoic acid (7.3 mmol, 1 g), to afford the *title* product as an off-white solid (7.3 mmol, 1.43 g). Yield = quantitative. LC-UV purity = 96%. The compound was not ionized by ESI⁺. ¹H-NMR (500 MHz, DMSO-d₆): δ = 7.28 (t, J = 7.8 Hz, 1H), 7.57 – 7.59 (m, 2H), 8.04 (d, J = 6.5 Hz, 1H), 8.92 (br s, 1H), 10.96 (br s, 1H). mp = 183-185°C, melting point is in accordance with lit. data (163°C).²⁸⁴

2-(4-thioureidophenyl)acetic acid (5d)

The reaction was carried out according to the general procedure 3, scale: 2-(4-aminophenyl)acetic acid (3.31 mmol, 500 mg), to afford the *title* product as an off-white solid (3.1 mmol, 651 mg). Yield = 93 %. LC-UV purity = 97%. LC-MS (ESI⁺) m/z = 211.05 for [M+H]⁺. ¹H-NMR (500 MHz, DMSO-d₆): δ = 3.34 (s, 2H), 5.00 (br s, 3H), 7.15 (d, J = 8.5 Hz, 2H), 7.30 (d, J = 8.2 Hz, 2H), 7.58 (br s, 1H), 10.2 (br s, 1H). ¹³C-NMR (125.7 MHz, DMSO-d₆): δ = 43.0, 122.7, 129.2, 133.4, 137.2, 173.9, 181.0. mp = 139-141°C (partially described).²⁸⁵

5-thioureidoisophthalic acid (5e)

The reaction was carried out according to the general procedure 3, scale: 5-aminoisophthalic acid (7.3 mmol, 1.32 g), to afford the *title* product as an off-white solid (7.3 mmol, 1.75 g). Yield = quantitative. LC-UV purity = 82%. The compound was not ionized by ESI⁺. ¹H-NMR (500 MHz, DMSO-d₆): δ = 7.53 (s, 1H), 8.09 – 8.18 (m, 3H), 9.18 (br s, 1H), 11.20 (br s, 1H). ¹³C-NMR (125.7 MHz, DMSO-d₆): δ = 124.8, 125.5, 137.3, 139.4, 170.4, 181.6. mp = 246-248°C.

2-hydroxy-4-thioureidobenzoic acid (5f)

The reaction was carried out according to the general procedure 3, scale: 4-aminosalicylic acid (7.3 mmol, 1.12 g) to afford the *title* product as an off-white solid (7.3 mmol, 1.55 g). Yield = quantitative. LC-UV purity = 70%. The compound was not ionized by ESI⁺. ¹H-NMR (500 MHz, DMSO-d₆): δ = 6.73 (dd, J = 2.2, 8.2 Hz, 1H), 6.96 (s, 1H), 7.30 – 7.50 (br s, labile H), 7.60 (d, J = 8.2 Hz, 1H), 7.56 – 7.70 (br s, labile H), 10.00 (s, 1H). mp = 185-187°C, melting point is in accordance with lit. data (179-180°C).²⁸⁶

4-methoxy-3-thioureidobenzoic acid (5g)

The reaction was carried out according to the general procedure 3, scale: 3-amino-4-methoxybenzoic acid (7.3 mmol, 1.22 g) to afford the *title* product as an off-white solid (7.3 mmol, 1.65 g). Yield = quant. LC-UV purity = 97%. LC-MS (ESI⁺) m/z = 226.79 for [M+H]⁺. ¹H-NMR (500 MHz, DMSO-d₆): δ = 3.80 (s, 3H), 5.33 (br s, labile H), 6.97 (d, J = 8.8 Hz, 1H), 7.52 (br s, 1H), 7.70 (dd, J = 1.9, 8.5 Hz, 1H), 8.10 (s, 1H). ¹³C-NMR (125.7 MHz, DMSO-d₆): δ = 55.7, 110.4, 126.5, 127.5, 127.7, 129.6, 154.2, 169.3, 181.6. mp = 241-243°C.

Phenylthiourea (5i)

Phenylisothiocyanate (8.37 mmol, 1 mL) was added to a solution of NH₄OH_(aq) (40 mL) and stirred at RT for 12h. After removal of volatile *in vacuo*, the white residue was triturated in water and filtered to obtain the *title* product as a white solid (8.15 mmol, 1.24 g). Yield = 97%. LC-UV purity > 99%. LC-MS (ESI⁺) m/z = 153.1 for [M+H]⁺. ¹H-NMR (500 MHz, DMSO-d₆): δ = 7.12 (t, J = 7.3 Hz, 1H), 7.32 (t, J = 7.3 Hz, 2H), 7.40 (d, J = 7.6 Hz, 2H), 9.70 (s, 1H). mp = 153-155°C, spectral data and melting point are in accordance with lit. data (153-154°C).²⁸⁷

1-(4-cyanophenyl)thiourea (5j)

A solution of 4-cyanophenyl isothiocyanate (6.24 mmol, 1 g) in $\text{NH}_4\text{OH}_{(\text{aq})}$ (80 mL) was stirred at RT for 12h. After cooling at 0°C , the mixture was filtrated to afford the *title* product as an off-white solid (4.85 mmol, 860 mg). Yield = 78%. LC-UV purity > 99%. The compound was not ionized by ESI^+ . $^1\text{H-NMR}$ (500 MHz, DMSO-d_6): δ = 7.75 (m, 4H), 10.07 (s, 1H). mp = $204\text{-}206^\circ\text{C}$, spectral data and melting point are in accordance with lit. data (239°C).^{283,288}

General procedure 4 for the preparation of 2-aminothiazole analogs:

An ethanolic solution of 2'-bromo-acetophenone derivative and aryl thiourea derivative at eqimolar ratio, corrected with respect to LC-UV purity, was heated at 80°C for 3-12h (reaction monitoring by TLC). The mixture was then cooled down to RT and water (twice more than EtOH v/v) was added. The mixture was stirred for 30 min and then filtrated. The obtained solid was washed twice with water to afford the product as a solid. When necessary, purification was performed (i) by recrystallization or washing with boiling MeCN (ii) by recrystallization or washing in $\text{H}_2\text{O}/\text{MeOH}$ (iii) by HPLC preparative to obtain the product with LC-UV purity higher than 95%.

4-((4-phenylthiazol-2-yl)amino)benzoic acid (2)

The reaction was carried out according to general procedure 4, scale: 2-bromo-acetophenone (0.51 mmol, 102 mg), 4-thioureidobenzoic acid (0.51 mmol, 100 mg), absolute EtOH (5 mL). Purification was performed by washing with boiling MeCN (5 mL) and hot filtration to afford the *title* product as a grey solid (0.24 mmol, 70 mg). Yield = 58%. LC-UV purity = 95%. The compound was not ionized by ESI^+ . $^1\text{H-NMR}$ (500 MHz, DMSO-d_6): δ = 7.33 (t, J = 6.9 Hz, 1H), 7.44 (t, J = 6.9 Hz, 3H), 7.84 (d, J = 8.5 Hz, 2H), 7.95 (d, J = 7.9 Hz, 4H), 10.70 (br s, 1H). $^{13}\text{C-NMR}$ (125.7 MHz, DMSO-d_6): δ = 104.1 (CH), 115.9 (2 x CH), 122.8 (C), 125.7 (2 x CH), 127.7 (CH), 128.6 (2 x CH), 130.8 (2 x CH), 134.3 (C), 144.9 (C), 150.2 (C), 162.2 (C), 167.0 (C). mp = $256\text{-}258^\circ\text{C}$ (in accordance with literature: 252°C).²⁷⁸

4-((4-(3-bromophenyl)thiazol-2-yl)amino)benzoic acid (3)

The reaction was carried out according to the general procedure 4, scale: 2-bromo-1-(3-bromophenyl)ethanone (0.36 mmol, 100 mg), 4-thioureidobenzoic acid (0.54 mmol, 106 mg), absolute EtOH (5 mL). Purification was performed by recrystallization in MeCN (5 mL) to afford the *title* product as a yellow solid (0.20 mmol, 75 mg). Yield = 56%. LC-UV purity = 95%. LC-MS (ESI^+) m/z = 374.62/376.65 for $[\text{M}+\text{H}]^+$. $^1\text{H-NMR}$ (500 MHz, DMSO-d_6): δ = 7.42 (t, J = 7.9 Hz, 1H), 7.52 (d, J = 7.1 Hz, 1H), 7.62 (s, 1H), 7.79 (d, J = 8.8 Hz, 2H), 7.93 – 7.98 (m, 3H), 8.11 (t, J = 1.6 Hz, 1H), 10.73 (s,

1H), 12.60 (br s, 1H). ¹³C-NMR (125.7 MHz, DMSO-d₆): δ = 105.7 (CH), 115.9 (2 x CH), 122.1 (C), 122.9 (C), 124.7 (CH), 128.0 (CH), 130.3 (CH), 130.8 (2 x CH), 130.9 (CH), 136.5 (C), 144.7 (C), 148.4 (C), 162.4 (C), 166.9 (C). mp = 281-283°C.

4-(3-nitrophenyl)-N-phenylthiazol-2-amine (6a)

The reaction was carried out according to the general procedure 4, scale: 2-bromo-3'-nitroacetophenone (0.66 mmol, 161 mg), phenylthiourea (0.66 mmol, 100 mg), absolute EtOH (5 mL). After removal of the solvents under reduced pressure, water (10 mL) and MeOH (2 mL) were added. The pH of the solution was adjusted to 9 with solid Na₂CO₃ and then stirred for 1h. After filtration and washing of the residual solid with water (3 x 5 mL), the product was obtained as a yellow solid (0.66 mmol, 196 mg). Yield = quantitative. LC-UV purity = 99%. LC-MS (ESI⁺) m/z = 298.06 for [M+H]⁺. ¹H-NMR (500 MHz, DMSO-d₆): δ = 6.99 (t, J = 6.9 Hz, 1H), 7.36 (t, J = 6.6 Hz, 2H), 7.65 – 7.71 (m, 4H), 8.14 (d, J = 7.3 Hz, 1H), 8.35 (d, J = 6.9 Hz, 1H), 8.69 (s, 1H), 10.39 (s, 1H). ¹³C-NMR (125.7 MHz, DMSO-d₆): δ = 105.6 (CH), 116.9 (2 x CH), 119.8 (CH), 121.4 (CH), 121.9 (CH), 129.0 (2 x CH), 130.1 (CH), 131.7 (CH), 135.9 (C), 140.9 (C), 147.6 (C), 148.2 (C), 163.5 (C). mp = 136-138 °C (in accordance with literature: 122-124 °C)²⁷⁶.

5-((4-(3-nitrophenyl)thiazol-2-yl)amino)isophthalic acid (6c)

The reaction was carried out according to the general procedure 4, scale: 2-bromo-1-(3-nitrophenyl)ethanone (0.42 mmol, 102 mg), 5-thioureidoisophthalic acid (0.63 mmol, 151 mg), EtOH absolute (5 mL). Purification was performed by washing with boiling MeCN (5 mL) and hot filtration to afford a yellow solid (0.36 mmol, 140 mg). Yield = 87%. LC-UV purity = 97%. LC-MS (ESI⁺) m/z = 385.59 for [M+H]⁺. ¹H-NMR (500 MHz, DMSO-d₆): δ = 7.71 (t, J = 7.6 Hz, 1H), 7.77 (s, 1H), 8.10 (s, 1H), 8.17 (d, J = 6.9 Hz, 1H), 8.38 (d, J = 6.3 Hz, 1H), 8.63 (s, 2H), 8.77 (s, 1H), 10.79 (s, 1H), 13.27 (br s, 1H). ¹³C-NMR (125.7 MHz, DMSO-d₆): δ = 106.6 (CH), 120.0 (CH), 121.1 (2 x CH), 122.2 (CH), 122.6 (CH), 130.1 (CH), 131.6 (CH), 132.1 (2 x C), 135.8 (C), 141.3 (C), 147.6 (C), 148.4 (C), 162.9 (C), 166.6 (2 x C). mp > 410°C.

2-(4-((4-(3- amino)phenyl) nitrophenyl)thiazol-2-yl) acetic acid (6d)

The reaction was carried out according to the general procedure 4, scale: 2-bromo-3'-nitroacetophenone (0.48 mmol, 117 mg), 2-(4-thioureidophenyl)acetic acid (0.48 mmol, 100 mg), EtOH (5 mL) to afford ethyl 2-(4-((4-(3-nitrophenyl)thiazol-2-yl)amino)phenyl) (0.41 mmol, 158 mg). Then, a mixture of ethyl 2-(4-((4-(3-nitrophenyl)thiazol-2-yl)amino)phenyl)acetate in THF (5 mL) and NaOH 0.5 M (1.3 mmol, 2.6 mL) was heated at 80°C for 4h. After removal of THF under reduced pressure, HCl 1M was added until pH = 1. The product was obtained after filtration as a

black solid (0.22 mmol, 78 mg). Yield = 73%. LC-UV purity = 96%. LC-MS (ESI⁺) m/z = 355.74 for [M+H]⁺. ¹H-NMR (500 MHz, DMSO-d₆): δ = 3.53 (s, 2H), 7.24 (d, J = 8.2 Hz, 2H), 7.64 (d, J = 8.2 Hz, 2H), 7.69 (s, 1H), 7.73 (t, J = 7.9 Hz, 1H), 8.16 (d, J = 7.9 Hz, 1H), 8.37 (d, J = 7.9 Hz, 1H), 8.70 (s, 1H), 10.43 (s, 1H). ¹³C-NMR (125.7 MHz, DMSO-d₆): δ = 39.7 (CH₂), 105.5 (CH), 116.9 (CH), 119.8 (CH), 122.0 (CH), 128.0 (C), 129.0 (CH), 130.2 (CH), 131.7 (CH), 135.9 (C), 139.5 (C), 147.6 (C), 148.2 (C), 163.6 (C), 172.8 (C). mp = 205-207 °C.

4-((4-(3-methoxyphenyl)thiazol-2-yl)amino)benzoic acid (7a)

The reaction was carried out according to the general procedure 4, scale: 2-bromo-3'-methoxyacetophenone (0.66 mmol, 152 mg), 4-thioureidobenzoic acid (0.51 mmol, 100 mg), EtOH (10 mL). Purification was performed by washing the residue with boiling MeCN (5 mL) and hot filtration to give a crude solid which was then purified by flash chromatography (cyclohexane/Acetone 50/50) to afford the *title* product as a yellow solid (0.09 mmol, 29 mg). Yield = 17%. LC-UV purity = 96%. LC-MS (ESI⁺) m/z = 327.10 for [M+H]⁺. ¹H-NMR (500 MHz, DMSO-d₆): δ = 3.83 (s, 3H), 6.91 (dd, J = 8.2, 2.2 Hz, 1H), 7.36 (t, J = 8.2 Hz, 1H), 7.48 (s, 2H), 7.53 (d, J = 7.9 Hz, 1H), 7.81 (d, J = 8.8 Hz, 2H), 7.94 (d, J = 8.8 Hz, 2H), 10.69 (s, 1H), 12.56 (br s, 1H). ¹³C-NMR (125.7 MHz, DMSO-d₆): δ = 55.0 (CH₃), 104.5 (CH), 111.1 (CH), 113.2 (CH), 115.8 (CH), 118.1 (CH), 122.8 (C), 129.7 (CH), 130.8 (CH), 135.6 (C), 144.8 (C), 150.0 (C), 159.5 (C), 162.1 (C), 167.0 (C). mp = 246-248°C.

4-((4-(4-methoxyphenyl)thiazol-2-yl)amino)benzoic acid (7b)

The reaction was carried out according to the general procedure 4, scale: 2-bromo-4'-methoxyacetophenone (0.71 mmol, 163 mg), 4-thioureidobenzoic acid (0.51 mmol, 100 mg), absolute EtOH (10 mL). Purification was performed by washing with boiling MeCN (5 mL) and hot filtration to afford the *title* product as a grey solid (0.15 mmol, 49 mg). Yield = 29%. LC-UV purity = 96%. LC-MS (ESI⁺) m/z = 327.09 for [M+H]⁺. ¹H-NMR (500 MHz, DMSO-d₆): δ = 3.80 (s, 3H), 7.00 (d, J = 7.3 Hz, 2H), 7.29 (s, 1H), 7.81 (d, J = 7.9 Hz, 2H), 7.87 (d, J = 7.9 Hz, 2H), 7.93 (d, J = 7.9 Hz, 2H), 10.65 (s, 1H), 12.54 (br s, 1H, O-H). ¹³C-NMR (125.7 MHz, DMSO-d₆): δ = 55.1 (CH₃), 101.9 (CH), 114.0 (2 x CH), 115.9 (2 x CH), 122.7 (C), 127.1 (2 x CH), 127.2 (C), 130.8 (2 x CH), 145.0 (C), 150.1 (C), 158.9 (C), 162.1 (C), 167.0 (C). mp = 266-268 °C (commercially available).

4-((4-(2,4-dimethoxyphenyl)thiazol-2-yl)amino)benzoic acid (7c)

The reaction was carried out according to the general procedure 4, scale: 2-bromo-1-(2,4-dimethoxyphenyl)ethanone (0.38 mmol, 100 mg), 4-thioureidobenzoic acid (0.58 mmol, 114 mg), EtOH (5 mL). Purification was performed by washing with boiling MeCN (5 mL) and hot filtration to

afford an off-white solid (0.25 mmol, 89 mg). Yield = 66%. LC-UV purity = 97%. LC-MS (ESI⁺) m/z = 356.78 for [M+H]⁺. ¹H-NMR (500 MHz, DMSO-d₆) δ = 3.81 (s, 3H), 3.91 (s, 3H), 6.65 – 6.67 (m, 2H), 7.31 (s, 1H), 7.81 (td, J = 2.2, 9.1 Hz, 2H), 7.93 (td, J = 2.2 Hz, 8.83 Hz, 2H), 8.08 – 8.10 (m, 1H), 10.58 (s, 1H), 12.56 (br s, 1H). ¹³C-NMR (125.7 MHz, DMSO-d₆): δ = 55.2 (CH₃), 55.5 (CH₃), 98.5 (CH), 105.2 (CH), 105.5 (CH), 115.7 (CH), 115.8 (C), 122.5 (C), 130.2 (CH), 130.7 (CH), 145.0 (C), 146.2 (C), 157.7(C), 159.8 (C), 160.3 (C), 167.0 (C). mp = 271-273°C.

4-((4-(2,4-dihydroxyphenyl)thiazol-2-yl)amino)benzoic acid (7d)

The reaction was carried out according to the general procedure 4, scale: 2-bromo-1-(2,4-dihydroxyphenyl)ethanone (0.43 mmol, 100 mg), 4-thioureidobenzoic acid (0.65 mmol, 127 mg), absolute EtOH (5 mL). Purification was performed by washing with boiling MeCN (5 mL) and hot filtration to afford the *title* product as yellow solid (0.38 mmol, 125 mg). Yield = 89%. LC-UV purity = 95% LC-MS (ESI⁺) m/z = 328.84 for [M+H]⁺. ¹H-NMR (500 MHz, DMSO-d₆): δ = 6.34 (dd, J = 8.4, 2.4 Hz, 1H), 6.36 (d, J = 2.3 Hz, 1H), 7.26 (s, 1H), 7.67 (d, J = 8.8 Hz, 2H), 7.76 (d, J = 8.2 Hz, 1H), 7.94 (d, J = 8.8 Hz, 2H), 9.48 (br s, 1H), 10.67 (s, 1H). ¹³C-NMR (125.7 MHz, DMSO-d₆): δ = 102.2 (CH), 102.8 (CH), 107.1 (CH), 111.6 (C), 116.0 (CH), 122.9 (C), 129.0 (CH), 130.8 (CH), 144.7 (C), 147.6 (C), 156.2(C), 158.1 (C), 161.2 (C), 166.9 (C). mp = 367-369°C.

4-((4-(5-bromo-2-hydroxyphenyl)thiazol-2-yl)amino)benzoic acid (7e)

The reaction was carried out according to the general procedure 4, scale: 2-bromo-1-(5-bromo-2-hydroxyphenyl)ethanone (0.34 mmol, 100 mg), 4-thioureidobenzoic acid (0.51 mmol, 100 mg), absolute EtOH (5 mL). Purification was performed by washing with boiling MeCN (5 mL) and hot filtration to afford a yellow solid (0.31 mmol, 120 mg). Yield = 90%. LC-UV purity = 98%. LC-MS (ESI⁺) m/z = 390.65/392.62 for [M+H]⁺. ¹H-NMR (500 MHz, DMSO-d₆) δ = 6.91 (d, J = 8.5 Hz, 1H), 7.31 (dd, J = 2.5, 8.5 Hz, 1H), 7.64 (s, 1H), 7.68 (d, J = 8.8 Hz, 2H), 7.94 (d, J = 9.1 Hz, 2H), 8.12 (d, J = 2.5 Hz, 1H), 10.74 (s, 1H), 10.84 (s, 1H), 12.60 (br s, 1H). ¹³C-NMR (125.7 MHz, DMSO-d₆): δ = 107.7 (CH), 110.3 (C), 116.0 (CH), 118.4 (CH), 122.1 (C), 123.1 (C), 130.3 (CH), 130.8 (CH), 130.9 (CH), 144.6 (C), 145.4 (C), 154.2 (C), 161.4 (C), 166.9 (C). mp = 312-314°C.

4-((4-(pyridin-2-yl)thiazol-2-yl)amino)benzoic acid (7f)

The reaction was carried out according to the general procedure 4, scale: 2-bromo-1-(pyridin-2-yl)ethanone hydrogen bromide (0.61 mmol, 171 mg), 4-thioureidobenzoic acid (0.51 mmol, 100 mg), absolute EtOH (10 mL). After water (5 mL) addition to the mixture, NH₄OH (30%) was added until complete dissolution. The pH of the solution was then adjusted to 2-3 by addition of aqueous HCl (1M) and the mixture was stirred for 30 min. The obtained solid was then filtrated and washed

with water (3 x 5 mL) to afford the *title* product as a yellow solid (0.28 mmol, 85 mg). Yield = 56%. LC-UV purity = 97%. LC-MS (ESI⁺) m/z = 298.07 for [M+H]⁺. ¹H-NMR (500 MHz, DMSO-d₆): δ = 7.83 (t, J = 5.5 Hz, 1H), 7.95 (m, 4H), 8.35, (br s, 1H), 8.50 (m, 2H), 8.79 (d, J = 5.4 Hz, 1H), 11.24 (br s, 1H). ¹³C-NMR (125.7 MHz, DMSO-d₆): δ = 114.8 (CH), 116.6 (2 x CH), 123.3 (CH), 124.7 (CH), 130.7 (2 x CH), 143.1 (CH), 144.2 (C), 144.6 (CH), 146.0 (C), 163.5 (C), 167.0 (C). mp = 274-276°C.

4-(thiazol-2-ylamino)benzoic acid (7g)

The reaction was carried out according to the general procedure 4, scale: 1,2-dichloro-1-ethoxyethane (0.41 mmol, 50 µL), 4-thioureidobenzoic acid (0.41 mmol, 80 mg), absolute EtOH (5 mL). Purification by semi-preparative HPLC (H₂O/MeCN/TFA: from 79/20/1 to 0/99/1 in 40 min) to afford ethyl 4-(thiazol-2-ylamino)benzoate as a white solid (0.09 mmol, 23 mg). Yield = 23%. LC-UV purity = 96%. LC-MS (ESI⁺) m/z = 249.01 for [M+H]⁺. The ethyl 4-(thiazol-2-ylamino)benzoate (0.085 mmol, 21 mg) obtained was directly hydrolyzed in a mixture of THF (2 mL) and aqueous 0.5 M NaOH (1.15 mmol, 2.3 mL) at reflux for 4h. Aqueous 1 M HCl was added until pH = 1 and then solvents were removed *in vacuo*. Crude product was purified by semi-preparative HPLC (H₂O/MeCN + 0.1% TFA: from 90/10 to 10/90 in 40 min) to afford the *title* product as a white solid (0.07 mmol, 16 mg). Yield = 86%. LC-UV purity > 99%. LC-MS (ESI⁺) m/z = 220.78 for [M+H]⁺. ¹H-NMR (500 MHz, DMSO-d₆): δ = 7.02 (d, J = 3.8 Hz, 1H), 7.33 (d, J = 3.8 Hz, 1H), 7.72 (d, J = 8.5 Hz, 2H), 7.88 (d, J = 8.8 Hz, 2H), 10.59 (s, 1H). ¹³C-NMR (125.7 MHz, DMSO-d₆): δ = 109.7 (CH), 115.7 (2 x CH), 122.5 (C), 130.7 (2 x CH), 138.8 (CH), 144.9 (C), 162.9 (C), 166.9 (C). mp = 270-272 °C (commercially available).²⁷⁷

4-((4-(tert-butyl)thiazol-2-yl)amino)benzoic acid (7h)

The reaction was carried out according to the general procedure 4, scale: 1-bromo-3,3-dimethylbutan-2-one (0.45 mmol, 60 µL), 4-thioureidobenzoic acid (0.41 mmol, 80 mg), absolute EtOH (5 mL). Purification was performed by washing with boiling MeCN (5 mL) and hot filtration to afford the *title* product as a white solid (0.10 mmol, 28 mg). Yield = 25%. LC-UV purity = 96%. LC-MS (ESI⁺) m/z = 277.04 for [M+H]⁺. ¹H-NMR (500 MHz, DMSO-d₆): δ = 1.28 (s, 9H), 6.53 (s, 1H), 7.70 (d, J = 8.5 Hz, 2H), 7.88 (d, J = 8.5 Hz, 2H), 10.48 (s, 1H), 12.49 (br s, 1H). ¹³C-NMR (125.7 MHz, DMSO-d₆): δ = 29.5 (CH₃), 34.3 (C), 100.5 (CH), 115.5 (CH), 122.3 (C), 130.6 (CH), 145.1 (C), 161.5 (C), 161.6 (C), 166.9 (C). mp = 280-282 °C.

4-((4-(thiophen-3-yl)thiazol-2-yl)amino)benzoic acid (7i)

The reaction was carried out according to the general procedure 4, scale: 2-bromo-1-(thiophen-3-yl)ethanone (0.41 mmol, 84 mg), 4-thioureidobenzoic acid (0.41 mmol, 80 mg), absolute EtOH

(5 mL). Purification was performed by washing with boiling MeCN (5 mL) and hot filtration by hot filtration to afford the *title* product as a brown solid (0.20 mmol, 59 mg). Yield = 48%. LC-UV purity = 96%. LC-MS (ESI⁺) m/z = 302.86 for [M+H]⁺. ¹H-NMR (500 MHz, DMSO-d₆): δ = 7.27 (s, 1H), 7.59 (m, 2H), 7.82 (m, 2H), 7.91 (m, 3H), 10.65 (s, 1H), 12.56 (br s, 1H). ¹³C-NMR (125.7 MHz, DMSO-d₆): δ = 103.4 (CH), 115.9 (2 x CH), 121.8 (CH), 122.7 (C), 125.9 (CH), 126.8 (CH), 130.7 (2 x CH), 136.6 (C), 144.8 (C), 146.6 (C), 162.1 (C), 166.9 (C). mp = 278-280 °C.

4-((4-(naphthalen-2-yl)thiazol-2-yl)amino)benzoic acid (7j)

The reaction was carried out according to the general procedure 4, scale: 2-bromo-1-(naphthalen-2-yl)ethanone (0.41 mmol, 102 mg), 4-thioureidobenzoic acid (0.41 mmol, 80 mg), absolute EtOH (5 mL). Purification was performed by washing with boiling MeCN (5 mL) and hot filtration to afford the *title* product as a brown solid (0.17 mmol, 59 mg). Yield = 42%. LC-UV purity = 95%. LC-MS (ESI⁺) m/z = 346.57 for [M+H]⁺. ¹H-NMR (500 MHz, DMSO-d₆): δ = 7.53 (m, 2H), 7.60 (s, 1H), 7.89 (d, J = 8.8 Hz, 2H), 7.93 (d, J = 7.9 Hz, 2H), 7.98 (m, 3H), 8.04 (d, J = 8.5 Hz, 1H), 8.08 (dd, J = 8.5, 1.9 Hz, 1H), 8.50 (s, 1H), 10.73 (s, 1H). ¹³C-NMR (125.7 MHz, DMSO-d₆): δ = 104.8 (CH), 116.0 (2 x CH), 122.8 (C), 123.9 (CH), 124.3 (CH), 126.0 (CH), 126.3 (CH), 127.5 (CH), 128.1 (CH), 128.2 (CH), 130.8 (2 x CH), 131.7 (C), 132.4 (C), 133.1 (C), 144.8 (C), 150.1 (C), 162.3 (C), 167.0 (C). mp = 294-296 °C.

4-((4-(2-oxo-2H-chromen-3-yl)thiazol-2-yl)amino)benzoic acid (7k)

The reaction was carried out according to the general procedure 4, scale: 3-(bromoacetyl)coumarin (0.45 mmol, 120 mg), 4-thioureidobenzoic acid (0.54 mmol, 106 mg), EtOH absolute (5 mL). Purification was performed by washing with boiling MeCN (5 mL) and hot filtration to afford the *title* product as a yellow solid (0.33 mmol, 120 mg). Yield = 73%. LC-UV purity = 96%. LC-MS (ESI⁺) m/z = 364.86 for [M+H]⁺. ¹H-NMR (500 MHz, DMSO-d₆): δ = 7.42 (t, J = 8.2 Hz, 1H), 7.46 (d, J = 8.5 Hz, 2H), 7.64 (t, J = 8.2 Hz, 1H), 7.88 (m, 3H), 7.99 (d, J = 8.8 Hz, 2H), 8.02 (d, J = 7.9 Hz, 1H), 8.75 (s, 1H), 10.75 (s, 1H). ¹³C-NMR (125.7 MHz, DMSO-d₆): δ = 110.8 (CH), 115.8 (CH), 116.2 (CH), 119.2 (C), 120.1 (C), 122.9 (C), 124.6 (CH), 129.0 (CH), 130.9 (CH), 131.7 (CH), 138.9 (CH), 143.6 (C), 144.6 (C), 152.3 (C), 158.7 (C), 161.7 (C), 167.0 (C). mp = 343-345 °C.

4-((4-(benzofuran-2-yl)thiazol-2-yl)amino)benzoic acid (7l)

The reaction was carried out according to the general procedure 4, scale: 1-(benzofuran-2-yl)-2-bromoethanone (0.42 mmol, 100 mg), 4-thioureidobenzoic acid (0.50 mmol, 99 mg), absolute EtOH (5 mL). Purification was performed by washing with boiling MeCN (5 mL) and hot filtration to afford a brown solid which was further purified by semi-preparative HPLC (H₂O/MeCN + 0.1% TFA:

from 70/30 to 0/100 in 45 min) to afford the *title* product as a yellow solid (0.19 mmol, 63 mg). Yield = 45%. LC-UV purity = 99%. LC-MS (ESI⁺) m/z = 336.96 for [M+H]⁺. ¹H-NMR (500 MHz, DMSO-d₆): δ = 7.28 (m, 2H), 7.34 (dd, J = 8.2, 1.3 Hz, 1H), 7.45 (s, 1H), 7.62 (d, J = 7.6 Hz, 1H), 7.70 (d, J = 7.3, 1H), 7.84 (d, J = 8.8 Hz, 2H), 7.95 (d, J = 8.8 Hz, 2H), 10.83 (s, 1H). ¹³C-NMR (125.7 MHz, DMSO-d₆): δ = 103.0 (CH), 106.4 (CH), 110.9 (CH), 116.1 (CH), 121.4 (CH), 123.0 (CH), 123.2 (C), 124.7 (CH), 128.4 (C), 130.7 (CH), 141.4 (C), 144.6 (C), 151.6 (C), 154.1 (C), 163.0 (C), 166.9 (C). mp = 296-298°C.

4-((4-(benzo[b]thiophen-5-yl)thiazol-2-yl)amino)benzoic acid (7m)

The reaction was carried out according to the general procedure 4, scale: 1-(1-benzothiophen-5-yl)-2-bromo-1-ethanone (0.39 mmol, 100 mg), 4-thioureidobenzoic acid (0.59 mmol, 115 mg), absolute EtOH (5 mL). The obtained solid was stirred in boiling MeCN (20 mL) and filtrated. The filtrate layer was concentrated and the remaining solid was then dissolved in hot MeOH (10 mL). After cooling at RT, water (10 mL) was added and the obtained solid was filtrated and washed with water (2 x 5 mL) to obtain the *title* product as a yellow solid (0.15 mmol, 51 mg). Yield = 38%. LC-UV purity = 95%. LC-MS (ESI⁺) m/z = 352.76 for [M+H]⁺. ¹H-NMR (500 MHz, DMSO-d₆): δ = 7.48 (s, 1H), 7.56 (d, J = 5.4 Hz, 1H), 7.79 (d, J = 5.4 Hz, 1H), 7.88 (d, J = 8.8 Hz, 2H), 7.94 – 7.99 (m, 3H), 8.04 (d, J = 8.5 Hz, 1H), 8.48 (d, J = 1.6 Hz, 1H), 10.70 (s, 1H), 12.52 (br s, 1H). ¹³C-NMR (125.7 MHz, DMSO-d₆): δ = 103.7 (CH), 115.9 (2 x CH), 120.7 (CH), 122.3 (CH), 122.7 (CH), 122.8 (C), 124.3 (CH), 128.0 (CH), 130.8 (3 x CH), 138.4 (C), 139.9 (C), 144.9 (C), 150.3 (C), 162.2 (C), 167.0 (C). mp = 353-355°C.

4-(naphthalen-2-yl)-N-phenylthiazol-2-amine (8a)

The reaction was carried out according to the general procedure 4, scale: 2-bromo-1-(naphthalen-2-yl)ethanone (0.66 mmol, 164 mg), phenylthiourea (0.66 mmol, 100 mg), absolute EtOH (15 mL). After water (25 mL) addition, the pH was adjusted to 9 with aqueous Na₂CO₃ (1M). The resulting mixture was cooled at 0°C and the precipitate was filtrated to afford the *title* product as a white solid (0.65 mmol, 195 mg). Yield = 98%. LC-UV purity > 99%. LC-MS (ESI⁺) m/z = 302.85 for [M+H]⁺. ¹H-NMR (500 MHz, DMSO-d₆): δ = 7.00 (t, J = 7.3 Hz, 1H), 7.39 (t, J = 8.2 Hz, 2H), 7.48 (s, 1H), 7.52 (qi, J = 8.2 Hz, 2H), 7.79 (d, J = 7.6 Hz, 2H), 7.91 (d, J = 7.9 Hz, 1H), 7.95 (d, J = 8.8 Hz, 1H), 8.00 (d, J = 7.9 Hz, 1H), 8.07 (dd, J = 8.5, 1.5 Hz, 1H), 10.32 (s, 1H). ¹³C-NMR (125.7 MHz, DMSO-d₆): δ = 103.6 (CH), 116.8 (CH), 121.2 (CH), 124.0 (CH), 124.1 (CH), 125.9 (CH), 126.3 (CH), 127.5 (CH), 128.0 (CH), 128.1 (CH), 129.0 (CH), 131.9 (C), 132.4 (C), 133.1 (C), 141.1 (C), 150.0 (C), 163.1 (C). mp = 148-150°C.

4-((4-(naphthalen-2-yl)thiazol-2-yl)amino)benzonitrile (8b)

The reaction was carried out according to the general procedure 4, scale: 2-bromo-2'-acetonaphthone (1.41 mmol, 351 mg), 1-(4-cyanophenyl)thiourea (1.41 mmol, 250 mg), EtOH absolute (5 mL). The resulting mixture was cooled at RT and aqueous Na₂CO₃ (1M) was added dropwise until pH = 8. After cooling at 0°C, the precipitate was filtrated and washed with H₂O (2 x 5 mL) to afford the *title* product as a slightly yellow solid (462 mg, 1.41 mmol). Yield = quantitative. LC-UV purity = 99%. LC-MS (ESI⁺) m/z = 327.94 for [M+H]⁺. ¹H-NMR (500 MHz, DMSO-d₆): δ = 7.51 (dt, J = 6.9, 1.3 Hz, 1H), 7.55 (dt, J = 6.9, 1.6 Hz, 1H), 7.61 (s, 1H), 7.81 (d, J = 8.8 Hz, 2H), 7.92 (d, J = 8.2 Hz, 1H), 7.96 (m, 3H), 8.01 (d, J = 7.9 Hz, 1H), 8.08 (dd, J = 8.5, 1.3 Hz, 1H). ¹³C-NMR (125.7 MHz, DMSO-d₆): δ = 101.8 (C), 105.2 (CH), 116.8 (CH), 119.6 (C), 123.9 (CH), 124.3 (CH), 126.0 (CH), 126.4 (CH), 127.5 (CH), 128.1 (CH), 131.6 (C), 132.4 (C), 133.1 (C), 133.5 (2 x CH), 145.2 (C), 150.2 (C), 162.4 (C). mp = 228-230°C.

3-((4-(naphthalen-2-yl)thiazol-2-yl)amino)benzoic acid (8c)

The reaction was carried out according to the general procedure 4, scale: 2-bromo-1-(naphthalen-2-yl)ethanone (0.40 mmol, 100 mg), 3-thioureidobenzoic acid (0.52 mmol, 102 mg), EtOH absolute (5 mL). The *title* product was obtained pure after filtration as a yellow solid (0.34 mmol, 118 mg). Yield = 86%. LC-UV purity = 98%. LC-MS (ESI⁺) m/z = 346.80 for [M+H]⁺. ¹H-NMR (500 MHz, DMSO-d₆): δ = 7.49 – 7.56 (m, 4H), 7.59 (d, J = 7.6 Hz, 1H), 7.90 – 7.98 (m, 4H), 8.08 (dd, J = 1.9, 8.5 Hz, 1H), 8.55 (s, 1H), 8.77 (s, 1H), 10.56 (s, 1H), 13.01 (br s, 1H). ¹³C-NMR (125.7 MHz, DMSO-d₆): δ = 104.1 (CH), 117.7 (CH), 120.8 (CH), 121.9 (CH), 123.8 (CH), 124.5 (CH), 126.0 (CH), 126.4 (CH), 127.5 (CH), 128.0 (CH), 128.1 (CH), 129.2 (CH), 131.5 (C), 131.8 (C), 132.4 (C), 133.2 (C), 141.3 (C), 149.8 (C), 162.7 (C), 167.4 (C). mp = 275-277°C.

4-methoxy-3-((4-(naphthalen-2-yl)thiazol-2-yl)amino)benzoic acid (8d)

The reaction was carried out according to the general procedure 4, scale: 2-bromo-1-(naphthalen-2-yl)ethanone (1 mmol, 250 mg), 3-methoxy-4-thioureidobenzoic acid (1.3 mmol, 294 mg), EtOH absolute (25 mL). Product was obtained pure after filtration as a yellow solid (0.94 mmol, 353 mg). Yield = 94%. LC-UV purity = 97%. LC-MS (ESI⁺) m/z = 376.82 for [M+H]⁺. ¹H-NMR (500 MHz, DMSO-d₆) δ = 3.97 (s, 3H), 7.14 (d, J = 8.5 Hz, 1H), 7.49 – 7.55 (m, 3H), 7.64 (dd, J = 2.2, 8.2 Hz, 1H), 7.91 – 7.96 (m, 3H), 8.07 (dd, J = 1.9, 8.5 Hz, 1H), 8.60 (d, J = 0.6 Hz, 1H), 9.70 (d, J = 2.2 Hz, 1H), 9.90 (s, 1H), 12.71 (br s, 1H). ¹³C-NMR (125.7 MHz, DMSO-d₆): δ = 55.9 (CH₃), 104.7 (CH), 110.0 (CH), 118.8 (CH), 122.9 (C), 123.5 (CH), 123.6 (CH), 124.5 (CH), 125.9 (CH), 126.3 (CH), 127.5 (CH), 127.9

(CH), 128.0 (CH), 129.9 (C), 131.8 (C), 132.3 (C), 133.2 (C), 149.1 (C), 150.8 (C), 162.7 (C), 167.5 (C). mp = 256-258°C.

2-hydroxy-4-((4-(naphthalen-2-yl)thiazol-2-yl)amino)benzoic acid (8e)

The reaction was carried out according to the general procedure 4, scale: 2-bromo-1-(naphthalen-2-yl)ethanone (0.50 mmol, 124 mg), 2-hydroxy-4-thioureidobenzoic acid (0.70 mmol, 149 mg), EtOH (5 mL). Purification was performed by washing with boiling MeCN (5 mL) and hot filtration to afford a yellow solid (0.37 mmol, 133 mg). Yield = 73%. LC-UV purity = 96%. LC-MS (ESI⁺) m/z = 362.84 for [M+H]⁺. ¹H-NMR (500 MHz, DMSO-d₆): δ = 7.19 (dd, J = 1.9, 8.8 Hz, 1H), 7.49 – 7.57 (m, 3H), 7.61 (s, 1H), 7.80 (d, J = 8.5 Hz, 1H), 7.92 (d, J = 7.9 Hz, 1H), 7.98 (d, J = 8.2 Hz, 2H), 8.07 (d, J = 8.5 Hz, 1H), 8.46 (s, 1H), 10.75 (s, 1H), 11.8 (br s, 1H). ¹³C-NMR (125.7 MHz, DMSO-d₆): δ = 103.0 (CH), 105.2 (CH), 105.6 (C), 108.4 (CH), 124.0 (CH), 124.2 (CH), 126.0 (CH), 126.5 (CH), 127.6 (CH), 128.1 (CH), 128.2 (CH), 131.3 (CH), 131.7 (C), 132.5 (C), 133.1 (C), 147.0 (C), 150.2 (C), 162.1 (C), 162.6 (C), 171.7 (C). mp = 221-223°C.

2-((4-(3-nitrophenyl)thiazol-2-yl)amino)benzoic acid (9)

A solution of HCl 37% (1 mL) and 1,4-dioxane (5 mL) containing 2-bromo-4-phenylthiazole (2.08 mmol, 500 mg) and 2-aminobenzoic acid (2.08 mmol, 286 mg) was heated at reflux for 60h. After solvents removal, the residual solid was washed with water (5 mL) and then with cold acetone (5 mL) to obtain a white solid which was further purified by flash chromatography (cyclohexane/EtOAc, from 7/3 to 0/100) to obtain a second white solid containing 75% of product (by HPLC). After a second purification by preparative HPLC (H₂O/MeCN - 1% formic acid, from 70/30 to 0/100), the pure title product was obtained as a white solid (0.04 mmol, 12 mg). Yield = 2%. LC-UV purity = 97%. LC-MS (ESI⁺) m/z = 297.08 for [M+H]⁺. ¹H-NMR (500 MHz, DMSO-d₆): δ = 7.07 (t, J = 7.9 Hz, 1H), 7.34 (t, J = 7.6 Hz, 1H), 7.45 (t, J = 7.6 Hz, 2H), 7.53 (s, 1H), 7.69 (td, J = 7.6, 1.6 Hz, 1H), 7.94 (d, J = 6.9 Hz, 2H), 8.02 (dd, J = 7.9, 1.6 Hz, 1H), 8.62 (d, J = 8.5 Hz, 1H), 11.48 (s, 1H). ¹³C-NMR (125.7 MHz, DMSO-d₆): δ = 104.6 (CH), 113.7 (C), 116.9 (CH), 120.4 (CH), 125.7 (CH), 127.8 (CH), 128.6 (CH), 131.4 (CH), 134.1, 134.7 (CH), 142.9 (C), 150.3 (C), 161.8 (C), 170.0 (C). mp = 95-97 °C.

Methyl 4-((4-(3-nitrophenyl)thiazol-2-yl)amino)benzoate (10)

Three drops of 95% H₂SO₄ were added to a mixture of 4-((4-(3-nitrophenyl)thiazol-2-yl)amino)benzoic acid (**1**) (0.14 mmol, 46 mg) in MeOH (5 mL) and the mixture was then heated at reflux for 2h. Na₂CO₃ 1 M was then added until pH = 10-11 and MeOH was removed under *vacuo*. The obtained solid was filtrated and washed with water (2 x 5 mL) to afford the *title*

product as a yellow solid (0.14 mmol, 49 mg). Yield = quantitative. LC-UV purity = 97%. LC-MS (ESI⁺) m/z = 356.01 for [M+H]⁺. ¹H-NMR (500 MHz, DMSO-d₆): δ = 3.82 (s, 3H), 7.74 – 7.84 (m, 4H), 7.96 (s, 2H), 8.17 (s, 1H), 8.40 (s, 1H), 8.71 (s, 1H), 10.83 (s, 1H). ¹³C-NMR (125.7 MHz, DMSO-d₆): δ = 51.7 (CH₃), 107.0 (CH), 116.1 (2 x CH), 119.9 (CH), 121.8 (C), 122.1 (CH), 130.3 (CH), 130.6 (2 x CH), 131.9 (CH), 135.7 (C), 144.9 (C), 147.8 (C), 148.3 (C), 162.6 (C), 165.8 (C). mp = 242-244 °C.

N-(methylsulfonyl)-4-((4-(naphthalen-2-yl)thiazol-2-yl)amino)benzamide (11a)

A solution of 4-((4-(naphthalen-2-yl)thiazol-2-yl)amino)benzoic acid (**7j**) (0.23 mmol, 80 mg), HATU (0.28 mmol, 106 mg) and DIPEA (0.69 mmol, 120 μL) in dry DMF (2 mL) was stirred under N₂ for 30 min. And then added to a solution of NaH (0.92 mmol, 22 mg) and MeSO₂NH₂ (1.15 mmol, 110 mg) in dry THF (2 mL) beforehand stirred at RT under N₂ for 30 min. The resulting mixture was stirred at RT for 4h. After removal of solvents under vacuo, residue was purified by semi-preparative HPLC (H₂O/MeCN + 0.1% TFA: from 40/60 to 0/100 in 50 min) followed by a second purification by semi-preparative HPLC (H₂O/MeCN + 0.1% TFA: from 25/75 to 20/80 in 45 min) to obtain the *title* product as a white solid (0.026 mmol, 11 mg). Yield = 11%. LC-UV purity = 99%. LC-MS (ESI⁺) m/z = 423.73 for [M+H]⁺. ¹H-NMR (500 MHz, acetone-d₆) δ = 3.40 (s, 3H), 7.48 (s, 1H), 7.49 – 7.56 (m, 2H), 7.92 (d, J = 7.9 Hz, 1H), 7.96 (d, J = 8.6 Hz, 1H), 7.99 (d, J = 8.0 Hz, 1H), 8.01 – 8.04 (m, 2H), 8.08 - 8.12 (m, 3H), 8.56 (s, 1H), 9.89 (brs, 1H), 10.49 (brs, 1H). ¹³C-NMR (125.7 MHz, acetone-d₆) δ = 42.8 (CH₃), 106.2 (CH), 118.3 (CH), 126.0 (CH), 126.2 (C), 126.8 (CH), 128.0 (CH), 128.3 (CH), 129.5 (CH), 130.1 (CH), 130.2 (CH), 131.8 (3 x CH), 134.0 (C), 135.1 (C), 135.7 (C), 153.1 (C), 167.1 (C). mp = 240-242°C.

4-((4-(naphthalen-2-yl)thiazol-2-yl)amino)-N-tosylbenzamide (11b)

4-methylbenzenesulfonamide (0.23 mmol, 39.5 mg), N-(3-Dimethylaminopropyl)-N'-ethylcarbodiimide hydrochloride (0.46 mmol, 88 mg) and 4-dimethylaminopyridine (0.46 mmol, 56 mg) were added to a solution of 4-((4-(naphthalen-2-yl)thiazol-2-yl)amino)benzoic acid (**7j**) (0.23 mmol, 80 mg) in CH₂Cl₂ (10 mL). The resulting mixture was stirred at RT under N₂ atmosphere for 36h. NH₄Cl_(aq) (10 mL) was added, and then H₂O (10 mL). The aqueous layer was extracted with CH₂Cl₂ (2 x 20 mL). The combined organic layers were dried with Na₂SO₄, filtrated and concentrated to give a brown solid which was further purified by semi-preparative HPLC (H₂O/MeCN + 0.1% TFA: from 30/70 to 0/100 in 45 min) to obtain the *title* product as a white solid (0.026 mmol, 13 mg). Yield = 11%. LC-UV purity = 97%. LC-MS (ESI⁺) m/z = 499.79 for [M+H]⁺. ¹H-NMR (500 MHz, acetone-d₆) δ = 2.43 (s, 3H), 7.43 (dt, J = 7.9, 0.6 Hz, 2H), 7.52 (m, 2H), 7.91 (dd, J = 7.9, 0.6 Hz, 1H), 7.94 (d, J = 9.1 Hz, 1H), 7.99 (m, 8H), 8.09 (dd, J = 8.5, 1.9 Hz, 1H), 8.54 (s, 1H). ¹³C-NMR (125.7 MHz, Acetone-d₆) δ = 22.5 (CH₃), 118.2 (CH), 125.9 (CH), 126.1 (C), 126.8 (CH), 127.9

(CH), 128.3 (CH), 129.5 (CH), 130.1 (CH), 130.2 (CH), 130.2 (CH), 131.2 (CH), 131.7 (CH), 133.9 (C), 135.0 (C), 135.6 (C), 139.2 (C), 146.3 (C), 147.3 (C), 152.8 (C), 164.2 (C), 165.9 (C). mp = 223-225°C.

General procedure 5 for the preparation of acetoxymethyl prodrug:

To a solution of the acid derivative (1 eq) in dry DMF (5 mL) under N₂ flow was added triethylamine (5 eq) and bromo-methylacetate (3 eq). After stirring for 12h, water (10 mL) was added and a precipitate occurred. The solid obtained after filtration was washed three times with water (5 mL) and further purified by semi-preparative HPLC (H₂O/MeCN: from 40/60 to 0/100 in 50 min) to obtain the desired product.

acetoxymethyl 4-((4-(naphthalen-2-yl)thiazol-2-yl)amino)benzoate (12a)

The reaction was carried out according to the general procedure 5, scale: 4-((4-(naphthalen-2-yl)thiazol-2-yl)amino)benzoic acid (**7j**) (0.14 mmol, 50 mg), Et₃N (0.7 mmol, 98 µL), bromo-methylacetate (0.43 mmol, 42 µL), DMF (5 mL), then H₂O (10 mL). After purification by semi-preparative HPLC, the product was obtained as an off-white solid (0.098 mmol, 41 mg). Yield = 70%. LC-UV purity = 95%. LC-MS (ESI⁺) m/z = 418.61 for [M+H]⁺. ¹H-NMR (500 MHz, acetone-d₆) δ = 2.11 (s, 3H), 5.98 (s, 2H), 7.47 (s, 1H), 7.49 – 7.55 (m, 2H), 7.91 (d, J = 8.2 Hz, 1H), 7.96 (d, J = 8.8 Hz, 1H), 8.03 – 8.06 (m, 5H), 8.12 (dd, J = 8.5, 1.9 Hz, 1H), 8.59 (s, 1H), 9.90 (s, 1H). ¹³C-NMR (125.7 MHz, acetone-d₆) δ = 21.6 (CH₃), 81.2 (CH₂), 106.2 (CH), 118.3 (CH), 123.3 (C), 125.9 (CH), 126.8 (CH), 127.9 (CH), 128.2 (CH), 129.5 (CH), 130.1 (CH), 130.3 (CH), 133.2 (CH), 134.04 (C), 135.1 (C), 135.7 (C), 148.0 (C), 153.2 (C), 164.3 (C), 166.2 (C), 171.1 (C). mp = 148-150°C.

acetoxymethyl 4-((4-(3-nitrophenyl)thiazol-2-yl)amino)benzoate (12b)

The reaction was carried out according to the general procedure 5, scale: 4-((4-(3-nitrophenyl)thiazol-2-yl)amino)benzoic acid (**1**) (0.26 mmol, 90 mg), Et₃N (1.3 mmol, 183 µL), bromo-methylacetate (0.79 mmol, 78 µL), DMF (5 mL), then H₂O (10 mL). After purification by semi-preparative HPLC, the product was obtained as an orange solid (0.11 mmol, 46 mg). Yield = 43%. LC-UV purity > 99%. LC-MS (ESI⁺) m/z = 413.60 for [M+H]⁺. ¹H-NMR (500 MHz, DMSO-d₆): δ = 2.11 (s, 3H), 5.91 (s, 2H), 7.73 (t, J = 8.2 Hz, 1H), 7.80 (s, 1H), 7.86 (d, J = 8.8 Hz, 2H), 7.97 (d, J = 8.8 Hz, 2H), 8.16 (ddd, J = 8.2, 2.2, 1.0 Hz, 1H), 8.40 (dt, J = 8.2, 1.0 Hz, 1H), 8.70 (t, J = 1.9 Hz, 1H), 10.94 (s, 1H). ¹³C-NMR (125.7 MHz, DMSO-d₆): δ = 20.5 (CH₃), 79.4 (CH₂), 107.2 (CH), 116.2 (CH), 119.9 (CH), 120.4 (C), 122.1 (CH), 130.3 (CH), 131.1 (CH), 131.9 (CH), 135.7 (C), 145.6 (C), 147.8 (C), 148.3 (C), 162.4 (C), 164.0 (C), 169.4 (C). mp = 169-171°C.

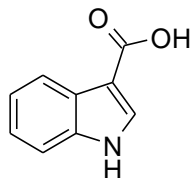
acetoxymethyl 4-((4-(thiophen-3-yl)thiazol-2-yl)amino)benzoate (12c)

The reaction was carried out according to the general procedure 5, scale: 4-((4-(thiophen-3-yl)thiazol-2-yl)amino)benzoic acid (**7i**) (0.25 mmol, 77 mg), Et₃N (1.25 mmol, 176 μ L), bromomethylacetate (0.76 mmol, 75 μ L), DMF (5 mL), then H₂O (10 mL). After purification by semi-preparative HPLC, the product was obtained as an off-white solid (0.04 mmol, 14 mg). Yield = 16%. LC-UV purity = 96%. LC-MS (ESI⁺) m/z = 374.66 for [M+H]⁺. ¹H-NMR (500 MHz, acetone-d₆) δ = 2.10 (s, 3H), 5.96 (s, 2H), 7.15 (s, 1H), 7.51 (dd, J = 5.0, 3.2 Hz, 1H), 7.60 (dd, J = 5.0, 1.3 Hz, 1H), 7.93 (dd, J = 3.2, 1.3 Hz, 1H), 7.98 (d, J = 9.0 Hz, 2H), 8.03 (d, J = 9.0 Hz, 2H), , 9.83 (s, 1H). ¹³C-NMR (125.7 MHz, acetone-d₆) δ = 21.6 (CH₃), 81.2 (CH₂), 105.0 (CH), 118.3 (CH), 123.2 (C), 123.8 (CH), 127.7 (CH), 128.1 (CH), 133.1 (CH), 139.0 (C), 148.0 (C), 149.5 (C), 164.2 (C), 166.2 (C), 171.7 (C). mp = 136-138°C.

6.1.3 Synthesis of compounds of chapter 3.4

All commercially available chemicals and solvents were purchased from Sigma-Aldrich, Acros Organics, Fischer scientific and Alfa Aesar. They were used without further purification, unless specified. ^1H NMR spectra were obtained on a Bruker ALS300 and DRX300 (300 MHz), and a DRX400 Bruker (400 MHz) using residual signal of deuterated NMR solvent as internal reference.²⁷⁴ Chemical shifts are expressed in parts per million (ppm), multiplicity of the signals are indicated by lower-case letters (singlet s, doublet d, triplet t, quadruplet q, multiplet m, broad singlet br s, doublet of triplet dt, triplet of doublet td, triplet of triplet tt) coupling constants are expressed in Hz, and deuterated solvents are either dimethylsulphoxide- d_6 or CDCl_3 . Analytical HPLC was performed on an Agilent Technology 1290 Infinity chromatographic system equipped with a 1260 Diode Array Detector and a single quadrupole 6120 Mass Spectrometer Detector (column: Zorbax Eclipse Plus C18, 2.1 x 50 mm, 1.8 μm ; temperature: 40°C). Solvent system was water/acetonitrile, each containing 0.1% of formic acid with an isocratic 90/10 elution during 0.5 min then a gradient till 10/90 over 5 min and kept during 1 min at 0.5 mL/min. Injection volume was typically 0.1 μL HPLC purities were measured at 254 nm. Electrospray ionization spectra (ESI) are obtained on an Agilent Technologies 6120 Quadrupole LC/MS. High Resolution Mass Spectrometry (HRMS) were performed on Bruker microTOF-Q II. Parallel syntheses were performed with a Radleys Tech system. Purifications are performed on silica gel 40-60 μm , 60A for normal phase. Thin Layer Chromatographies (TLC) (thickness: 200 μm , particle size: 25 μm) were purchased from Fluka Analytical. When specified, products were obtained in different batches according to their HPLC purity. In this case, analytical and biological data were obtained from the most pure batch.

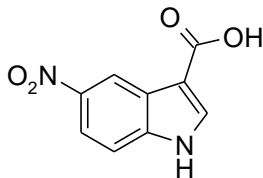
1H-Indole-3-carboxylic acid (5a)



To a solution of 1H-indole-3-carbonitrile (13.4 mmol, 1.9 g) in water (50 mL) was added a solution of NaOH (147 mmol, 5.9 g) in water (50 mL). The mixture was then heated at reflux under argon for 24h. This aqueous layer was washed with 3 x 20 mL of EtOAc and then acidified until pH = 1 with HCl 1M. A white precipitate occurred and it was filtered, washed with HCl 1M to give the *title* compound as a white solid (9.24 mmol, 1.49 g). Yield = 69 %. Chemical formula: $\text{C}_9\text{H}_7\text{NO}_2$.

Molecular weight: 161.16 g.mol⁻¹. LC/MS (ESI): 95 % pure, *m/z* [M + H]⁺: 162. ¹H-NMR (300 MHz, DMSO-d₆) δ = 7.09 – 7.23 (m, 2H), 7.41 – 7.50 (m, 1H), 7.96 – 8.04 (m, 2H), 11.80 (s, 1H).²⁸⁹

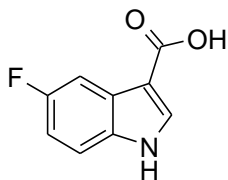
5-Nitro-1H-indole-3-carboxylic acid (5c)



General procedure 1 for the preparation of indole-3-carboxylic acids

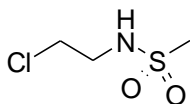
TFAA (42 mmol, 5.9 mL) was added dropwise to a solution of 5-nitro-1H-indole (18.5 mmol, 3 g) in dry DMF (25 mL) at 0°C under argon. After the end of the addition, the mixture was heated at reflux for 12h. Solvent was removed under reduced pressure and crude was taken off with water (50 mL) and a solution of NaOH (250 mmol, 10 g) in water (100 mL) was added. The resulting mixture was then heated at reflux for 12h. The solution was washed with Et₂O (4 x 50 mL) and then acidified with HCl 1M until pH = 2. The resulting solid was filtered and dried to afford the *title* compound (16.8 mmol, 3.46 g). Yield = 91 %. Chemical formula: C₉H₆N₂O₄. Molecular weight: 206.158 g.mol⁻¹. LC/MS (ESI): 97 % pure, *m/z* [M + H]⁺: 207.4. ¹H-NMR (300 MHz, DMSO-d₆) δ = 7.68 (d, *J* = 9.0, 1H), 8.09 (dd, *J* = 2.4, 9.0, 1H), 8.27 (d, *J* = 2.9, 1H), 8.89 (d, *J* = 2.4, 1H), 12.52 – 12.58 (m, 2H). mp: 244-245°C. Spectral data and melting point are in accordance with literature reference.²⁹⁰

5-Fluoro-1H-indole-3-carboxylic acid (5b)



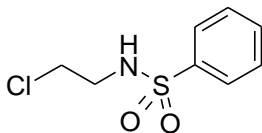
The reaction was carried out according to General procedure 1 with the corresponding scale: 5-fluoro-1H-indole (22.2 mmol, 3 g), TFAA (50 mmol, 7.1 mL), DMF (22 mL) then NaOH (300 mmol, 12 g), water (70 mL). The *title* compound (20.0 mmol, 3.59 g) was isolated as a grey solid. Yield = 90 %. Chemical formula: C₉H₆FNO₂. Molecular weight: 179.15 g.mol⁻¹. LC/MS (ESI): 95 % pure, *m/z* [M + H]⁺: 180. ¹H-NMR (300 MHz, DMSO-d₆) δ = 7.03 (td, *J* = 2.6, 9.2, 1H), 7.48 (dd, *J* = 4.6, 8.9, 1H), 7.64 (dd, *J* = 2.7, 10.0, 1H), 8.05 (d, *J* = 3.0, 1H), 11.99 (s, 1H). mp > 410°C.²⁹¹

N-(2-Chloroethyl)methanesulfonamide (10a)



To a slurry of 2-chloroethylamine hydrochloride (70 mmol, 8.12 g) in MeCN (150 mL) at 5°C was added dropwise and simultaneously Et₃N (140 mmol, 19.7 mL) and MeSO₂Cl (70 mmol, 5.42 mL) were also added during 30 min. After 30 min at 5°C, the mixture was slowly allowed to warm at RT and the stirring was pursued during 3h. The mixture became slightly orange. After removal of solvent, residue was taken off with water, the resulting aqueous phase was saturated with NaCl and extracted with CH₂Cl₂ (6 x 50 mL). The combined organic layers were dried on Na₂SO₄, filtered and the solvent was removed under vacuum to give a brown oil (5.87 g) which was purified on a normal phase silica gel column (cyclohexane/EtOAc: 6/4) to afford the *title* compound as a yellow oil which crystallized at -18°C (19.9 mmol, 3.13 g). Yield = 28 %. Chemical formula: C₃H₈ClNO₂S. Molecular weight: 157.62 g.mol⁻¹. LC/MS (ESI): not UV visible, *m/z* [M + H]⁺: not ionizable. ¹H-NMR (300 MHz, CDCl₃) δ = 3.02 (s, 3H), 3.49 (td, *J* = 5.2, 6.2, 2H), 3.68 (dd, *J* = 5.17, 6.1, 2H), 4.80 (s, 1H).

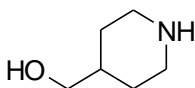
N-(2-Chloroethyl)benzenesulfonamide (10b)



To a mixture of 2-chloroethylamine hydrochloride (43.1 mmol, 5 g) solubilized in CH₂Cl₂ (100 mL) and H₂O (50 mL) at 10°C was added K₂CO₃ (43.1 mmol, 5.7 g) followed by chlorosulfonylbenzene (43.1 mmol, 5.5 mL). The reaction was stirred during 3h, with a temperature kept at 10±3°C and the pH value was maintained around 7-8 with K₂CO₃. The mixture was then allowed to warm up at RT for 2h. Layers were partitioned and aqueous one was extracted with CH₂Cl₂ (2 x 100 mL). After recrystallization in *i*Pr₂O (50 mL, 70°C then RT), the *title* compound was obtained as a white solid (28.9 mmol, 6.36 g). Yield = 67 %. Chemical formula: C₈H₁₀ClNO₂S. Molecular weight: 219.69 g.mol⁻¹. LC/MS (ESI): 86 % pure at 254 nm, *m/z* [M + H]⁺: not ionizable. ¹H-NMR (CDCl₃, 300 MHz): δ

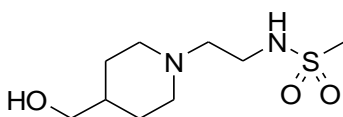
= 3.32 (q, $J = 6.0$, 2H), 3.56 (t, $J = 6.0$, 2H), 4.97 (br s, 1H), 7.51 – 7.64 (m, 3H), 7.87 – 7.89 (m, 2H). mp: 70-72°C. Melting point is in accordance with lit. data (70°C).²⁹²

(Piperidin-4-yl)methanol (13)



A solution of ethyl isonipecotate (77.9 mmol, 12.24 g) in anhydrous THF (80 mL) was added dropwise under argon to an ice-cooled suspension of LiAlH_4 (97.3 mmol, 3.69 g) in anhydrous THF (250 mL). After 30 min, the mixture was allowed to warm at room temperature and stirred for 20h. After treatment with water (4.8 mL), $\text{NaOH}_{(\text{aq})}$ 1M (4.8 mL), and water (9.6 mL) the solution was stirred with diethyl ether (200 mL) for 30 min. The slurry was then filtered and washed with diethyl ether (3 x 100 mL). Solvents were removed under vacuum to afford the *title* compound as a colorless oil (77.9 mmol, 8.97 g). Yield = 100 %. Chemical formula: $\text{C}_6\text{H}_{13}\text{NO}$. Molecular weight: 115.17 $\text{g}\cdot\text{mol}^{-1}$. LC/MS (ESI): not UV visible, m/z $[\text{M} + \text{H}]^+$: 116.2. $^1\text{H-NMR}$ (300 MHz, CDCl_3) $\delta = 1.06 - 1.22$ (m, 2H), 1.61 (s, 1H), 1.67 – 1.77 (m, 2H), 2.00 (s, 3H), 2.60 (td, $J = 2.6, 12.2$, 2H), 3.03 – 3.16 (m, 2H), 3.44 – 3.47 (m, 2H). Spectral data are in accordance with lit. data.²⁶⁴

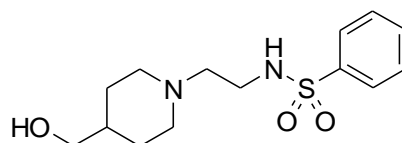
N-[2-[4-(Hydroxymethyl)-1-piperidinyl]ethyl]methanesulphonamide (14a)



To an ice-cooled solution of (piperidin-4-yl)methanol (67.7 mmol, 7.8 g) in MeCN (70 mL) was added dropwise a N-(2-chloroethyl)methanesulfonamide (54.1 mmol, 8.45 g) solution in MeCN (50 mL). After the end of the addition, the mixture was allowed to warm at RT and stirred over 2 days. Then a 4 % aqueous solution of NaOH (200 mL) was added dropwise. The mixture was extracted with CH_2Cl_2 (6 x 100 mL) and the combined organic layers were dried on MgSO_4 and then filtered. After solvent removal, a yellow oil was obtained and was further purified by normal phase silica gel column ($\text{CH}_2\text{Cl}_2/\text{EtOH}$: 5/5) to afford the *title* compound as a yellow oil (16.2 mmol, 3.8 g). Yield = 30 %. Chemical formula: $\text{C}_9\text{H}_{20}\text{N}_2\text{O}_3\text{S}$. Molecular weight: 236.34 $\text{g}\cdot\text{mol}^{-1}$. LC/MS (ESI): not UV visible, m/z $[\text{M} + \text{H}]^+$: not ionizable. $^1\text{H-NMR}$ (300 MHz, CDCl_3) $\delta = 1.20$ (t, $J = 7.0$,

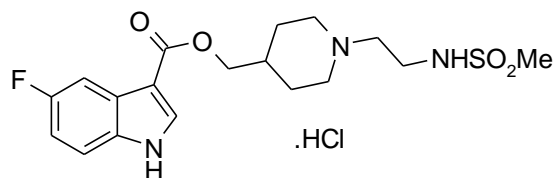
2H), 1.51 (s, 1H), 1.69 – 1.77 (m, 2H), 1.97 – 2.06 (m, 2H), 2.45 – 2.57 (m, 2H), 2.87 (d, $J = 11.6$, 2H), 2.96 (s, 3H), 3.10 – 3.25 (m, 2H), 3.49 (d, $J = 6.3$, 2H). Spectral data are in accordance with lit. data.²⁶⁵

N-[2-[4-(Hydroxymethyl)-1-piperidinyl]ethyl]phenylsulfonamide (14b)



To a solution of piperidin-4-ylmethanol (17.4 mmol, 2 g) in MeCN (50 mL) were added DIPEA (35 mmol, 6.1 mL) and N-(2-chloroethyl)benzenesulfonamide (17.4 mmol, 3.82 g). The mixture was heated at reflux under argon for 3h. The solvent was evaporated under reduced pressure to give a white solid which was washed with water (2 x 75 mL) to give the *title* compound as a white solid (13.2 mmol, 3.95 g). Yield = 76 %. Chemical formula: C₁₄H₂₂N₂O₃S. Molecular weight: 298.41 g.mol⁻¹. LC/MS (ESI): 95 %, m/z [M + H]⁺: 299.3. ¹H-NMR (300 MHz, DMSO-d₆) $\delta = 1.25$ (d, $J = 14.5$, 2H), 1.50 – 1.62 (m, 2H), 1.69 – 1.97 (m, 2H), 2.33 (s, 2H), 2.73 (d, $J = 9.6$, 2H), 2.86 (t, $J = 6.9$, 2H), 3.19 (dd, $J = 3.8, 6.2$, 2H), 4.40 (d, $J = 6.0$, 1H), 7.61 (qdd, $J = 1.9, 3.6, 8.8$, 4H), 7.81 (dd, $J = 1.7, 8.0$, 2H).

(1-(2-(Methylsulfonamido)ethyl)piperidin-4-yl)methyl 5-fluoro-1H-indole-3-carboxylate hydrochloride (15a)



General procedure 2 for the preparation of (1-(2-(Phenyl-/methyl-sulfonamido)ethyl)piperidin-4-yl)methyl 1H-indole-3-carboxylate

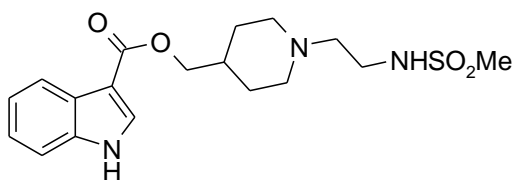
Thionyl chloride (5.6 mmol, 406 μ L) was slowly added to a suspension of 5-fluoro-1H-indole-3-carboxylic acid (1.12 mmol, 200 mg) in dry CH₂Cl₂ (10 mL) under argon, then the mixture was heated at reflux for 24h. After removal of the volatiles under reduced pressure, the residue was immediately put under argon atmosphere then taken off with dry CH₂Cl₂ (10 mL) and N-[2-[4-(hydroxymethyl)-1-piperidinyl]ethyl]methylsulfonamide (1.10 mmol, 260 mg) was added. The

resulting mixture was heated at reflux under argon for 24h. After removal of the solvent under vacuum, the resulting brown solid was taken off with water (50 mL) and then the aqueous layer was saturated with NaCl and extracted with CH₂Cl₂ (5 x 50 mL). The combined organic layers were washed with brine, dried on Na₂SO₄, filtered and solvents were removed under vacuum. The resulting grey solid was purified on a 20 g normal phase silica column with eluent (CH₂Cl₂/MeOH 90/10 to 75/25) to afford the product as brown foam (0.34 mmol, 134 mg). Yield = 30 %. The product was directly engaged in the next step.²⁹³

General procedure 3 for the preparation of hydrochloride acid salt

To a solution of (1-(2-(methylsulfonylamido)ethyl)piperidin-4-yl)methyl 5-fluoro-1H-indole-3-carboxylate (0.16 mmol, 62 mg) in MeOH (3 mL) was slowly added acetyl chloride (0.48 mmol, 34 μ L). After removal of solvent under reduced pressure, the residue was taken off with CHCl₃ (3 x 5 mL) and evaporated 3 times then with Et₂O (3 x 5 mL) to afford the *title* compound as a solid (0.16 mmol, 73 mg). Yield = quantitative. Chemical formula: C₁₈H₂₅FCIN₃O₄S. Molecular weight: 433.93 g.mol⁻¹. LCMS (ESI): (2012/02/22) 96 % pure at 254 nm, *m/z* [M + H]⁺: 398.2. HRMS (ESI) *m/z*: calcd. for C₁₈H₂₆FCIN₃O₄S: 398.1544; [M+H]⁺ found: 398.1536. ¹H-NMR (400 MHz, DMSO-d₆) δ = 12.24 (s, 1H), 10.61 (s, 1H), 8.27 – 8.18 (m, 1H), 7.62 (dd, *J* = 2.8, 9.8, 1H), 7.51 (dd, *J* = 4.6, 9.1, 2H), 7.06 (td, *J* = 2.7, 9.2, 1H), 4.23 – 4.07 (m, 2H), 3.53 (s, 3H), 3.15 (s, 2H), 2.98 (s, 3H), 2.11 – 1.84 (m, 4H), 1.76 (d, *J* = 13.1, 2H), 1.35 (d, *J* = 5.8, 2H). ¹³C NMR (101 MHz, DMSO-d₆) δ = 25.7, 26.7, 30.4, 33.0, 34.4, 37.2, 51.7, 55.7, 66.2, 105.2, 106.4, 110.8, 113.8, 126.3, 133.1, 157.1, 159.5, 164.0.

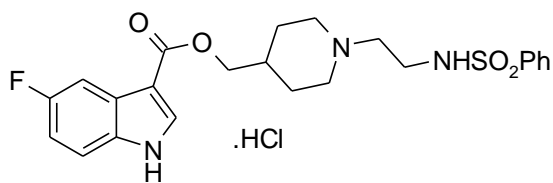
(1-(2-(Methylsulfonylamido)ethyl)piperidin-4-yl)methyl 1H-indole-3-carboxylate (15b)



The reaction was carried out according to the general procedure 2 with the corresponding scale: 1H-indole-3-carboxylic acid (1.67 mmol, 270 mg), SOCl₂ (8.35 mmol, 606 μ L), CH₂Cl₂ (10 mL), then N-[2-[4-(hydroxymethyl)-1-piperidinyl]ethyl]methylsulphonamide (1.58 mmol, 373 mg), CH₂Cl₂ (10 mL). The crude was purified without work-up on a normal phase silica gel chromatography (CH₂Cl₂/MeOH 90/10) to afford the *title* compound as brown foam (0.83 mmol, 313 mg). Yield = 50 %. Chemical formula: C₁₈H₂₅N₃O₄S. Molecular weight: 379.48 g.mol⁻¹. LCMS (ESI): 98 % pure, *m/z* [M + H]⁺: 380.2. HRMS (ESI) *m/z*: calcd. for C₁₈H₂₆N₃O₄S: 380.1639; [M+H]⁺ found: 380.1629. ¹H NMR (400 MHz, DMSO-d₆) δ = 1.75 (s, 2H), 1.83 – 1.94 (m, 2H), 1.93 – 2.05 (m,

1H), 2.92 (s, 2H), 2.97 (s, 3H), 3.07 (q, $J = 7.7, 8.1$, 2H), 4.14 (d, $J = 5.9$, 2H), 7.14 – 7.26 (m, 2H), 7.41 – 7.54 (m, 2H), 7.96 – 8.02 (m, 1H), 8.15 (d, $J = 3.0$, 1H), 10.81 (s, 1H), 12.14 (d, $J = 3.1$, 1H). ^{13}C NMR (101 MHz, DMSO- d_6) $\delta = 18.6, 33.2, 37.6, 38.9, 40.1, 40.2, 51.8, 56.0, 66.2, 106.2, 107.0, 112.4, 116.1, 120.4, 121.4, 122.4, 125.6, 132.8, 136.5, 164.4$.

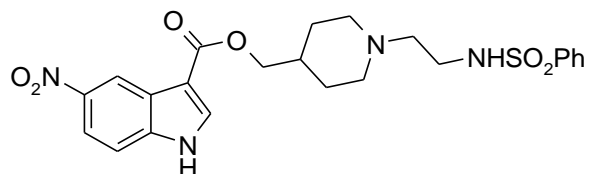
(1-(2-(Phenylsulfonamido)ethyl)piperidin-4-yl)methyl 5-fluoro-1H-indole-3-carboxylate hydrochloride (15c)



The reaction was carried out according to the general procedure 2 with the corresponding scale: 5-fluoro-1H-indole-3-carboxylic acid (1.67 mmol, 300 mg), SOCl_2 (8.35 mmol, 605 μL), CH_2Cl_2 (10 mL), then *N*-[2-[4-(hydroxymethyl)-1-piperidinyl]ethyl]phenylsulphonamide (1.67 mmol, 498 mg), CH_2Cl_2 (10 mL). For the purification, a normal phase silica gel column ($\text{CH}_2\text{Cl}_2/\text{EtOH}/\text{NH}_3(\text{aq})$ 95.5/4/0.5) was used to afford the product as a brown foam (0.65 mmol, 299 mg). Yield = 39 %. LC/MS (ESI): 86 % pure, m/z $[\text{M} + \text{H}]^+$: 460.2 The product was directly engaged in the next step.

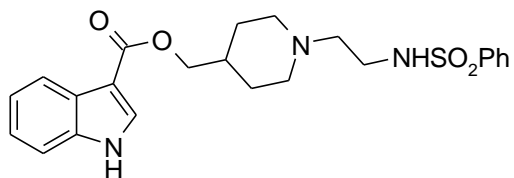
The reaction was carried out according to the general procedure 3 with the corresponding scale: (1-(2-(phenylsulfonamido)ethyl)piperidin-4-yl)methyl 5-fluoro-1H-indole-3-carboxylate (0.28 mmol, 131 mg), MeOH (3 mL), acetyl chloride (0.86 mmol, 61 μL). After removal of solvent under reduced pressure, residue was washed with diethyl ether (3 x 3 mL). MeOH (3 mL) was added onto the resulting solid (120 mg) and heated at reflux for 15 min. The insoluble part was separated and washed with diethyl ether (2 x 3 mL). This operation was repeated two times to obtain the *title* compound as a white solid (64 mg, 0.13 mmol). Yield = 46 %. Chemical formula: $\text{C}_{23}\text{H}_{28}\text{FN}_3\text{O}_4\text{S}$. Molecular weight: 496.00 $\text{g}\cdot\text{mol}^{-1}$. LC/MS (ESI): 98 % pure at 254 nm, m/z $[\text{M} + \text{H}]^+$: 460.2. HRMS (ESI) m/z : calcd. for $\text{C}_{23}\text{H}_{29}\text{FN}_3\text{O}_4\text{S}$: 460.1701 $[\text{M} + \text{H}]^+$; found: 460.1704. ^1H -NMR (400 MHz, DMSO- d_6) $\delta = 1.74$ (tt, $J = 7.1, 13.6$, 2H), 1.89 (d, $J = 13.6$, 2H), 1.93 – 2.07 (m, 1H), 2.97 (q, $J = 11.3$, 2H), 3.07 – 3.27 (m, 5H), 3.40 – 3.54 (m, 2H), 4.13 (d, $J = 5.9$, 2H), 7.06 (td, $J = 2.7, 9.2$, 1H), 7.50 (dd, $J = 4.6, 8.9$, 1H), 7.58 – 7.72 (m, 4H), 7.85 (dd, $J = 1.8, 7.0$, 2H), 8.18 (d, $J = 5.6$, 1H), 8.23 (d, $J = 3.1$, 1H), 10.53 (s, 1H), 12.24 (d, $J = 3.4$, 1H). ^{13}C NMR (101 MHz, DMSO- d_6) $\delta = 25.5, 32.8, 37.1, 40.2, 48.6, 51.6, 55.3, 66.1, 105.0, 105.2, 106.3, 106.4, 110.6, 110.8, 113.7, 113.8, 126.2, 126.3, 126.6, 126.6, 129.4, 132.8, 133.1, 134.4, 139.7, 157.1, 159.4, 164.0$. mp: 227-228°C

(1-(2-(Phenylsulfonamido)ethyl)piperidin-4-yl)methyl 5-nitro-1H-indole-3-carboxylate (15d)



The reaction was carried out according to the general procedure 2 with the corresponding scale: 5-nitro-1H-indole-3-carboxylic acid (1.45 mmol, 300 mg), SOCl₂ (7.25 mmol, 526 μ L), CH₂Cl₂ (10 mL), then N-[2-[4-(hydroxymethyl)-1-piperidiny]ethyl]phenylsulphonamide (1.45 mmol, 432 mg), CH₂Cl₂ (10 mL). After the work-up, the resulting brown solid (512 mg) was taken off with MeOH (25 mL) and the insoluble part was removed by filtration. After removal of solvents, the resulting yellow solid was washed with EtOAc (3 x 20 mL) and Et₂O (2 x 20 mL) to afford the *title* compound as a yellow solid (0.385 mmol, 187 mg). Yield = 26 %. Chemical formula: C₂₃H₂₆N₄O₆S. Molecular weight: 486.55 g.mol⁻¹. LC/MS (ESI): 90 % pure, *m/z* [M + H]⁺: 487.2. HRMS (ESI) *m/z*: calcd. for C₂₃H₂₇N₄O₆S: 487.1646 [M+H]⁺; found: 487.1628. ¹H-NMR (300 MHz, DMSO-d₆) δ = 1.49 (s, 2H), 1.83 (d, *J* = 13.4, 3H), 2.73 (t, *J* = 2.0, 2H), 3.01 (s, 4H), 4.17 (d, *J* = 6.0, 2H), 7.57 – 7.72 (m, 4H), 7.83 (dd, *J* = 1.7, 8.0, 2H), 8.11 (dd, *J* = 2.4, 9.0, 1H), 8.40 (s, 1H), 8.86 (d, *J* = 2.3, 1H), 12.66 (s, 1H). ¹³C NMR (101 MHz, DMSO-d₆) δ = 26.4, 51.9, 67.0, 108.4, 113.3, 116.9, 117.8, 125.0, 126.6, 129.3, 132.6, 136.3, 139.6, 140.1, 142.4, 163.5. mp: 201-202°C.

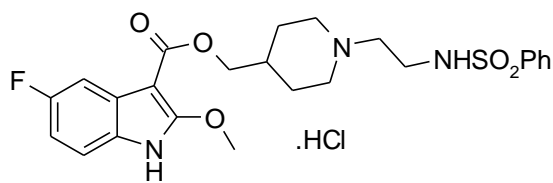
(1-(2-(Phenylsulfonamido)ethyl)piperidin-4-yl)methyl 1H-indole-3-carboxylate (15e)



The reaction was carried out according to the general procedure 2 with the corresponding scale: SOCl₂ (4.65 mmol, 337 μ L), 1H-indole-3-carboxylic acid (0.93 mmol, 150 mg), dry CH₂Cl₂ (10 mL), N-[2-[4-(hydroxymethyl)piperidin-1-yl]ethyl]benzenesulfonamide (1.12 mmol, 333 mg). The resulting grey solid was purified on a 20 g normal phase silica column with eluent CH₂Cl₂/MeOH 95/5 to give oil (154 mg) containing the product. This fraction was further purified on a 40 g normal phase silica column with eluent CH₂Cl₂/MeOH 97/3 to give the *title* compound as a white solid (0.068 mmol, 30 mg). Yield = 7 %. Chemical formula: C₂₃H₂₇N₃O₄S. Molecular weight: 441.55

g.mol⁻¹. LC/MS (ESI): 80 % pure, m/z [M + H]⁺: 442.2. ¹H-NMR (300 MHz, DMSO-d₆) δ = 1.24 (d, J = 9.1, 2H), 1.66 (d, J = 11.4, 3H), 1.87 (t, J = 11.1, 2H), 2.28 (t, J = 6.8, 2H), 2.72 (d, J = 10.6, 2H), 2.85 (t, J = 6.9, 2H), 4.07 (d, J = 5.9, 2H), 7.15 – 7.22 (m, 2H), 7.45 – 7.50 (m, 1H), 7.52 – 7.68 (m, 3H), 7.77 – 7.85 (m, 2H), 7.94 – 8.00 (m, 1H), 8.07 (s, 1H), 11.94 (s, 1H).

(1-(2-(Phenylsulfonamido)ethyl)piperidin-4-yl)methyl 5-fluoro-2-methoxy-1H-indole-3-carboxylate hydrochloride (16)



To a solution of (1-(2-(phenylsulfonamido)ethyl)piperidin-4-yl)methyl 5-fluoro-1H-indole-3-carboxylate (0.32 mmol, 148 mg) in dry CHCl₃ (7 mL) was added *N*-chlorosuccinimide (0.39 mmol, 52 mg). The mixture was heated at reflux under argon for 4h. After removal of solvent under reduced pressure, the residue was taken off with MeOH (10 mL) and heated at reflux under argon for 12h. After removal of solvent under vacuum, the resulting brown foam (207 mg) was purified on a normal phase silica gel column (CH₂Cl₂/MeOH 9/1) to afford the product as brown foam (0.22 mmol, 109 mg). Yield = 56 %. LC/MS (ESI): 99 % pure at 254 nm, m/z [M + H]⁺: 490.2. The product was directly engaged in the next step.

The reaction was carried out according to the general procedure 3 with the corresponding scale: (1-(2-(phenylsulfonamido)ethyl)piperidin-4-yl)methyl 5-fluoro-2-methoxy-1H-indole-3-carboxylate (0.22 mmol, 109 mg), MeOH (3 mL), acetyl chloride (0.70 mmol, 50 μ L). The crude oil was dissolved in boiling methanol (3 mL) and then cooled to -18°C overnight. A white precipitate occurred. After removal of MeOH, the resulting solid was washed with methanol (1 x 2 mL) and with diethyl ether (3 x 2 mL). MeOH (3 mL) was added to the resulting solid and heated at reflux for 15 min. The insoluble part was separated and then washed with diethyl ether (2 x 3 mL). This purification was repeated once to give the *title* compound as a white solid (0.07 mmol, 38 mg). Yield = 33 %. Chemical formula: C₂₄H₂₉FCIN₃O₅S. Molecular weight: 526.03 g.mol⁻¹. LC/MS (ESI): 99 % pure at 254 nm, m/z [M + H]⁺: 490.2. HRMS (ESI) m/z : calcd. for C₂₄H₃₀FCIN₃O₅S: 490.1806; [M+H]⁺ found: 498.1800. ¹H-NMR (400 MHz, DMSO-d₆) δ = 1.54 – 1.69 (m, 2H), 1.88 (d, J = 12.9, 2H), 1.97 (s, 1H), 2.96 (q, J = 11.2, 2H), 3.11 (t, J = 5.6, 2H), 3.16 (s, 1H), 3.18 (d, J = 6.3, 2H), 3.40 (s, 2H), 3.48 (d, J = 12.0, 2H), 4.07 (d, J = 6.4, 2H), 4.11 (s, 3H), 6.88 (ddd, J = 2.7, 8.6, 9.6, 1H), 7.30 (dd, J = 4.7, 8.7,

1H), 7.45 (dd, J = 2.7, 10.2, 1H), 7.59 – 7.71 (m, 3H), 7.82 – 7.88 (m, 2H), 8.16 (t, J = 5.9, 1H), 10.42 (d, J = 67.8, 1H), 12.27 (s, 1H). ¹³C NMR (101 MHz, DMSO) δ = 25.8, 33.0, 37.1, 38.9, 39.1, 39.3, 39.5, 39.6, 39.7, 39.8, 39.9, 40.0, 40.2, 40.2, 48.6, 51.6, 55.4, 58.8, 65.6, 86.5, 86.5, 104.6, 104.9, 107.8, 108.1, 112.1, 112.2, 126.6, 126.9, 127.1, 127.2, 129.4, 132.8, 139.7, 157.2, 158.5, 159.5, 163.2. mp: 195-196°C.

6.2 Biology

6.2.1 Biology of the chapter 3.1

Radiometric kinase assays

CK2 radiometric kinase assay was performed as previously described in Prudent *et al.* ¹⁵¹. Production and purification of GST-rhCK2a mutants were performed as described in the paper of Moucadel *et al.* ¹⁵⁰ and inhibitors were tested following the CK2 radiometric kinase assay procedure. ATP concentrations were 100 μM if not stated otherwise. Substrate dependent phosphorylation assays on nucleolin, Six1 and CK2 β auto-phosphorylation were performed following the CK2 radiometric kinase assay with CK2 $\alpha_2\beta_2$, the reaction was quenched by Laemmli buffer and samples were submitted to electrophoresis in NuPAGE buffer (150 V for 75 min) using pre-cast 4-12 % gradient gel (Bio-Rad). Proteins were stained using Coomassie blue (InstantBlue™, Expedeon, Cambridge, UK) and phosphorylation status measured using a phosphorimager PMI (BIO-RAD) and quantified with ImageJ.

Temperature-dependent circular dichroism (TdCD)

All single Far-UV-CD spectra were recorded using a Jasco-1500 spectropolarimeter (Gross-Umstadt, Germany). All spectra were recorded using a 1 mm path-length quartz cell, 1 nm bandwidth, 100 nm/min scan speed and 3 accumulations, within a wavelength range of 195 to 250 nm. GST-CK2a protein was diluted at 5 μM with 10 mM KH_2PO_4 and 50 mM Na_2SO_4 , pH 7.4. Ligand binding was tested at 50 μM for compound **5**, 6.25 μM for compound **7** and 6.25 μM for CX-4945 with a final methanol concentration of 0.8 % (v/v). Compound **7** and CX-4945 concentrations were limited by their solubility in the methanol stock. Spectra in absence of protein were recorded and subtracted from the experimental spectra. Temperature ramping experiments were performed from 20 °C to 86 °C, and prior to each recording point, the sample was allowed to equilibrate for 30 sec at ± 0.1 °C from the desired temperature. Midpoint unfolding temperatures (T_m) were determined using Thermal Denaturation multi-Analysis software.

Protein-ligand interactions by NMR

NMR experiments were recorded on a 600 MHz spectrometer at 293 K in PBS pH 7.3, 10 mM NaCl, MgCl₂ 2 mM, 10 % D₂O. 1D experiments were performed using a excitation sculpting pulse sequence. Saturation Transfer Difference was performed with on-resonance protein saturation at 0.6 ppm using 2 s saturation time. 7-azaindole was used as a reference compound to test the STD-competition with CX-4945. STD experiments were performed using 5 μM CK2α protein in the presence of 4 mM MgCl₂. STD factors were measured as previously reported ²²¹, and the values were normalized by assigning the value 100 % to the highest STD factor. Concentrations of the molecules AMP-PNP, 7-azaindole and compound **5** were 500 μM, and concentration of CX-4945 was 100 μM.

Molecular modeling and docking

Structures of the catalytic subunit of the human CK2 enzyme were retrieved from the Pocketome database ²⁸⁷. Including the multiple chains within each structure, there was a total of 72 structures. Candidate ligand docking locations were delineated as shown in figure 3, one comprising the canonical ATP binding site, and another the proposed allosteric binding site. Prior to docking, the kinase structures were completed by rebuilding and optimization of the missing side-chains and the hydrogen atoms in the presence of co-crystallized ligands (if any). Compounds **1-7** presented here, as well as ATP and CX-4945 were docking to each of the two sites in each of the available structures using ICM (Molsoft L.L.C.) ²⁸⁸ (The ICM docking procedure and scoring are presented in the supporting procedures).

Top ranking predicted ligand poses were inspected manually, taking into account the pose consistency between multiple compounds in the series as well as interactions with the residues highlighted by site-directed mutagenesis. From this analysis, it became clear that the backbone conformation with the largest distance between the αC-helix and the middle β-strand of the N-terminal lobe is most compatible with the proposed model of binding. Based on this consideration, PDB 3JUH was selected as a backbone template for further studies. Val66Ala and Met163Leu mutations in the ATP binding pocket of this structure were reverted back to their wild-type amino-acids. Residue side-chains in the allosteric pocket were conformationally optimized in the presence of docked compounds to resemble pocket shape observed in PDB 3FWQ. The optimized model was used for the second round of compound docking using the ICM grid potential based protocol described in the supporting procedures. Top-ranking poses of compounds (including CX-4945 and ATP) from this round are presented.

ICM docking procedure

The ICM docking engine predicts ligand poses by stochastic global optimization of the flexible ligand molecule (represented in internal coordinates) inside a set of pre-calculated grid potential maps representing the binding pocket of the receptor^{289–291} and including (i) van der Waals (represented as Lennard-Jones potential for hydrogen, carbon and “large atom” probes); (ii) electrostatic potential (calculated by the Coulomb formula with the distance-dependent dielectric constant of $4r$); (iii) hydrogen bonding potential combining the donor and acceptor fields; (iv) apolar surface energy. Prior to sampling, multiple starting poses of the ligand were generated by exhaustively sampling the ligand *in vacuo* and overlaying each of the resulting conformations onto the binding pocket in four principal orientations. The sampling phase was performed using biased probability Monte Carlo optimization²⁸⁸ of rotational, translational, and torsional variables of the ligand in an attempt to achieve the global minimum of the objective energy function that combines ligand interactions with the receptor grid potentials and the explicit (full-atom) interactions within the ligand itself (“ligand strain”). Top-ranking predicted poses of the ligand were combined with the full-atom representation of the receptor pocket and evaluated with ICM ligand binding score²⁹² calculated as $S_{bind} = E_{int} + T\Delta S_{Tor} + E_{vw} + \alpha_1 \times E_{el} + \alpha_2 \times E_{hb} + \alpha_3 \times E_{hp} + \alpha_4 \times E_{sf}$. Here E_{vw} , E_{el} , E_{hb} , E_{hp} , and E_{sf} are Van der Waals, electrostatic, hydrogen bonding, non-polar and polar atom solvation energy differences between bound and unbound states, E_{int} is the ligand internal strain, ΔS_{Tor} is its conformational entropy loss upon binding, $T = 300$ K, and α_i are ligand- and protein-independent constants that have been previously optimized on a diverse screening benchmark.

Cell culture

The human kidney carcinoma cell line (786-O) was cultured in RPMI 1640 medium (Gibco) supplemented with 10 % (v/v) fetal calf serum, penicillin (100 U/mL) and streptomycin (100 µg/mL) at 37 °C in 5 % CO₂ atmosphere. Experiments were performed in RPMI 1640 (GIBCO) supplemented with 0.1 % or 0.5 % (v/v) fetal serum, penicillin (100 U/mL) and streptomycin (100 µg/mL) 37 °C in 5 % CO₂ atmosphere.

Cell viability assay

Cells were plated into 96-well plates at 1×10^4 cells/well. The following day, the culture medium was replaced with fresh medium containing the inhibitors at various concentrations. DMSO (0.25 %) and cell free wells were used as control. After 24 h, 50 µL of (3-(4,5-dimethylthiazol-2-yl)-2,5-diphenyltetrazolium bromide) (MTT) solution in PBS (5 mg/mL) were added in each well and the

plate incubated for 2 h at 37 °C in 5 % CO₂ atmosphere. Then, 80 µL of SDS (10 %) containing 0.01 M HCl were added in each well and gently stirred at RT for 4 h. Absorbance was measured at 570 nm with a microplate reader (Infinite 200 Pro, Tecan). Results are the average of a triplicate experiment with a standard deviation lower than 10 %. EC₅₀ was determined by linear interpolation after transformation to log[c] scale.

CK2 inhibition in cells

Cells were plated into 6-well plates at 3 x 10⁵ cells/well. The following day, the culture medium was replaced with fresh medium containing the inhibitors at various concentrations or DMSO (0.5 %) as reference. After incubation for 24 h, medium was removed, cells were washed with cold PBS and frozen at -80°C. The phosphorylation status of two protein substrates of CK2 (α-catenin and Akt1) was measured by Western Blot analysis of cell extracts.

Western Blot analysis

Primary antibodies were α-catenin (phospho-Ser641) antibody from SAB Signalway Antibody, Akt1-(phospho-Ser129) antibody from Abgent, anti-GAPDH mAb from Ambion. Secondary antibodies were peroxidase-conjugated affinity pure Goat anti-rabbit IgG (#111035003) and peroxidase-conjugated affinity pure Goat anti-mouse IgG (#115035003) from Jackson Immuno Research. Cells were lysed in RIPA buffer (10 mM Tris-HCl pH 7.4, 150 mM NaCl, 1 % Triton X-100, 0.1 % SDS, 0.5 % DOC and 1 mM EDTA) containing both protease- and phosphatase-inhibitor cocktails (Sigma-Aldrich; P8340, P2850, P5726). Cell homogenates were quantified using BCA protein Assay kit (Thermo Scientific). SDS-PAGE was performed using pre-cast 4-12 % gradient gel (Bio-Rad) and submitted to electrophoresis in NuPAGE buffer (150 V for 75 min). Separated proteins at 20 µg/lane were transferred to PVDF membranes (100 V for 60 min). Blotted membranes were blocked during 1 h at room temperature with saturation buffer (1 % BSA in Tris Buffer Saline 10 mM, Tween 0.1 % (TBST)), and then incubated with primary antibody diluted in saturation buffer, for 2 h or overnight. After 3 washes with TBST, secondary antibodies were added for 1 h. Luminata Forte Western HRP substrate (Millipore) was added and membranes were read with Fusion Fx7 (PerkinElmer). Anti-GAPDH was used as loading control. Images were analyzed and band intensities were quantified using ImageJ software. EC₅₀ were determined by fitting band intensities in function of inhibitor concentration to a sigmoid equation using SigmaPlot.

Cell transfection and imaging

The cDNA encoding GFP-CK2a was subcloned from pEGFP-CK2a vector²⁴⁵ into pMSCV-puro plasmid. Viral particles were produced and stable expression of EGFP-CK2a was accomplished by transfection of 786-O cells followed by 1 µg/ml puromycin-mediated selection. 786-O pEGFP-CK2a cells were seeded on Lab-Tek™ slides. After treatment with DMSO, compound **7** (40 µM) or CX-4945 (8 µM) for 12 h, cells were washed twice with PBS and fixed with 4 % paraformaldehyde for 10 min at 20 °C. Nuclei were stained with Hoechst-33342 (Sigma-Aldrich) for 30 min and cells were washed with PBS (3 x 15 min). Images were acquired with a Zeiss ApoTome microscope and analyzed using Zen software. Fluorescence intensity, exposure times and post-acquisition modifications were kept identical for all the samples.

Screening of compound selectivity against a kinase panel

Kinase selectivity of compound **1** and **7** were assessed using the Kinase Profiler service offered by Life Technologies. The assays were performed with ATP concentration adjusted to the respective Km of each kinase in the presence of 50 µM inhibitor. Inhibition, expressed as the percent of activity determined in the absence of inhibitor, was calculated from the residual activity measured in the presence of 50 µM inhibitor.

6.2.2 Biology of the chapter 3.2

Radiometric kinase assays

CK2 radiometric kinase assay was performed as previously described in Prudent *et al.*¹⁵¹ Production and purification of GST-rhCK2a mutants were performed as described in the paper of Moucadel *et al.*¹⁵⁰ and inhibitors were tested following the CK2 radiometric kinase assay procedure. ATP concentrations were 100 μ M if not stated otherwise.

Cell culture

The human kidney carcinoma cell line (786-O) was cultured in RPMI 1640 medium (Gibco) supplemented with 10% (v/v) fetal calf serum, penicillin (100 U/mL) and streptomycin (100 μ g/mL) at 37 °C in 5% CO₂ atmosphere. Experiments were performed in RPMI 1640 (GIBCO) supplemented with 0.1% or 0.5% (v/v) fetal serum, penicillin (100 U/mL) and streptomycin (100 μ g/mL) 37 °C in 5% CO₂ atmosphere.

Cell viability assay

Cells were plated into 96-well plates at 1×10^4 cells/well. The following day, the culture medium was replaced with fresh medium containing the inhibitors at various concentrations. DMSO (0.25%) and cell free wells were used as control. After 24 h, 50 μ L of (3-(4,5-dimethylthiazol-2-yl)-2,5-diphenyltetrazolium bromide) (MTT) solution in PBS (5 mg/mL) were added in each well and the plate incubated for 2 h at 37 °C in 5 % CO₂ atmosphere. Then, 80 μ L of SDS (10%) containing 0.01 M HCl were added in each well and gently stirred at RT for 4 h. Absorbance was measured at 570 nm with a microplate reader (Infinite 200 Pro, Tecan). Results are the average of a triplicate experiment with a standard deviation lower than 10%. EC₅₀ was determined by linear interpolation after transformation to log[c] scale.

CK2 inhibition in cells

Cells were plated into 6-well plates at 3×10^5 cells/well. The following day, the culture medium was replaced with fresh medium containing the inhibitors at various concentrations or DMSO (0.5%) as reference. After incubation for 24 h, medium was removed, cells were washed with cold PBS and frozen at -80°C. The phosphorylation status of two protein substrates of CK2 (α -catenin and Akt1) was measured by Western Blot analysis of cell extracts.

Western Blot analysis

Primary antibodies were α -catenin (phospho-Ser641) antibody from SAB Signalway Antibody, Akt1-(phosphor-Ser129) antibody from Abgent, anti-GAPDH mAb from Ambion, anti-Akt1, anti- α -catenin, anti-PARP, anti-survivin. Secondary antibodies were peroxidase-conjugated affinity pure Goat anti-rabbit IgG (#111035003) and peroxidase-conjugated affinity pure Goat anti-mouse IgG (#115035003) from Jackson Immuno Research. Cells were lysed in RIPA buffer (10 mM Tris-HCl pH 7.4, 150 mM NaCl, 1% Triton X-100, 0.1% SDS, 0.5% DOC and 1 mM EDTA) containing both protease- and phosphatase-inhibitor cocktails (Sigma-Aldrich; P8340, P2850, P5726). Cell homogenates were quantified using BCA protein Assay kit (Thermo Scientific). SDS-PAGE was performed using pre-cast 4-12% gradient gel (Bio-Rad) and submitted to electrophoresis in NuPAGE buffer (150 V for 75 min). Separated proteins at 20 μ g/lane were transferred to PVDF membranes (100 V for 60 min). Blotted membranes were blocked during 1 h at room temperature with saturation buffer (1 % BSA in Tris Buffer Saline 10 mM, Tween 0.1% (TBST)), and then incubated with primary antibody diluted in saturation buffer, for 2 h or overnight. After 3 washes with TBST, secondary antibodies were added for 1 h. Luminata Forte Western HRP substrate (Millipore) was added and membranes were read with Fusion Fx7 (PerkinElmer). Anti-GAPDH was used as loading control. Images were analyzed and band intensities were quantified using ImageJ software.

6.2.3 Biology of the chapter 3.3

Cell culture

The human kidney carcinoma cell line (786-O) was cultured in RPMI 1640 medium (Gibco) supplemented with 10 % (v/v) fetal calf serum, penicillin (100 U/mL) and streptomycin (100 µg/mL) at 37°C in 5 % CO₂ atmosphere. MCF10A and MCF10A-Δβ cells were cultured as described²⁹³. HeLa cells were cultured in DMEM with 10 % (v/v) fetal calf serum, penicillin (100 U/mL) and streptomycin (100 µg/mL) at 37°C in 5 % CO₂ atmosphere.

Monitoring of the CK2α/CK2β interaction in cells

HeLa cells were seeded on Lab-Tek™. After treatment with DMSO, TAT-Pc (30 µM) or CX-4945 (12 µM) for 6h, cells were washed twice with PBS and fixed with 4 % paraformaldehyde for 10 min at 20° C, followed by permeabilization with 0.5% Triton X100. CK2α/CK2β interactions in cells were measured following the procedure of the DuoLink™ kit (Olink Bioscience). Images were acquired with a Zeiss ApoTome microscope and analyzed using Zen software. Quantification was performed using the BlobFinder software²⁵⁰.

Cell immunostaining and imaging

786-O, MCF10A or MCF10A-Δβ cells were seeded on Lab-Tek™. After treatment with DMSO, TAT-Pc (30 µM) or CX-4945 (12 µM) for 12h, cells were washed twice with PBS and fixed with 4 % paraformaldehyde for 10 min at 20° C followed by permeabilization with 0.5% Triton X100. The following primary antibodies were diluted in TBS containing 0.1% Tween20. They were purchased from Santa Cruz Biotechnology for anti-CK2α sc6479 (1/200); anti-CK2β (6D5) sc-12739 (1/200); anti-CK2α' (C-20) sc-6481 (1/200); anti-EGFR (1005) sc-03 (1/200); anti-p21 (C-19) sc-397 (1/200); and from BD Pharmingen™ for Anti-Human CD107a (LAMP1) Clone H4A3 (RUO) (1/500). Cells were washed with PBS (3 x 15 min) and the secondary antibodies were Cy3-labeled donkey-anti-goat, Dy649-labeled donkey-anti-mouse IgG, and Cy3-labeled goat-anti-rabbit IgG. Nuclei were stained with Hoechst-33342 (Sigma-Aldrich) for 30 min and cells were washed with PBS (3 x 15 min). Images were acquired with a Zeiss ApoTome microscope and analyzed using Zen software. Fluorescence intensity, exposure times and post-acquisition modifications were kept identical for all the samples.

Cell viability assay

Cells were plated into 96-well plates at 1×10^4 cells/well. The following day, the culture medium was replaced with fresh medium (90 μ L) containing the inhibitors at various concentrations. DMSO (0.25 %) and cell free wells were used as control. After 24 h, 10 μ L of PrestoBlue® solution were added in each well and the plate incubated for 1 h at 37° C in 5 % CO₂ atmosphere. Results are the average of a triplicate experiment with a standard deviation lower than 10 %.

Western Blot analysis

Cells were plated into 6-well plates at 3×10^5 cells/well. The following day, the culture medium was replaced with fresh medium containing the inhibitors at various concentrations or DMSO (0.5 %) as reference. After incubation for 48 h, medium was removed, cells were washed with cold PBS and frozen at -80°C. Primary antibodies were α -catenin (phospho-Ser641) antibody from SAB Signalway Antibody, anti- α -catenin, Akt1-(phosphor-Ser129) antibody from Abgent, anti-Akt1-(phosphor-Ser473), anti-Akt1, anti-p21, anti-p21-(phosphor-Thr145), anti-GAPDH mAb from Ambion, anti-SNAIL1 from Cell signaling, anti-HSP90. Secondary antibodies were peroxidase-conjugated affinity pure Goat anti-rabbit IgG (#111035003) and peroxidase-conjugated affinity pure Goat anti-mouse IgG (#115035003) from Jackson Immuno Research. Cells were lysed in RIPA buffer (10 mM Tris-HCl pH 7.4, 150 mM NaCl, 1 % Triton X-100, 0.1 % SDS, 0.5 % DOC and 1 mM EDTA) containing both protease- and phosphatase-inhibitor cocktails (Sigma-Aldrich; P8340, P2850, P5726). Cell homogenates were quantified using BCA protein Assay kit (Thermo Scientific). SDS-PAGE was performed using pre-cast 4-12 % gradient gel (Bio-Rad) and submitted to electrophoresis in NuPAGE buffer (150 V for 75 min). Separated proteins at 20 μ g/lane were transferred to PVDF membranes (100 V for 60 min). Blotted membranes were blocked during 1 h at room temperature with saturation buffer (1 % BSA in Tris Buffer Saline 10 mM, Tween 0.1 % (TBST)), and then incubated with primary antibody diluted in saturation buffer, for 2 h or overnight. After 3 washes with TBST, secondary antibodies were added for 1 h. Luminata Forte Western HRP substrate (Millipore) was added and membranes were read with Fusion Fx7 (PerkinElmer). Anti-HSP90 and/or anti-GAPDH were used as loading control.

6.2.4 Biology of the chapter 3.4

CK2 β -independent and CK2 β (+)-dependent substrates

The following peptide substrates were employed: a canonical CK2 peptide substrate RRREDEESDDEE phosphorylated equally by CK2 α and CK2 α 2 β 2 (CK2 β -independent peptide substrate), and MSGDEMIFDPTMSKKKKKKKP (eIF2 peptide) exclusively phosphorylated by CK2 α 2 β 2 (CK2 β -dependent peptide substrate).²⁹⁴

CK2 kinase assays were performed in a final assay volume of 18 mL containing 3 mL of compounds, 3 mL of CK2 α (36 ng) and a mixture of 100 μ M peptide substrate, 10 mM MgCl₂, and 1 μ Ci [γ ³²P]-ATP. Final concentration of ATP was 100 μ M if not specified otherwise. Assays were performed under linear kinetic conditions for 5 min at room temperature before termination by the addition of 60 μ L of 4% TCA. ³²P incorporation in peptide substrate was determined as previously described.²⁹⁵

Surface Plasmon Resonance (SPR)

SPR binding studies were performed using a Reichert SR7000DC instrument optical biosensor (Reichert Technologies) equipped with a CMD500m sensor chip obtained from XanTec Bioanalytics. CK2 α was immobilized by a capturing approach using a monoclonal anti-GST antibody (27 kDa, Clone GST-R 6G9 produced in rat, SAB4200055 Sigma Aldrich). Prior to use, the anti-GST antibodies were purified twice by micro dialysis at 4°C (Membrane: dialysis tubing benzoylated, 9 mm, D2272-5FT) in 10 mM sodium acetate, pH = 5. Anti-GST antibodies were immobilized using amine-coupling chemistry at 12°C. The surfaces of all two flow cells were activated for 7 min with a 1:1 mixture of 0.1 M NHS (N-hydroxysuccinimide) and 0.1 M EDC (3-(N,N-dimethylamino) propyl-N-ethylcarbodiimide) at a flow rate of 10 μ L/min. The antibody at a concentration of 30 μ g/ml in 10 mM sodium acetate, pH 5.0, was immobilized at a density of 2000 RU on flow cell 2; flow cell 1 was left blank to serve as a reference surface. All the surfaces were blocked with a 3 min injection at 10 μ L/min of 1 M ethanolamine, pH 8.0. GST tagged CK2 α at a concentration of 50 μ g/mL in 10 mM HEPES, 150 mM NaCl, 3 mM EDTA, 0.005% (v/v) polysorbate 20, pH = 7.4 was captured at a density of 900 RU on flow cell 2.

SPR Kd determination

To collect kinetic binding data, analytes in 10 mM HEPES, 150 mM NaCl, 3 mM EDTA, 0.005 % (v/v) polysorbate 20, 1% DMSO (v/v), pH = 7.4 were injected over the two flow cells at concentrations of 100, 50, 25, 12.5, 6.25, 3.12, 1.56 μ M at a flow rate of 25 μ L/min and at a temperature of 25°C. The complex was allowed to associate and dissociate for 120 s. Duplicate injections (in random order) of each sample and a buffer blank were flowed over the two surfaces. Affinities were obtained after treatments (DMSO calibration, blank and references subtractions) using the software Scrubber 2.0c.

Cell culture

MCF10 were cultured as described.²⁹³

Cell viability assay

Cells were plated into 96-well plates at 1×10^4 cells/well. The following day, the culture medium was replaced with fresh medium (90 μ L) containing the inhibitors at various concentrations. DMSO (0.25 %) and cell free wells were used as control. After 24 h, 10 μ L of PrestoBlue® solution were added in each well and the plate incubated for 1 h at 37° C in 5 % CO₂ atmosphere. Results are the average of a triplicate experiment with a standard deviation lower than 10 %. EC₅₀ was determined by linear interpolation after transformation to log[c] scale.

Western Blot analysis

Cells were plated into 6-well plates at 3×10^5 cells/well. The following day, the culture medium was replaced with fresh medium containing the inhibitors at various concentrations or DMSO (0.5 %) as reference. After incubation for 48 h, medium was removed, cells were washed with cold PBS and frozen at -80°C. Primary antibodies were anti-p21, anti-p21-(phosphor-Thr145), anti-HSP90. Secondary antibodies were peroxidase-conjugated affinity pure Goat anti-rabbit IgG (#111035003) and peroxidase-conjugated affinity pure Goat anti-mouse IgG (#115035003) from Jackson Immuno Research. Cells were lysed in RIPA buffer (10 mM Tris-HCl pH 7.4, 150 mM NaCl, 1 % Triton X-100, 0.1 % SDS, 0.5 % DOC and 1 mM EDTA) containing both protease- and phosphatase-inhibitor cocktails (Sigma-Aldrich; P8340, P2850, P5726). Cell homogenates were quantified using BCA protein Assay kit (Thermo Scientific). SDS-PAGE was performed using pre-cast 4-12 % gradient gel (Bio-Rad) and submitted to electrophoresis in NuPAGE buffer (150 V for 75 min). Separated proteins at 20 μ g/lane were transferred to PVDF membranes (100 V for 60 min). Blotted membranes were blocked during 1 h at room temperature with saturation buffer (1

% BSA in Tris Buffer Saline 10 mM, Tween 0.1 % (TBST)), and then incubated with primary antibody diluted in saturation buffer, for 2 h or overnight. After 3 washes with TBST, secondary antibodies were added for 1 h. Luminata Forte Western HRP substrate (Millipore) was added and membranes were read with Fusion Fx7 (PerkinElmer). Anti-HSP90 was used as loading control.

References

- (1) de Magalhães, J. P. How Ageing Processes Influence Cancer. *Nat. Rev. Cancer* **2013**, *13* (5), 357–365.
- (2) GBD 2013 Mortality and Causes of Death Collaborators. Global, Regional, and National Age-Sex Specific All-Cause and Cause-Specific Mortality for 240 Causes of Death, 1990–2013: A Systematic Analysis for the Global Burden of Disease Study 2013. *Lancet* **2015**, *385* (9963), 117–171.
- (3) Jemal, A.; Bray, F.; Center, M. M.; Ferlay, J.; Ward, E.; Forman, D. Global Cancer Statistics. *CA. Cancer J. Clin.* **2011**, *61* (2), 69–90.
- (4) Hanahan, D.; Weinberg, R. A. The Hallmarks of Cancer. *Cell* **2000**, *100* (1), 57–70.
- (5) Hanahan, D.; Weinberg, R. A. Hallmarks of Cancer: The next Generation. *Cell* **2011**, *144* (5), 646–674.
- (6) Dephoure, N.; Gould, K. L.; Gygi, S. P.; Kellogg, D. R. Mapping and Analysis of Phosphorylation Sites: A Quick Guide for Cell Biologists. *Mol. Biol. Cell* **2013**, *24* (5), 535–542.
- (7) Manning, G.; Whyte, D. B.; Martinez, R.; Hunter, T.; Sudarsanam, S. The Protein Kinase Complement of the Human Genome. *Science* **2002**, *298* (5600), 1912–1934.
- (8) Manning, G.; Plowman, G. D.; Hunter, T.; Sudarsanam, S. Evolution of Protein Kinase Signaling from Yeast to Man. *Trends Biochem. Sci.* **2002**, *27* (10), 514–520.
- (9) Kannan, N.; Taylor, S. S.; Zhai, Y.; Venter, J. C.; Manning, G. Structural and Functional Diversity of the Microbial Kinome. *PLoS Biol.* **2007**, *5* (3), e17.
- (10) Knighton, D. R.; Zheng, J. H.; Ten Eyck, L. F.; Ashford, V. A.; Xuong, N. H.; Taylor, S. S.; Sowadski, J. M. Crystal Structure of the Catalytic Subunit of Cyclic Adenosine Monophosphate-Dependent Protein Kinase. *Science* **1991**, *253* (5018), 407–414.
- (11) Smyth, L. A.; Collins, I. Measuring and Interpreting the Selectivity of Protein Kinase Inhibitors. *J. Chem. Biol.* **2009**, *2* (3), 131–151.
- (12) Taylor, S. S.; Kornev, A. P. Protein Kinases: Evolution of Dynamic Regulatory Proteins. *Trends Biochem. Sci.* **2011**, *36* (2), 65–77.
- (13) Zhang, J.; Yang, P. L.; Gray, N. S. Targeting Cancer with Small Molecule Kinase Inhibitors. *Nat. Rev. Cancer* **2009**, *9* (1), 28–39.
- (14) Williams, R.; Berndt, A.; Miller, S.; Hon, W.-C.; Zhang, X. Form and Flexibility in Phosphoinositide 3-Kinases. *Biochem. Soc. Trans.* **2009**, *37* (Pt 4), 615–626.

- (15) Kornev, A. P.; Taylor, S. S.; Ten Eyck, L. F. A Helix Scaffold for the Assembly of Active Protein Kinases. *Proc. Natl. Acad. Sci.* **2008**, *105* (38), 14377.
- (16) Kornev, A. P.; Haste, N. M.; Taylor, S. S.; Ten Eyck, L. F. Surface Comparison of Active and Inactive Protein Kinases Identifies a Conserved Activation Mechanism. *Proc. Natl. Acad. Sci.* **2006**, *103* (47), 17783.
- (17) Hopkins, A. L.; Groom, C. R. The Druggable Genome. *Nat. Rev. Drug Discov.* **2002**, *1* (9), 727–730.
- (18) Collett, M. S.; Erikson, R. L. Protein Kinase Activity Associated with the Avian Sarcoma Virus Src Gene Product. *Proc. Natl. Acad. Sci. U. S. A.* **1978**, *75* (4), 2021–2024.
- (19) Cohen, P. Protein Kinases - the Major Drug Targets of the Twenty-First Century? *Nat. Rev. Drug Discov.* **2002**, *1* (4), 309–315.
- (20) Kesselheim, A. S.; Avorn, J. The Most Transformative Drugs of the Past 25 Years: A Survey of Physicians. *Nat. Rev. Drug Discov.* **2013**.
- (21) Protein Kinase Inhibitor. *Wikipedia, the free encyclopedia*; 2014.
- (22) European Medicines Agency - Find medicine - European public assessment reports http://www.ema.europa.eu/ema/index.jsp?curl=pages/medicines/landing/epar_search.jsp&mid=WC0b01ac058001d12 (accessed Jul 26, 2014).
- (23) Burnett, G.; Kennedy, E. P. The Enzymatic Phosphorylation of Proteins. *J. Biol. Chem.* **1954**, *211* (2), 969–980.
- (24) Hathaway, G. M.; Traugh, J. A. Cyclic Nucleotide-Independent Protein Kinases from Rabbit Reticulocytes. Purification of Casein Kinases. *J. Biol. Chem.* **1979**, *254* (3), 762–768.
- (25) Villar-Palasi, C.; Kumon, A. Purification and Properties of Dog Cardiac Troponin T Kinase. *J. Biol. Chem.* **1981**, *256* (14), 7409–7415.
- (26) Cohen, P.; Yellowlees, D.; Aitken, A.; Donella-Deana, A.; Hemmings, B. A.; Parker, P. J. Separation and Characterisation of Glycogen Synthase Kinase 3, Glycogen Synthase Kinase 4 and Glycogen Synthase Kinase 5 from Rabbit Skeletal Muscle. *Eur. J. Biochem. FEBS* **1982**, *124* (1), 21–35.
- (27) Meggio, F.; Pinna, L. A. One-Thousand-and-One Substrates of Protein Kinase CK2? *FASEB J.* **2003**, *17* (3), 349–368.
- (28) Niefind, K.; Guerra, B.; Ermakowa, I.; Issinger, O. G. Crystal Structure of Human Protein Kinase CK2: Insights into Basic Properties of the CK2 Holoenzyme. *EMBO J.* **2001**, *20* (19), 5320–5331.
- (29) *The PyMOL Molecular Graphics System*; Schrödinger, LCC.

- (30) Niefind, K.; Guerra, B.; Pinna, L. A.; Issinger, O.-G.; Schomburg, D. Crystal Structure of the Catalytic Subunit of Protein Kinase CK2 from Zea Mays at 2.1 Å Resolution. *EMBO J.* **1998**, *17* (9), 2451–2462.
- (31) Niefind, K.; Raaf, J.; Issinger, O.-G. Protein Kinase CK2: From Structures to Insights. *Cell. Mol. Life Sci.* **2009**, *66* (11), 1800–1816.
- (32) Niefind, K.; Pütter, M.; Guerra, B.; Issinger, O. G.; Schomburg, D. GTP plus Water Mimic ATP in the Active Site of Protein Kinase CK2. *Nat. Struct. Biol.* **1999**, *6* (12), 1100–1103.
- (33) Yde, C. W.; Ermakova, I.; Issinger, O.-G.; Niefind, K. Inclining the Purine Base Binding Plane in Protein Kinase CK2 by Exchanging the Flanking Side-Chains Generates a Preference for ATP as a Cosubstrate. *J. Mol. Biol.* **2005**, *347* (2), 399–414.
- (34) Nolen, B.; Taylor, S.; Ghosh, G. Regulation of Protein Kinases; Controlling Activity through Activation Segment Conformation. *Mol. Cell* **2004**, *15* (5), 661–675.
- (35) Battistutta, R.; Lolli, G. Structural and Functional Determinants of Protein Kinase CK2α: Facts and Open Questions. *Mol. Cell. Biochem.* **2011**, *356*, 67–73.
- (36) Bischoff, N.; Raaf, J.; Olsen, B.; Bretner, M.; Issinger, O.-G.; Niefind, K. Enzymatic Activity with an Incomplete Catalytic Spine: Insights from a Comparative Structural Analysis of Human CK2α and Its Paralogous Isoform CK2α'. *Mol. Cell. Biochem.* **2011**, *356*, 57–65.
- (37) Klopfleisch, K.; Issinger, O.-G.; Niefind, K. Low-Density Crystal Packing of Human Protein Kinase CK2 Catalytic Subunit in Complex with Resorufin or Other Ligands: A Tool to Study the Unique Hinge-Region Plasticity of the Enzyme without Packing Bias. *Acta Crystallogr. D Biol. Crystallogr.* **2012**, *68* (Pt 8), 883–892.
- (38) Pargellis, C.; Tong, L.; Churchill, L.; Cirillo, P. F.; Gilmore, T.; Graham, A. G.; Grob, P. M.; Hickey, E. R.; Moss, N.; Pav, S.; Regan, J. Inhibition of p38 MAP Kinase by Utilizing a Novel Allosteric Binding Site. *Nat. Struct. Biol.* **2002**, *9* (4), 268–272.
- (39) Schindler, T.; Bornmann, W.; Pellicena, P.; Miller, W. T.; Clarkson, B.; Kuriyan, J. Structural Mechanism for STI-571 Inhibition of Abelson Tyrosine Kinase. *Science* **2000**, *289* (5486), 1938–1942.
- (40) Hari, S. B.; Merritt, E. A.; Maly, D. J. Sequence Determinants of a Specific Inactive Protein Kinase Conformation. *Chem. Biol.* **2013**, *20* (6), 806–815.
- (41) Jakobi, R.; Traugh, J. A. Site-Directed Mutagenesis and Structure/function Studies of Casein Kinase II Correlate Stimulation of Activity by the Beta Subunit with Changes in Conformation and ATP/GTP Utilization. *Eur. J. Biochem. FEBS* **1995**, *230* (3), 1111–1117.
- (42) Pinna, L. A. *Protein Kinase CK2*; Wiley-Blackwell: Ames, Iowa, USA, 2013.

- (43) Guerra, B.; Siemer, S.; Boldyreff, B.; Issinger, O. G. Protein Kinase CK2: Evidence for a Protein Kinase CK2beta Subunit Fraction, Devoid of the Catalytic CK2alpha Subunit, in Mouse Brain and Testicles. *FEBS Lett.* **1999**, *462* (3), 353–357.
- (44) Xu, X.; Toselli, P. A.; Russell, L. D.; Seldin, D. C. Globozoospermia in Mice Lacking the Casein Kinase II Alpha' Catalytic Subunit. *Nat. Genet.* **1999**, *23* (1), 118–121.
- (45) Bischoff, N.; Olsen, B.; Raaf, J.; Bretner, M.; Issinger, O.-G.; Niefind, K. Structure of the Human Protein Kinase CK2 Catalytic Subunit CK2a' and Interaction Thermodynamics with the Regulatory Subunit CK2β. *J. Mol. Biol.* **2011**, *407*, 1–12.
- (46) Olsen, B. B.; Rasmussen, T.; Niefind, K.; Issinger, O.-G. Biochemical Characterization of CK2alpha and Alpha' Paralogues and Their Derived Holoenzymes: Evidence for the Existence of a Heterotrimeric CK2alpha'-Holoenzyme Forming Trimeric Complexes. *Mol. Cell. Biochem.* **2008**, *316* (1-2), 37–47.
- (47) Chantalat, L.; Leroy, D.; Filhol, O.; Nueda, A.; Benitez, M. J.; Chambaz, E. M.; Cochet, C.; Dideberg, O. Crystal Structure of the Human Protein Kinase CK2 Regulatory Subunit Reveals Its Zinc Finger-Mediated Dimerization. *EMBO J.* **1999**, *18* (11), 2930–2940.
- (48) Lolli, G.; Ranchio, A.; Battistutta, R. Active Form of the Protein Kinase CK2a2β2 Holoenzyme Is a Strong Complex with Symmetric Architecture. *ACS Chem. Biol.* **2014**, *9* (2), 366-71
- (49) Raaf, J.; Brunstein, E.; Issinger, O. G.; Niefind, K. The Interaction of CK2alpha and CK2beta, the Subunits of Protein Kinase CK2, Requires CK2beta in a Preformed Conformation and Is Enthalpically Driven. *Protein Sci.* **2008**, *17* (12), 2180–2186.
- (50) Laudet, B.; Barette, C.; Dulery, V.; Renaudet, O.; Dumy, P.; Metz, A.; Prudent, R.; Deshiere, A.; Dideberg, O.; Filhol, O.; others. Structure-Based Design of Small Peptide Inhibitors of Protein Kinase CK2 Subunit Interaction. *Biochem. J.* **2007**, *408* (3), 363-373
- (51) Raaf, J.; Guerra, B.; Neundorf, I.; Bopp, B.; Issinger, O.-G.; Jose, J.; Pietsch, M.; Niefind, K. First Structure of Protein Kinase CK2 Catalytic Subunit with an Effective CK2β-Competitive Ligand. *ACS Chem. Biol.* **2013**, *8* (5), 901-907.
- (52) Lolli, G.; Pinna, L. A.; Battistutta, R. Structural Determinants of Protein Kinase CK2 Regulation by Auto-Inhibitory Polymerization. *ACS Chem. Biol.* **2012**, *7* (7), 1158-1163.
- (53) O-charoenrat, P.; Rusch, V.; Talbot, S. G.; Sarkaria, I.; Viale, A.; Socci, N.; Ngai, I.; Rao, P.; Singh, B.; others. Casein Kinase II Alpha Subunit and C1-Inhibitor Are Independent Predictors of Outcome in Patients with Squamous Cell Carcinoma of the Lung. *Clin. Cancer Res.* **2004**, *10* (17), 5792–5803.

- (54) Laramas, M.; Pasquier, D.; Filhol, O.; Ringeisen, F.; Descotes, J.-L.; Cochet, C. Nuclear Localization of Protein Kinase CK2 Catalytic Subunit (CK2a) Is Associated with Poor Prognostic Factors in Human Prostate Cancer. *Eur. J. Cancer* **2007**, *43* (5), 928–934.
- (55) Kim, J. S.; Eom, J. I.; Cheong, J.-W.; Choi, A. J.; Lee, J. K.; Yang, W. I.; Min, Y. H. Protein Kinase CK2 as an Unfavorable Prognostic Marker and Novel Therapeutic Target in Acute Myeloid Leukemia. *Clin. Cancer Res.* **2007**, *13* (3), 1019–1028.
- (56) Giusiano, S.; Cochet, C.; Filhol, O.; Duchemin-Pelletier, E.; Secq, V.; Bonnier, P.; Carcopino, X.; Boubli, L.; Birnbaum, D.; Garcia, S.; Iovanna, J.; Charpin, C. Protein Kinase CK2a Subunit over-Expression Correlates with Metastatic Risk in Breast Carcinomas: Quantitative Immunohistochemistry in Tissue Microarrays. *Eur. J. Cancer* **2011**, *47* (5), 792–801.
- (57) Lin, K.-Y.; Tai, C.; Hsu, J.-C.; Li, C.-F.; Fang, C.-L.; Lai, H.-C.; Hseu, Y.-C.; Lin, Y.-F.; Uen, Y.-H. Overexpression of Nuclear Protein Kinase CK2 a Catalytic Subunit (CK2a) as a Poor Prognosticator in Human Colorectal Cancer. *PLoS ONE* **2011**, *6* (2), e17193.
- (58) Zheng, Y.; McFarland, B. C.; Drygin, D.; Yu, H.; Bellis, S. L.; Kim, H.; Bredel, M.; Benveniste, E. N. Targeting Protein Kinase CK2 Suppresses Prosurvival Signaling Pathways and Growth of Glioblastoma. *Clin. Cancer Res.* **2013**, *19* (23), 6484–6494.
- (59) Bae, J. S.; Park, S.-H.; Kim, K. M.; Kwon, K. S.; Kim, C. Y.; Lee, H. K.; Park, B.-H.; Park, H. S.; Lee, H.; Moon, W. S.; Chung, M. J.; Sylvester, K. G.; Jang, K. Y. CK2a Phosphorylates DBC1 and Is Involved in the Progression of Gastric Carcinoma and Predicts Poor Survival of Gastric Carcinoma Patients. *Int. J. Cancer* **2014**, *136* (4), 797–809.
- (60) Roelants, C.; Giacosa, S.; Duchemin-Pelletier, E.; McLeer-Florin, A.; Tisseyre, C.; Aubert, C.; Champelovier, P.; Boutonnat, J.; Descotes, J. L.; Rambeaud, J.-J.; Arnoux, V.; Long, J.-A.; Pasquier, D.; Laramas, M.; Kassem, M.; David-Boudet, L.; Schoutteten, L.; Bestgen, B.; Pillet, C.; Cochet, C.; Filhol, O. Dysregulated Expression of Protein Kinase CK2 in Renal Cancer. In *Protein Kinase CK2 Cellular Function in Normal and Disease States*; Ahmed, K., Issinger, O.-G., Szyszka, R., Eds.; Springer International Publishing: Cham, 2015; pp 241–257.
- (61) Pinna, L. A. *Protein Kinase CK2*; John Wiley & Sons, 2012.
- (62) Dominguez, I.; Sonenshein, G. E.; Seldin, D. C. Protein Kinase CK2 in Health and Disease: CK2 and Its Role in Wnt and NF- κ B Signaling: Linking Development and Cancer. *Cell. Mol. Life Sci.* **2009**, *66* (11-12), 1850–1857.
- (63) Eddy, S. F. Inducible I B Kinase/I B Kinase Expression Is Induced by CK2 and Promotes Aberrant Nuclear Factor- B Activation in Breast Cancer Cells. *Cancer Res.* **2005**, *65* (24), 11375–11383.

- (64) Chantome, A.; Pance, A.; Gauthier, N.; Vandroux, D.; Chenu, J.; Solary, E.; Jeannin, J.-F.; Reveneau, S. Casein Kinase II-Mediated Phosphorylation of NF- κ B p65 Subunit Enhances Inducible Nitric-Oxide Synthase Gene Transcription in Vivo. *J. Biol. Chem.* **2004**, *279* (23), 23953–23960.
- (65) Ji, H.; Wang, J.; Nika, H.; Hawke, D.; Keezer, S.; Ge, Q.; Fang, B.; Fang, X.; Fang, D.; Litchfield, D. W.; Aldape, K.; Lu, Z. EGF-Induced ERK Activation Promotes CK2-Mediated Disassociation of α -Catenin from β -Catenin and Transactivation of β -Catenin. *Mol. Cell* **2009**, *36* (4), 547–559.
- (66) Ruzzene, M.; Pinna, L. A. Addiction to Protein Kinase CK2: A Common Denominator of Diverse Cancer Cells? *Biochim. Biophys. Acta* **2010**, *1804* (3), 499–504.
- (67) *Protein Kinase CK2*; Pinna, L. A., Ed.; The Wiley-IUBMB series on biochemistry and molecular biology; Wiley-Blackwell: Ames, Iowa, USA, 2013.
- (68) Borgo, C.; Cesaro, L.; Salizzato, V.; Ruzzene, M.; Massimino, M. L.; Pinna, L. A.; Donella-Deana, A. Aberrant Signalling by Protein Kinase CK2 in Imatinib-Resistant Chronic Myeloid Leukaemia Cells: Biochemical Evidence and Therapeutic Perspectives. *Mol. Oncol.* **2013**, *7* (6), 1103–1115.
- (69) Zanin, S.; Borgo, C.; Girardi, C.; O'Brien, S. E.; Miyata, Y.; Pinna, L. A.; Donella-Deana, A.; Ruzzene, M. Effects of the CK2 Inhibitors CX-4945 and CX-5011 on Drug-Resistant Cells. *PLoS ONE* **2012**, *7* (11), e49193.
- (70) Tsai, C.-F.; Wang, Y.-T.; Yen, H.-Y.; Tsou, C.-C.; Ku, W.-C.; Lin, P.-Y.; Chen, H.-Y.; Nesvizhskii, A. I.; Ishihama, Y.; Chen, Y.-J. Large-Scale Determination of Absolute Phosphorylation Stoichiometries in Human Cells by Motif-Targeting Quantitative Proteomics. *Nat. Commun.* **2015**, *6*, 6622.
- (71) Toczyski, D. P.; Galgoczy, D. J.; Hartwell, L. H. CDC5 and CKII Control Adaptation to the Yeast DNA Damage Checkpoint. *Cell* **1997**, *90* (6), 1097–1106.
- (72) Bidwai, A. P.; Reed, J. C.; Glover, C. V. Cloning and Disruption of CKB1, the Gene Encoding the 38-kDa Beta Subunit of *Saccharomyces Cerevisiae* Casein Kinase II (CKII). Deletion of CKII Regulatory Subunits Elicits a Salt-Sensitive Phenotype. *J. Biol. Chem.* **1995**, *270* (18), 10395–10404.
- (73) Buchou, T.; Vernet, M.; Blond, O.; Jensen, H. H.; Pointu, H.; Olsen, B. B.; Cochet, C.; Issinger, O.-G.; Boldyreff, B. Disruption of the Regulatory Beta Subunit of Protein Kinase CK2 in Mice Leads to a Cell-Autonomous Defect and Early Embryonic Lethality. *Mol. Cell. Biol.* **2003**, *23* (3), 908–915.
- (74) Huillard, E.; Ziercher, L.; Blond, O.; Wong, M.; Deloulme, J.-C.; Souchelnytskyi, S.; Baudier, J.; Cochet, C.; Buchou, T. Disruption of CK2beta in Embryonic Neural Stem Cells

- Compromises Proliferation and Oligodendrogenesis in the Mouse Telencephalon. *Mol. Cell. Biol.* **2010**, 30 (11), 2737–2749.
- (75) Deshiere, A.; Duchemin-Pelletier, E.; Spreux, E.; Ciais, D.; Forcet, C.; Cochet, C.; Filhol, O. Regulation of Epithelial to Mesenchymal Transition: CK2 β on Stage. *Mol. Cell. Biochem.* **2011**, 356 (1-2), 11–20.
- (76) Deshiere, A.; Duchemin-Pelletier, E.; Spreux, E.; Ciais, D.; Combes, F.; Vandembrouck, Y.; Couté, Y.; Mikaelian, I.; Giusiano, S.; Charpin, C.; Cochet, C.; Filhol, O. Unbalanced Expression of CK2 Kinase Subunits Is Sufficient to Drive Epithelial-to-Mesenchymal Transition by Snail1 Induction. *Oncogene* **2012**, 32 (11), 1373–1383.
- (77) Bibby, A. C.; Litchfield, D. W. The Multiple Personalities of the Regulatory Subunit of Protein Kinase CK2: CK2 Dependent and CK2 Independent Roles Reveal a Secret Identity for CK2beta. *Int. J. Biol. Sci.* **2005**, 1 (2), 67–79.
- (78) Qiu, S.; Xiao, Z.; Piao, C.; Zhang, J.; Dong, Y.; Cui, W.; Liu, X.; Zhang, Y.; Du, J. AMPK α 2 Reduces Renal Epithelial Transdifferentiation and Inflammation after Injury through Interaction with CK2 β . *J. Pathol.* **2015** [Epub ahead of print].
- (79) Filhol, O.; Baudier, J.; Delphin, C.; Loue-Mackebach, P.; Chambaz, E. M.; Cochet, C. Casein Kinase II and the Tumor Suppressor Protein P53 Associate in a Molecular Complex That Is Negatively Regulated upon P53 Phosphorylation. *J. Biol. Chem.* **1992**, 267 (29), 20577–20583.
- (80) Appel, K.; Wagner, P.; Boldyreff, B.; Issinger, O. G.; Montenarh, M. Mapping of the Interaction Sites of the Growth Suppressor Protein p53 with the Regulatory Beta-Subunit of Protein Kinase CK2. *Oncogene* **1995**, 11 (10), 1971–1978.
- (81) Guerra, B.; Issinger, O. G. Protein Kinase CK2 and Its Role in Cellular Proliferation, Development and Pathology. *Electrophoresis* **1999**, 20 (2), 391–408.
- (82) Romero-Oliva, F.; Allende, J. E. Protein p21(WAF1/CIP1) Is Phosphorylated by Protein Kinase CK2 in Vitro and Interacts with the Amino Terminal End of the CK2 Beta Subunit. *J. Cell. Biochem.* **2001**, 81 (3), 445–452.
- (83) Theis-Febvre, N.; Filhol, O.; Froment, C.; Cazales, M.; Cochet, C.; Monsarrat, B.; Ducommun, B.; Baldin, V. Protein Kinase CK2 Regulates CDC25B Phosphatase Activity. *Oncogene* **2003**, 22 (2), 220–232.
- (84) Burnett, R. T.; Smith-Doiron, M.; Stieb, D.; Cakmak, S.; Brook, J. R. Effects of Particulate and Gaseous Air Pollution on Cardiorespiratory Hospitalizations. *Arch. Environ. Health* **1999**, 54 (2), 130–139.

- (85) Shimada, K.; Kondo, K.; Yamanishi, K. Human Herpesvirus 6 Immediate-Early 2 Protein Interacts with Heterogeneous Ribonucleoprotein K and Casein Kinase 2. *Microbiol. Immunol.* **2004**, *48* (3), 205–210.
- (86) Chen, M.; Li, D.; Krebs, E. G.; Cooper, J. A. The Casein Kinase II Beta Subunit Binds to Mos and Inhibits Mos Activity. *Mol. Cell. Biol.* **1997**, *17* (4), 1904–1912.
- (87) Lieberman, S. L.; Ruderman, J. V. CK2 Beta, Which Inhibits Mos Function, Binds to a Discrete Domain in the N-Terminus of Mos. *Dev. Biol.* **2004**, *268* (2), 271–279.
- (88) Guerra, B.; Issinger, O.-G.; Wang, J. Y. J. Modulation of Human Checkpoint Kinase Chk1 by the Regulatory Beta-Subunit of Protein Kinase CK2. *Oncogene* **2003**, *22* (32), 4933–4942.
- (89) Hagemann, C.; Kalmes, A.; Wixler, V.; Wixler, L.; Schuster, T.; Rapp, U. R. The Regulatory Subunit of Protein Kinase CK2 Is a Specific A-Raf Activator. *FEBS Lett.* **1997**, *403* (2), 200–202.
- (90) Bolanos-Garcia, V. M.; Fernandez-Recio, J.; Allende, J. E.; Blundell, T. L. Identifying Interaction Motifs in CK2 β – a Ubiquitous Kinase Regulatory Subunit. *Trends Biochem. Sci.* **2006**, *31* (12), 654–661.
- (91) Cozza, G.; Meggio, F.; Moro, S. The Dark Side of Protein Kinase CK2 Inhibition. *Curr. Med. Chem.* **2011**, *18* (19), 2867–2884.
- (92) Siddiqui-Jain, A.; Drygin, D.; Streiner, N.; Chua, P.; Pierre, F.; O'Brien, S. E.; Bliesath, J.; Omori, M.; Huser, N.; Ho, C.; Proffitt, C.; Schwaebel, M. K.; Ryckman, D. M.; Rice, W. G.; Anderes, K. CX-4945, an Orally Bioavailable Selective Inhibitor of Protein Kinase CK2, Inhibits Prosurvival and Angiogenic Signaling and Exhibits Antitumor Efficacy. *Cancer Res.* **2010**, *70* (24), 10288–10298.
- (93) Nakanishi, I.; Murata, K.; Nagata, N.; Kurono, M.; Kinoshita, T.; Yasue, M.; Miyazaki, T.; Takei, Y.; Nakamura, S.; Sakurai, A.; Iwamoto, N.; Nishiwaki, K.; Nakaniwa, T.; Sekiguchi, Y.; Hirasawa, A.; Tsujimoto, G.; Kitaura, K. Identification of Protein Kinase CK2 Inhibitors Using Solvent Dipole Ordering Virtual Screening. *Eur. J. Med. Chem.* **2015**, *96*, 396–404.
- (94) Prudent, R.; Mouchadel, V.; López-Ramos, M.; Aci, S.; Laudet, B.; Mouawad, L.; Barette, C.; Einhorn, J.; Einhorn, C.; Denis, J.-N.; Bisson, G.; Schmidt, F.; Roy, S.; Lafanechere, L.; Florent, J.-C.; Cochet, C. Expanding the Chemical Diversity of CK2 Inhibitors. *Mol. Cell. Biochem.* **2008**, *316* (1-2), 71–85.
- (95) Cozza, G.; Pinna, L. A.; Moro, S. Protein Kinase CK2 Inhibitors: A Patent Review. *Expert Opin. Ther. Pat.* **2012**, *22* (9), 1081–1097.

- (96) Prudent, R.; Sautel, C. F.; Cochet, C. Structure-Based Discovery of Small Molecules Targeting Different Surfaces of Protein-Kinase CK2. *Biochim. Biophys. Acta BBA - Proteins Proteomics* **2010**, *1804* (3), 493–498.
- (97) Battistutta, R.; Cozza, G.; Pierre, F.; Papinutto, E.; Lolli, G.; Sarno, S.; O'Brien, S. E.; Siddiqui-Jain, A.; Haddach, M.; Anderes, K.; Ryckman, D. M.; Meggio, F.; Pinna, L. A. Unprecedented Selectivity and Structural Determinants of a New Class of Protein Kinase CK2 Inhibitors in Clinical Trials for the Treatment of Cancer. *Biochemistry (Mosc.)* **2011**, *50* (39), 8478–8488.
- (98) Graczyk, P. P. Gini Coefficient: A New Way To Express Selectivity of Kinase Inhibitors against a Family of Kinases †. *J. Med. Chem.* **2007**, *50* (23), 5773–5779.
- (99) Kim, H.; Choi, K.; Kang, H.; Lee, S.-Y.; Chi, S.-W.; Lee, M.-S.; Song, J.; Im, D.; Choi, Y.; Cho, S. Identification of a Novel Function of CX-4945 as a Splicing Regulator. *PLoS One* **2014**, *9* (4), e94978.
- (100) Battistutta, R.; Cozza, G.; Pierre, F.; Papinutto, E.; Lolli, G.; Sarno, S.; O'Brien, S. E.; Siddiqui-Jain, A.; Haddach, M.; Anderes, K.; Ryckman, D. M.; Meggio, F.; Pinna, L. A. Unprecedented Selectivity and Structural Determinants of a New Class of Protein Kinase CK2 Inhibitors in Clinical Trials for the Treatment of Cancer. *Biochemistry (Mosc.)* **2011**, *50* (39), 8478–8488.
- (101) Cozza, G.; Mazzorana, M.; Papinutto, E.; Bain, J.; Elliott, M.; di Maira, G.; Gianoncelli, A.; Pagano, M. A.; Sarno, S.; Ruzzene, M.; Battistutta, R.; Meggio, F.; Moro, S.; Zagotto, G.; Pinna, L. A. Quinalizarin as a Potent, Selective and Cell-Permeable Inhibitor of Protein Kinase CK2. *Biochem. J.* **2009**, *421* (3), 387–395.
- (102) Anastassiadis, T.; Deacon, S. W.; Devarajan, K.; Ma, H.; Peterson, J. R. Comprehensive Assay of Kinase Catalytic Activity Reveals Features of Kinase Inhibitor Selectivity. *Nat. Biotechnol.* **2011**, *29* (11), 1039–1045.
- (103) Pagano, M. A.; Bain, J.; Kazimierczuk, Z.; Sarno, S.; Ruzzene, M.; Di Maira, G.; Elliott, M.; Orzeszko, A.; Cozza, G.; Meggio, F.; Pinna, L. A. The Selectivity of Inhibitors of Protein Kinase CK2: An Update. *Biochem. J.* **2008**, *415* (3), 353–365.
- (104) Tubi, L. Q.; Gurrieri, C.; Brancalion, A.; Bonaldi, L.; Bertorelle, R.; Manni, S.; Pavan, L.; Lessi, F.; Zambello, R.; Trentin, L.; Inhibition of Protein Kinase CK2 with the Clinical-Grade Small ATP-Competitive Compound CX-4945 or by RNA Interference Unveils Its Role in Acute Myeloid Leukemia Cell Survival, p53-Dependent Apoptosis and Daunorubicin-Induced Cytotoxicity. *J. Hematol. Oncol. J Hematol Oncol* **2013**, *6* (1), 78.
- (105) Bian, Y.; Han, J.; Kannabiran, V.; Mohan, S.; Cheng, H.; Friedman, J.; Zhang, L.; VanWaes, C.; Chen, Z. MEK Inhibitor PD-0325901 Overcomes Resistance to CK2 Inhibitor CX-4945

- and Exhibits Anti-Tumor Activity in Head and Neck Cancer. *Int. J. Biol. Sci.* **2015**, *11* (4), 411–422.
- (106) Perea, S. E.; Reyes, O.; Puchades, Y.; Mendoza, O.; Vispo, N. S.; Torrens, I.; Santos, A.; Silva, R.; Acevedo, B.; López, E.; Falcón, V.; Alonso, D. F. Antitumor Effect of a Novel Proapoptotic Peptide That Impairs the Phosphorylation by the Protein Kinase 2 (casein Kinase 2). *Cancer Res.* **2004**, *64* (19), 7127–7129.
- (107) Perea, S. E.; Baladron, I.; Garcia, Y.; Perera, Y.; Lopez, A.; Soriano, J. L.; Batista, N.; Palau, A.; Hernández, I.; Farina, H.; Garcia, I.; Gonzalez, L.; Gil, J.; Rodriguez, A.; Solares, M.; Santana, A.; Cruz, M.; Lopez, M.; Valenzuela, C.; Reyes, O.; López-Saura, P. A.; González, C. A.; Díaz, A.; Castellanos, L.; Sanchez, A.; Betancourt, L.; Besada, V.; González, L. J.; Garay, H.; Gómez, R.; Gómez, D. E.; Alonso, D. F.; Perrin, P.; Renualt, J.-Y.; Sigman, H.; Herrera, L.; Acevedo, B. CIGB-300, a Synthetic Peptide-Based Drug That Targets the CK2 Phosphoacceptor Domain. Translational and Clinical Research. *Mol. Cell. Biochem.* **2011**, *356* (1-2), 45–50.
- (108) Solares, A. M.; Santana, A.; Baladrón, I.; Valenzuela, C.; González, C. A.; Díaz, A.; Castillo, D.; Ramos, T.; Gómez, R.; Alonso, D. F.; Herrera, L.; Sigman, H.; Perea, S. E.; Acevedo, B. E.; López-Saura, P. Safety and Preliminary Efficacy Data of a Novel Casein Kinase 2 (CK2) Peptide Inhibitor Administered Intralesionally at Four Dose Levels in Patients with Cervical Malignancies. *BMC Cancer* **2009**, *9* (1), 146-155.
- (109) Enkvist, E.; Viht, K.; Bischoff, N.; Vahter, J.; Saaver, S.; Raidaru, G.; Issinger, O.-G.; Niefind, K.; Uri, A. A Subnanomolar Fluorescent Probe for Protein Kinase CK2 Interaction Studies. *Org. Biomol. Chem.* **2012**, *10* (43), 8645-8653.
- (110) Niefind, K.; Yde, C. W.; Ermakova, I.; Issinger, O.-G. Evolved to Be Active: Sulfate Ions Define Substrate Recognition Sites of CK2 α and Emphasise Its Exceptional Role within the CMGC Family of Eukaryotic Protein Kinases. *J. Mol. Biol.* **2007**, *370* (3), 427–438.
- (111) Monod, J.; Jacob, F. Teleonomic Mechanisms in Cellular Metabolism, Growth, and Differentiation. *Cold Spring Harb. Symp. Quant. Biol.* **1961**, *26*, 389–401.
- (112) Changeux, J.-P. 50th Anniversary of the Word "Allosteric." *Protein Sci. Publ. Protein Soc.* **2011**, *20* (7), 1119–1124.
- (113) Pardee, A. B.; Yates, R. A. Control of Pyrimidine Biosynthesis in Escherichia Coli by a Feed-Back Mechanism. *J. Biol. Chem.* **1956**, *221* (2), 757–770.
- (114) Umbarger, H. E. Evidence for a Negative-Feedback Mechanism in the Biosynthesis of Isoleucine. *Science* **1956**, *123* (3202), 848.
- (115) Adelberg, E. A.; Umbarger, H. E. Isoleucine and Valine Metabolism in Escherichia Coli. V. Alpha-Ketoisovaleric Acid Accumulation. *J. Biol. Chem.* **1953**, *205* (1), 475–482.

- (116) Monod, J.; Wyman, J.; Changeux, J. P. On the Nature of Allosteric Transitions: A Plausible Model. *J. Mol. Biol.* **1965**, *12*, 88–118.
- (117) Changeux, J.-P. Allostery and the Monod-Wyman-Changeux Model after 50 Years. *Annu. Rev. Biophys.* **2012**, *41*, 103–133.
- (118) Koshland, D. E., Jr; Némethy, G.; Filmer, D. Comparison of Experimental Binding Data and Theoretical Models in Proteins Containing Subunits. *Biochemistry (Mosc.)* **1966**, *5* (1), 365–385.
- (119) Cooper, A.; Dryden, D. T. Allostery without Conformational Change. A Plausible Model. *Eur. Biophys. J. EBJ* **1984**, *11* (2), 103–109.
- (120) Szilágyi, A.; Nussinov, R.; Csermely, P. Allo-Netwrok Drugs: Extension of the Allosteric Drug Concept to Protein- Protein Interaction and Signaling Networks. *Curr. Top. Med. Chem.* **2013**, *13* (1), 64–77.
- (121) Druker, B. J.; Tamura, S.; Buchdunger, E.; Ohno, S.; Segal, G. M.; Fanning, S.; Zimmermann, J.; Lydon, N. B. Effects of a Selective Inhibitor of the Abl Tyrosine Kinase on the Growth of Bcr-Abl Positive Cells. *Nat. Med.* **1996**, *2* (5), 561–566.
- (122) Sordella, R.; Bell, D. W.; Haber, D. A.; Settleman, J. Gefitinib-Sensitizing EGFR Mutations in Lung Cancer Activate Anti-Apoptotic Pathways. *Science* **2004**, *305* (5687), 1163–1167.
- (123) Sun, L.; Liang, C.; Shirazian, S.; Zhou, Y.; Miller, T.; Cui, J.; Fukuda, J. Y.; Chu, J.-Y.; Nematalla, A.; Wang, X.; Chen, H.; Sistla, A.; Luu, T. C.; Tang, F.; Wei, J.; Tang, C. Discovery of 5-[5-Fluoro-2-Oxo-1,2-Dihydroindol-(3Z)-Ylidenemethyl]-2,4-Dimethyl-1H-Pyrrole-3-Carboxylic Acid (2-Diethylaminoethyl)amide, a Novel Tyrosine Kinase Inhibitor Targeting Vascular Endothelial and Platelet-Derived Growth Factor Receptor Tyrosine Kinase. *J. Med. Chem.* **2003**, *46* (7), 1116–1119.
- (124) Hauschild, A.; Grob, J.-J.; Demidov, L. V.; Jouary, T.; Gutzmer, R.; Millward, M.; Rutkowski, P.; Blank, C. U.; Miller, W. H.; Kaempgen, E.; Martín-Algarra, S.; Karaszewska, B.; Mauch, C.; Chiarion-Sileni, V.; Martín, A.-M.; Swann, S.; Haney, P.; Mirakhur, B.; Guckert, M. E.; Goodman, V.; Chapman, P. B. Dabrafenib in BRAF-Mutated Metastatic Melanoma: A Multicentre, Open-Label, Phase 3 Randomised Controlled Trial. *Lancet* **2012**, *380* (9839), 358–365.
- (125) Foda, Z. H.; Seeliger, M. A. Kinase Inhibitors: An Allosteric Add-On. *Nat. Chem. Biol.* **2014**, *10* (10), 796–797.
- (126) Nussinov, R.; Tsai, C.-J. Allostery in Disease and in Drug Discovery. *Cell* **2013**, *153* (2), 293–305.

- (127) Martin, M. P.; Alam, R.; Betzi, S.; Ingles, D. J.; Zhu, J.-Y.; Schönbrunn, E. A Novel Approach to the Discovery of Small-Molecule Ligands of CDK2. *Chembiochem Eur. J. Chem. Biol.* **2012**, *13* (14), 2128–2136.
- (128) Betzi, S.; Alam, R.; Martin, M.; Lubbers, D. J.; Han, H.; Jakkaraj, S. R.; Georg, G. I.; Schönbrunn, E. Discovery of a Potential Allosteric Ligand Binding Site in CDK2. *ACS Chem. Biol.* **2011**, *6* (5), 492–501.
- (129) Palmieri, L.; Rastelli, G. α C Helix Displacement as a General Approach for Allosteric Modulation of Protein Kinases. *Drug Discov. Today* **2013**, *18* (7-8), 407–414.
- (130) Arencibia, J. M.; Pastor-Flores, D.; Bauer, A. F.; Schulze, J. O.; Biondi, R. M. AGC Protein Kinases: From Structural Mechanism of Regulation to Allosteric Drug Development for the Treatment of Human Diseases. *Biochim. Biophys. Acta* **2013**, *1834* (7), 1302–1321.
- (131) Biondi, R. M.; Cheung, P. C.; Casamayor, A.; Deak, M.; Currie, R. A.; Alessi, D. R. Identification of a Pocket in the PDK1 Kinase Domain That Interacts with PIF and the C-Terminal Residues of PKA. *EMBO J.* **2000**, *19* (5), 979–988.
- (132) Hindie, V.; Stroba, A.; Zhang, H.; Lopez-Garcia, L. A.; Idrissova, L.; Zeuzem, S.; Hirschberg, D.; Schaeffer, F.; Jørgensen, T. J. D.; Engel, M.; Alzari, P. M.; Biondi, R. M. Structure and Allosteric Effects of Low-Molecular-Weight Activators on the Protein Kinase PDK1. *Nat. Chem. Biol.* **2009**, *5* (10), 758–764.
- (133) Wilhelm, A.; Lopez-Garcia, L. A.; Busschots, K.; Fröhner, W.; Maurer, F.; Boettcher, S.; Zhang, H.; Schulze, J. O.; Biondi, R. M.; Engel, M. 2-(3-Oxo-1,3-Diphenylpropyl)malonic Acids as Potent Allosteric Ligands of the PIF Pocket of Phosphoinositide-Dependent Kinase-1: Development and Prodrug Concept. *J. Med. Chem.* **2012**, *55* (22), 9817–9830.
- (134) Engel, M.; Hindie, V.; Lopez-Garcia, L. A.; Stroba, A.; Schaeffer, F.; Adrian, I.; Imig, J.; Idrissova, L.; Nastainczyk, W.; Zeuzem, S.; Alzari, P. M.; Hartmann, R. W.; Piiper, A.; Biondi, R. M. Allosteric Activation of the Protein Kinase PDK1 with Low Molecular Weight Compounds. *EMBO J.* **2006**, *25* (23), 5469–5480.
- (135) Busschots, K.; Lopez-Garcia, L. A.; Lammi, C.; Stroba, A.; Zeuzem, S.; Piiper, A.; Alzari, P. M.; Neimanis, S.; Arencibia, J. M.; Engel, M.; Schulze, J. O.; Biondi, R. M. Substrate-Selective Inhibition of Protein Kinase PDK1 by Small Compounds That Bind to the PIF-Pocket Allosteric Docking Site. *Chem. Biol.* **2012**, *19* (9), 1152–1163.
- (136) Lopez-Garcia, L. A.; Schulze, J. O.; Fröhner, W.; Zhang, H.; Süß, E.; Weber, N.; Navratil, J.; Amon, S.; Hindie, V.; Zeuzem, S.; Jørgensen, T. J. D.; Alzari, P. M.; Neimanis, S.; Engel, M.; Biondi, R. M. Allosteric Regulation of Protein Kinase PKC ζ by the N-Terminal C1 Domain and Small Compounds to the PIF-Pocket. *Chem. Biol.* **2011**, *18* (11), 1463–1473.

- (137) Barnett, S. F.; Defeo-Jones, D.; Fu, S.; Hancock, P. J.; Haskell, K. M.; Jones, R. E.; Kahana, J. A.; Kral, A. M.; Leander, K.; Lee, L. L.; Malinowski, J.; McAvoy, E. M.; Nahas, D. D.; Robinson, R. G.; Huber, H. E. Identification and Characterization of Pleckstrin-Homology-Domain-Dependent and Isoenzyme-Specific Akt Inhibitors. *Biochem. J.* **2005**, 385 (Pt 2), 399–408.
- (138) Ashwell, M. A.; Lapierre, J.-M.; Brassard, C.; Bresciano, K.; Bull, C.; Cornell-Kennon, S.; Eathiraj, S.; France, D. S.; Hall, T.; Hill, J.; Kelleher, E.; Khanapurkar, S.; Kizer, D.; Koerner, S.; Link, J.; Liu, Y.; Makhija, S.; Moussa, M.; Namdev, N.; Nguyen, K.; Nicewonger, R.; Palma, R.; Szwaya, J.; Tandon, M.; Uppalapati, U.; Vensel, D.; Volak, L. P.; Volckova, E.; Westlund, N.; Wu, H.; Yang, R.-Y.; Chan, T. C. K. Discovery and Optimization of a Series of 3-(3-Phenyl-3H-imidazo[4,5-B]pyridin-2-Yl)pyridin-2-Amines: Orally Bioavailable, Selective, and Potent ATP-Independent Akt Inhibitors. *J. Med. Chem.* **2012**, 55 (11), 5291–5310.
- (139) Lindsley, C. W.; Zhao, Z.; Leister, W. H.; Robinson, R. G.; Barnett, S. F.; Defeo-Jones, D.; Jones, R. E.; Hartman, G. D.; Huff, J. R.; Huber, H. E.; Duggan, M. E. Allosteric Akt (PKB) Inhibitors: Discovery and SAR of Isozyme Selective Inhibitors. *Bioorg. Med. Chem. Lett.* **2005**, 15 (3), 761–764.
- (140) Wu, W.-I.; Voegtli, W. C.; Sturgis, H. L.; Dizon, F. P.; Vigers, G. P. A.; Brandhuber, B. J. Crystal Structure of Human AKT1 with an Allosteric Inhibitor Reveals a New Mode of Kinase Inhibition. *PLoS One* **2010**, 5 (9), e12913.
- (141) Sebolt-Leopold, J. S.; Dudley, D. T.; Herrera, R.; Van Becelaere, K.; Wiland, A.; Gowan, R. C.; Teclé, H.; Barrett, S. D.; Bridges, A.; Przybranowski, S.; Leopold, W. R.; Saltiel, A. R. Blockade of the MAP Kinase Pathway Suppresses Growth of Colon Tumors in Vivo. *Nat. Med.* **1999**, 5 (7), 810–816.
- (142) Delaney, A. M.; Printen, J. A.; Chen, H.; Fauman, E. B.; Dudley, D. T. Identification of a Novel Mitogen-Activated Protein Kinase Kinase Activation Domain Recognized by the Inhibitor PD 184352. *Mol. Cell. Biol.* **2002**, 22 (21), 7593–7602.
- (143) Ohren, J. F.; Chen, H.; Pavlovsky, A.; Whitehead, C.; Zhang, E.; Kuffa, P.; Yan, C.; McConnell, P.; Spessard, C.; Banotai, C.; Mueller, W. T.; Delaney, A.; Omer, C.; Sebolt-Leopold, J.; Dudley, D. T.; Leung, I. K.; Flamme, C.; Warmus, J.; Kaufman, M.; Barrett, S.; Teclé, H.; Hasemann, C. A. Structures of Human MAP Kinase Kinase 1 (MEK1) and MEK2 Describe Novel Noncompetitive Kinase Inhibition. *Nat. Struct. Mol. Biol.* **2004**, 11 (12), 1192–1197.
- (144) Smith, C. K.; Windsor, W. T. Thermodynamics of Nucleotide and Non-ATP-Competitive Inhibitor Binding to MEK1 by Circular Dichroism and Isothermal Titration Calorimetry. *Biochemistry (Mosc.)* **2007**, 46 (5), 1358–1367.

- (145) Abe, H.; Kikuchi, S.; Hayakawa, K.; Iida, T.; Nagahashi, N.; Maeda, K.; Sakamoto, J.; Matsumoto, N.; Miura, T.; Matsumura, K.; Seki, N.; Inaba, T.; Kawasaki, H.; Yamaguchi, T.; Kakefuda, R.; Nanayama, T.; Kurachi, H.; Hori, Y.; Yoshida, T.; Kakegawa, J.; Watanabe, Y.; Gilmartin, A. G.; Richter, M. C.; Moss, K. G.; Laquerre, S. G. Discovery of a Highly Potent and Selective MEK Inhibitor: GSK1120212 (JTP-74057 DMSO Solvate). *ACS Med. Chem. Lett.* **2011**, *2* (4), 320–324.
- (146) Flaherty, K. T.; Infante, J. R.; Daud, A.; Gonzalez, R.; Kefford, R. F.; Sosman, J.; Hamid, O.; Schuchter, L.; Cebon, J.; Ibrahim, N.; Kudchadkar, R.; Burris, H. A.; Falchook, G.; Algazi, A.; Lewis, K.; Long, G. V.; Puzanov, I.; Lebowitz, P.; Singh, A.; Little, S.; Sun, P.; Allred, A.; Ouellet, D.; Kim, K. B.; Patel, K.; Weber, J. Combined BRAF and MEK Inhibition in Melanoma with BRAF V600 Mutations. *N. Engl. J. Med.* **2012**, *367* (18), 1694–1703.
- (147) Morris, E. J.; Jha, S.; Restaino, C. R.; Dayananth, P.; Zhu, H.; Cooper, A.; Carr, D.; Deng, Y.; Jin, W.; Black, S.; Long, B.; Liu, J.; Dinunzio, E.; Windsor, W.; Zhang, R.; Zhao, S.; Angagaw, M. H.; Pinheiro, E. M.; Desai, J.; Xiao, L.; Shipps, G.; Hruza, A.; Wang, J.; Kelly, J.; Paliwal, S.; Gao, X.; Babu, B. S.; Zhu, L.; Daublain, P.; Zhang, L.; Lutterbach, B. A.; Pelletier, M. R.; Philippar, U.; Siliphaivanh, P.; Witter, D.; Kirschmeier, P.; Bishop, W. R.; Hicklin, D.; Gilliland, D. G.; Jayaraman, L.; Zawel, L.; Fawell, S.; Samatar, A. A. Discovery of a Novel ERK Inhibitor with Activity in Models of Acquired Resistance to BRAF and MEK Inhibitors. *Cancer Discov.* **2013**, *3* (7), 742–750.
- (148) Chaikuad, A.; M C Tacconi, E.; Zimmer, J.; Liang, Y.; Gray, N. S.; Tarsounas, M.; Knapp, S. A Unique Inhibitor Binding Site in ERK1/2 Is Associated with Slow Binding Kinetics. *Nat. Chem. Biol.* **2014**, *10* (10), 853–860.
- (149) Raaf, J.; Issinger, O.-G.; Niefind, K. First Inactive Conformation of CK2 α , the Catalytic Subunit of Protein Kinase CK2. *J. Mol. Biol.* **2009**, *386* (5), 1212–1221.
- (150) Moucadel, V.; Prudent, R.; Sautel, C. F.; Teillet, F.; Barette, C.; Lafanechere, L.; Receveur-Brechot, V.; Cochet, C. Antitumoral Activity of Allosteric Inhibitors of Protein Kinase CK2. *Oncotarget* **2011**, *2* (12), 997.
- (151) Prudent, R.; Moucadel, V.; Laudet, B.; Barette, C.; Lafanechère, L.; Hasenknopf, B.; Li, J.; Bareyt, S.; Lacôte, E.; Thorimbert, S.; Malacria, M.; Gouzerh, P.; Cochet, C. Identification of Polyoxometalates as Nanomolar Noncompetitive Inhibitors of Protein Kinase CK2. *Chem. Biol.* **2008**, *15* (7), 683–692.
- (152) Cozza, G.; Zanin, S.; Sarno, S.; Costa, E.; Girardi, C.; Ribaudo, G.; Salvi, M.; Zagotto, G.; Ruzzene, M.; Pinna, L. A. Design, Validation and Efficacy of Bi-Substrate Inhibitors Specifically Affecting Ecto-CK2 Kinase Activity. *Biochem. J.* **2015** [Epub ahead of print].

- (153) Rual, J.-F.; Venkatesan, K.; Hao, T.; Hirozane-Kishikawa, T.; Dricot, A.; Li, N.; Berriz, G. F.; Gibbons, F. D.; Dreze, M.; Ayivi-Guedehoussou, N.; Klitgord, N.; Simon, C.; Boxem, M.; Milstein, S.; Rosenberg, J.; Goldberg, D. S.; Zhang, L. V.; Wong, S. L.; Franklin, G.; Li, S.; Albala, J. S.; Lim, J.; Fraughton, C.; Llamosas, E.; Cevik, S.; Bex, C.; Lamesch, P.; Sikorski, R. S.; Vandenhaute, J.; Zoghbi, H. Y.; Smolyar, A.; Bosak, S.; Sequerra, R.; Doucette-Stamm, L.; Cusick, M. E.; Hill, D. E.; Roth, F. P.; Vidal, M. Towards a Proteome-Scale Map of the Human Protein-Protein Interaction Network. *Nature* **2005**, *437* (7062), 1173–1178.
- (154) Venkatesan, K.; Rual, J.-F.; Vazquez, A.; Stelzl, U.; Lemmens, I.; Hirozane-Kishikawa, T.; Hao, T.; Zenkner, M.; Xin, X.; Goh, K.-I.; Yildirim, M. A.; Simonis, N.; Heinzmann, K.; Gebreab, F.; Sahalie, J. M.; Cevik, S.; Simon, C.; de Smet, A.-S.; Dann, E.; Smolyar, A.; Vinayagam, A.; Yu, H.; Szeto, D.; Borick, H.; Dricot, A.; Klitgord, N.; Murray, R. R.; Lin, C.; Lalowski, M.; Timm, J.; Rau, K.; Boone, C.; Braun, P.; Cusick, M. E.; Roth, F. P.; Hill, D. E.; Tavernier, J.; Wanker, E. E.; Barabási, A.-L.; Vidal, M. An Empirical Framework for Binary Interactome Mapping. *Nat. Methods* **2009**, *6* (1), 83–90.
- (155) CCSB Interactome Database <http://interactome.dfci.harvard.edu/> (accessed Sep 27, 2014).
- (156) Jones, S.; Thornton, J. M. Principles of Protein-Protein Interactions. *Proc. Natl. Acad. Sci. U. S. A.* **1996**, *93* (1), 13–20.
- (157) Lo Conte, L.; Chothia, C.; Janin, J. The Atomic Structure of Protein-Protein Recognition Sites. *J. Mol. Biol.* **1999**, *285* (5), 2177–2198.
- (158) Clackson, T.; Wells, J. A. A Hot Spot of Binding Energy in a Hormone-Receptor Interface. *Science* **1995**, *267* (5196), 383–386.
- (159) Arkin, M. R.; Wells, J. A. Small-Molecule Inhibitors of Protein-protein Interactions: Progressing towards the Dream. *Nat. Rev. Drug Discov.* **2004**, *3* (4), 301–317.
- (160) Kozakov, D.; Hall, D. R.; Chuang, G. Y.; Cencic, R.; Brenke, R.; Grove, L. E.; Beglov, D.; Pelletier, J.; Whitty, A.; Vajda, S. Structural Conservation of Druggable Hot Spots in Protein-protein Interfaces. *Proc. Natl. Acad. Sci.* **2011**, *108* (33), 13528–13533.
- (161) London, N.; Raveh, B.; Schueler-Furman, O. Druggable Protein-Protein Interactions-from Hot Spots to Hot Segments. *Curr. Opin. Chem. Biol.* **2013**, *17* (6), 952–959.
- (162) Eyrisch, S.; Helms, V. Transient Pockets on Protein Surfaces Involved in Protein-Protein Interaction. *J. Med. Chem.* **2007**, *50* (15), 3457–3464.
- (163) Morelli, X.; Bourgeas, R.; Roche, P. Chemical and Structural Lessons from Recent Successes in Protein-protein Interaction Inhibition (2P2I). *Curr. Opin. Chem. Biol.* **2011**, *15* (4), 475–481.

- (164) Bourgeas, R.; Basse, M.-J.; Morelli, X.; Roche, P. Atomic Analysis of Protein-Protein Interfaces with Known Inhibitors: The 2P2I Database. *PLoS ONE* **2010**, *5* (3), e9598.
- (165) Hajduk, P. J.; Greer, J. A Decade of Fragment-Based Drug Design: Strategic Advances and Lessons Learned. *Nat. Rev. Drug Discov.* **2007**, *6* (3), 211–219.
- (166) Oltersdorf, T.; Elmore, S. W.; Shoemaker, A. R.; Armstrong, R. C.; Augeri, D. J.; Belli, B. A.; Bruncko, M.; Deckwerth, T. L.; Dinges, J.; Hajduk, P. J.; Joseph, M. K.; Kitada, S.; Korsmeyer, S. J.; Kunzer, A. R.; Letai, A.; Li, C.; Mitten, M. J.; Nettlesheim, D. G.; Ng, S.; Nimmer, P. M.; O'Connor, J. M.; Oleksijew, A.; Petros, A. M.; Reed, J. C.; Shen, W.; Tahir, S. K.; Thompson, C. B.; Tomaselli, K. J.; Wang, B.; Wendt, M. D.; Zhang, H.; Fesik, S. W.; Rosenberg, S. H. An Inhibitor of Bcl-2 Family Proteins Induces Regression of Solid Tumours. *Nature* **2005**, *435* (7042), 677–681.
- (167) Hann, C. L.; Daniel, V. C.; Sugar, E. A.; Dobromilskaya, I.; Murphy, S. C.; Cope, L.; Lin, X.; Hierman, J. S.; Wilburn, D. L.; Watkins, D. N.; Rudin, C. M. Therapeutic Efficacy of ABT-737, a Selective Inhibitor of BCL-2, in Small Cell Lung Cancer. *Cancer Res.* **2008**, *68* (7), 2321–2328.
- (168) Tsao, D. H. H.; Sutherland, A. G.; Jennings, L. D.; Li, Y.; Rush, T. S.; Alvarez, J. C.; Ding, W.; Dushin, E. G.; Dushin, R. G.; Haney, S. A. Discovery of Novel Inhibitors of the ZipA/FtsZ Complex by NMR Fragment Screening Coupled with Structure-Based Design. *Bioorg. Med. Chem.* **2006**, *14* (23), 7953–7961.
- (169) Van Molle, I.; Thomann, A.; Buckley, D. L.; So, E. C.; Lang, S.; Crews, C. M.; Ciulli, A. Dissecting Fragment-Based Lead Discovery at the von Hippel-Lindau Protein:Hypoxia Inducible Factor 1 α Protein-Protein Interface. *Chem. Biol.* **2012**, *19* (10), 1300–1312.
- (170) Barelier, S.; Pons, J.; Marcillat, O.; Lancelin, J. M.; Krimm, I. Fragment-Based Deconstruction of Bcl-xL Inhibitors. *J. Med. Chem.* **2010**, *53* (6), 2577–2588.
- (171) Barile, E.; Pellicchia, M. NMR-Based Approaches for the Identification and Optimization of Inhibitors of Protein-Protein Interactions. *Chem. Rev.* **2014**, *114* (9), 4749–4963.
- (172) Lipinski, C. A.; Lombardo, F.; Dominy, B. W.; Feeney, P. J. Experimental and Computational Approaches to Estimate Solubility and Permeability in Drug Discovery and Development Settings. *Adv. Drug Deliv. Rev.* **2001**, *46* (1-3), 3–26.
- (173) Sperandio, O.; Reynès, C. H.; Camproux, A.-C.; Villoutreix, B. O. Rationalizing the Chemical Space of Protein–protein Interaction Inhibitors. *Drug Discov. Today* **2010**, *15* (5-6), 220–229.
- (174) Jochim, A. L.; Arora, P. S. Systematic Analysis of Helical Protein Interfaces Reveals Targets for Synthetic Inhibitors. *ACS Chem. Biol.* **2010**, *5* (10), 919–923.

- (175) Azzarito, V.; Long, K.; Murphy, N. S.; Wilson, A. J. Inhibition of α -Helix-Mediated Protein-Protein Interactions Using Designed Molecules. *Nat. Chem.* **2013**, *5* (3), 161–173.
- (176) Bullock, B. N.; Jochim, A. L.; Arora, P. S. Assessing Helical Protein Interfaces for Inhibitor Design. *J. Am. Chem. Soc.* **2011**, *133* (36), 14220–14223.
- (177) Vassilev, L. T.; Vu, B. T.; Graves, B.; Carvajal, D.; Podlaski, F.; Filipovic, Z.; Kong, N.; Kammlott, U.; Lukacs, C.; Klein, C.; Fotouhi, N.; Liu, E. A. In Vivo Activation of the p53 Pathway by Small-Molecule Antagonists of MDM2. *Science* **2004**, *303* (5659), 844–848.
- (178) Aeluri, M.; Chamakuri, S.; Dasari, B.; Guduru, S. K. R.; Jimmidi, R.; Jogula, S.; Arya, P. Small Molecule Modulators of Protein-Protein Interactions: Selected Case Studies. *Chem. Rev.* **2014**, *114* (9), 4640–94
- (179) Shangary, S.; Wang, S. Small-Molecule Inhibitors of the MDM2-p53 Protein-Protein Interaction to Reactivate p53 Function: A Novel Approach for Cancer Therapy. *Annu. Rev. Pharmacol. Toxicol.* **2009**, *49*, 223.
- (180) Khoo, K. H.; Hoe, K. K.; Verma, C. S.; Lane, D. P. Drugging the p53 Pathway: Understanding the Route to Clinical Efficacy. *Nat. Rev. Drug Discov.* **2014**, *13* (3), 217–236.
- (181) Vu, B.; Wovkulich, P.; Pizzolato, G.; Lovey, A.; Ding, Q.; Jiang, N.; Liu, J.-J.; Zhao, C.; Glenn, K.; Wen, Y.; Tovar, C.; Packman, K.; Vassilev, L.; Graves, B. Discovery of RG7112: A Small-Molecule MDM2 Inhibitor in Clinical Development. *ACS Med. Chem. Lett.* **2013**, *4* (5), 466–469.
- (182) Ding, Q.; Zhang, Z.; Liu, J.-J.; Jiang, N.; Zhang, J.; Ross, T. M.; Chu, X.-J.; Bartkovitz, D.; Podlaski, F.; Janson, C.; Tovar, C.; Filipovic, Z. M.; Higgins, B.; Glenn, K.; Packman, K.; Vassilev, L. T.; Graves, B. Discovery of RG7388, a Potent and Selective p53-MDM2 Inhibitor in Clinical Development. *J. Med. Chem.* **2013**, *56* (14), 5979–5983.
- (183) Wang, S.; Sun, W.; Zhao, Y.; McEachern, D.; Meaux, I.; Barrière, C.; Stuckey, J. A.; Meagher, J. L.; Bai, L.; Liu, L.; Hoffman-Luca, C. G.; Lu, J.; Shangary, S.; Yu, S.; Bernard, D.; Aguilar, A.; Dos-Santos, O.; Besret, L.; Guerif, S.; Pannier, P.; Gorge-Bernat, D.; Debussche, L. SAR405838: An Optimized Inhibitor of MDM2-p53 Interaction That Induces Complete and Durable Tumor Regression. *Cancer Res.* **2014**, *4* (20), 5855–5865.
- (184) Sun, D.; Li, Z.; Rew, Y.; Gribble, M.; Bartberger, M. D.; Beck, H. P.; Canon, J.; Chen, A.; Chen, X.; Chow, D.; Deignan, J.; Duquette, J.; Eksterowicz, J.; Fisher, B.; Fox, B. M.; Fu, J.; Gonzalez, A. Z.; Gonzalez-Lopez De Turiso, F.; Houze, J. B.; Huang, X.; Jiang, M.; Jin, L.; Kayser, F.; Liu, J. J.; Lo, M.-C.; Long, A. M.; Lucas, B.; McGee, L. R.; McIntosh, J.; Mihalic, J.; Oliner, J. D.; Osgood, T.; Peterson, M. L.; Roveto, P.; Saiki, A. Y.; Shaffer, P.; Toteva, M.; Wang, Y.; Wang, Y. C.; Wortman, S.; Yakowec, P.; Yan, X.; Ye, Q.; Yu, D.; Yu, M.; Zhao, X.; Zhou, J.; Zhu, J.; Olson, S. H.; Medina, J. C. Discovery of AMG 232, a Potent, Selective, and

- Orally Bioavailable MDM2-p53 Inhibitor in Clinical Development. *J. Med. Chem.* **2014**, *57* (4), 1454–1472.
- (185) Moll, U. M.; Petrenko, O. The MDM2-p53 Interaction. *Mol. Cancer Res. MCR* **2003**, *1* (14), 1001–1008.
- (186) Shangary, S.; Wang, S. Small-Molecule Inhibitors of the MDM2-p53 Protein-Protein Interaction to Reactivate p53 Function: A Novel Approach for Cancer Therapy. *Annu. Rev. Pharmacol. Toxicol.* **2009**, *49*, 223–241.
- (187) Nero, T. L.; Morton, C. J.; Holien, J. K.; Wielens, J.; Parker, M. W. Oncogenic Protein Interfaces: Small Molecules, Big Challenges. *Nat. Rev. Cancer* **2014**, *14* (4), 248–262.
- (188) Milroy, L.-G.; Grossmann, T. N.; Hennig, S.; Brunsveld, L.; Ottmann, C. Modulators of Protein–Protein Interactions. *Chem. Rev.* **2014**, *114* (9), 4695–4748.
- (189) Guharoy, M.; Chakrabarti, P. Secondary Structure Based Analysis and Classification of Biological Interfaces: Identification of Binding Motifs in Protein-Protein Interactions. *Bioinforma. Oxf. Engl.* **2007**, *23* (15), 1909–1918.
- (190) Gavenonis, J.; Sheneman, B. A.; Siegert, T. R.; Eshelman, M. R.; Kritzer, J. A. Comprehensive Analysis of Loops at Protein-Protein Interfaces for Macrocyclic Design. *Nat. Chem. Biol.* **2014**, *10* (9), 716–722.
- (191) Pasquale, E. B. Eph-Ephrin Bidirectional Signaling in Physiology and Disease. *Cell* **2008**, *133* (1), 38–52.
- (192) Qin, H.; Noberini, R.; Huan, X.; Shi, J.; Pasquale, E. B.; Song, J. Structural Characterization of the EphA4-Ephrin-B2 Complex Reveals New Features Enabling Eph-Ephrin Binding Promiscuity. *J. Biol. Chem.* **2010**, *285* (1), 644–654.
- (193) Murai, K. K.; Nguyen, L. N.; Koolpe, M.; McLennan, R.; Krull, C. E.; Pasquale, E. B. Targeting the EphA4 Receptor in the Nervous System with Biologically Active Peptides. *Mol. Cell. Neurosci.* **2003**, *24* (4), 1000–1011.
- (194) Lamberto, I.; Qin, H.; Noberini, R.; Premkumar, L.; Bourgin, C.; Riedl, S. J.; Song, J.; Pasquale, E. B. Distinctive Binding of Three Antagonistic Peptides to the Ephrin-Binding Pocket of the EphA4 Receptor. *Biochem. J.* **2012**, *445* (1), 47–56.
- (195) Noberini, R.; Koolpe, M.; Peddibhotla, S.; Dahl, R.; Su, Y.; Cosford, N. D. P.; Roth, G. P.; Pasquale, E. B. Small Molecules Can Selectively Inhibit Ephrin Binding to the EphA4 and EphA2 Receptors. *J. Biol. Chem.* **2008**, *283* (43), 29461–29472.
- (196) Qin, H.; Shi, J.; Noberini, R.; Pasquale, E. B.; Song, J. Crystal Structure and NMR Binding Reveal That Two Small Molecule Antagonists Target the High Affinity Ephrin-Binding Channel of the EphA4 Receptor. *J. Biol. Chem.* **2008**, *283* (43), 29473–29484.

- (197) Giorgio, C.; Hassan Mohamed, I.; Flammini, L.; Barocelli, E.; Incerti, M.; Lodola, A.; Tognolini, M. Lithocholic Acid Is an Eph-Ephrin Ligand Interfering with Eph-Kinase Activation. *PLoS One* **2011**, *6* (3), e18128.
- (198) Wu, B.; Zhang, Z.; Noberini, R.; Barile, E.; Giulianotti, M.; Pinilla, C.; Houghten, R. A.; Pasquale, E. B.; Pellecchia, M. HTS by NMR of Combinatorial Libraries: A Fragment-Based Approach to Ligand Discovery. *Chem. Biol.* **2013**, *20* (1), 19–33.
- (199) Liu, Z.; Sun, C.; Olejniczak, E. T.; Meadows, R. P.; Betz, S. F.; Oost, T.; Herrmann, J.; Wu, J. C.; Fesik, S. W. Structural Basis for Binding of Smac/DIABLO to the XIAP BIR3 Domain. *Nature* **2000**, *408* (6815), 1004–1008.
- (200) Oost, T. K.; Sun, C.; Armstrong, R. C.; Al-Assaad, A.-S.; Betz, S. F.; Deckwerth, T. L.; Ding, H.; Elmore, S. W.; Meadows, R. P.; Olejniczak, E. T.; Oleksijew, A.; Oltersdorf, T.; Rosenberg, S. H.; Shoemaker, A. R.; Tomaselli, K. J.; Zou, H.; Fesik, S. W. Discovery of Potent Antagonists of the Antiapoptotic Protein XIAP for the Treatment of Cancer. *J. Med. Chem.* **2004**, *47* (18), 4417–4426.
- (201) Schimmer, A. D.; Welsh, K.; Pinilla, C.; Wang, Z.; Krajewska, M.; Bonneau, M.-J.; Pedersen, I. M.; Kitada, S.; Scott, F. L.; Bailly-Maitre, B.; Glinsky, G.; Scudiero, D.; Sausville, E.; Salvesen, G.; Nefzi, A.; Ostresh, J. M.; Houghten, R. A.; Reed, J. C. Small-Molecule Antagonists of Apoptosis Suppressor XIAP Exhibit Broad Antitumor Activity. *Cancer Cell* **2004**, *5* (1), 25–35.
- (202) Grembecka, J.; He, S.; Shi, A.; Purohit, T.; Muntean, A. G.; Sorenson, R. J.; Showalter, H. D.; Murai, M. J.; Belcher, A. M.; Hartley, T.; Hess, J. L.; Cierpicki, T. Menin-MLL Inhibitors Reverse Oncogenic Activity of MLL Fusion Proteins in Leukemia. *Nat. Chem. Biol.* **2012**, *8* (3), 277–284.
- (203) Filhol, O.; Martiel, J.-L.; Cochet, C. Protein Kinase CK2: A New View of an Old Molecular Complex. *EMBO Rep.* **2004**, *5* (4), 351–355.
- (204) Raaf, J.; Bischoff, N.; Klopffleisch, K.; Brunstein, E.; Olsen, B. B.; Vilc, G.; Litchfield, D. W.; Issinger, O.-G.; Niefind, K. Interaction between CK2 α and CK2 β , the Subunits of Protein Kinase CK2: Thermodynamic Contributions of Key Residues on the CK2 α Surface. *Biochemistry* **2011**, *50* (4), 512–522.
- (205) Hochscherf, J.; Lindenblatt, D.; Steinkrüger, M.; Yoo, E.; Ulucan, O.; Herzig, S.; Issinger, O.-G.; Helms, V.; Götz, C.; Neundorf, I.; Niefind, K.; Pietsch, M. Development of a High-Throughput Screening-Compatible Assay to Identify Inhibitors of the CK2 α /CK2 β Interaction. *Anal. Biochem.* **2014**, *468C*, 4–14.
- (206) Laudet, B.; Moucadel, V.; Prudent, R.; Filhol, O.; Wong, Y.-S.; Royer, D.; Cochet, C. Identification of Chemical Inhibitors of Protein-Kinase CK2 Subunit Interaction. *Mol. Cell. Biochem.* **2008**, *316* (1-2), 63–69.

- (207) Raaf, J.; Brunstein, E.; Issinger, O.-G.; Niefind, K. The CK2 α /CK2 β Interface of Human Protein Kinase CK2 Harbors a Binding Pocket for Small Molecules. *Chem. Biol.* **2008**, *15* (2), 111–117.
- (208) Solimini, N. L.; Luo, J.; Elledge, S. J. Non-Oncogene Addiction and the Stress Phenotype of Cancer Cells. *Cell* **2007**, *130* (6), 986–988.
- (209) Chua, P.; Pierre, F.; Whitten, J. Serine-Threonine Protein Kinase and Parp Modulators. WO/2008/028168, March 7, 2008.
- (210) Engel, M. The PIF Pocket of AGC Kinases: A Target Site for Allosteric Modulators and Protein-Protein Interaction Inhibitors. In *Protein-Protein Interactions in Drug Discovery*; Dömling, A., Ed.; Wiley-VCH Verlag GmbH & Co. KGaA: Weinheim, Germany, 2013; pp 187–223.
- (211) Huang, X.; Shipps, G. W.; Cheng, C. C.; Spacciapoli, P.; Zhang, X.; McCoy, M. A.; Wyss, D. F.; Yang, X.; Achab, A.; Soucy, K.; Montavon, D. K.; Murphy, D. M.; Whitehurst, C. E. Discovery and Hit-to-Lead Optimization of Non-ATP Competitive MK2 (MAPKAPK2) Inhibitors. *ACS Med. Chem. Lett.* **2011**, *2* (8), 632–637.
- (212) Filhol, O.; Cochet, C. Cellular Functions of Protein Kinase CK2: A Dynamic Affair. *Cell. Mol. Life Sci.* **2009**, *66* (11-12), 1830–1839.
- (213) Litchfield, D. W. Protein Kinase CK2: Structure, Regulation and Role in Cellular Decisions of Life and Death. *Biochem. J.* **2003**, *369* (Pt 1), 1–15.
- (214) Ferguson, A. D.; Sheth, P. R.; Basso, A. D.; Paliwal, S.; Gray, K.; Fischmann, T. O.; Le, H. V. Structural Basis of CX-4945 Binding to Human Protein Kinase CK2. *FEBS Lett.* **2011**, *585* (1), 104–110.
- (215) Irina Kufareva; Ruben Abagyan. Strategies to Overcome the Induced Fit Effects in Molecular Docking. In *Computational Biophysics to Systems Biology (CBSB08)*; Ulrich H. E. Hansmann, Jan H. Meinke, Sandipan Mohanty, Walter Nadler, Olav Zimmermann, Eds.; John von Neumann Institute for Computing, Jülich, NIC Series, 2008; Vol. 40, pp 1–6.
- (216) Irina Kufareva; Beatrice Laudet; Claude Cochet; Ruben Abagyan. Structure-Based Discovery of Small Molecules That Modulate Kinase Activity by Disrupting the Subunit Interaction: Application to CK2. *Protein Sci.* **2008**, *17*, Suppl 1:265.
- (217) Gouron, A.; Milet, A.; Jamet, H. Conformational Flexibility of Human Casein Kinase Catalytic Subunit Explored by Metadynamics. *Biophys. J.* **2014**, *106* (5), 1134–1141.
- (218) Guerra, B.; Bischoff, N.; Bdzhola, V. G.; Yarmoluk, S. M.; Issinger, O.-G.; Golub, A. G.; Niefind, K. A Note of Caution on the Role of Halogen Bonds for Protein Kinase/inhibitor Recognition Suggested by High- and Low-Salt CK2 α Complex Structures. *ACS Chem. Biol.* **2015**, *10* (7), 1654–60.

- (219) Kroe, R. R.; Regan, J.; Proto, A.; Peet, G. W.; Roy, T.; Landro, L. D.; Fuschetto, N. G.; Pargellis, C. A.; Ingraham, R. H. Thermal Denaturation: A Method to Rank Slow Binding, High-Affinity P38alpha MAP Kinase Inhibitors. *J. Med. Chem.* **2003**, *46* (22), 4669–4675.
- (220) Fedorov, O.; Marsden, B.; Pogacic, V.; Rellos, P.; Müller, S.; Bullock, A. N.; Schwaller, J.; Sundström, M.; Knapp, S. A Systematic Interaction Map of Validated Kinase Inhibitors with Ser/Thr Kinases. *Proc. Natl. Acad. Sci. U. S. A.* **2007**, *104* (51), 20523–20528.
- (221) Mayer, M.; Meyer, B. Group Epitope Mapping by Saturation Transfer Difference NMR to Identify Segments of a Ligand in Direct Contact with a Protein Receptor. *J. Am. Chem. Soc.* **2001**, *123* (25), 6108–6117.
- (222) Lee, B.; Richards, F. M. The Interpretation of Protein Structures: Estimation of Static Accessibility. *J. Mol. Biol.* **1971**, *55* (3), 379–400.
- (223) Ji, H.; Wang, J.; Nika, H.; Hawke, D.; Keezer, S.; Ge, Q.; Fang, B.; Fang, X.; Fang, D.; Litchfield, D. W.; Aldape, K.; Lu, Z. EGF-Induced ERK Activation Promotes CK2-Mediated Disassociation of α -Catenin from β -Catenin and Transactivation of β -Catenin. *Mol. Cell* **2009**, *36* (4), 547–559.
- (224) Di Maira, G.; Salvi, M.; Arrigoni, G.; Marin, O.; Sarno, S.; Brustolon, F.; Pinna, L. A.; Ruzzene, M. Protein Kinase CK2 Phosphorylates and Upregulates Akt/PKB. *Cell Death Differ.* **2005**, *12* (6), 668–677.
- (225) Li, D.; Dobrowolska, G.; Krebs, E. G. The Physical Association of Casein Kinase 2 with Nucleolin. *J. Biol. Chem.* **1996**, *271* (26), 15662–15668.
- (226) Pfaff, M.; Anderer, F. A. Casein Kinase II Accumulation in the Nucleolus and Its Role in Nucleolar Phosphorylation. *Biochim. Biophys. Acta* **1988**, *969* (1), 100–109.
- (227) Schwab, M. S.; Dreyer, C. Protein Phosphorylation Sites Regulate the Function of the Bipartite NLS of Nucleolin. *Eur. J. Cell Biol.* **1997**, *73* (4), 287–297.
- (228) Filhol, O.; Giacosa, S.; Wallez, Y.; Cochet, C. Protein Kinase CK2 in Breast Cancer: The CK2 β Regulatory Subunit Takes Center Stage in Epithelial Plasticity. *Cell. Mol. Life Sci. CMLS* **2015**, *72* (17), 3305–3322.
- (229) Cozza, G.; Meggio, F.; Moro, S. The Dark Side of Protein Kinase CK2 Inhibition. *Curr. Med. Chem.* **2011**, *18* (19), 2867–2884.
- (230) Prudent, R.; Cochet, C. New Protein Kinase CK2 Inhibitors: Jumping out of the Catalytic Box. *Chem. Biol.* **2009**, *16* (2), 112–120.
- (231) Teclé, H.; Shao, J.; Li, Y.; Kothe, M.; Kazmirski, S.; Penzotti, J.; Ding, Y.-H.; Ohren, J.; Moshinsky, D.; Coli, R.; Jhawar, N.; Bora, E.; Jacques-O'Hagan, S.; Wu, J. Beyond the MEK-Pocket: Can Current MEK Kinase Inhibitors Be Utilized to Synthesize Novel Type III NCKIs?

- Does the MEK-Pocket Exist in Kinases Other than MEK? *Bioorg. Med. Chem. Lett.* **2009**, *19* (1), 226–229.
- (232) Solit, D. B.; Garraway, L. A.; Pratilas, C. A.; Sawai, A.; Getz, G.; Basso, A.; Ye, Q.; Lobo, J. M.; She, Y.; Osman, I.; Golub, T. R.; Sebolt-Leopold, J.; Sellers, W. R.; Rosen, N. BRAF Mutation Predicts Sensitivity to MEK Inhibition. *Nature* **2006**, *439* (7074), 358–362.
- (233) Grant, B. J.; Gorfe, A. A.; McCammon, J. A. Large Conformational Changes in Proteins: Signaling and Other Functions. *Curr. Opin. Struct. Biol.* **2010**, *20* (2), 142–147.
- (234) Weikl, T. R.; Paul, F. Conformational Selection in Protein Binding and Function. *Protein Sci. Publ. Protein Soc.* **2014**, *23* (11), 1508–1518.
- (235) Bae, J. S.; Park, S.-H.; Kim, K. M.; Kwon, K. S.; Kim, C. Y.; Lee, H. K.; Park, B.-H.; Park, H. S.; Lee, H.; Moon, W. S.; Chung, M. J.; Sylvester, K. G.; Jang, K. Y. CK2 α Phosphorylates DBC1 and Is Involved in the Progression of Gastric Carcinoma and Predicts Poor Survival of Gastric Carcinoma Patients. *Int. J. Cancer J. Int. Cancer* **2015**, *136* (4), 797–809.
- (236) Filhol, O.; Giacosa, S.; Wallez, Y.; Cochet, C. Protein Kinase CK2 in Breast Cancer: The CK2 β Regulatory Subunit Takes Center Stage in Epithelial Plasticity. *Cell. Mol. Life Sci. CMLS* **2015**, *72* (17), 3305–3322.
- (237) Clive, D. L. J.; Hisaindee, S.; Coltart, D. M. Derivatized Amino Acids Relevant to Native Peptide Synthesis by Chemical Ligation and Acyl Transfer. *J. Org. Chem.* **2003**, *68* (24), 9247–9254.
- (238) Marzabadi, M. R.; Wong, W. C.; Noble, S. A.; Desai, M. N. Selective NPY (Y5) Antagonists. US6989379B1, 2006.
- (239) Satoshi Nakano; Daisuke Saito. Method for Producing Isothiocyanate Compound Having Carboxyl Group. US20100312000A1, 2010.
- (240) Wilhelm, A.; Lopez-Garcia, L. A.; Busschots, K.; Fröhner, W.; Maurer, F.; Boettcher, S.; Zhang, H.; Schulze, J. O.; Biondi, R. M.; Engel, M. 2-(3-Oxo-1,3-Diphenylpropyl)malonic Acids as Potent Allosteric Ligands of the PIF Pocket of Phosphoinositide-Dependent Kinase-1: Development and Prodrug Concept. *J. Med. Chem.* **2012**, *55* (22), 9817–9830.
- (241) Meanwell, N. A. Synopsis of Some Recent Tactical Application of Bioisosteres in Drug Design. *J. Med. Chem.* **2011**, *54* (8), 2529–2591.
- (242) Abad-Zapatero, C.; Metz, J. T. Ligand Efficiency Indices as Guideposts for Drug Discovery. *Drug Discov. Today* **2005**, *10* (7), 464–469.
- (243) Davis, M. I.; Hunt, J. P.; Herrgard, S.; Ciceri, P.; Wodicka, L. M.; Pallares, G.; Hocker, M.; Treiber, D. K.; Zarrinkar, P. P. Comprehensive Analysis of Kinase Inhibitor Selectivity. *Nat. Biotechnol.* **2011**, *29* (11), 1046–1051.

- (244) Singer, E. A.; Gupta, G. N.; Marchalik, D.; Srinivasan, R. Evolving Therapeutic Targets in Renal Cell Carcinoma. *Curr. Opin. Oncol.* **2013**, *25* (3), 273–280.
- (245) Filhol, O.; Nueda, A.; Martel, V.; Gerber-Scokaert, D.; Benitez, M. J.; Souchier, C.; Saoudi, Y.; Cochet, C. Live-Cell Fluorescence Imaging Reveals the Dynamics of Protein Kinase CK2 Individual Subunits. *Mol. Cell. Biol.* **2003**, *23* (3), 975–987.
- (246) Frankel, A. D.; Pabo, C. O. Cellular Uptake of the Tat Protein from Human Immunodeficiency Virus. *Cell* **1988**, *55* (6), 1189–1193.
- (247) Green, M.; Loewenstein, P. M. Autonomous Functional Domains of Chemically Synthesized Human Immunodeficiency Virus Tat Trans-Activator Protein. *Cell* **1988**, *55* (6), 1179–1188.
- (248) Schwarze, S. R.; Hruska, K. A.; Dowdy, S. F. Protein Transduction: Unrestricted Delivery into All Cells? *Trends Cell Biol.* **2000**, *10* (7), 290–295.
- (249) Söderberg, O.; Gullberg, M.; Jarvius, M.; Ridderstråle, K.; Leuchowius, K.-J.; Jarvius, J.; Wester, K.; Hydbring, P.; Bahram, F.; Larsson, L.-G.; Landegren, U. Direct Observation of Individual Endogenous Protein Complexes in Situ by Proximity Ligation. *Nat. Methods* **2006**, *3* (12), 995–1000.
- (250) Allalou, A.; Wählby, C. BlobFinder, a Tool for Fluorescence Microscopy Image Cytometry. *Comput. Methods Programs Biomed.* **2009**, *94* (1), 58–65.
- (251) Yewale, C.; Baradia, D.; Vhora, I.; Patil, S.; Misra, A. Epidermal Growth Factor Receptor Targeting in Cancer: A Review of Trends and Strategies. *Biomaterials* **2013**, *34* (34), 8690–8707.
- (252) So, K. S.; Kim, C. H.; Rho, J. K.; Kim, S. Y.; Choi, Y. J.; Song, J. S.; Kim, W. S.; Choi, C. M.; Chun, Y. J.; Lee, J. C. Autophagosome-Mediated EGFR down-Regulation Induced by the CK2 Inhibitor Enhances the Efficacy of EGFR-TKI on EGFR-Mutant Lung Cancer Cells with Resistance by T790M. *PLoS One* **2014**, *9* (12), e114000.
- (253) Jackman, D. M.; Miller, V. A.; Cioffredi, L.-A.; Yeap, B. Y.; Jänne, P. A.; Riely, G. J.; Ruiz, M. G.; Giaccone, G.; Sequist, L. V.; Johnson, B. E. Impact of Epidermal Growth Factor Receptor and KRAS Mutations on Clinical Outcomes in Previously Untreated Non-Small Cell Lung Cancer Patients: Results of an Online Tumor Registry of Clinical Trials. *Clin. Cancer Res. Off. J. Am. Assoc. Cancer Res.* **2009**, *15* (16), 5267–5273.
- (254) Xiong, Y.; Hannon, G. J.; Zhang, H.; Casso, D.; Kobayashi, R.; Beach, D. p21 Is a Universal Inhibitor of Cyclin Kinases. *Nature* **1993**, *366* (6456), 701–704.
- (255) Harper, J. W.; Adami, G. R.; Wei, N.; Keyomarsi, K.; Elledge, S. J. The p21 Cdk-Interacting Protein Cip1 Is a Potent Inhibitor of G1 Cyclin-Dependent Kinases. *Cell* **1993**, *75* (4), 805–816.

- (256) Romero-Oliva, F.; Allende, J. E. Protein p21WAF1/CIP1 Is Phosphorylated by Protein Kinase CK2 in Vitro and Interacts with the Amino Terminal End of the CK2 Beta Subunit. *J. Cell. Biochem.* **2001**, *81* (3), 445–452.
- (257) Pierre, F.; Chua, P. C.; O'Brien, S. E.; Siddiqui-Jain, A.; Bourbon, P.; Haddach, M.; Michaux, J.; Nagasawa, J.; Schwaebe, M. K.; Stefan, E.; Vialettes, A.; Whitten, J. P.; Chen, T. K.; Darjanian, L.; Stansfield, R.; Bliesath, J.; Drygin, D.; Ho, C.; Omori, M.; Proffitt, C.; Streiner, N.; Rice, W. G.; Ryckman, D. M.; Anderes, K. Pre-Clinical Characterization of CX-4945, a Potent and Selective Small Molecule Inhibitor of CK2 for the Treatment of Cancer. *Mol. Cell. Biochem.* **2011**, *356* (1-2), 37–43.
- (258) Esteve, V.; Canela, N.; Rodriguez-Vilarrupla, A.; Aligué, R.; Agell, N.; Mingarro, I.; Bachs, O.; Pérez-Payá, E. The Structural Plasticity of the C Terminus of p21Cip1 Is a Determinant for Target Protein Recognition. *Chembiochem Eur. J. Chem. Biol.* **2003**, *4* (9), 863–869.
- (259) Rossig, L.; Jadidi, A. S.; Urbich, C.; Badorff, C.; Zeiher, A. M.; Dimmeler, S. Akt-Dependent Phosphorylation of p21Cip1 Regulates PCNA Binding and Proliferation of Endothelial Cells. *Mol. Cell. Biol.* **2001**, *21* (16), 5644–5657.
- (260) Rodríguez-Vilarrupla, A.; Díaz, C.; Canela, N.; Rahn, H. P.; Bachs, O.; Agell, N. Identification of the Nuclear Localization Signal of p21(cip1) and Consequences of Its Mutation on Cell Proliferation. *FEBS Lett.* **2002**, *531* (2), 319–323.
- (261) Park, C. M.; Kim, S. Y.; Park, W. K.; Park, N. S.; Seong, C. M. Synthesis and Structure–activity Relationship of 1H-Indole-3-Carboxylic Acid Pyridine-3-Ylamides: A Novel Series of 5-HT_{2C} Receptor Antagonists. *Bioorg. Med. Chem. Lett.* **2008**, *18* (14), 3844–3847.
- (262) Hopkins, C. R.; Czekaj, M.; Kaye, S. S.; Gao, Z.; Pribish, J.; Pauls, H.; Liang, G.; Sides, K.; Cramer, D.; Cairns, J.; others. Design, Synthesis, and Biological Activity of Potent and Selective Inhibitors of Mast Cell Tryptase. *Bioorg. Med. Chem. Lett.* **2005**, *15* (11), 2734–2737.
- (263) Oxford, A. W.; Whitehead, J. W. F.; Knight, J. 3-Piperidinylmethylcarboxylate Substituted Indoles. EP0501322A1, September 2, 1992.
- (264) Boyer, N.; Gloanec, P.; De Nanteuil, G.; Jubault, P.; Quirion, J.-C. Synthesis of α,α -Difluoro- β -Amino Esters or Gem-Difluoro- β -Lactams as Potential Metalloprotease Inhibitors. *Eur. J. Org. Chem.* **2008**, *2008* (25), 4277–4295.
- (265) Lopez-Rodriguez, M. L.; Benhamu, B.; Viso, A.; Morcillo, M. J.; Murcia, M.; Orensanz, L.; Alfaro, M. J.; Martín, M. I. Benzimidazole Derivatives. Part 1: Synthesis and Structure±Activity Relationships of New Benzimidazole-4-Carboxamides and Carboxylates as Potent and Selective 5-HT₄ Receptor Antagonists. *Bioorg. Med. Chem.* **1999**, *7*, 2271–2781.

- (266) Gaster, L. M.; Joiner, G. F.; King, F. D.; Wyman, P. A.; Sutton, J. M.; Bingham, S.; Ellis, E. S.; Sanger, G. J.; Wardle, K. A. N-[(1-Butyl-4-Piperidinyl) Methyl]-3, 4-Dihydro-2H-[1, 3] Oxazino [3, 2-A] Indole-10-Carboxamide Hydrochloride: The First Potent and Selective 5-HT₄ Receptor Antagonist Amide with Oral Activity. *J. Med. Chem.* **1995**, 38 (24), 4760–4763.
- (267) López-Ramos, M.; Prudent, R.; Moucadel, V.; Sautel, C. F.; Barette, C.; Lafanechère, L.; Mouawad, L.; Grierson, D.; Schmidt, F.; Florent, J.-C.; Filippakopoulos, P.; Bullock, A. N.; Knapp, S.; Reiser, J.-B.; Cochet, C. New Potent Dual Inhibitors of CK2 and Pim Kinases: Discovery and Structural Insights. *FASEB J. Off. Publ. Fed. Am. Soc. Exp. Biol.* **2010**, 24 (9), 3171–3185.
- (268) Liu, D.; Liu, Z.; Jiang, D.; Dackiw, A. P.; Xing, M. Inhibitory Effects of the Mitogen-Activated Protein Kinase Kinase Inhibitor CI-1040 on the Proliferation and Tumor Growth of Thyroid Cancer Cells with BRAF or RAS Mutations. *J. Clin. Endocrinol. Metab.* **2007**, 92 (12), 4686–4695.
- (269) Fischmann, T. O.; Smith, C. K.; Mayhood, T. W.; Myers, J. E.; Reichert, P.; Mannarino, A.; Carr, D.; Zhu, H.; Wong, J.; Yang, R.-S.; Le, H. V.; Madison, V. S. Crystal Structures of MEK1 Binary and Ternary Complexes with Nucleotides and Inhibitors. *Biochemistry (Mosc.)* **2009**, 48 (12), 2661–2674.
- (270) Oda, K.; Matsuoka, Y.; Funahashi, A.; Kitano, H. A Comprehensive Pathway Map of Epidermal Growth Factor Receptor Signaling. *Mol. Syst. Biol.* **2005**, 1, 2005.0010.
- (271) Abbas, T.; Dutta, A. p21 in Cancer: Intricate Networks and Multiple Activities. *Nat. Rev. Cancer* **2009**, 9 (6), 400–414.
- (272) Zunszain, P. A.; Ghuman, J.; Komatsu, T.; Tsuchida, E.; Curry, S. Crystal Structural Analysis of Human Serum Albumin Complexed with Hemin and Fatty Acid. *BMC Struct. Biol.* **2003**, 3, 6.
- (273) Liu, X.; Wright, M.; Hop, C. E. C. A. Rational Use of Plasma Protein and Tissue Binding Data in Drug Design. *J. Med. Chem.* **2014**, 57 (20), 8238–8248.
- (274) Gottlieb, H. E.; Kotlyar, V.; Nudelman, A. NMR Chemical Shifts of Common Laboratory Solvents as Trace Impurities. *J. Org. Chem.* **1997**, 62 (21), 7512–7515
- (275) Guha-Sircar, S.; Patnaik, Khirod Kumar. Preparation of Antibacterials from Organomercurials. *J. Indian Chem. Soc.* **1950**, 27, 535–538.
- (276) Potewar, T. M.; Ingale, S. A.; Srinivasan, K. V. Catalyst-Free Efficient Synthesis of 2-Aminothiazoles in Water at Ambient Temperature. *Tetrahedron* **2008**, 64 (22), 5019–5022.
- (277) Wan, Y.; Gray, N. S. Compounds and Compositions as Protein Kinase Inhibitors. WO2007016228 (A2), February 8, 2007.
- (278) Mahapatra, R. *J. Indian Chem. Soc.* **1953**, 30, 398.

- (279) Gottlieb, H. E.; Kotlyar, V.; Nudelman, A. NMR Chemical Shifts of Common Laboratory Solvents as Trace Impurities. *J. Org. Chem.* **1997**, *62* (21), 7512–7515.
- (280) Pravst, I.; Zupan, M.; Stavber, S. Halogenation of Ketones with N-Halosuccinimides under Solvent-Free Reaction Conditions. *Tetrahedron* **2008**, *64* (22), 5191–5199.
- (281) Kumar, R. S.; Kulangiappar, K.; Kulandainathan, M. A. Convenient Electrochemical Method for the Synthesis of α -Bromo Alkyl Aryl Ketones. *Synth. Commun.* **2010**, *40* (12), 1736–1742.
- (282) Borowitz, I. J.; Parnes, H. Kinetics and Mechanism of the Reaction of Triphenylphosphine with α -Haloacetophenones. *J. Org. Chem.* **1967**, *32* (11), 3560–3564.
- (283) Hay, M. P.; Turcotte, S.; Flanagan, J. U.; Bonnet, M.; Chan, D. A.; Sutphin, P. D.; Nguyen, P.; Giaccia, A. J.; Denny, W. A. 4-Pyridylanilinothiazoles That Selectively Target von Hippel–Lindau Deficient Renal Cell Carcinoma Cells by Inducing Autophagic Cell Death. *J. Med. Chem.* **2010**, *53* (2), 787–797.
- (284) Browne, D. W.; Dyson, G. M. The Inhibitory Effect of Substituents in Chemical Reactions. Part III. The Reactivity of the Isothiocyano-Group in Substituted Arylthiocarbimides. *J. Chem. Soc.* **1934**, 178.
- (285) Richter. *Pharmazie* **1974**, *29*, 307.
- (286) Seligman, R. B.; Bost, R. W.; McKee, R. L. Some Derivatives of P-Aminosalicylic Acid. *J. Am. Chem. Soc.* **1953**, *75* (24), 6334–6335.
- (287) Katritzky, A. R.; Kirichenko, N.; Rogovoy, B. V.; Kister, J.; Tao, H. Synthesis of Mono- and N,N-Disubstituted Thioureas and N-Acylthioureas. *Synthesis* **2004**, *11*, 1799–1805.
- (288) Cohen, Victor Israel; Reynaud, Pierre; Moreau, Robert Cesar. Synthesis of Some 1,3-disubstituted Thioureas Containing Thioamide Groups. *Bull. Soc. Chim. Fr.* **1965**, *8*, 2314–2317.
- (289) Yan, X.; Xue-ping, S.; Xiu-guo, Z.; Wan-ping, T. Insecticidal Activity of Compounds from the South China Sea Invertebrate Scapharca Subcrenata. *Chem. Nat. Compd.* **2015**, *51* (4), 800–802.
- (290) Swain, C.; Baker, R.; Kneen, C.; Herbert, R.; Moseley, J.; Saunders, J.; Seward, E.; Stevenson, G.; Beer, M. Novel 5-HT₃ Antagonists: Indol-3-Ylspiro (azabicycloalkane-3, 5'(4'H) Oxazoles). *J. Med. Chem.* **1992**, *35* (6), 1019–1031.
- (291) Kalir, A.; Balderman, D. Improved Synthesis of Some Fluoroindoles. *Isr. J. Chem.* **1968**, *6* (6), 927–932.
- (292) Hideaki, S.; Tatsuo, K.; Hiroshige, T.; Hirotoshi, N.; Hiromu, H.; Tatsumi, N.; Seiichi, A.; Masayuki, M. Process for Producing Sulfonylamides. 3956385, 1976.

- (293) Gaster, L. M.; Wyman, P. A. Condensed Indoles Derivatives as 5-HT₄ Receptor Antagonists. US5998409A, December 7, 1999.
- (294) Kufareva, I.; Ilatovskiy, A. V.; Abagyan, R. Pocketome: An Encyclopedia of Small-Molecule Binding Sites in 4D. *Nucleic Acids Res.* **2012**, *40* (Database issue), D535–D540.
- (295) Abagyan, R.; Totrov, M. Biased Probability Monte Carlo Conformational Searches and Electrostatic Calculations for Peptides and Proteins. *J. Mol. Biol.* **1994**, *235* (3), 983–1002.
- (296) Totrov, M.; Abagyan, R. Flexible Protein-Ligand Docking by Global Energy Optimization in Internal Coordinates. *Proteins* **1997**, *Suppl 1*, 215–220.
- (297) Totrov, M.; Abagyan, R. Protein-Ligand Docking as an Energy Optimization Problem. In *Drug-Receptor Thermodynamics: Introduction and Applications*; Raffa RB, 2001; pp 603–624.
- (298) Fernández-Recio, J.; Totrov, M.; Abagyan, R. Soft Protein-Protein Docking in Internal Coordinates. *Protein Sci. Publ. Protein Soc.* **2002**, *11* (2), 280–291.
- (299) Schapira, M.; Totrov, M.; Abagyan, R. Prediction of the Binding Energy for Small Molecules, Peptides and Proteins. *J. Mol. Recognit. JMR* **1999**, *12* (3), 177–190.
- (300) Debnath, J.; Muthuswamy, S. K.; Brugge, J. S. Morphogenesis and Oncogenesis of MCF-10A Mammary Epithelial Acini Grown in Three-Dimensional Basement Membrane Cultures. *Methods San Diego Calif* **2003**, *30* (3), 256–268.
- (301) Poletto, G.; Vilardell, J.; Marin, O.; Pagano, M. A.; Cozza, G.; Sarno, S.; Falqués, A.; Itarte, E.; Pinna, L. A.; Meggio, F. The Regulatory Beta Subunit of Protein Kinase CK2 Contributes to the Recognition of the Substrate Consensus Sequence. A Study with an eIF2 Beta-Derived Peptide. *Biochemistry (Mosc.)* **2008**, *47* (32), 8317–8325.
- (302) Filhol, O.; Cochet, C.; Wedegaertner, P.; Gill, G. N.; Chambaz, E. M. Coexpression of Both Alpha and Beta Subunits Is Required for Assembly of Regulated Casein Kinase II. *Biochemistry (Mosc.)* **1991**, *30* (46), 11133–11140

